NAVAL POSTGRADUATE SCHOOL
Monterey, California

DISSERTATION

SOFT DECISION DIVERSITY CODED DS/DPSK SYSTEMS IN PULSE-JAMMED MULTIPATH-FADING CHANNELS

by

Charles W. Victory

March 1999

Dissertation Advisors: Charles W. Therrien
Tri T. Ha

Approved for public release; distribution is unlimited.

DTIC QUALITY INSPECTED 2

19990401 119

REPORT DOCUMENTATION PAGE

Form Approved
OMB No. 0704-0188

Public reporting burden for this collection of information is estimated to average 1 hour per response, including the time reviewing instructions, searching existing data sources gathering and maintaining the data needed, and completing and reviewing the collection of information. Send comments regarding this burden estimate or any other aspect of this collection of information, including suggestions for reducing this burden to Washington Headquarters Services, Directorate for Information Operations and Reports, 1215 Jefferson Davis Highway, Suite 1204, Arlington, VA 22202-4302, and to the Office of Management and Budget, Paperwork Reduction Project (0704-0188), Washington, DC 20503.

1. AGENCY USE ONLY (Leave Blank)	2. REPORT DATE	3. REPORT TYPE AND DATES COVERED
	March 1999	Doctoral Dissertation

4. TITLE AND SUBTITLE
SOFT DECISION DIVERSITY CODED DS/DPSK SYSTEMS IN PULSE-JAMMED MULTIPATH-FADING CHANNELS

5. FUNDING NUMBERS

6. AUTHOR(S)
Charles W. Victory

7. PERFORMING ORGANIZATION NAME(S) AND ADDRESS(ES)
Naval Postgraduate School
Monterey, CA 93943-5000

8. PERFORMING ORGANIZATION REPORT NUMBER

9. SPONSORING/ MONITORING AGENCY NAME(S) AND ADDRESS(ES)

10. SPONSORING/ MONITORING AGENCY REPORT NUMBER

11. SUPPLEMENTARY NOTES
The views expressed in this dissertation are those of the author and do not reflect the official policy or position of the Department of Defense or the United States Government.

12a. DISTRIBUTION / AVAILABILITY STATEMENT
Approved for public release; distribution is unlimited

12b. DISTRIBUTION CODE

13. ABSTRACT *(Maximum 200 words)*

The performance of a Direct Sequence Spread Spectrum system utilizing Differential Phase Shift-Keying modulation over a fading channel in the presence of pulse noise interference and additive white Gaussian noise is considered. Time and spatial diversity receivers utilizing various normalization schemes and post-detection selection combining are employed to overcome performance limitations inherent in the adverse environments. Numerical results are presented over a range of environmental conditions demonstrating the efficacy of such receivers. The performance analysis is extended through the utilization of convolutional coding and soft decision Viterbi decoding. Here the performance of the maximum likelihood decoding operation is expressed in terms of an equivalent uncoded system for both the Rayleigh and Rician fading channel with interference effects. Numerical results are then presented demonstrating the efficacy of such a receiver.

14. SUBJECT TERMS	15. NUMBER OF PAGES
Wireless communications, Direct Sequence Spread Spectrum, Differential Phase Shift-Keying, Convolutional coding, Viterbi decoding	207
	16. PRICE CODE

17. SECURITY CLASSIFICATION OF REPORT	18. SECURITY CLASSIFICATION OF THIS PAGE	19. SECURITY CLASSIFICATION OF ABSTRACT	20. LIMITATION OF ABSTRACT
Unclassified	Unclassified	Unclassified	UL

Approved for public release; distribution is unlimited

SOFT DECISION DIVERSITY CODED DS/DPSK SYSTEMS IN PULSE-JAMMED MULTIPATH-FADING CHANNELS

Charles William Victory
Lieutenant Commander, United States Navy
B.S., SUNY Maritime College, 1985
M.S., U.S. Naval Postgraduate School, 1993

DOCTOR OF PHILOSOPHY IN ELECTRICAL ENGINEERING

from the

NAVAL POSTGRADUATE SCHOOL
March 1999

Author: Charles William Victory
Charles William Victory

Approved By:

Charles W. Therrien
Charles W. Therrien, Professor
Dept. of Electrical & Computer Engr.
Dissertation and Committee Supervisor

Tri T. Ha
Tri T. Ha, Professor
Dept. of Electrical & Computer Engr.
Dissertation Supervisor

Roberto Cristi, Associate Professor
Dept. of Electrical & Computer Engr.

Murali Tummala
Murali Tummala, Professor
Dept. of Electrical & Computer Engr.

Andres Larraza, Assistant Professor
Dept. of Physics

Approved By:
Jeffrey B. Knorr, Chairman, Dept. of
Electrical and Computer Engr.

Approved By:
Anthony Ciavarelli, Acting Associate Provost for Instruction

ABSTRACT

The performance of a Direct Sequence Spread Spectrum system utilizing Differential Phase Shift-Keying modulation over a fading channel in the presence of pulse noise interference and additive white Gaussian noise is considered. Time and spatial diversity receivers utilizing various normalization schemes and post-detection selection combining are employed to overcome performance limitations inherent in certain adverse environments. Numerical results are presented over a range of environmental conditions demonstrating the efficacy of such receivers. The performance analysis is extended through the utilization of convolutional coding and soft decision Viterbi decoding. The performance of the maximum likelihood decoding operation is expressed in terms of an equivalent uncoded system for both the Rayleigh and Rician fading channel with interference effects. Numerical results are then presented demonstrating the efficacy of such a receiver.

TABLE OF CONTENTS

LIST OF FIGURES

LIST OF SYMBOLS

E_b/N_0 - signal energy-to-thermal noise density ratio

E_b/N_I - signal energy-to-interference noise density ratio

α^2 - direct path signal energy

$2\sigma_a^2$ - diffuse (multipath) signal energy

γ - ratio of direct path signal energy-to-diffuse signal energy

ρ - fraction of time for which jammer is "on"

ρ_1 - fraction of bits which experience case I jamming events

ρ_2 - fraction of bits which experience case II jamming events

β - ratio of the number of case I jamming events to case II jamming events

L - time diversity order

M - spatial diversity order

σ_n^2 - thermal noise variance

$\sigma_{I_j}^2$ - interference noise variance

σ_j^2 - total conditional noise variance

$\sigma_{1_j}^2$ - total conditional variance for signal branch

$\sigma_{2_j}^2$ - total conditional variance for non-signal branch

Γ_L - inverse of signal energy-to-total conditional noise variance ratio when using time diversity

Γ_M - inverse of signal energy-to-total conditional noise variance ratio when using spatial diversity

r_c - code rate

ν - constraint length

d - Hamming distance; the number of bits for which two code words are different

$P_2(d)$ - probability of decoder error for all code words a distance d from the correct code word

ACKNOWLEDGEMENTS

Without question, the pursuit of a Ph.D. degree has been an extremely challenging task and the most difficult that I have ever set out to accomplish. It was definitely worth the effort and the amount of personal satisfaction is great. I am truly grateful and would like to extend my personal thanks and gratitude to several people. First I must thank God, who has always been there to answer my prayers. I thank my wife. No other person knows the depth of what I was feeling during this process. She has absorbed it all with me and has been my "Rock of Gibraltar." There is no better friend in the world to me than you, Charlene. I must also thank my primary research advisor, Tri Ha. Tri, you have been so instrumental in directing my efforts and keeping me on track. You helped me believe that I could and would make it through the program. You provided a breath of fresh air when I needed it most. You have been a great mentor and friend. Thank you. Thanks to my chairman, Charlie Therrien. Charlie, you have been so instrumental in my development as an electrical engineer over the years. You are a true professional at what you do and also have been a great mentor. Thank you also to the rest of my committee, especially Murali and Roberto. They have also played a big part in my development over the years and have been very supportive. Also a special thanks to Dr. Clark Robertson who taught many of the Communications courses for which I was enrolled. I truly enjoyed your classes!! I also thank my parents, who pushed me at a young age through a competitive high school which taught me discipline and gave me a solid background for which to draw on. I would also like to thank my younger brother, Dr. James Victory. Jim, having gone through a EE Ph.D. program of your own, you were there to empathize with me as I progressed through. Thanks to Helen and Jerry for your support and prayers for me. A very special thanks to my kids, whom I absolutely adore, Sarah, Olivia and Alyssa. It was always nice to know that at the end of a day, I would be coming home to your unconditional love.

I. INTRODUCTION

The field of *wireless communications* including the areas of mobile cellular and Personal Communications Services (PCS) has experienced rapid and expansive growth in recent years. The high demand to communicate in a mobile environment is pushing the need for wireless providers to upgrade existing systems. Traditional analog systems are being supplanted by digital systems to improve performance and increase capacity. The performance of a mobile radio communications link is governed by several factors. One of the most detrimental effects to a mobile radio channel is that of multipath fading [1,2]. Fading is caused when several replicas of the transmitted signal are accepted by the receiver where they may constructively and destructively add to each other. The result is that the signal-to-noise ratio may take large swings in magnitude greatly effecting the reliability of the link. The effects are most detrimental when there is no line sight (LOS) path between the transmitter and receiver. This type of channel is termed the Rayleigh channel. Another element that limits the performance of the mobile radio channel is that of the ubiquitous additive white Gaussian noise (AWGN). In a military setting, in addition to the previous mentioned factors, the channel may experience pulse noise interference. Pulse noise interference occurs when a source outside the normal communications channel transmits electromagnetic energy into the channel in short bursts with the goal of disrupting effective communication between the end users. For a digital communications link, short bursts of this sort can be extremely deleterious to maintaining a reliable communications link. Ideally one would like to eliminate the effects of the pulse noise jammer while maintaining signal integrity. Several digital techniques, such as direct sequence spread spectrum and forward error correction (FEC) coding, have been shown to be effective in the mitigation of pulse noise interference [10]. If the jammer is smart however, significant degradation to the communications link may still occur. In worst case jamming scenarios, the use of spread spectrum and FEC may not be enough to restore a reliable communications link.

In this dissertation, maximum-likelihood (ML) solutions which minimize the probability of bit error are sought. The performance of coded Direct Sequence Differential Phase Shift-Keying (DS-DPSK) over a Rayleigh fading channel in the presence of pulse noise interference and AWGN has been considered [29]. Here to combat the effects of pulse noise interference, a non-maximum likelihood (ML) soft-limiter receiver with a non-adaptive threshold in tandem with a combination

of antenna diversity and spread spectrum diversity are utilized. ML receivers with an adaptive threshold, such as the self-normalized and noise-normalized receivers, have been shown to be extremely effective in combatting partial band interference in Fast-Frequency Hopped Frequency Shift-Keying (FSK) systems [14-18]. Part of the work in this dissertation will be to apply the techniques of self-normalization and noise-normalization to a DS-DPSK system to mitigate the effects of pulse noise interference. Up until now, no such attempt has been made to do so. The next two chapters investigate these topics. In chapter IV, a new technique is introduced where the receiver employs spatial diversity and selects the maximum from a set of multiple antenna post-detected outputs. The resulting technique is termed First Order Post-Detection Selection Combining (PDSC1). This receiver type has the attribute of path independent performance which provides an extra measure of reliability to the system. In a military setting, this extra measure of reliability is highly desirable. In chapter V, the performance of the PDSC1 receiver employing both spatial and time diversity is investigated. In chapter VI, convolutional coding is employed and receiver performances using the Viterbi decoding algorithm is analyzed. In addition the performance of the linear receiver will be analyzed. The linear receiver utilizes diversity combining without any limiting device. The performance of this receiver has been shown to be extremely effective in improving performance in signal fading environments provided a sufficient signal-to-noise ratio is maintained at the receiver [5]. The performance of the linear receiver will be used here as a benchmark for which to compare the other non-linear receivers.

The main results of this dissertation will show that the noise-normalized and self-normalized receivers are most effective in mitigating the effects of pulse noise interference and signal fading. The additional noncoherent combining losses incurred by the linear receiver in the combined pulse-jammed, multipath fading channel prove to be too significant to overcome and performance subsequently degrades. The linear receiver performance degrades further when convolutional coding is employed. Performance improvement of the noise-normalized and self-normalized receivers with convolutional coding is significant in comparison to the uncoded systems. The combined use of time diversity with convolutional coding produces the best results for these receivers. The performance of the PDSC1 receiver is shown to be inferior to either the self-normalized or noise-normalized receivers. The PDSC1 receiver performance degrades with the addition of time diversity as a result of noncoherent combining losses.

Throughout this dissertation, a constant information bit rate is assumed. A power-limited environment is therefore assumed and additional bandwidth is available to help improve system performance. While it may not be always realistic to assume unlimited bandwidth, the work here could be extended to bandlimited cases through some system modifications. Pulse shaping could be employed to reduce the amount of intersymbol interference (ISI). In cases where ISI cannot be avoided, spread spectrum diversity utilizing a Rake receiver and/or channel equalization techniques [5, 29] may be included in the system.

II. DS-DPSK WITH SELF-NORMALIZATION AND L-FOLD DIVERSITY IN A FADING CHANNEL

In this chapter, the performance of a DS-DPSK spread spectrum system over a Rician frequency nonselective, slowly fading channel in the presence of pulsed noise interference and AWGN is considered. The system employs L-fold time diversity with i of L channels, i = 1,2,... L experiencing interference at any given point in time. A model block diagram of the system transmitter/channel/receiver is shown in Figure 2.1. In the interleaving frame at the transmitter, N data bits are consecutively repeated L times for a total of M = LN transmission bits. The M bits are then interleaved in such a fashion so that adjacent repeated bits are separated by a time greater than the coherence time of the channel. This allows for independent reception of each of the L diversity transmissions [5]. The data is then differentially encoded via the DPSK modulator prior to "spreading" by the Direct Sequence Spread Spectrum (DSSS) spreader. At the receiver, the data is "despread", demodulated via a DPSK receiver, deinterleaved and combined. The performance of a self-normalized receiver utilizing soft decision equal gain combining is considered. To begin the discussion, the optimum receiver for detection of a DPSK signal in AWGN over a frequency nonselective slowly fading Rician channel is considered. A brief overview of Direct Sequence Spread Spectrum is then provided followed by a description of the pulsed noise interference model. The bit error probability of the self-normalized receiver is then derived.

A. OPTIMUM DETECTION OF DPSK IN AWGN OVER A FREQUENCY NONSELECTIVE SLOWLY FADING RICIAN CHANNEL

The general form of a DPSK signal may be written as

$$s(t) = \sqrt{\frac{2}{T}} A[c_0 p_T(t) + c_1 p_T(t-T)]\cos\omega_c t \qquad (2.1)$$

for $0 \le t \le 2T$, with $c_0 c_1 = 1$ representing bit 0 and $c_0 c_1 = -1$ representing bit 1. The function $p_T(t)$ represents a rectangular pulse of unit amplitude on the bit interval $0 \le t \le T$. The carrier frequency is denoted by ω_c. Note that the signals representing bit 0 and bit 1 are orthogonal to each other over the 2-bit interval, 2T.

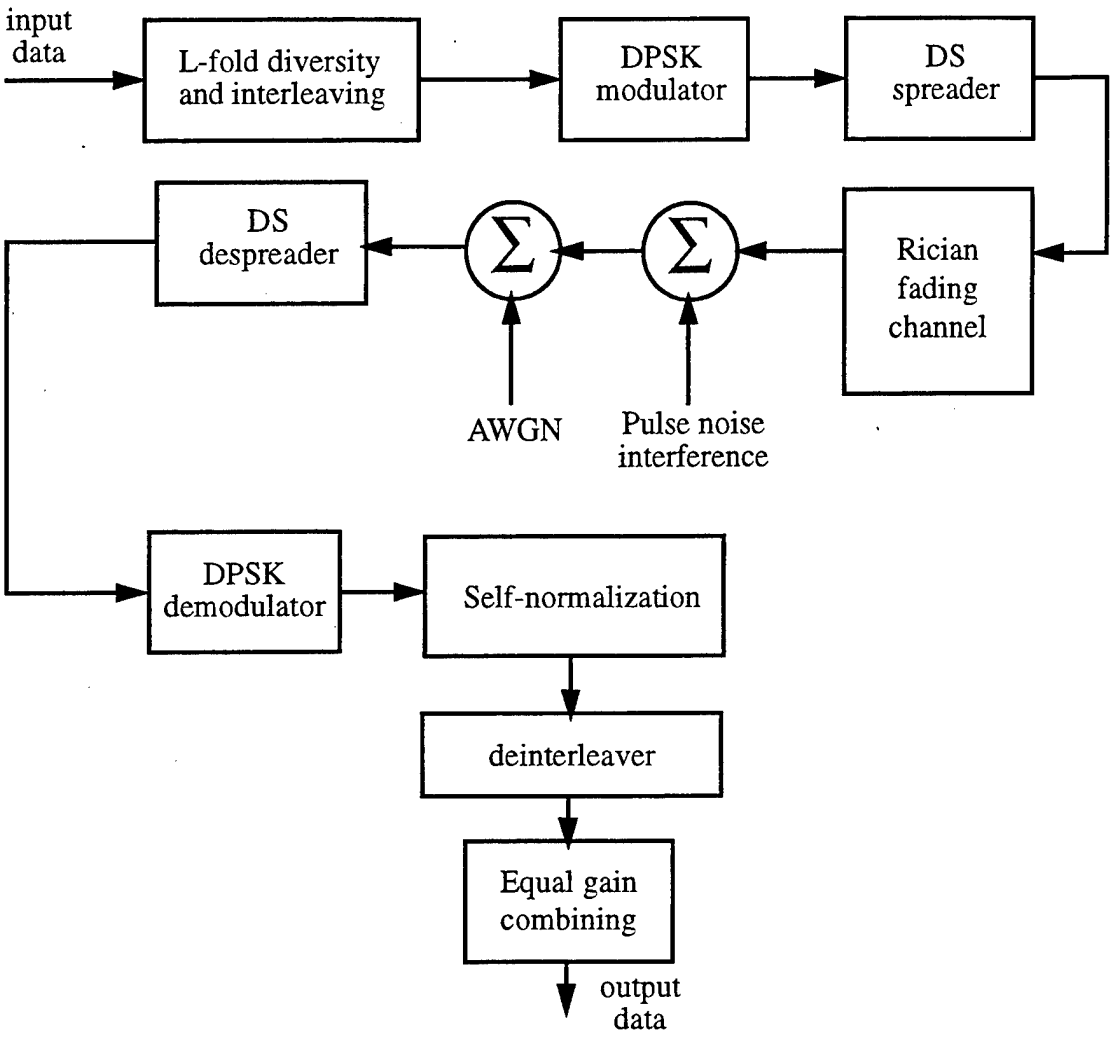

Figure 2.1: Transmitter/channel/receiver model of DS-DPSK over fading channel and in the presence of pulse noise interference and AWGN.

The received signal over a Rician channel has the general form

$$r(t) = \sqrt{\frac{2}{T}}\alpha(t)d(t)\cos(\omega_c t + \theta) + \sqrt{\frac{2}{T}}\sum_{i=1}^{N} A_i(t)d(t)\cos(\omega_c t + \theta + \phi_i(t)) + n(t) \qquad (2.2)$$

where $d(t) = [c_0 p_T(t) + c_1 p_T(t-T)]$ represents the data and $n(t)$ is AWGN (thermal noise) with power spectral density (PSD) $N_0/2$. The first term in the expression for $r(t)$ represents the

direct path component of the received signal with amplitude $\alpha(t)$ and phase offset θ. The second term represents the diffuse component due to the presence of multipath whose amplitude fluctuates due to the time-varying amplitude function $A_i(t)$ and phase function $\phi_i(t)$. This phase function is equal to $\omega_c\tau_i$ with τ_i representing the time delay of the i^{th} multipath component of the received signal. If the carrier frequency is large, relatively small time delays can cause large phase shifts in the $\phi_i(t)$ (modulo 2π). The result is that the received signal paths may add constructively when the received paths are in phase, producing large signal amplitudes; or add destructively when the paths are out of phase, producing very weak signal returns. If it is assumed that $A_i(t)$ and $\alpha(t)$ are constant over the 2-bit signaling interval, $A_i(t)$ may be replaced with A_i and $\alpha(t)$ with α. If it is further assumed that the phase function $\phi_i(t)$ varies slowly over the 2-bit interval then $\phi_i(t)$ may be replaced by ϕ_i. Both assumptions are equivalent to saying the 2-bit signal duration is much less than the coherence time of the channel. A channel of this sort is said to be *slowly fading*. The received signal can now be rewritten as

$$r(t) = \sqrt{\frac{2}{T}}\alpha d(t)\cos(\omega_c t + \theta) + \sqrt{\frac{2}{T}}\sum_{i=1}^{N} A_i d(t)\cos(\omega_c t + \theta + \phi_i) + n(t) \tag{2.3}$$

A channel is said to be frequency nonselective when the bandwidth of the transmitted signal is less than the coherence bandwidth of the channel. This occurs when the time duration of the signal is greater than the time duration of the impulse response of the channel. In this situation, intersymbol interference (ISI) is not present.

The optimum receiver for noncoherent detection of orthogonal signals in AWGN according to the Bayes criterion is shown in Figure 2.2 [4, 5]. The signals $h_1(t)$ and $h_2(t)$ are replicas of the transmitted signal representing bits 0 and 1 respectively. A square law detector receiver with identical detection performance is shown in Figure 2.3. In this figure the upper branch corresponds to the bit 1 detector while the lower corresponds to the bit 0 detector.

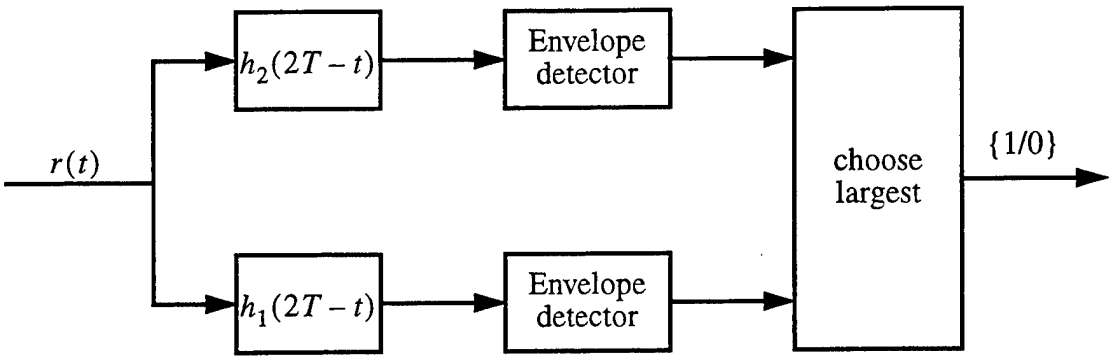

Figure 2.2: Matched filter receiver for noncoherent detection of DPSK in AWGN.

An important figure of merit for any digital communications system is the probability of bit error. In a binary system such as DPSK, the probability of bit error is P_b = Pr[bit 1 detected|bit 0 sent]Pr[bit 0 sent] + Pr[bit 0 detected|bit 1 sent]Pr[bit 1 sent]. A binary symmetric channel is assumed, therefore Pr[bit 1 detected|bit 0 sent] = Pr[bit 0 detected|bit 1 sent]. If is further assumed each bit is equally likely to be sent, then the expression reduces to P_b = Pr[bit 1 detected|bit 0 sent] = Pr[bit 0 detected|bit 1 sent]. The case of either bit 1 or 0 being sent may therefore be considered in determining the overall probability of bit error.

If it is assumed bit 0 is sent, the outputs of the detector branches before the squaring operation are given by

$$Y_{1c} = \pm 2\alpha\cos\theta \pm \sum_{i=1}^{n} 2A_i\cos(\theta + \phi_i) + N_{1c} \tag{2.4a}$$

$$Y_{1s} = \pm 2\alpha\sin\theta \pm \sum_{i=1}^{n} 2A_i\sin(\theta + \phi_i) + N_{1s} \tag{2.4b}$$

$$Y_{2c} = N_{2c} \tag{2.4c}$$

$$Y_{2s} = N_{2s} \tag{2.4d}$$

where

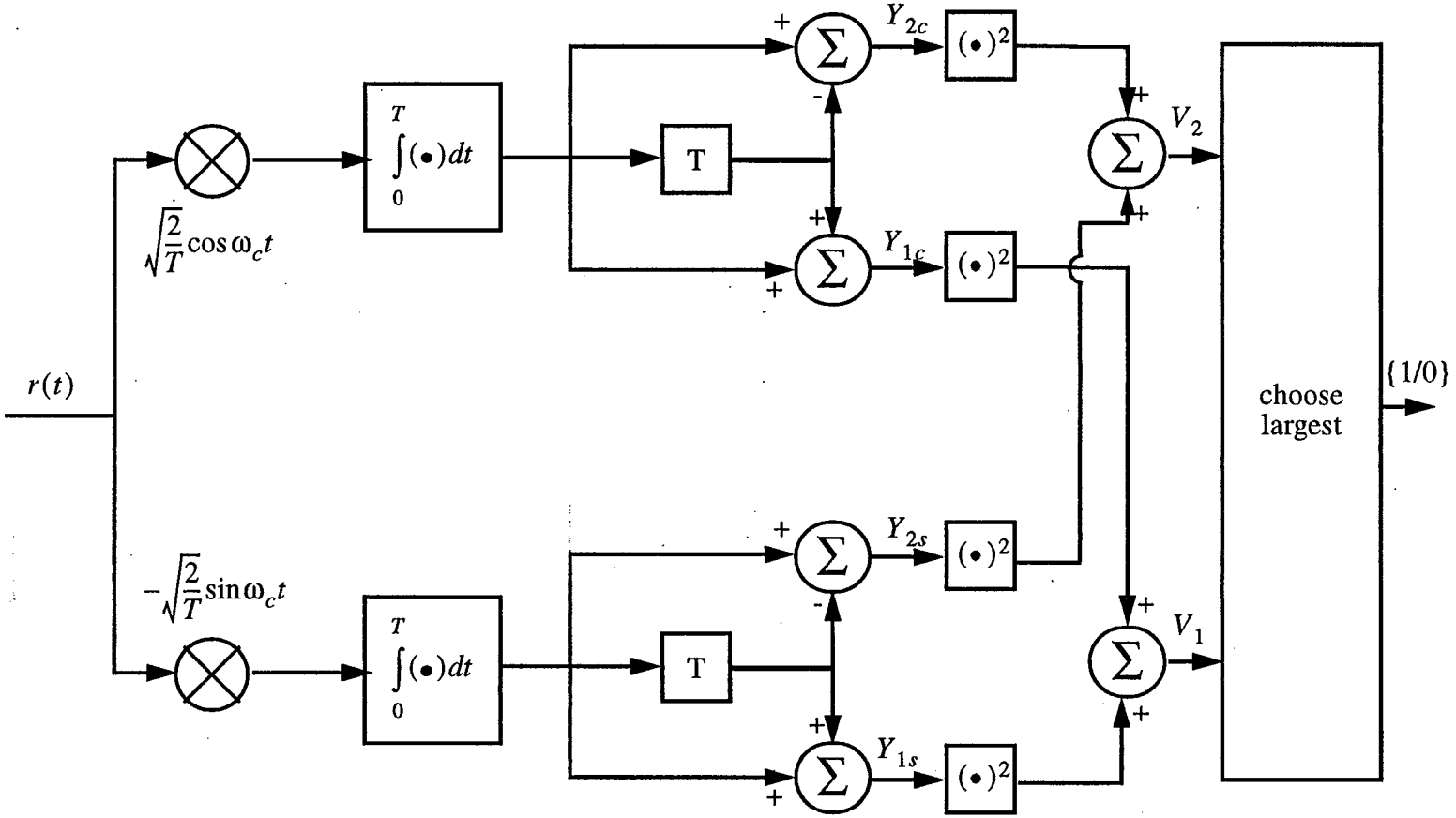

Figure 2.3: Square Law receiver for optimum detection of DPSK in AWGN.

$$N_{1c} = N_{1c_0} + N_{1c_T} \tag{2.5a}$$

$$N_{2c} = N_{1c_0} - N_{1c_T} \tag{2.5b}$$

$$N_{1s} = N_{1s_0} + N_{1s_T} \tag{2.5c}$$

$$N_{2s} = N_{1s_0} - N_{1s_T} \tag{2.5d}$$

and

$$N_{1c_0} = \sqrt{\frac{2}{T}} \int_0^T n(t) \cos \omega_c t dt \tag{2.6a}$$

$$N_{1c_T} = \sqrt{\frac{2}{T}} \int_T^{2T} n(t) \cos \omega_c t dt \tag{2.6b}$$

$$N_{1s_0} = \sqrt{\frac{2}{T}} \int_0^T n(t) \sin \omega_c t dt \tag{2.6c}$$

$$N_{1s_T} = \sqrt{\frac{2}{T}} \int_T^{2T} n(t) \sin \omega_c t dt \tag{2.6d}$$

The quantities $N_{1c_0}, N_{1c_T}, N_{1s_0}, N_{1s_T}$ are uncorrelated, Gaussian random variables and therefore are independent. In addition they are identically distributed with zero mean and variance $\sigma_0^2 = N_0/2$. N_{1c}, N_{1s}, N_{2c}, N_{2s} are also independent, identically distributed (iid) Gaussian random variables with zero mean and variance $\sigma_n^2 = 2\sigma_0^2 = N_0$.

Referring again to equations 2.4a and 2.4b, the phases, ϕ_i, are modeled as independent uniform random variables over the range $[0,2\pi]$ since no prior knowledge of their values is assumed. In the limit as the number of paths N becomes large, by the Central Limit Theorem the first and second terms of equations 2.4a and 2.4b together can be modeled as non-zero mean Gaussian random variables. Therefore, Y_{1c} and Y_{1s} are Gaussian random variables with mean

$\pm 2\alpha\cos\theta$ and $\pm 2\alpha\sin\theta$ respectively, and with common variance equal to $(\sigma_n^2 + 4\sigma_a^2)$. In addition, due to the orthogonality of the sine and cosine functions, Y_{1c} and Y_{1s} are independent Gaussian random variables whose joint distribution is

$$f_{Y_{1c},Y_{1s}}(y_{1c}, y_{1s}|0) = \frac{1}{2\pi(4\sigma_a^2 + \sigma_n^2)} \times$$

$$\exp\left(-\frac{1}{2(4\sigma_a^2 + \sigma_n^2)}[(y_{1c} \mp 2\alpha\cos\theta)^2 + (y_{1s} \mp 2\alpha\sin\theta)^2]\right) \qquad (2.7)$$

The decision statistic V_1 is now the sum of two squared non-zero mean Gaussian random variables and is a noncentral Chi-squared random variable with 2 degrees of freedom [8]. Its distribution is

$$f_{V_1}(v_1|0) = \frac{1}{2(4\sigma_a^2 + \sigma_n^2)}\exp\left(-\frac{1}{2(4\sigma_a^2 + \sigma_n^2)}(v_1 + 4\alpha^2)\right)I_0\left(\frac{2\alpha\sqrt{v_1}}{(4\sigma_a^2 + \sigma_n^2)}\right)u(v_1) \qquad (2.8)$$

where $I_0(x)$ is the modified Bessel function of the first kind of zero order and $u(x)$ is the unit step function. In a similar fashion, the decision statistic V_2 is the sum of two squared zero mean Gaussian random variables and is therefore a central Chi-squared random variable with 2 degrees of freedom. Its distribution is

$$f_{V_2}(v_2|0) = \frac{1}{2\sigma_n^2}\exp\left(-\frac{v_2}{2\sigma_n^2}\right)u(v_2) \qquad (2.9)$$

since there is no signal component on this branch. Due to the orthogonality of the 2 branches, V_1 and V_2 are also independent random variables. Equations 2.4a and 2.4b can also be expressed in the following equivalent forms

$$Y_{1c} = R\cos\psi + N_{1c} \qquad (2.10a)$$

$$Y_{1s} = R\sin\psi + N_{1s} \qquad (2.10b)$$

where $R = \sqrt{X^2 + Y^2}$, $\psi = \arctan\left(\frac{Y}{X}\right)$ and

$$X = 2\alpha\cos\theta + \sum_{i=1}^{n} 2A_i\cos(\theta + \phi_i) \qquad (2.11a)$$

$$Y = 2\alpha\sin\theta + \sum_{i=1}^{n} 2A_i\sin(\theta + \phi_i) \qquad (2.11b)$$

R may then be identified as a Rician random variable. The average signal energy over this 2-bit interval, which is the second moment of R, is $4\alpha^2 + 8\sigma_a^2$. The average signal energy over a 1-bit interval, denoted by E_b, is $\alpha^2 + 2\sigma_a^2$ [5].

If either a noise-normalizer or self-normalizer were not employed, then the optimum decision logic at this point according to the Bayes criterion would be to pick the detector branch corresponding to the larger of V_1 and V_2. Before introducing the normalizing schemes, the model and underlying assumptions of the pulsed noised interference is described in detail. Before this however, the general underlying principles of Direct Sequence Spread Spectrum (DSSS) are described.

B. DIRECT SEQUENCE SPREAD SPECTRUM

The purpose of a DSSS system is two-fold. First the signal is spread to mitigate the possibility of detection of the information signal by unwanted users. Systems of this sort are termed Low Probability of Detection (LPD) systems. Secondly, if an unwanted user can detect the DSSS signal, then the DSSS system should minimize the possibility that the unwanted user can decipher the encoded message. Systems of this nature are called Low Probability of Interception (LPI) systems.

To produce a DSSS signal, a rectangular pulse shaped bipolar binary wave representing the information signal with bit duration T_b, bit rate $R_b = 1/T_b$ and noise equivalent bandwidth $B = R_b$, is multiplied ideally by a random bipolar binary wave called the chipping sequence of bit rate $R_c = kR_b$ where $k \gg 1$. The resulting sequence forms the DSSS signal. It has a Power Spectral Density (PSD) whose maximum magnitude is k times smaller than the maximum magnitude of the PSD of the information signal and whose noise equivalent bandwidth is k times larger than that of the information signal. Truly random binary waves cannot be generated in practice however and

signals called pseudorandom sequences are employed to modulate the information signal. These pseudorandom sequences are deterministic signals with ideally many of the same properties of a truly random binary wave. Demodulation of the DSSS signal occurs when the same sequence that was used to generate the modulated signal is used to multiply the signal at the receiver to recover the resulting information signal. This requires the codes at the transmitter and receiver to be in bit and code synchronization. For this dissertation, bit and code synchronization between transmitter and receiver is assumed to exist. More information about spread spectrum systems can be found in [10].

C. PULSE NOISE INTERFERENCE MODEL

The pulse noise interference model will now be described. The wideband pulse noise interference model to be described is based upon the assumption that the jammer bandwidth is at least as wide as the bandwidth of the transmitted DSSS signal, allowing the jammer to avoid detection at the receiver. It is assumed that an interferer jams a fraction ρ of the information bits ($0 \leq \rho \leq 1$). The fraction of bits not jammed is equal to thus ($1-\rho$). Pulse noise jamming is explicitly defined for the case of $\rho < 1$. The interfering signal is modeled as white Gaussian noise whose PSD is $N_I/2\rho$ when the jammer is on and 0 when the jammer is off. The total average PSD is then equal to $N_I/2$. Allowing for the possibility that either 2 consecutive bits, 1 bit, or no bits of the DPSK signal may be jammed, the following event space for these three cases is defined:

I_1- Event that either the first bit contains interference and the second bit does not, or that the second bit contains interference and the first bit does not ($\{I, NI\} \cup \{NI, I\}$).

I_2- Event that the first bit and the second bit both contain interference {I,I}.

I_3- Event that neither the first bit nor the second bit contain interference {NI,NI}.

The probabilities of the three events are defined as $Pr(I_1) = \rho_1$, $Pr(I_2) = \rho_2$ and $Pr(I_3) = (1-\rho_1-\rho_2)$ where $0 \leq \rho_1, \rho_2 \leq 1$. It is assumed that the jammer noise component is present equally in branches V_1 and V_2. The jammer noise variances at the receiver branches just prior to the squaring operation for the three cases are $\sigma^2_{I_1} = N_I/2\rho$, $\sigma^2_{I_2} = N_I/\rho$, and $\sigma^2_{I_3} = 0$. The total conditional noise variance is defined as $\sigma^2_j = \sigma^2_n + \sigma^2_{I_j}$ for $j = 1,2,3$. The total conditional variance for branch

1 of our receiver is $\sigma_{1_j}^2 = (4\sigma_a^2 + \sigma_j^2)$ and for branch 2, $\sigma_{2_j}^2 = \sigma_j^2$ for $j = 1,2,3$. The densities for V_1, (equation 2.8) and V_2, (equation 2.9) conditioned on the 3 jammer cases can be reexpressed respectively as

$$f_{V_1}(v_1|0, I_j) = \frac{1}{2\sigma_{1_j}^2}\exp\left(-\frac{1}{2\sigma_{1_j}^2}(v_1 + 4\alpha^2)\right)I_0\left(\frac{2\alpha\sqrt{v_1}}{\sigma_{1_j}^2}\right)u(v_1) \qquad (2.12)$$

$$f_{V_2}(v_2|0, I_j) = \frac{1}{2\sigma_{2_j}^2}\exp\left(-\frac{v_2}{2\sigma_{2_j}^2}\right)u(v_2) \qquad (2.13)$$

The relationships between the parameters ρ, ρ_1 and ρ_2 are now derived. Consider an interleaved frame of M bits shown with K jammed bursts per frame each consisting of H bits, as shown in Figure 2.4.

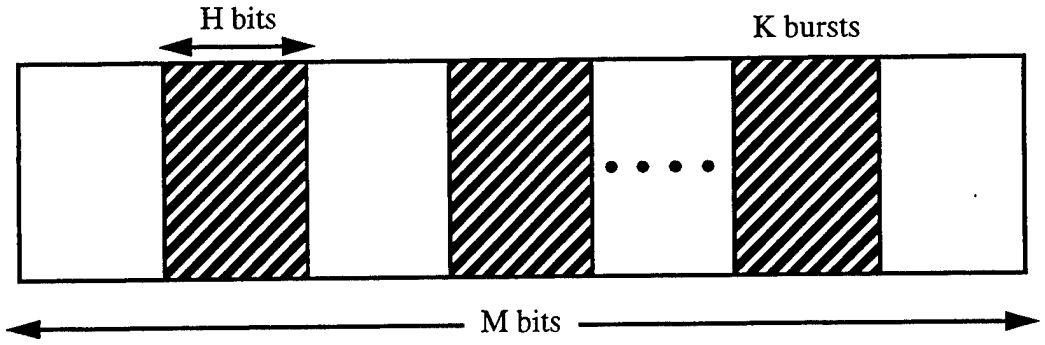

Figure 2.4: Interleaved frame of M bits

From this figure the following is ascertained. First, there are a total of n = KH jammed bits per frame and therefore ρ = n/M. The variable n_1 is defined to be the number of type I_1 bits in the frame. Since there are 2 edges for each burst, there are a total of n_1 = 2K type I_1 bits in the frame. This gives ρ_1 = n_1/M. The variable n_2 is defined to be the number of type I_2 bits in the frame. There are a total of (H-1) type I_2 bits in a burst for a total of n_2 = K(H-1) type I_2 bits in the frame. This gives ρ_2 = n_2/M. Now n_1+n_2 = 2K+K(H-1) = K+KH = K+n. Therefore n = n_1+n_2-K. Further since ρ = n/M = $(n_1+n_2-K)/M = \rho_1 + \rho_2 - (K/M) = \rho_1 + \rho_2 - (n_1/2M)$, it follows that

$$\rho = \frac{\rho_1}{2} + \rho_2 \qquad (2.14)$$

D. SELF-NORMALIZED RECEIVER

It has been shown that the use of the self-normalized receiver shown in Figure 2.5

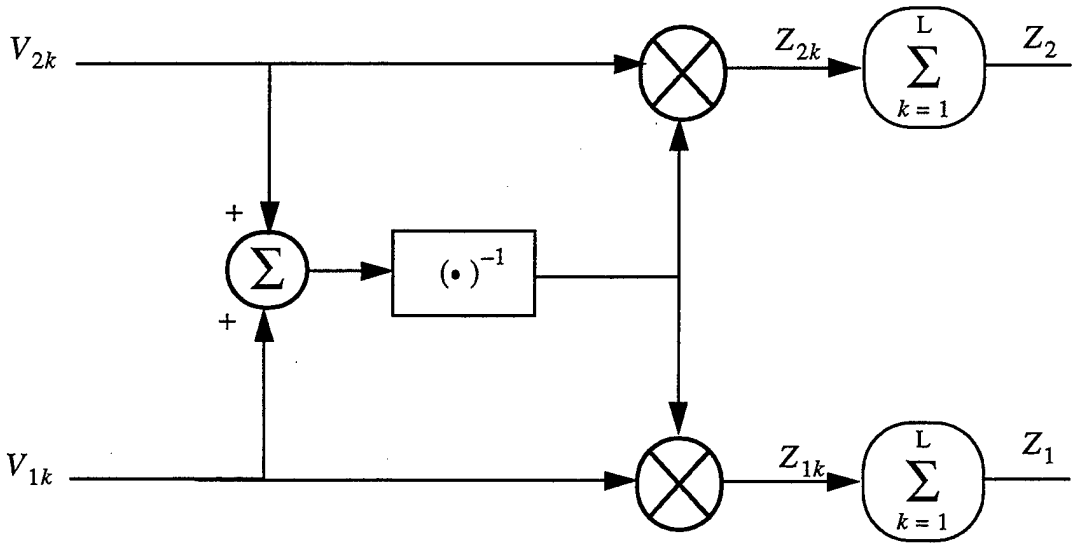

Figure 2.5: Self-Normalized receiver

can improve the worst case performances of a frequency-hopped BFSK signal under partial band jamming interference over a Rician channel [14]. In an analogous way, it is sought to improve the performance of a DPSK system employing time diversity under pulse noise interference over a Rician channel.

For the L-fold diversity receiver shown, a constant bit rate system is assumed. The duration of a bit for each diversity transmission is $T_L = T_b/L$ for a bit rate of $R_L = R_bL$ and average energy $E_L = E_b/L$. Therefore as L increases with R_b fixed, R_L increases and E_L decreases. The inputs to the self-normalized receiver for the k^{th} diversity reception are V_{1k} and V_{2k}. The density functions for V_{1k} and V_{2k} are the same as derived for V_1 and V_2 before, with the exception that E_b is now replaced with E_L. The random variables Z_{1k} and Z_{2k} are defined as

$$Z_{1k} = \frac{V_{1k}}{V_{1k} + V_{2k}} \tag{2.15a}$$

$$Z_{2k} = \frac{V_{2k}}{V_{1k} + V_{2k}} \tag{2.15b}$$

and

$$Z_{1k} + Z_{2k} = 1 \tag{2.15c}$$

Summing both sides of equation 2.15c over L and rearranging terms yields

$$Z_2 = L - Z_1 \tag{2.16}$$

The maximum value of either Z_{1k} or Z_{2k} is 1 and either Z_1 or Z_2 is L. Herein lies the motivation for the use of the self-normalized receiver. If the jammer decides on a strategy of pulsing on an intermittent basis ($\rho \ll 1$), the instantaneous power (proportional to $1/\rho$) will be large allowing that jammed reception to possibly dominate the decision variable at the output of the diversity combiner. Giving each diversity reception a weight of no more than 1 out of L effectively limits the capability of any single reception from dominating the receiver.

The optimum decision logic at the output of the combiners according to the Bayes criteria is to choose the larger of the two branches. The probability of bit error as a function of the diversity L is then

$$P_b(L) = P_r(Z_1 < Z_2 | 0, I_j; L) \tag{2.17}$$

Substituting equation 2.16 into 2.17 yields

$$P_b(L) = P_r(Z_1 < L/2 | 0, I_j; L) \tag{2.18}$$

Implicit in this statement is that each of the L diversity bits may be either case I_1, I_2 or I_3 bits as previously defined. Since this set of events is complete, $L = i_1 + i_2 + i_3$, where i_1, i_2 and i_3 represent the number of case I_1, I_2 or I_3 bits respectively. L is therefore a function of i_1, i_2 and i_3 and equation 2.18 is explicitly written as

$$P_b(L,i_1,i_2) = P_r(Z_1 < L/2 | 0, I_j; L, i_1, i_2) \tag{2.19}$$

where i_3 has been deliberately excluded since it is just a function of L, i_1 and i_2.

The derivation of the density function of the random variable Z_{1k} is now described. If an auxiliary random variable $W = V_{1k} + V_{2k}$ is defined, then the following relationships may also be written:

$$\begin{bmatrix} Z_{1k} \\ W \end{bmatrix} = \begin{bmatrix} \frac{1}{W} & 0 \\ 1 & 1 \end{bmatrix} \begin{bmatrix} V_{1k} \\ V_{2k} \end{bmatrix} \tag{2.21a}$$

$$\begin{bmatrix} V_{1k} \\ V_{2k} \end{bmatrix} = \begin{bmatrix} W & 0 \\ -W & 1 \end{bmatrix} \begin{bmatrix} Z_{1k} \\ W \end{bmatrix} \tag{2.21b}$$

The joint density function for Z_{1k} and W is

$$f_{Z_{1k},W}(z_{1k}, w) = f_{V_{1k},V_{2k}}(v_{1k} = wz_{1k}, v_{2k} = w(1-z_{1k}))\ J(Z_{1k}, W) \tag{2.22}$$

where $J(Z_{1k}, W)$ is the Jacobian of the transformation. Substituting equations 2.12 and 2.13 in equation 2.22 gives

$$f_{Z_{1k},W}(z_{1k}, w|0, \mathrm{I}_j) = \frac{w}{4\sigma_{1_j}^2\sigma_{2_j}^2}\exp\left(-\frac{w(1-z_{1k})}{2\sigma_{2_j}^2}\right)\exp\left(-\frac{wz_{1k}+4\alpha^2}{2\sigma_{1_j}^2}\right)\mathrm{I}_0\left(\frac{2\alpha\sqrt{wz_{1k}}}{\sigma_{1_j}^2}\right)\times$$

$$u(wz_{1k})u(w(1-z_{1k})) \tag{2.23}$$

Since $0 \le w \le \infty$ and $0 \le z_{1k} \le 1$, the arguments of the unit step functions in equation 2.23 are both non-negative quantities and may be replaced by z_{1k} and w respectively.

The marginal density for Z_{1k} is then given by

$$f_{Z_{1k}}(z_{1k}|0, \mathrm{I}_j) = \int_0^\infty f_{Z_{1k},W}(z_{1k}, w|0, \mathrm{I}_j)dw \tag{2.24}$$

The explicit form of equation 2.24 is derived in Appendix A and has the form

$$f_{Z_{1k}}(z_{1k}|0, \mathrm{I}_j) = \left(\frac{[((\gamma+1)\Gamma_\mathrm{L})^3 + 2((\gamma+1)\Gamma_\mathrm{L})^2(1+(1-z_{1k})) + 4(\gamma+1)\Gamma_\mathrm{L}(1-z_{1k})]}{[(\gamma+1)\Gamma_\mathrm{L} + 2(1-z_{1k})]^3} + \right.$$

$$\left.\frac{[2\gamma z_{1k}((\gamma+1)\Gamma_\mathrm{L})^2]}{[(\gamma+1)\Gamma_\mathrm{L} + 2(1-z_{1k})]^3}\right)\times\exp\left(-\frac{2\gamma(1-z_{1k})}{(\gamma+1)\Gamma_\mathrm{L} + 2(1-z_{1k})}\right)u(z_{1k}) \tag{2.25}$$

where $\gamma = \frac{\alpha^2}{2\sigma_a^2}$ is the ratio of direct signal power to diffuse signal power, $\Gamma_L = \left(\frac{E_L}{N_0}\right)^{-1} + \left(\frac{E_L}{\sigma_{I_j}^2}\right)^{-1} \cdot \left(\frac{E_L}{N_0}\right)$ is the average signal energy to thermal noise density ratio and $\left(\frac{E_L}{\sigma_{I_j}^2}\right)$ is the average signal energy-to-interference noise power ratio (SIR) for case $I_j, j = 1,2,3$. The SIR is equal to $SIR = \frac{2E_L\rho}{N_I}$, $SIR = \frac{E_L\rho}{N_I}$, $SIR = \infty$, for cases I_1, I_2, and I_3 respectively.

The L diversity receptions are modeled as independent events. The conditional density for Z_1 may thus be obtained by convolution of the L conditional probability density functions of Z_{1k}. This may be done equivalently with greater numerical efficiency in the Laplace domain, the expression for which is

$$f_{Z_1}(z_1|0, I_j; L, i_1, i_2) = \mathcal{L}^{-1}\Big([\mathcal{L}(f_{Z_{1k}}(z_{1k}|0, I_1))]^{i_1} \times [\mathcal{L}(f_{Z_{1k}}(z_{1k}|0, I_2))]^{i_2} \times [\mathcal{L}(f_{Z_{1k}}(z_{1k}|0, I_3))]^{(L-i_1-i_2)}\Big) \quad (2.26)$$

where $\mathcal{L}$ and $\mathcal{L}^{-1}$ denote the forward and inverse Laplace transforms. Since each of the L diversity receptions are modeled as independent events, the probability distribution for (L, i_1, i_2) is derived from a *multinomial* distribution and is given by

$$Pr(L, i_1, i_2) = \frac{L!}{i_1! i_2! (L-i_1-i_2)!} \rho_1^{i_1} \rho_2^{i_2} (1-\rho_1-\rho_2)^{(L-i_1-i_2)} \quad (2.27)$$

The density function for Z_1 conditioned on bit 0 being sent may be obtained by averaging the conditional density for Z_1 in equation 2.26 over the probability distribution in equation 2.27. The expression is

$$f_{Z_1}(z_1|0) = \sum_{i_2=0}^{L} \sum_{i_1=0}^{L-i_2} f_{Z_1}(z_1|0, I_j; L, i_1, i_2) Pr(L, i_1, i_2) \quad (2.28)$$

Finally the expression for probability of bit error follows from equation 2.19 and is

$$P_b = \int_0^{L/2} f_{Z_1}(z_1|0)dz_1 \qquad (2.29)$$

This last expression must be evaluated numerically.

E. NUMERICAL RESULTS

The probability of bit error, P_b as a function of γ with no pulse noise jamming, a signal energy to thermal noise density ratio of $E_b/N_0 = 15$ dB, and with diversity as a parameter is shown in Figure 2.6.

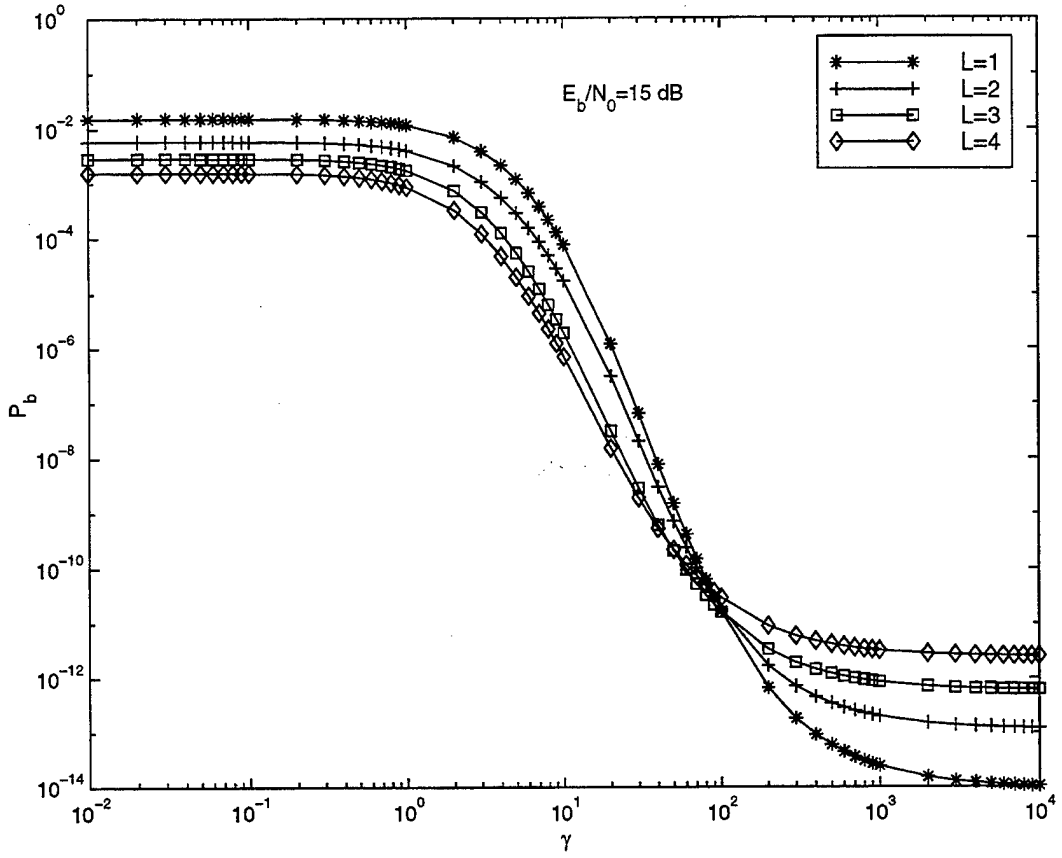

Figure 2.6: Probability of bit error as a function of γ with no pulse noise jamming, $E_b/N_0 = 15$ dB and with diversity as a parameter.

For $\gamma > 100$, noncoherent combining losses dominate the performance. Noncoherent combining loss is defined to be the additional amount of signal-to-noise ratio required by a diversity system

to attain the same level of performance as a system with no diversity. This type of loss is prevalent in the Gaussian channel where there is no signal fading. Noncoherent combining losses increase for increasing levels of diversity and are inversely proportional to the signal-to-noise ratio [5]. For $\gamma < 100$, gains against signal fading are achieved as diversity order is increased. For $\gamma < 1$, receiver performance is relatively unchanged for each diversity order as the ratio of direct to diffuse signal power approaches the Rayleigh limit ($\gamma = 0$). In this dissertation, the performance for fading parameters which are common to the mobile radio channel, typically $0 \leq \gamma \leq 5$, are investigated.

In the following analysis, receiver worst case performance is determined. Worst case performance represents a composite performance by obtaining the value of the jamming fraction ρ that produced the highest probability of bit error as a function of the signal energy to interference noise density ratio, E_b/N_I. Worst case performance implies that the jammer can determine the current value of E_b/N_I and reallocate the resources in an adaptive fashion. Worst case performance was determined by numerical search since no analytical solution could be produced. In determining worst case performance, a large range of combinations of case I_1 and I_2 events were considered. There were two scenarios which produced identical worst case performance results for any particular value of E_b/N_I. They are

$$\rho_2 = 0, \rho = \frac{\rho_1}{2} \tag{2.30}$$

$$\rho_1 = 0, \rho = \rho_2 \tag{2.31}$$

where the non-zero values of ρ_1 and ρ_2 are equal. A simple illustration would best explain this result. Figure 2.7 plots the instantaneous jammer power levels (normalized to unity) as a function of time for the worst case scenarios described in equations 2.30 and 2.31 (case I and case II shown). It is seen that although the values of ρ will be different in the two scenarios, the jammer noise variances as previously defined will be the same over any 2-bit interval. Equation 2.14 may be rewritten as

$$\rho = \rho_2\left(1 + \frac{\beta}{2}\right) \tag{2.32}$$

where $\beta = \rho_1/\rho_2$. It is evident that $\beta = \infty$ corresponds to equation 2.30 while $\beta = 0$ corresponds to equation 2.31. It is also of interest to determine for a fixed ρ, the worst case β. Figure 2.8 shows the performance curves for the probability of bit error as a function of E_b/N_I with $E_b/N_0 = 15$ dB, a diversity of $L = 4$, $\gamma = 0$ and $\rho = 0.05$ with β as a parameter. Of the curves shown, the case of $\beta = \infty$ produced the worst performance over the entire range of E_b/N_I. The performance difference between the two extreme cases ($\beta = 0$ and $\beta = \infty$) is significant for E_b/N_I below 10 dB. A similar result was observed for $E_b/N_0 = 15$ dB, a diversity of $L = 4$, $\gamma = 0$ and $\rho = 0.5$, shown in Figure 2.9.

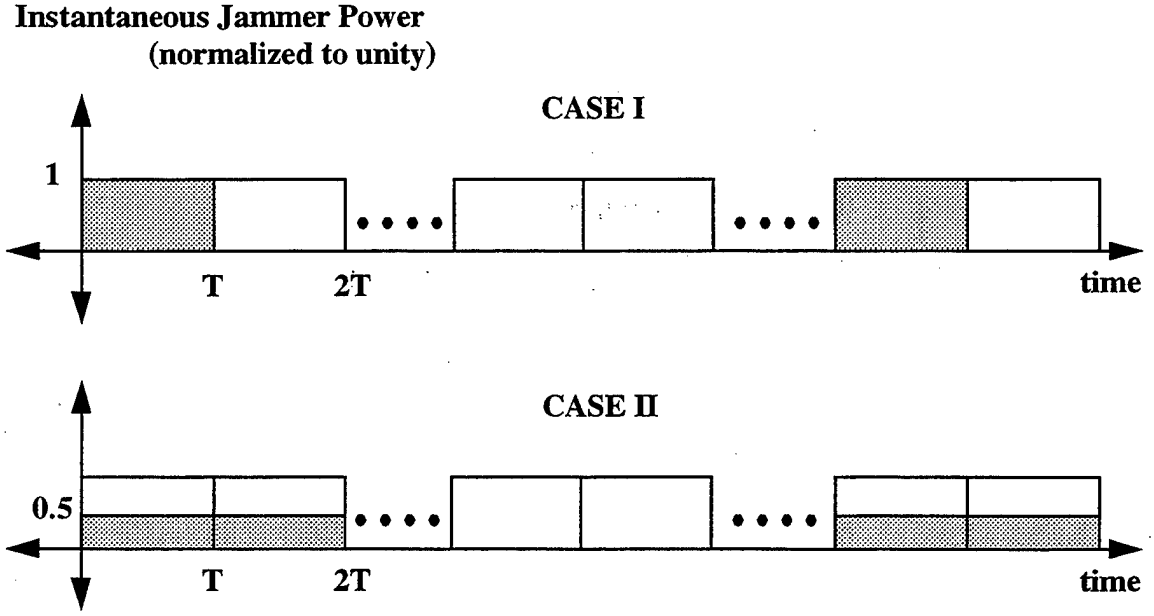

Figure 2.7: Schematic representation of worst case jamming scenarios with instantaneous jammer power (normalized to unity) plotted as a function of time.

These experiments were repeated for moderate fading ($\gamma = 5$) for the same values of E_b/N_0, diversity, and ρ. These results are shown in Figures 2.10 and 2.11. Similar performance trends are observed for these cases. These results suggest that when the jammer's peak power is fixed and where strong or moderate fading occur, the optimum jamming strategy (from the jammer's point of view) is to jam isolated bits rather than adjacent bits, especially for low E_b/N_I. Figures 2.12 and 2.13 show the performance curves with $E_b/N_0 = 15$ dB, a diversity of $L = 4$, $\gamma = 1000$ (a very strong direct signal) and $\rho = 0.05, 0.5$ respectively. Although a very strong signal may not be a realistic scenario for the mobile radio channel, it is shown here for completeness. In each case, it

is seen that there is a distinct crossover in the performance curves for $\beta = 0$ and $\beta = \infty$. In the case of the former, it occurs at about $E_b/N_I = 17$ dB and in the case of the latter at $E_b/N_I = 9$ dB. Such curves are also beneficial because if the jammer cannot adapt its strategy and has a fixed ρ, it tells the jammer which of the two jamming strategies produces worse performance for a particular fading condition.

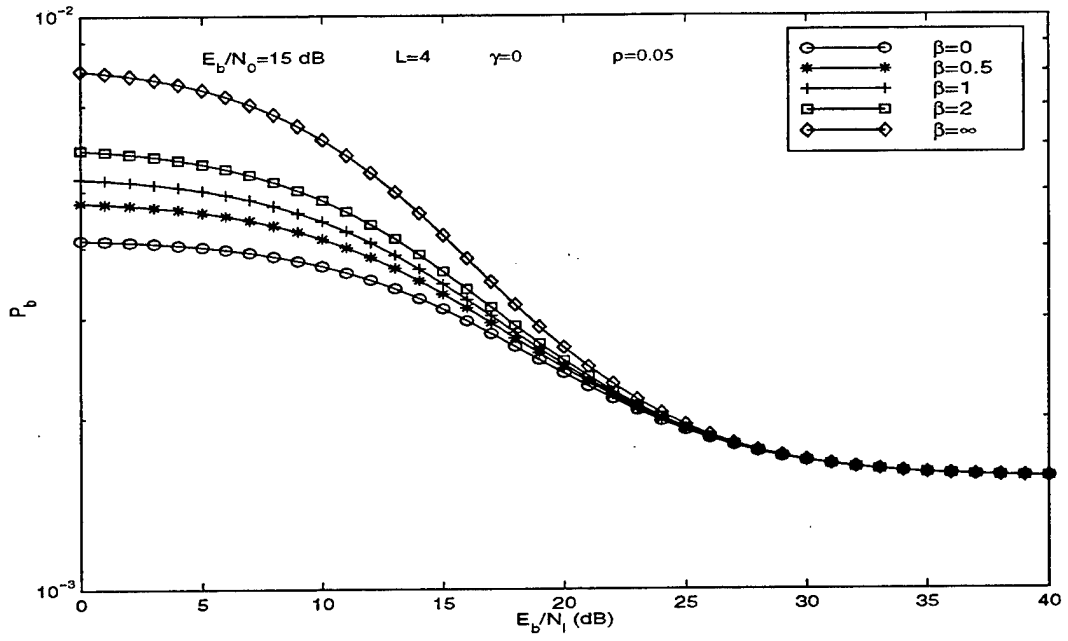

Figure 2.8: Performance of self-normalized receiver for $E_b/N_0 = 15$ dB, a diversity of $L = 4$, $\gamma = 0$ and $\rho = 0.05$ with β as a parameter.

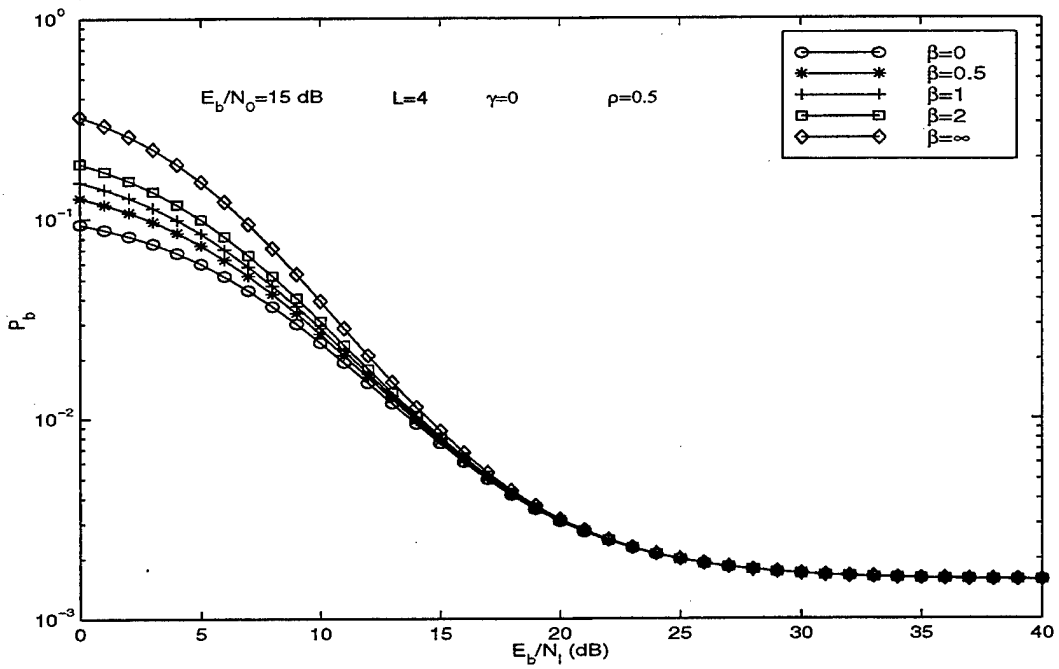

Figure 2.9: Performance of self-normalized receiver for $E_b/N_0 = 15$ dB, a diversity of $L = 4$, $\gamma = 0$ and $\rho = 0.5$ with β as a parameter.

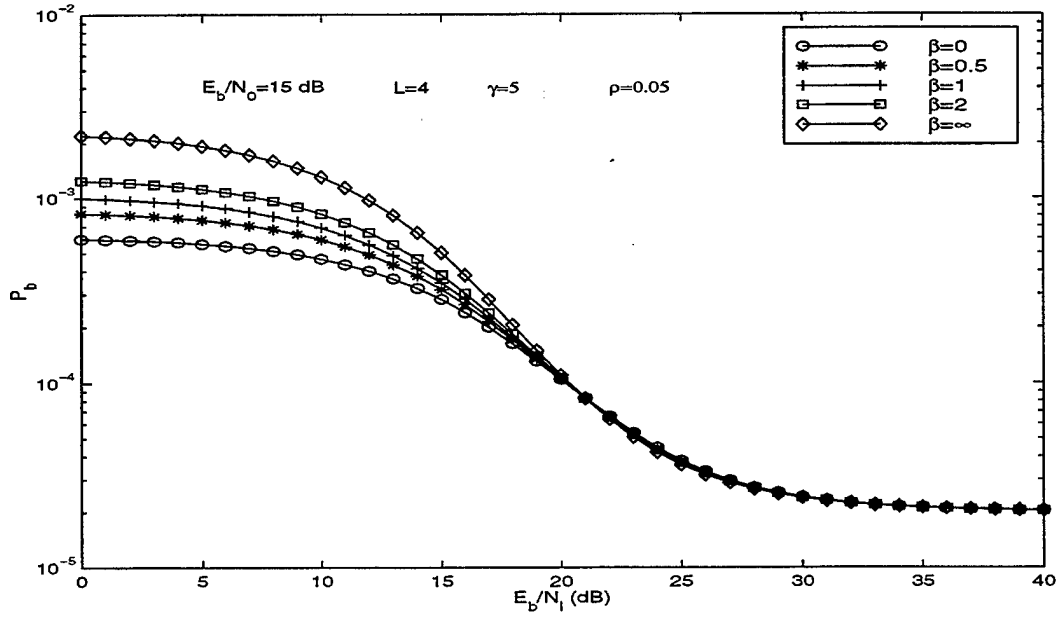

Figure 2.10: Performance of self-normalized receiver for $E_b/N_0 = 15$ dB, a diversity of $L = 4$, $\gamma = 5$ and $\rho = 0.05$ with β as a parameter.

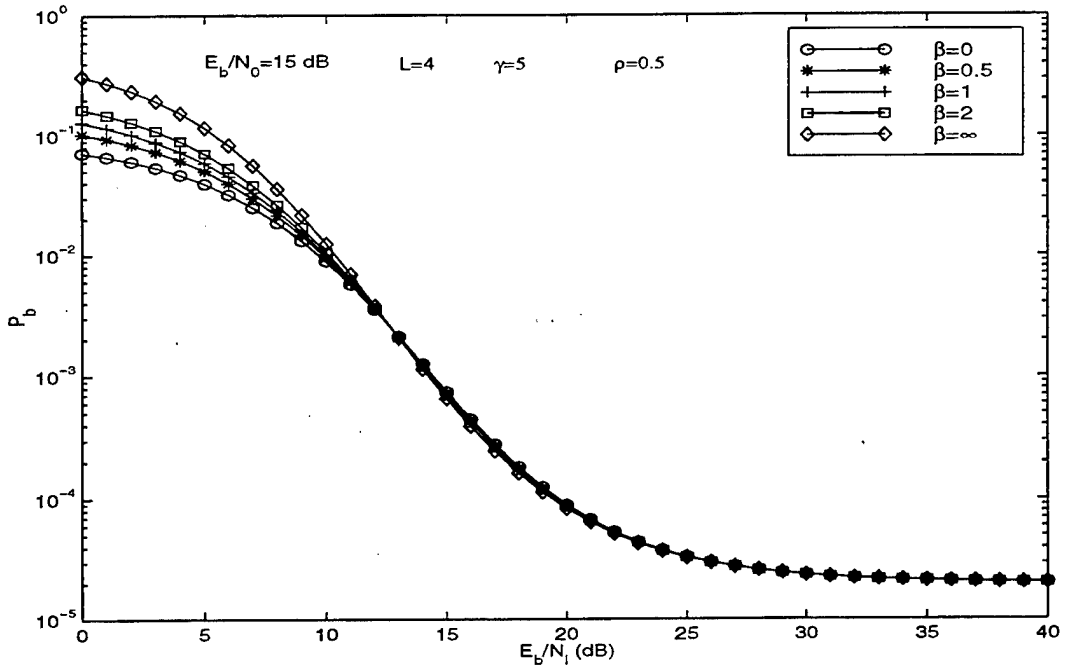

Figure 2.11: Performance of self-normalized receiver for $E_b/N_0 = 15$ dB, a diversity of $L = 4$, $\gamma = 5$ and $\rho = 0.5$ with β as a parameter.

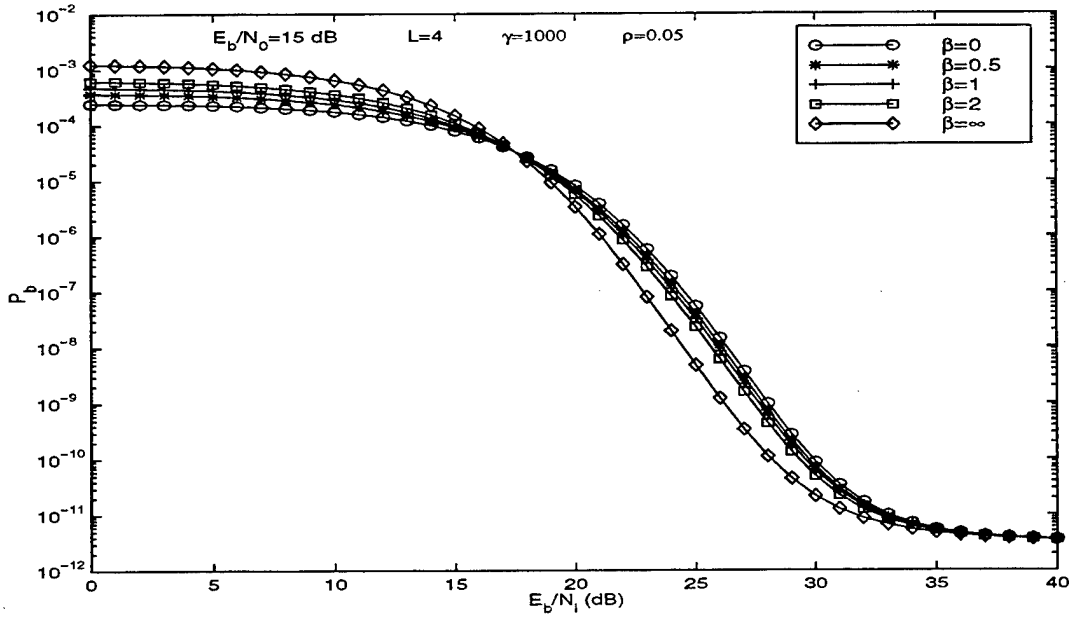

Figure 2.12: Performance of self-normalized receiver for $E_b/N_0 = 15$ dB, a diversity of $L = 4$, $\gamma = 1000$ and $\rho = 0.05$ with β as a parameter.

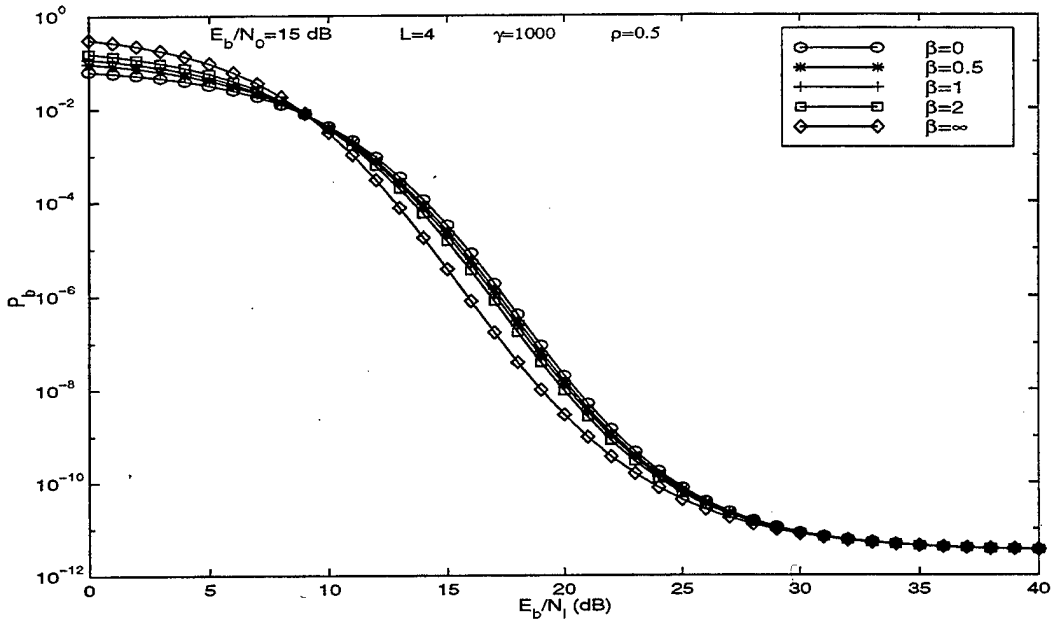

Figure 2.13: Performance of self-normalized receiver for $E_b/N_0 = 15$ dB, a diversity of $L = 4$, $\gamma = 1000$ and $\rho = 0.5$ with β as a parameter.

The performance of the self-normalized receiver under the conditions of worst case jamming as a function of the parameter ρ are now analyzed. The values of ρ corresponding to equation 2.31 ($\beta = 0$) have been arbitrarily selected since both jamming scenarios result in the same performance. Performance curves of the self-normalized receiver for diversity orders L = 1,3,4 and jammer fractions $\rho = 0.01, 0.1, 0.25, 1$, $E_b/N_0 = 15$ dB and $\gamma = 0$ are shown in Figures 2.14-2.16. For either case of diversity, it is seen that the self-normalized receiver has completely negated the effects of pulse noise jamming since the worst case performance curve coincides with the continuous jamming curve ($\rho = 1$). A comparison of worst case performance curves for diversities of order 1 through 4 is given in Figure 2.17. It can be seen from that figure that there are significant gains achieved against signal fading for E_b/N_I greater than approximately 15 dB. Below E_b/N_I=10 dB, noncoherent combining losses become significant. For error probabilities on the order shown, some sort of error correction coding would be necessary to ensure reliable communications.

Performance curves of the self-normalized receiver for diversity orders L = 1,3,4 and jammer fractions $\rho = 0.01, 0.1, 0.25, 1$, E_b/N_0=15 dB and $\gamma = 5$ are shown in Figures 2.18-2.20.

For a diversity of order L = 1, it is seen that pulse noise jamming results in a significant performance reduction for E_b/N_I in the range of approximately 10-20 dB. Notice also for this curve that the optimum value of ρ decreases as E_b/N_I increases. As the diversity is increased to L = 4 however, the self-normalized receiver virtually eliminates the effectiveness of the pulse noise jammer. A comparison of worst case performance curves for diversities of order 1 through 4 is shown in Figure 2.21. Significant gains are again achieved above E_b/N_I = 15 dB while noncoherent combining losses become a factor below E_b/N_I = 10 dB.

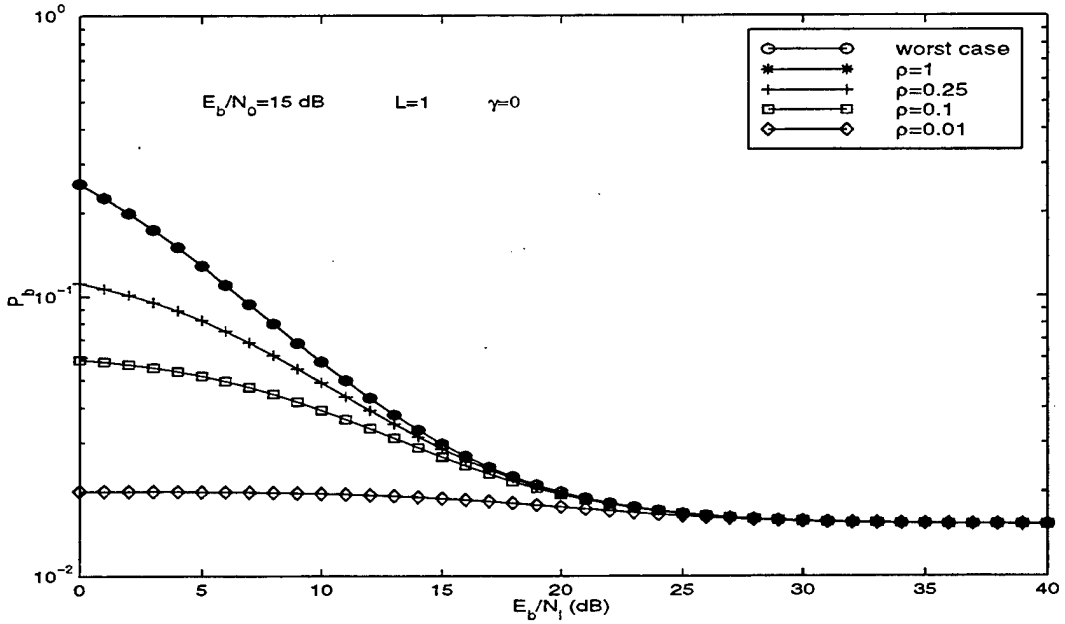

Figure 2.14: Performance of self-normalized receiver for pulse jamming fractions ρ = 1, 0.25, 0.1, 0.01 and worst case for diversity order L = 1, E_b/N_0 = 15 dB and γ = 0.

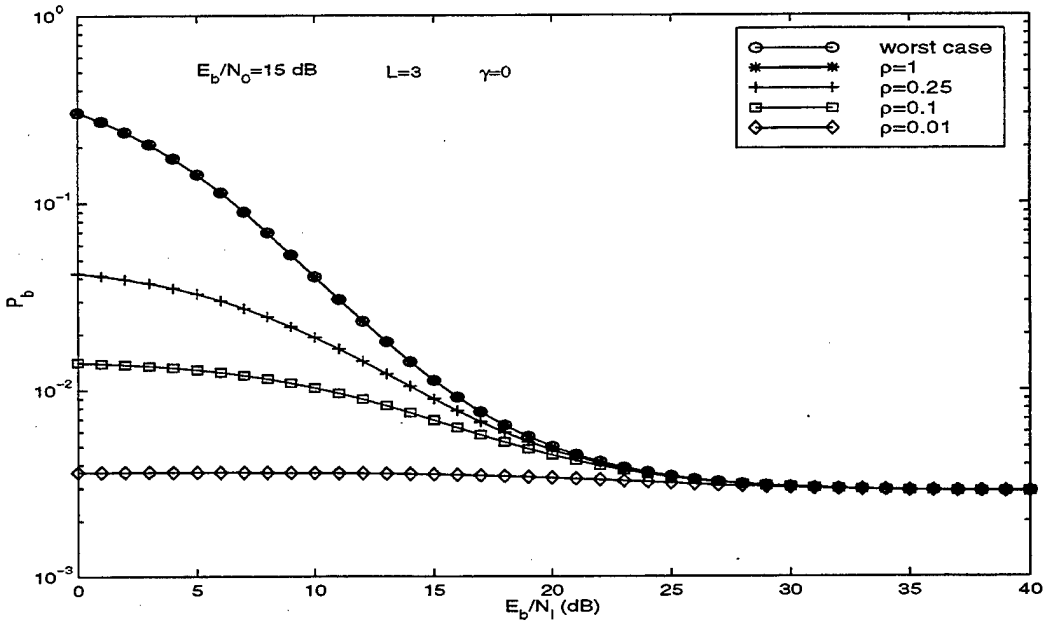

Figure 2.15: Performance of self-normalized receiver for pulse jamming fractions $\rho = 1, 0.25, 0.1, 0.01$ and worst case for diversity order $L = 3$, $E_b/N_0 = 15$ dB and $\gamma = 0$.

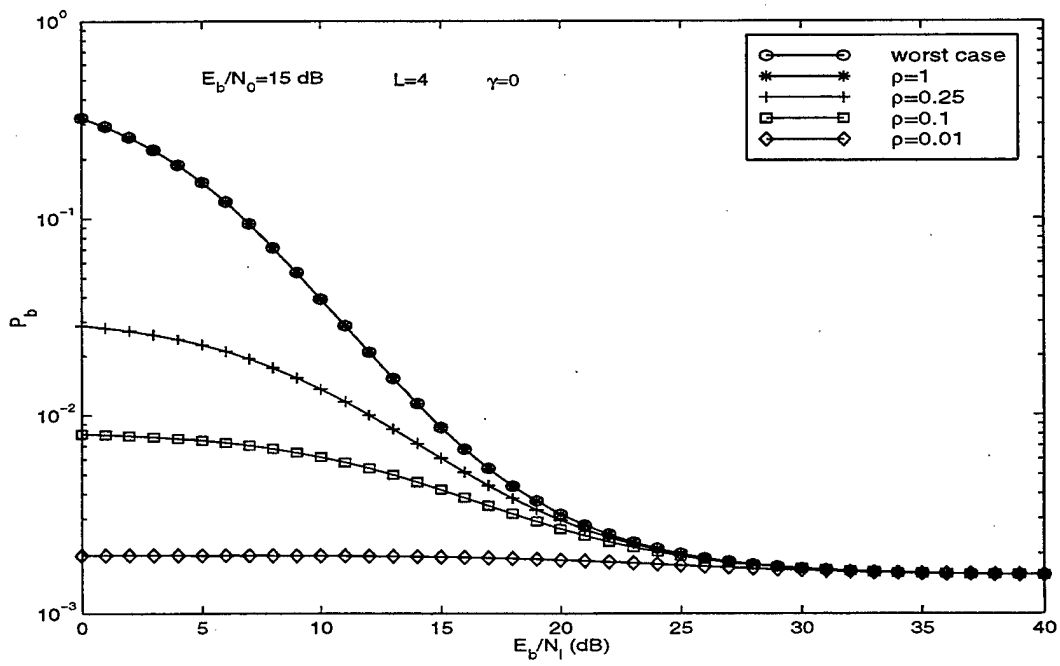

Figure 2.16: Performance of self-normalized receiver for pulse jamming fractions $\rho = 1, 0.25, 0.1, 0.01$ and worst case for diversity order $L = 4$, $E_b/N_0 = 15$ dB and $\gamma = 0$.

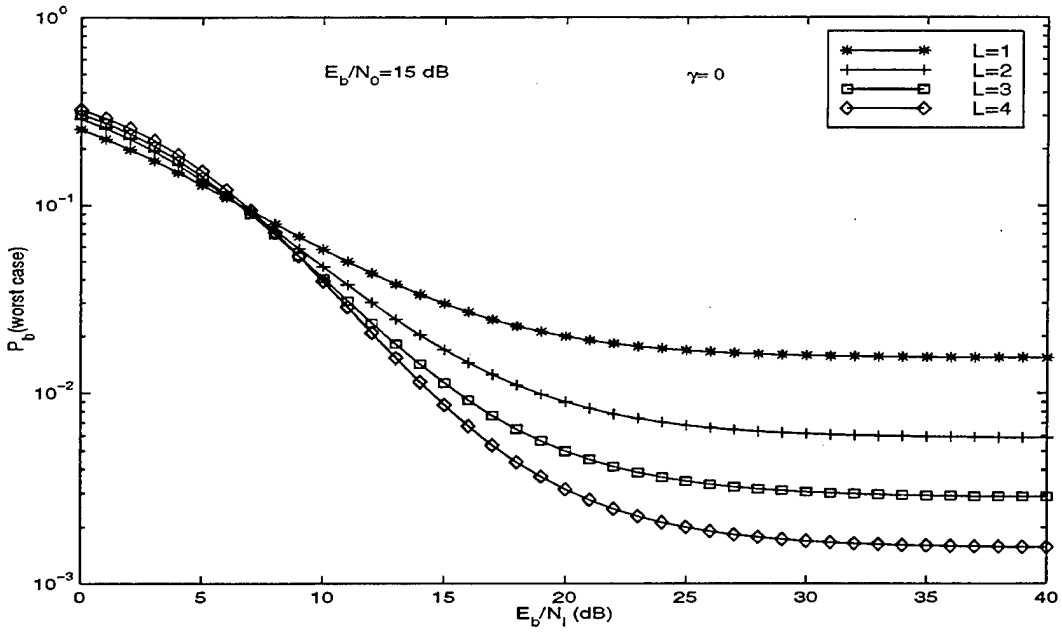

Figure 2.17: Worst case performance of self-normalized receiver in presence of pulse noise interference for diversity orders L = 1,2,3,4, E_b/N_0 = 15 dB and $\gamma = 0$.

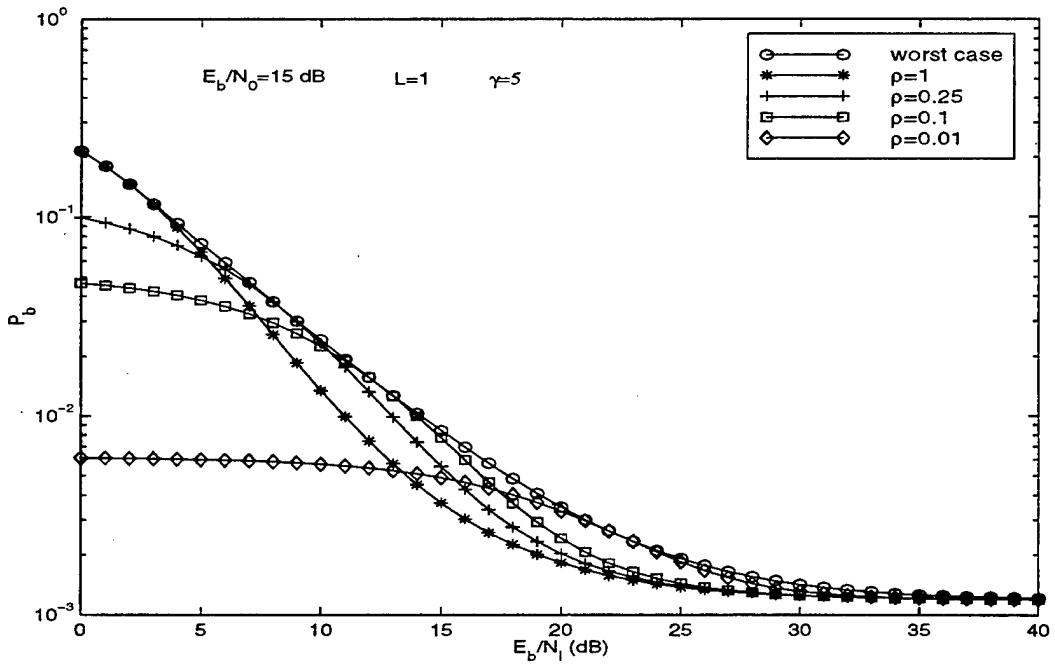

Figure 2.18: Performance of self-normalized receiver for pulse jamming fractions $\rho = 1, 0.25, 0.1, 0.01$ and worst case for diversity order L = 1, E_b/N_0 = 15 dB and $\gamma = 5$.

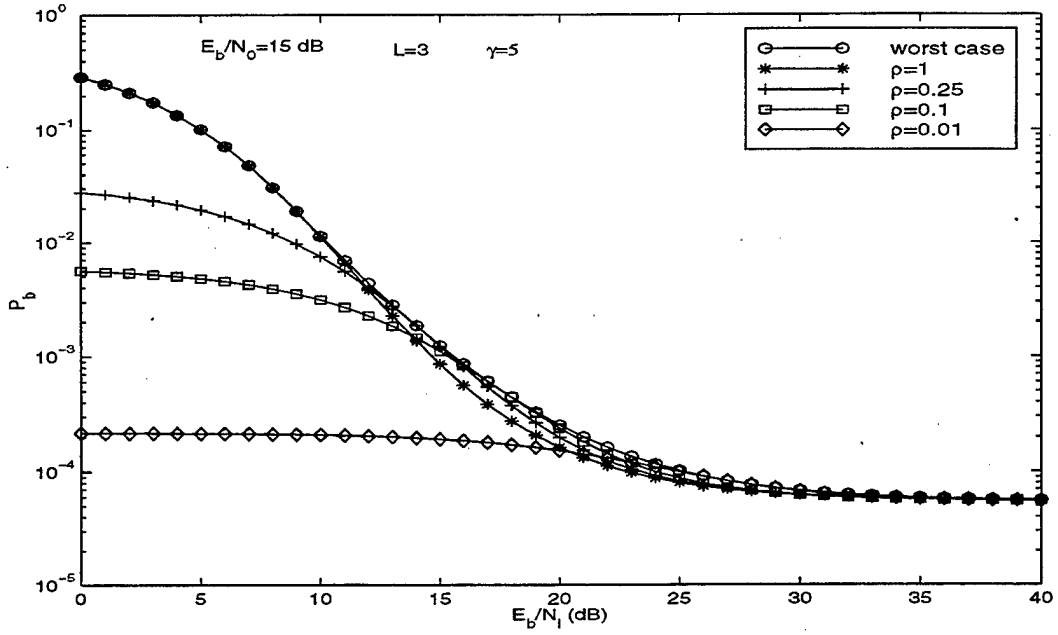

Figure 2.19: Performance of self -normalized receiver for pulse jamming fractions $\rho = 1, 0.25, 0.1, 0.01$ and worst case for diversity order $L = 3$, $E_b/N_0 = 15$ dB and $\gamma = 5$.

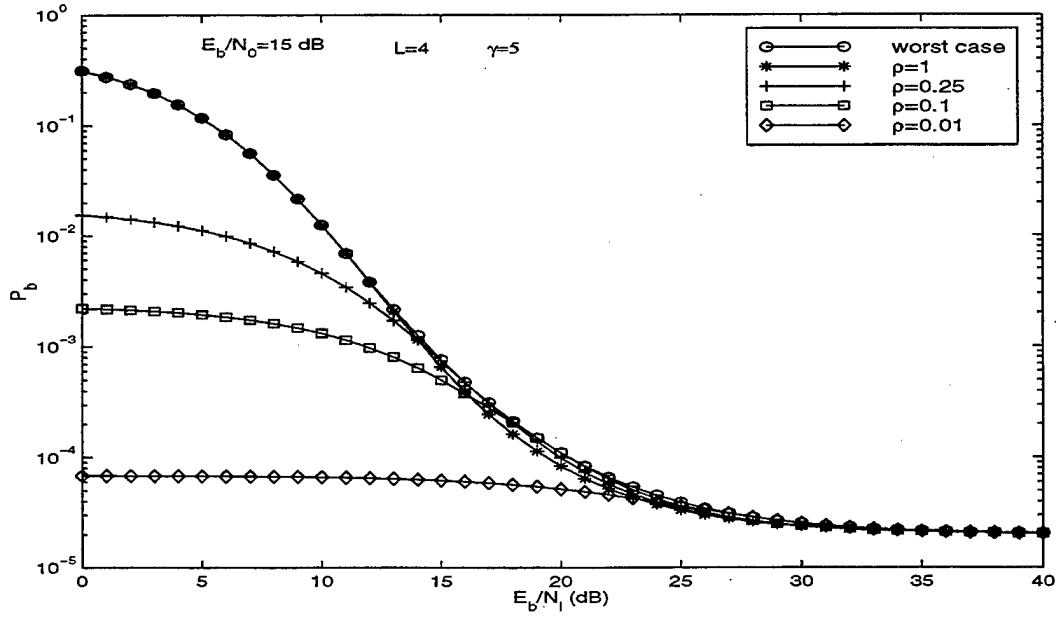

Figure 2.20: Performance of self -normalized receiver for pulse jamming fractions $\rho = 1, 0.25, 0.1, 0.01$ and worst case for diversity order $L = 4$, $E_b/N_0 = 15$ dB and $\gamma = 5$.

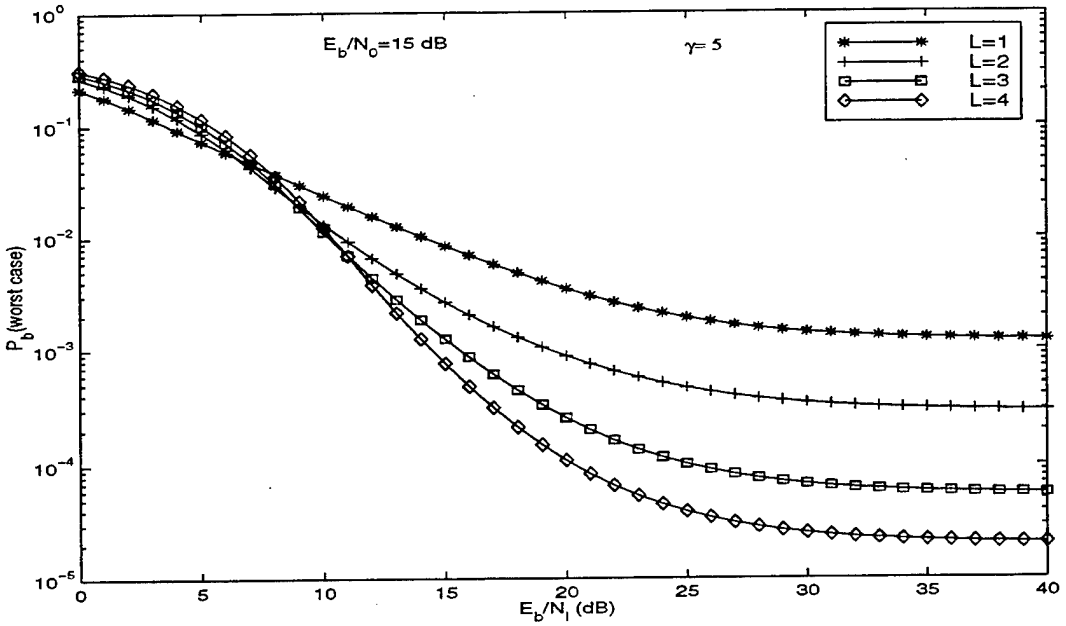

Figure 2.21: Worst case performance of self-normalized receiver in presence of pulse noise interference for diversity orders L = 1,2,3,4, E_b/N_0 = 15 dB and γ = 5.

Another indicator of the effectiveness of the self-normalized receiver is that for increasing diversity order and fixed value of E_b/N_I, the optimum value of ρ increases. This result is seen in Figure 2.22 where the optimum value of ρ is plotted as a function of diversity order with E_b/N_0 = 15 dB, γ = 5 and E_b/N_I as a parameter. The increasing value of ρ for increasing diversity order at a given E_b/N_I is an indicator that the self-normalized receiver has forced the jammer to adopt a more continuous form of jamming. It is observed that pulse noise jamming is most effective at higher values of E_b/N_I where higher levels of diversity are required to render the pulse noise jammer ineffective. An intuitive way to explain why pulse noise jamming is more effective at higher values of E_b/N_I is to compare its effects to that of a fading channel. It has been observed that as the average jammer noise power decreases (or E_b/N_I increases), the most efficient use of this power is to jam in a less frequent fashion (smaller ρ) with stronger bursts of energy (instantaneous jammer power $\sim 1/\rho$). In this way, some bits experience very low signal-to-noise ratio while others experience relatively very high signal-to-noise ratio. This is analogous to a fading channel which produces the same type of fluctuations in signal-to-noise ratio which is very deleterious to the effective performance of a digital communications link.

Figures 2.23 and 2.24 shows the optimum value of ρ as a function of γ with diversity order as a parameter and with E_b/N_0 = 15 dB for E_b/N_I equal to 20 dB and 30 dB respectively. It is observed that the overall trend results in the optimum value of ρ decreases for increasing γ. From these plots, it is seen that there appears to be a lower limit as to the effectiveness of pulse noise jamming. For example, for a diversity order of L = 4, pulse noise jamming is no longer effective below $\gamma = 2$. For γ greater than 3, higher order diversities would be required to render the pulse noise jammer completely ineffective. It is therefore concluded that pulse noise jamming effectiveness increases for increasing γ.

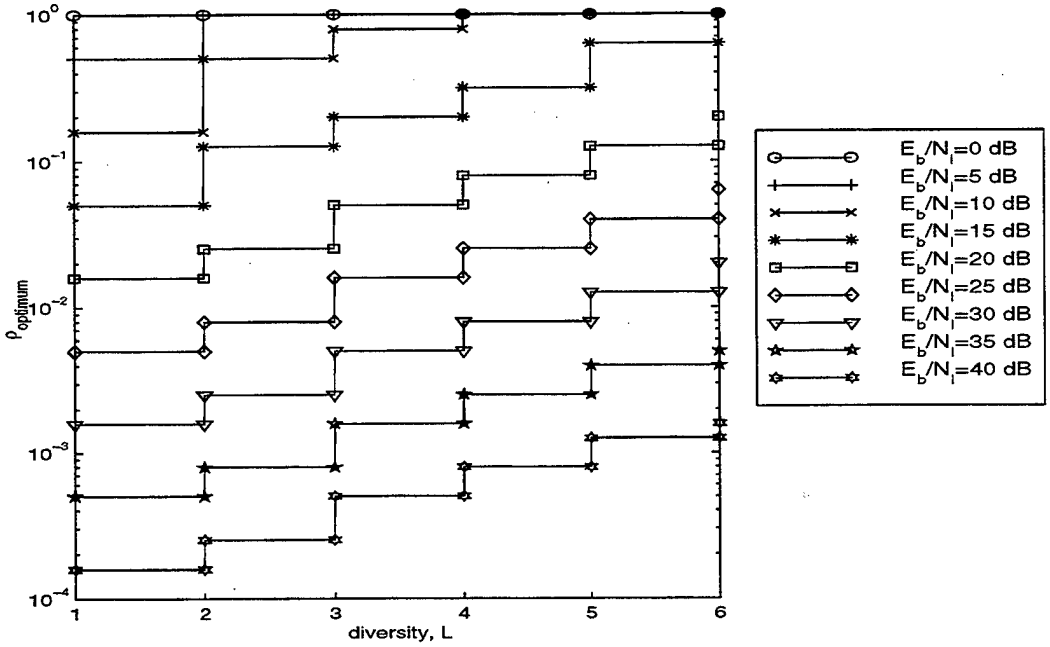

Figure 2.22: Optimum value of ρ as a function of diversity order with E_b/N_0 = 15 dB, $\gamma = 5$ and E_b/N_I as a parameter.

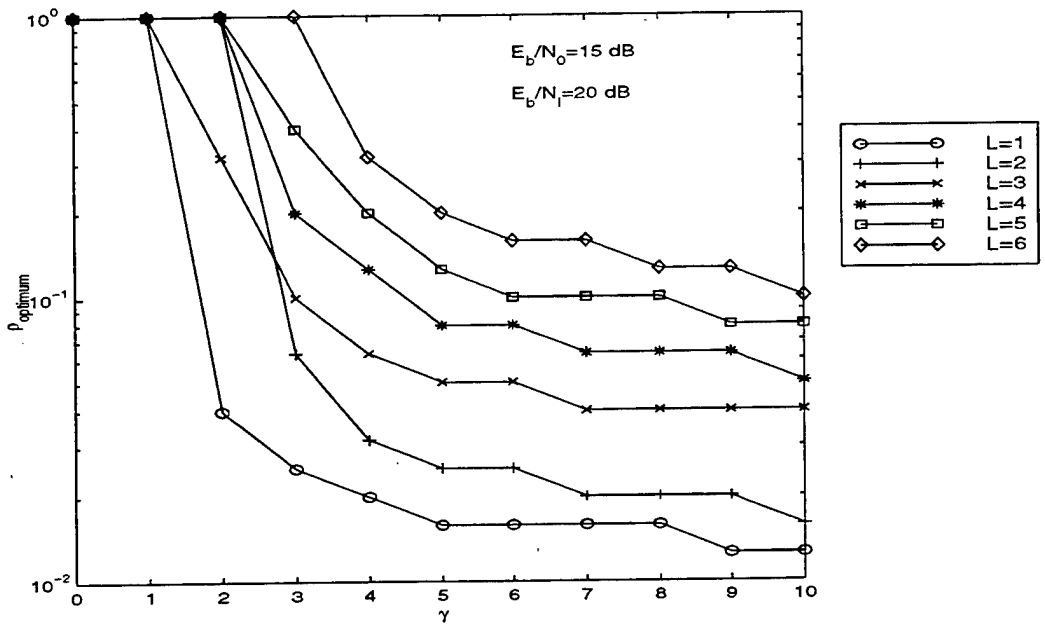

Figure 2.23: Optimum value of ρ as a function of γ with diversity order as a parameter for E_b/N_0 = 15 dB and E_b/N_I = 20 dB.

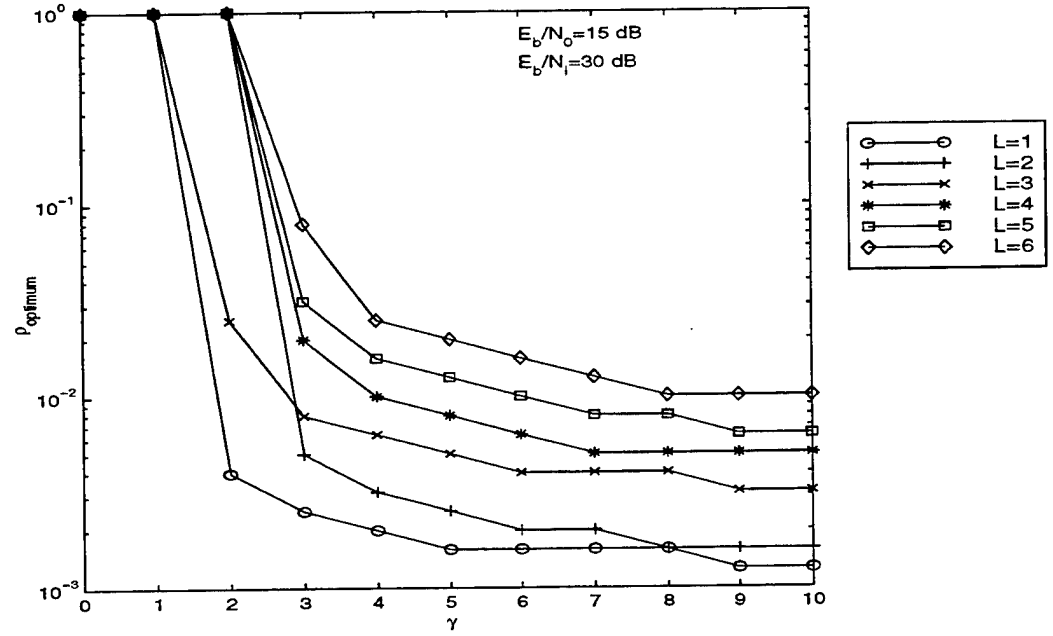

Figure 2.24: Optimum value of ρ as a function of γ with diversity order as a parameter for E_b/N_0 = 15 dB and E_b/N_I = 30 dB.

F. CHAPTER CONCLUSIONS

The performance of a DS-DPSK spread spectrum system with self-normalized receiver over a Rician frequency nonselective, slowly fading channel in the presence of pulsed noise interference and AWGN has been considered. The receiver employs L-fold time diversity and soft decision equal gain combining. A multinomial probability distribution was used to characterize the distribution of pulsed noise interference events. The events included the possibility that either 1, 2 consecutive or none of the signal bits were jammed. A analytical solution to the probability of bit error was not available. In the numerical analysis, for fixed values of the jamming fraction ρ, worst case performance was determined as a function of the signal energy-to-interference noise density ratio, E_b/N_I and β, the ratio of fraction of 1-bit jammed events to 2-bit jammed events. It was seen for severe and moderate fading, the best strategy for the jammer is to jam alternating bits rather than adjacent bits. The worst case performance of the self-normalized receiver as a function of the parameter ρ under conditions of severe and moderate fading was analyzed. It was determined that the self-normalized receiver was effective in mitigating the effects of pulse noise jamming for both fading conditions. For the moderate fading condition, the optimum value of ρ to produce worst case performance was observed as a function of diversity with E_b/N_I as a parameter. It was determined that pulse noise jamming is most effective at higher values of E_b/N_I and that increasing the diversity order forces the jammer to a more continuous form of jamming. The optimum value of ρ to produce worst case performance was observed as a function of γ with diversity as a parameter. It was concluded that pulse noise jamming effectiveness increased for increasing γ and decreased for increasing diversity order. This was observed for values of γ between 0 and 10.

III. DS-DPSK WITH NOISE-NORMALIZATION AND L-FOLD DIVERSITY IN A FADING CHANNEL

In this chapter, the performance of a noise-normalized DS-DPSK spread spectrum system over a Rician frequency-nonselective, slowly fading channel in the presence of pulsed noise interference and AWGN is considered. Where the self-normalized receiver normalizes the detector outputs by a combination of signal and noise, the noise-normalized receiver normalizes by a factor equal to the noise power which includes both AWGN and the pulsed noise interference. In this sense, the noise-normalized receiver is an idealization of the self-normalized receiver. The noise-normalized receiver assumes accurate measurement of the noise present at the receiver whereas the self-normalized receiver assumes no knowledge of the noise power. One may view the noise-normalized receiver as a limiting case of ideal performance of the self-normalized receiver. The self-normalized receiver however would be much simpler to implement in practice. The same jammer model used in the analysis for the self-normalized receiver is assumed here. Therefore the inputs to the noise-normalized receiver are identical to that of the self-normalized receiver. A block diagram of the noise-normalized receiver is shown in Figure 3.1.

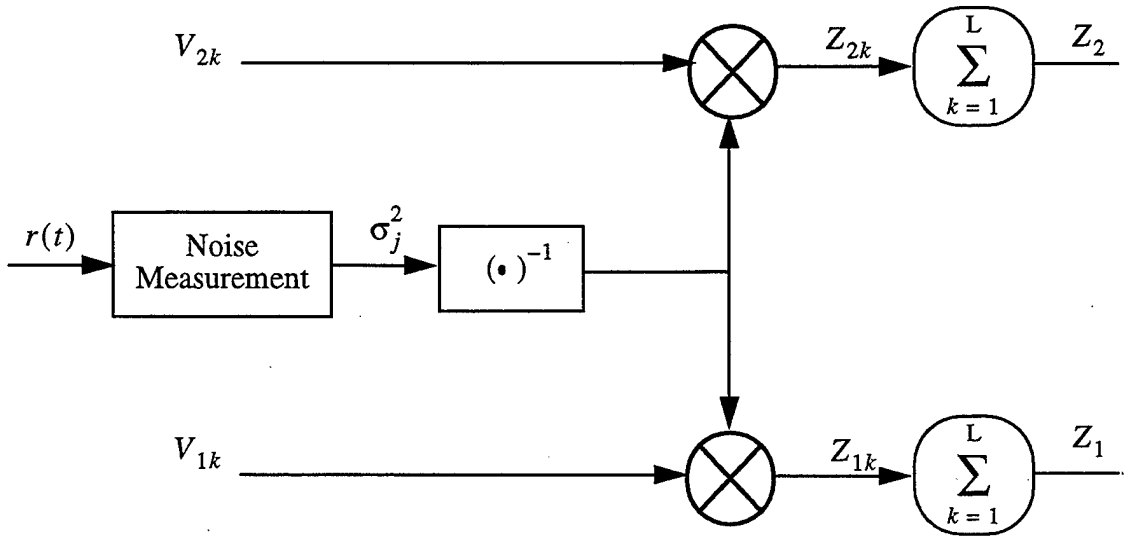

Figure 3.1: Noise normalized receiver structure.

Here $r(t)$ is the received signal and σ_j^2 for j = 1,2,3 is the total conditional noise variance as before. The equations for the determination of the probability of bit error are now derived.

A. BIT ERROR PROBABILITY

Since the inputs V_{1k} and V_{2k} to the noise-normalized receiver are identical to the inputs of the self-normalized receiver, the probability density functions of these statistics assuming a bit 0 is sent, are respectively

$$f_{V_{1k}}(v_{1k}|0, \mathrm{I}_j) = \frac{1}{2\sigma_{1_j}^2}\exp\left(-\frac{1}{2\sigma_{1_j}^2}(v_{1k}+4\alpha^2)\right)\mathrm{I}_0\left(\frac{2\alpha\sqrt{v_{1k}}}{\sigma_{1_j}^2}\right)u(v_{1k}) \tag{3.1}$$

and

$$f_{V_{2k}}(v_{2k}|0, \mathrm{I}_j) = \frac{1}{2\sigma_{2_j}^2}\exp\left(-\frac{v_{2k}}{2\sigma_{2_j}^2}\right)u(v_{2k}) \tag{3.2}$$

The conditional density for the random variable Z_1 can be expressed from equation 2.26 as

$$f_{Z_1}(z_1|0, \mathrm{I}_j;\mathrm{L}, \mathrm{i}_1, \mathrm{i}_2) = \mathcal{L}^{-1}([\mathcal{L}(f_{Z_{1k}}(z_{1k}|0, \mathrm{I}_1)^{\otimes \mathrm{i}_1})]\times[\mathcal{L}(f_{Z_{1k}}(z_{1k}|0, \mathrm{I}_2)^{\otimes \mathrm{i}_2})]\times$$
$$[\mathcal{L}(f_{Z_{1k}}(z_{1k}|0, \mathrm{I}_3)^{\otimes(\mathrm{L}-\mathrm{i}_1-\mathrm{i}_2)})]) \tag{3.3}$$

where $\otimes i_j$ represents i_j fold self-convolution. The density function for the random variable $Z_{1k} = V_{1k}/\sigma_j^2$ is

$$f_{Z_{1k}}(z_{1k}|0, \mathrm{I}_j) = f_{V_{1k}}(v_{1k}= z_{1k}\sigma_j^2|0, \mathrm{I}_j)\ J(Z_{1k}) \tag{3.4}$$

where $J(Z_{1k}) = \sigma_j^2$ is the Jacobian of the transformation. By substituting equation 3.1, the density function for the random variable Z_{1k} is found to be

$$f_{Z_{1k}}(z_{1k}|0, \mathrm{I}_j) = \frac{\sigma_j^2}{2\sigma_{1_j}^2}\exp\left(-\frac{1}{2\sigma_{1_j}^2}(z_{1k}\sigma_j^2+4\alpha^2)\right)\mathrm{I}_0\left(\frac{2\alpha\sqrt{z_{1k}\sigma_j^2}}{\sigma_{1_j}^2}\right)u(z_{1k}) \tag{3.5}$$

since $u(z_{1k}) = u(z_{1k}\sigma_j^2)$. The density function for Z_{2k} may be determined from equation 3.5 by setting $\alpha = 0$, $Z_{1k} = Z_{2k}$ and recalling that $\sigma_{2_j}^2 = \sigma_j^2$. The result is

$$f_{Z_{2k}}(z_{2k}|0, I_j) = \frac{1}{2}\exp\left(-\frac{z_{2k}}{2}\right)u(z_{2k}) \tag{3.6}$$

Note that the density function for the non-signal branch is not a function of the signal or the noise. The Laplace transform of the density function for Z_{1k} is shown to be (Appendix B, section B.1),

$$F_{Z_{1k}}(s|0, I_j) = \frac{\sigma_j^2}{2\sigma_{1_j}^2\left(s + \frac{\sigma_j^2}{2\sigma_{1_j}^2}\right)}\exp\left(-\frac{2\alpha^2}{\sigma_{1_j}^2}\right)\exp\left(\frac{\alpha^2\sigma_j^2}{\sigma_{1_j}^4\left(s + \frac{\sigma_j^2}{2\sigma_{1_j}^2}\right)}\right) \tag{3.7}$$

The expression for $f_{Z_{1k}}(z_{1k}|0, I_j)^{\otimes i_j}$ is then given as

$$f_{Z_{1k}}(z_{1k}|0, I_j)^{\otimes i_j} = \mathcal{L}^{-1}([F_{Z_{1k}}(s|0, I_j)]^{i_j}) \tag{3.8}$$

which is shown to be (Appendix B, section B.2)

$$f_{Z_{1k}}(z_{1k}|0, I_1)^{\otimes i_j} = \left(\frac{(\gamma+1)\Gamma_L}{2(2+(\gamma+1)\Gamma_L)}\right)\exp\left(-\frac{4\gamma i_j + (\gamma+1)\Gamma_L z_{1k}}{2(2+(\gamma+1)\Gamma_L)}\right)$$

$$\left(\frac{z_{1k}(\gamma+1)\Gamma_L}{4\gamma i_j}\right)^{\left(\frac{i_j-1}{2}\right)} I_{i_j-1}\left(\sqrt{\frac{4\gamma(\gamma+1)\Gamma_L z_{1k} i_j}{(2+(\gamma+1)\Gamma_L)^2}}\right)u(z_{1k}) \tag{3.9}$$

where $\gamma = \frac{\alpha^2}{2\sigma_a^2}$ and $\Gamma_L = \left(\frac{E_L}{N_0}\right)^{-1} + \left(\frac{E_L}{\sigma_{I_j}^2}\right)^{-1}$. Assuming the same jammer model as before, the density function for the random variable Z_1 is

$$f_{Z_1}(z_1|0) = \sum_{i_2=0}^{L}\sum_{i_1=0}^{L-i_2} f_{Z_1}(z_1|0, I_j; L, i_1, i_2)\Pr(L, i_1, i_2) \tag{3.10}$$

where

$$\Pr(L, i_1, i_2) = \frac{L!}{i_1! i_2! (L-i_1-i_2)!}\rho_1^{i_1}\rho_2^{i_2}(1-\rho_1-\rho_2)^{(L-i_1-i_2)} \tag{3.11}$$

is the multinomial probability distribution. Equation 3.10 must be evaluated numerically. The density function for the random variable Z_2 may be written as

$$f_{Z_2}(z_2|0) = f_{Z_{2k}}(z_{2k}|0, I_j)^{\otimes L} \tag{3.12}$$

since Z_2 is independent of the three jamming events. Equation 3.12 is a special case of equation B.24 of Appendix B and is given as

$$f_{Z_2}(z_2|0) = \frac{\exp\left(-\frac{z_2}{2}\right) z_2^{(L-1)}}{2^L(L-1)!} u(z_2) \tag{3.13}$$

which is recognizable as a *Chi-squared* probability density function with 2L degrees of freedom [4, 5]. The probability of bit error is given by

$$P_b = P_r(Z_1 < Z_2|0) \tag{3.14}$$

Expressing this in terms of the density functions for the random variables Z_1 and Z_2 yields

$$P_b = \int_0^\infty \int_0^{z_2} f_{Z_1, Z_2}(z_1, z_2|0) dz_1 dz_2 \tag{3.15}$$

The joint density function for the random variables Z_1 and Z_2 in equation 3.15 is the product of the two marginal density functions $f_{Z_1}(z_1|0)$ and $f_{Z_2}(z_2|0)$ since Z_1 and Z_2 are independent random variables. Equation 3.15 must also be evaluated numerically.

B. NUMERICAL RESULTS

The probability of bit error, P_b as a function of γ with no pulse noise jamming, a bit energy to thermal noise density ratio of E_b/N_0 = 15 dB, and with diversity as a parameter is shown in Figure 3.2. If the performance of the noise-normalized receiver is compared to that of the self-normalized receiver (Figure 2.6) for a diversity of L = 4 and severe Rayleigh fading (approximately $\gamma < 3$), it is seen that there is almost an order of magnitude better performance in probability of bit error for the noise-normalized receiver than the self-normalized receiver.

For the noise-normalized receiver, worst case performance was produced under the conditions outlined in equations 2.30 and 2.31; this was also the case for the self-normalized receiver.

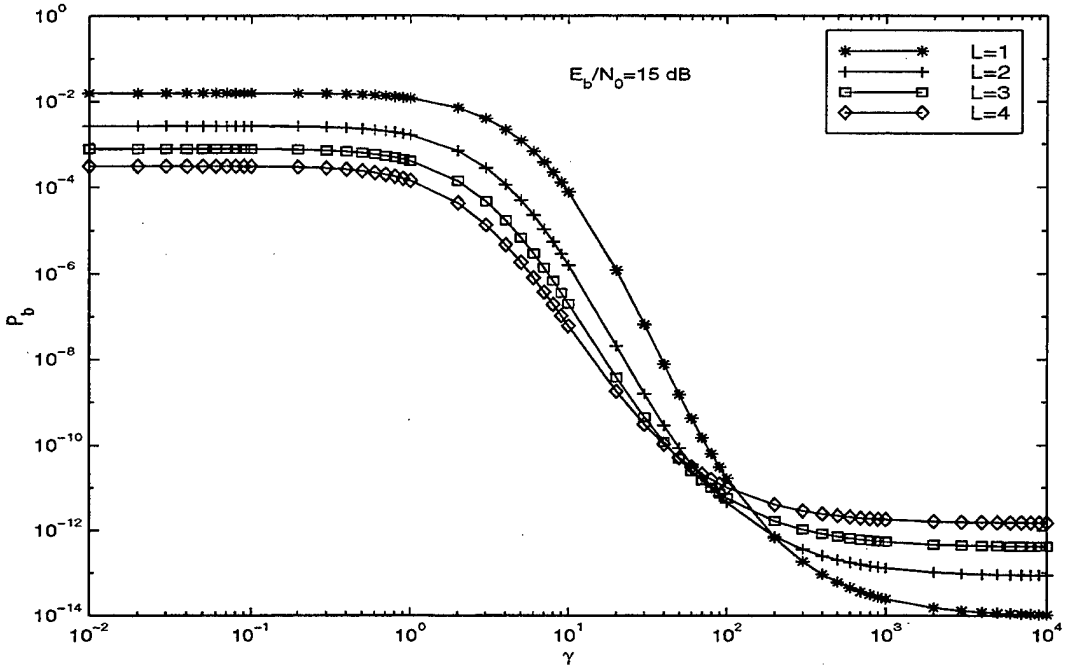

Figure 3.2: Probability of bit error for the noise-normalized receiver as a function of γ with no pulse noise jamming, $E_b/N_0 = 15$ dB and with diversity as a parameter.

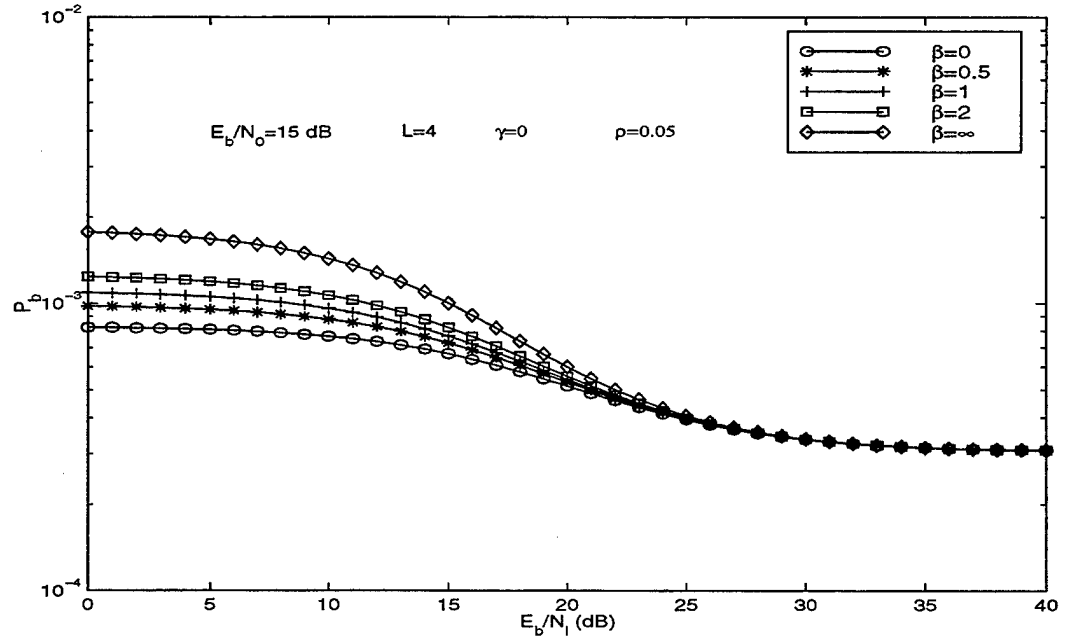

Figure 3.3: Performance of noise-normalized receiver for $E_b/N_0 = 15$ dB, a diversity of $L = 4$, $\gamma = 0$ and $\rho = 0.05$ with β as a parameter.

Figure 3.3 shows the performance curves for the probability of bit error as a function of E_b/N_I with $E_b/N_0 = 15$ dB, a diversity of $L = 4$, $\gamma = 0$ and $\rho = 0.05$ with β as a parameter. It is seen that the case of $\beta = \infty$ produces the worst performance over the entire range of E_b/N_I. Below approximately 15 dB, there is marked jammer advantage by jamming individual bits (case $\beta = \infty$) compared to jamming consecutive bits (case $\beta = 0$). Figure 3.4 shows the performance curves for the probability of bit error as a function of E_b/N_I with $E_b/N_0 = 15$ dB, a diversity of $L = 4$, $\gamma = 0$ and $\rho = 0.5$ with β as a parameter. Below approximately $E_b/N_I = 15$ db, a significant performance degradation for all cases of β is observed. This is much more than the degradation observed in the case of $\rho = 0.05$. Similar results were observed in the case of moderate signal fading ($\gamma = 5$), shown in Figures 3.5 and 3.6 for $\rho = 0.05, 0.5$ respectively. These results are similar to what was observed for the self-normalized receiver. Figures 3.7 and 3.8 show the performance curves for the probability of bit error as a function of E_b/N_I with $E_b/N_0 = 15$ dB, a diversity of $L = 4$, $\gamma = 1000$ (a very strong direct signal), with β as a parameter and $\rho = 0.05, 0.5$ respectively. As observed with the self-normalized receiver, there are distinct crossover points where the worst performance curve shifts from the case of $\beta = \infty$ to $\beta = 0$. This occurs at approximately $E_b/N_I = 20$ dB for $\rho = 0.05$ and $E_b/N_I = 10$ dB for $\rho = 0.5$.

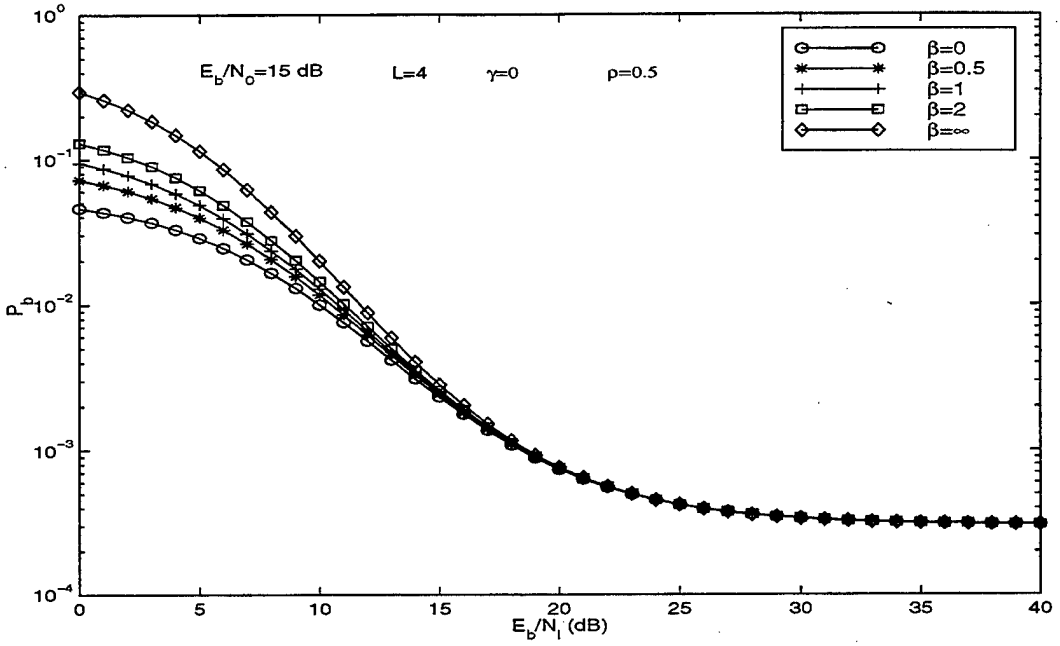

Figure 3.4: Performance of noise-normalized receiver for $E_b/N_0 = 15$ dB, a diversity of $L = 4$, $\gamma = 0$ and $\rho = 0.5$ with β as a parameter.

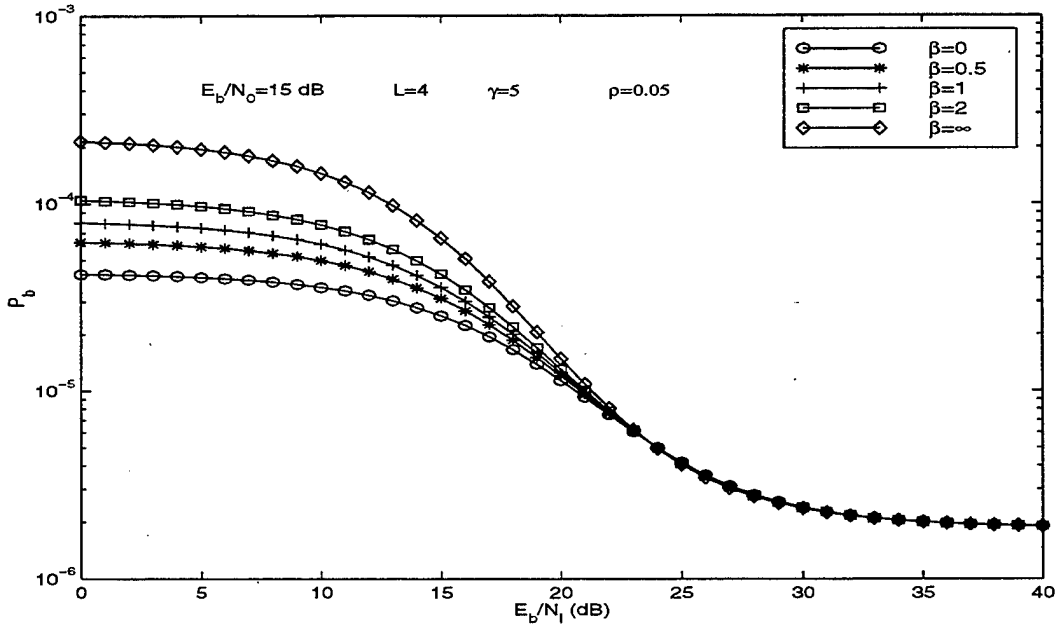

Figure 3.5: Performance of noise-normalized receiver for $E_b/N_0 = 15$ dB, a diversity of $L = 4$, $\gamma = 5$ and $\rho = 0.05$ with β as a parameter.

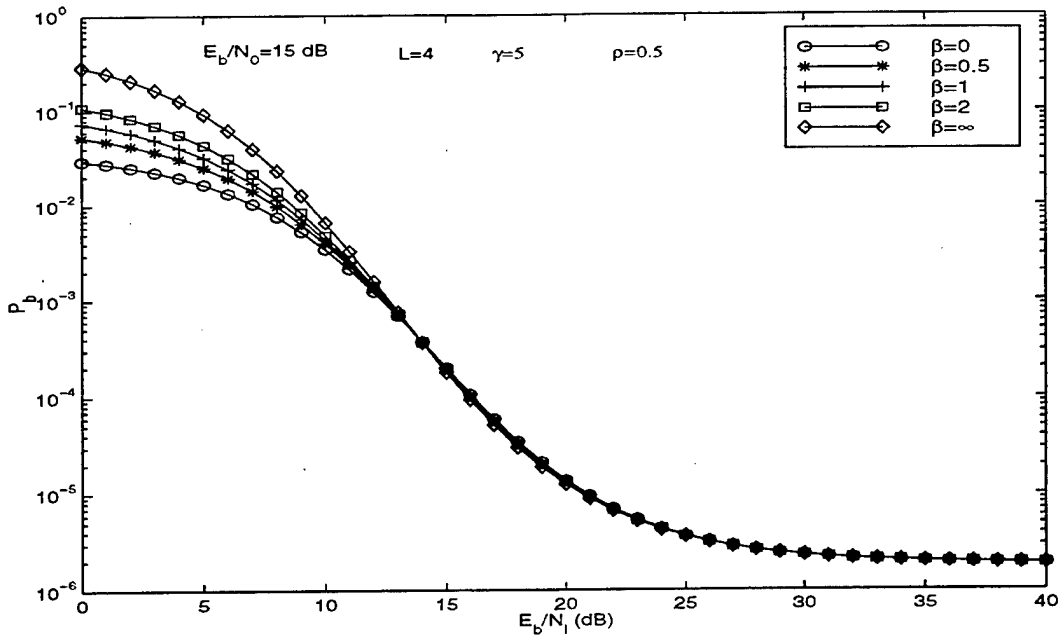

Figure 3.6: Performance of noise-normalized receiver for $E_b/N_0 = 15$ dB, a diversity of $L = 4$, $\gamma = 5$ and $\rho = 0.5$ with β as a parameter.

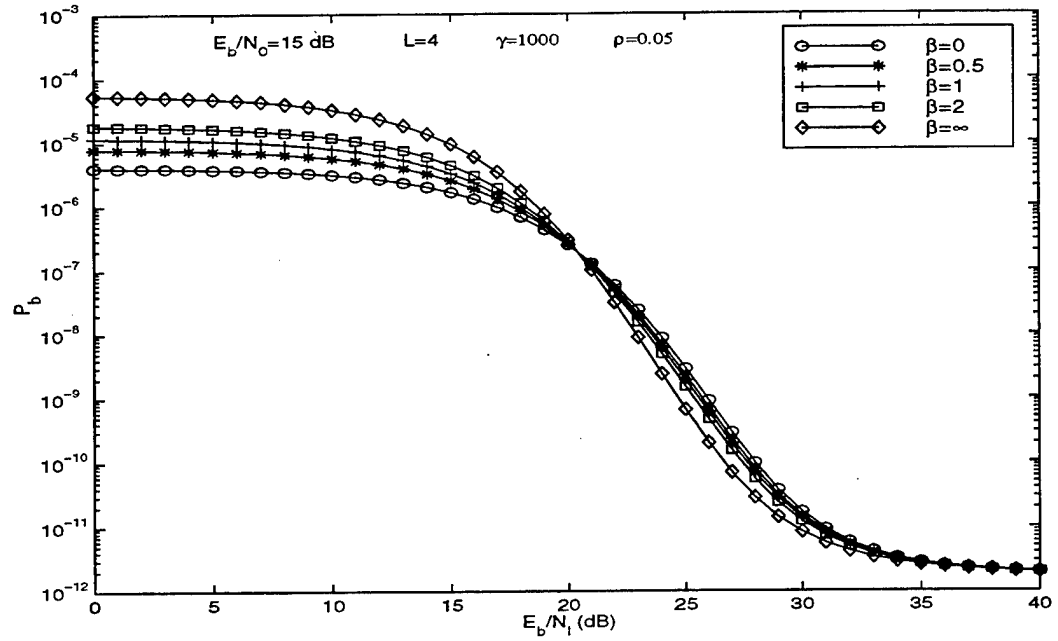

Figure 3.7: Performance of noise-normalized receiver for $E_b/N_0 = 15$ dB, a diversity of $L = 4$, $\gamma = 1000$ and $\rho = 0.05$ with β as a parameter.

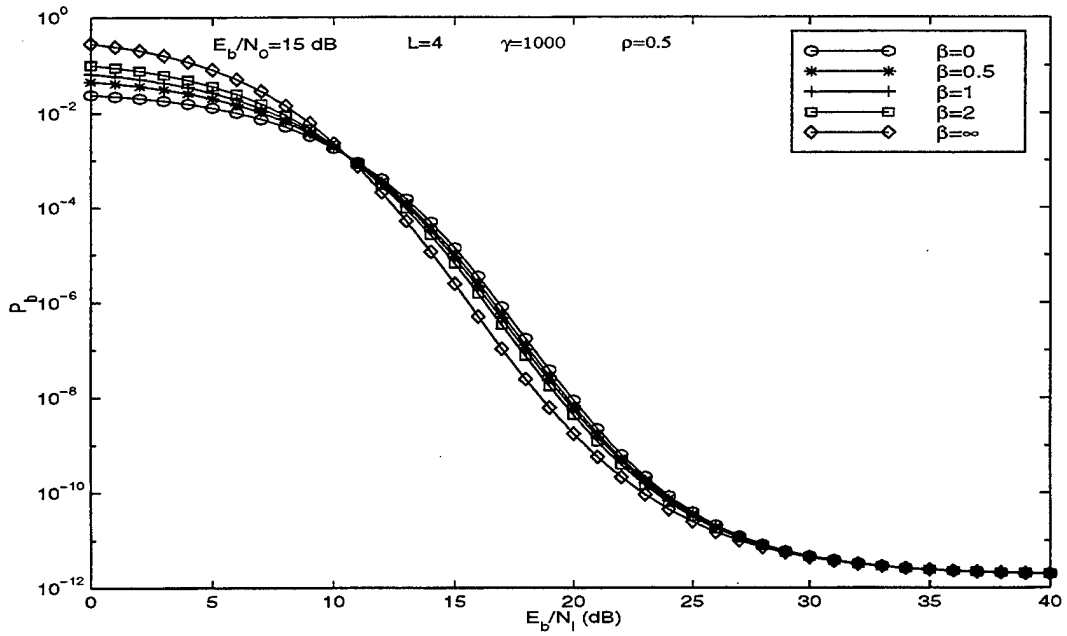

Figure 3.8: Performance of noise-normalized receiver for $E_b/N_0 = 15$ dB, a diversity of $L = 4$, $\gamma = 1000$ and $\rho = 0.5$ with β as a parameter.

The performance of the noise-normalized receiver under the conditions of worst case jamming is now analyzed. The values of ρ corresponding to equation 2.31 have been selected to be consistent with the values of ρ selected for the self-normalized receiver. Performance curves of the noise-normalized receiver for diversity orders $L = 1,3,4$ and jammer fractions $\rho = 0.01$, 0.1, 0.25, 1 and worst case, $E_b/N_0 = 15$ dB and $\gamma = 0$ are shown in Figures 3.9-3.11. As in the case of the self-normalized receiver, it is seen for either diversity value that the noise-normalized receiver has completely negated the effects of pulse noise jamming. That is, the worst case performance curve coincides with the continuous jamming curve ($\rho = 1$). By comparing the performance of the noise-normalized receiver with no diversity ($L = 1$) with the self-normalized receiver (Figure 2.14), it is seen that their performances are identical. This is not surprising since the SNR at the outputs of both receivers are the same. A comparison of worst case performance curves for diversities of order 1 through 4 is shown in Figure 3.12. It is seen that a diversity of order $L = 2$ is sufficient to dramatically improve receiver performance. Below $E_b/N_I = 5$ dB, noncoherent combining losses occur but are rather small. Figure 3.13 shows a worst case performance

comparison between the noise-normalized and self-normalized receivers in the presence of pulse noise interference for diversity orders L = 1,4, E_b/N_0 = 15 dB and γ = 0. In shifting from no diversity to a diversity of order L = 4, it is observed that the noise-normalized receiver provides superior performance to the self-normalized receiver. There is a significant performance difference for E_b/N_I greater than approximately 10 dB. Below this point, the performance difference is small. Noncoherent combining losses occur over a smaller range (E_b/N_I < 5 dB) with smaller magnitude for the noise-normalized receiver compared to the self-normalized receiver (E_b/N_I < 10dB).

Performance curves of the noise-normalized receiver for diversity orders L = 1,3,4 and jammer fractions ρ = 0.01, 0.1, 0.25, 1 and worst case, E_b/N_0 = 15 dB and γ = 5 are shown in Figures 3.14 - 3.16. With no diversity, it is seen that pulse noise jamming results in a significant performance reduction in the range 10 dB < E_b/N_I < 25 dB. As the diversity order is increased to L = 4 however, the noise-normalized receiver has virtually eliminated the effectiveness of the pulse noise jammer. A comparison of worst case performance curves for diversities of order 1 through 4 is shown in Figure 3.17. A diversity of order L = 2 is seen to be sufficient to achieve more than an order of magnitude performance improvement for E_b/N_I > 20 dB. Non-coherent combining losses, although still rather small, are noticed for E_b/N_I < 7 dB and are larger in magnitude than for the severe fading case (γ = 0). Figure 3.18 shows a performance comparison between the noise-normalized and self-normalized receivers in the presence of pulse noise interference for diversity orders L = 1,4, E_b/N_0 = 15 dB and γ = 5. The noise-normalized receiver once again demonstrates superior performance compared to the self-normalized receiver. At approximately E_b/N_I > 30 dB, there is an order of magnitude improved performance for the noise-normalized receiver when compared to the self-normalized receiver. The difference in receiver performance over this range of signal-to-interference ratios is more than what was observed for the severe fading case. Noncoherent combining losses are more noticeable for both receivers than was the case for severe fading.

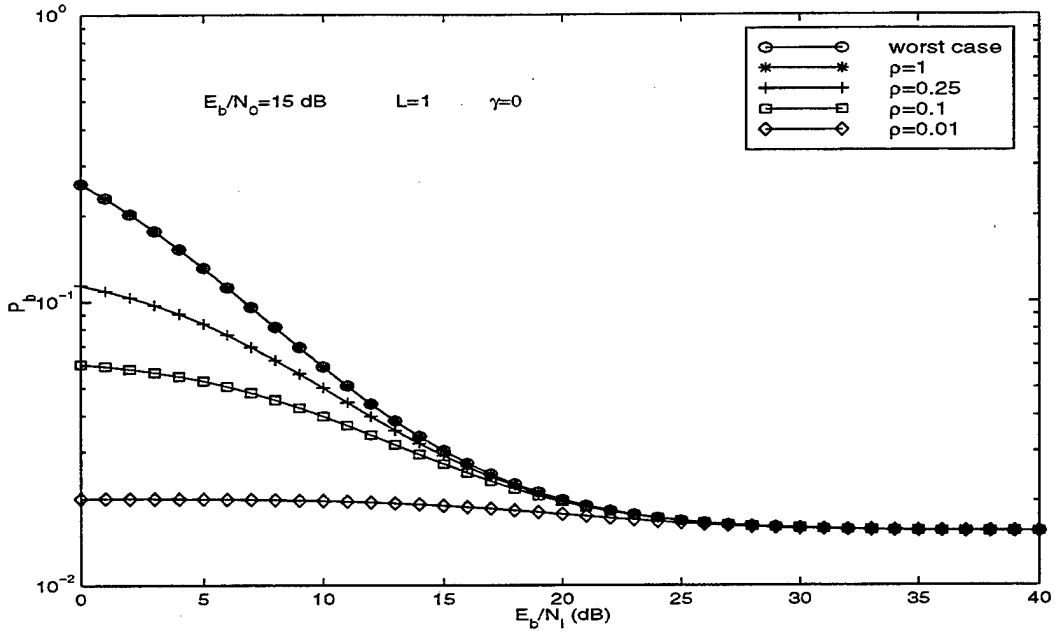

Figure 3.9: Performance of noise-normalized receiver for pulse jamming fractions $\rho = 1, 0.25, 0.1, 0.01$ and worst case for diversity order $L = 1$, $E_b/N_0 = 15$ dB and $\gamma = 0$.

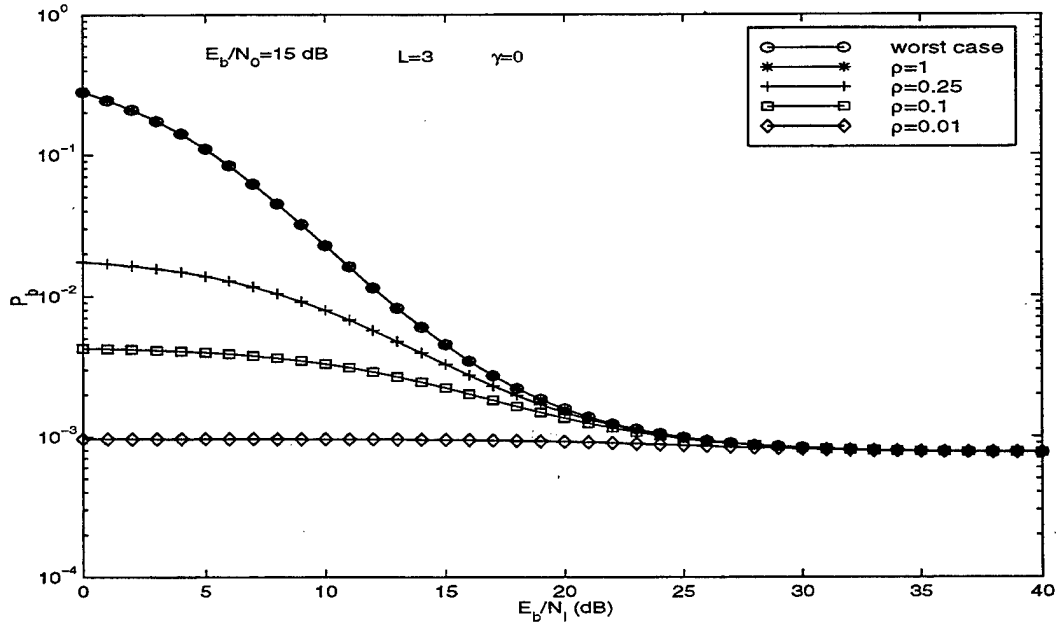

Figure 3.10: Performance of noise-normalized receiver for pulse jamming fractions $\rho = 1, 0.25, 0.1, 0.01$ and worst case for diversity order $L = 3$, $E_b/N_0 = 15$ dB and $\gamma = 0$.

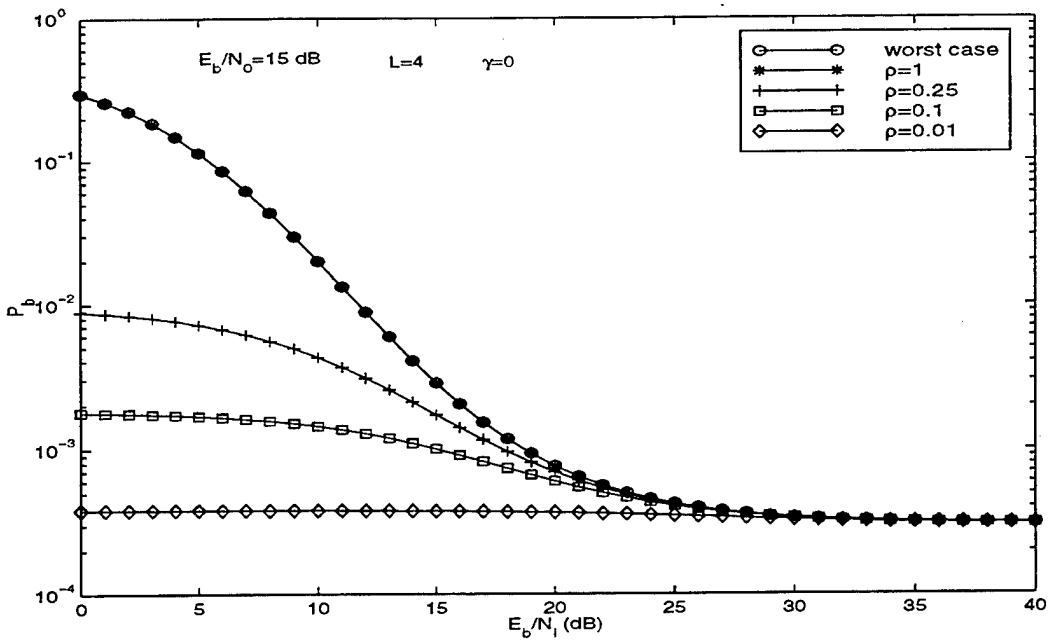

Figure 3.11: Performance of noise-normalized receiver for pulse jamming fractions $\rho = 1, 0.25, 0.1, 0.01$ and worst case for diversity order $L = 4$, $E_b/N_0 = 15$ dB and $\gamma = 0$.

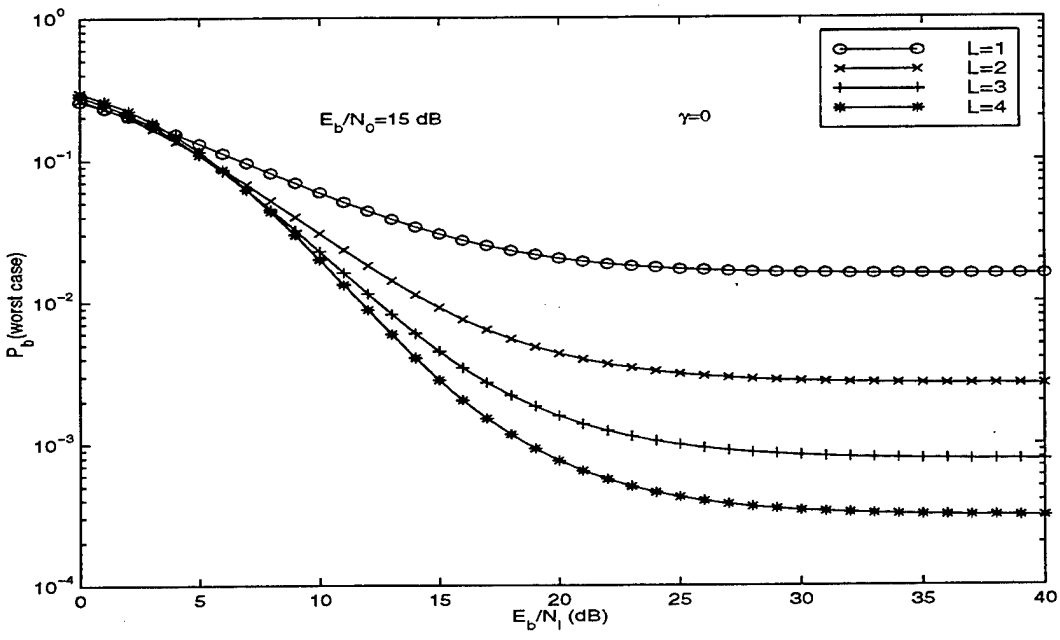

Figure 3.12: Worst case performance of noise-normalized receiver in presence of pulse noise interference for diversity orders $L = 1,2,3,4$, $E_b/N_0 = 15$ dB and $\gamma = 0$.

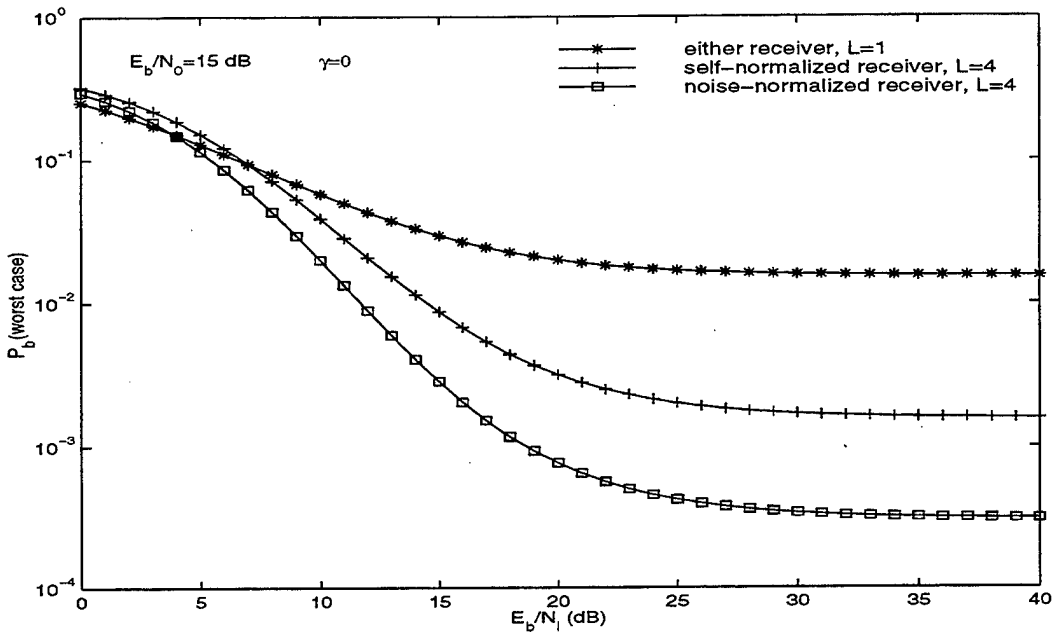

Figure 3.13: Worst case performance comparison between noise-normalized and self-normalized receivers in presence of pulse noise interference for diversity orders L = 1,4, E_b/N_0 = 15 dB and $\gamma = 0$.

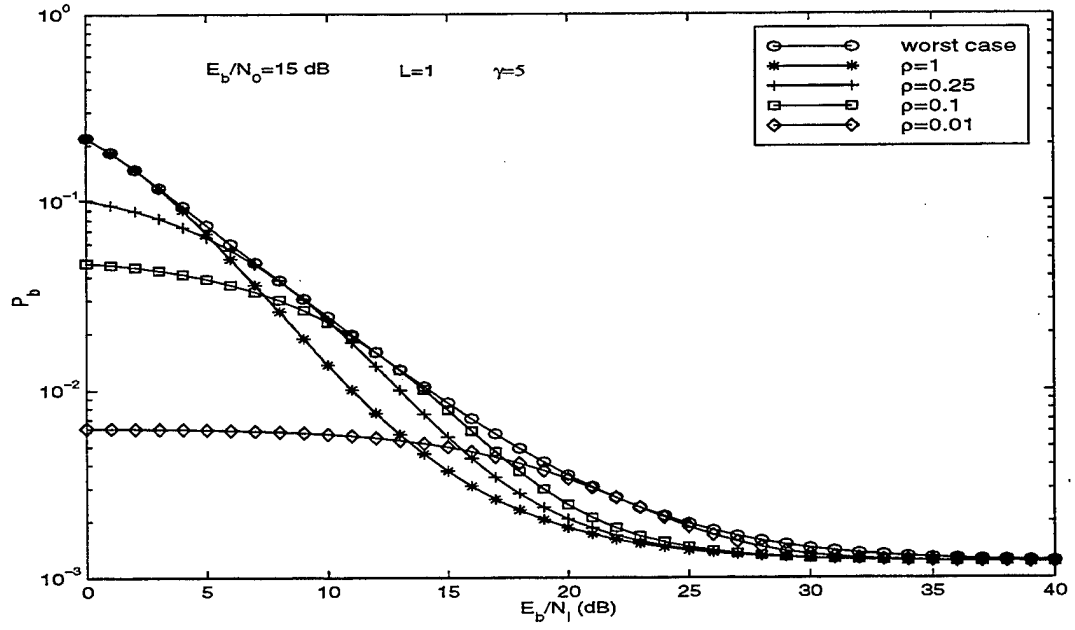

Figure 3.14: Performance of noise-normalized receiver for pulse jamming fractions $\rho = 1, 0.25, 0.1, 0.01$ and worst case for diversity order L = 1, E_b/N_0 = 15 dB and $\gamma = 5$.

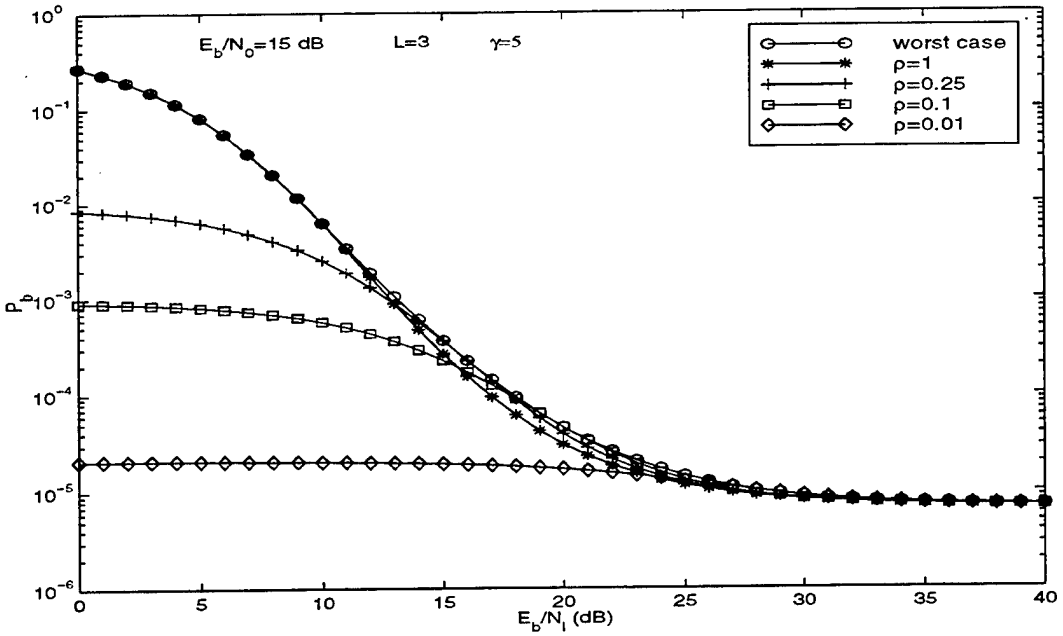

Figure 3.15: Performance of noise-normalized receiver for pulse jamming fractions $\rho = 1, 0.25, 0.1, 0.01$ and worst case for diversity order $L = 3$, $E_b/N_0 = 15$ dB and $\gamma = 5$.

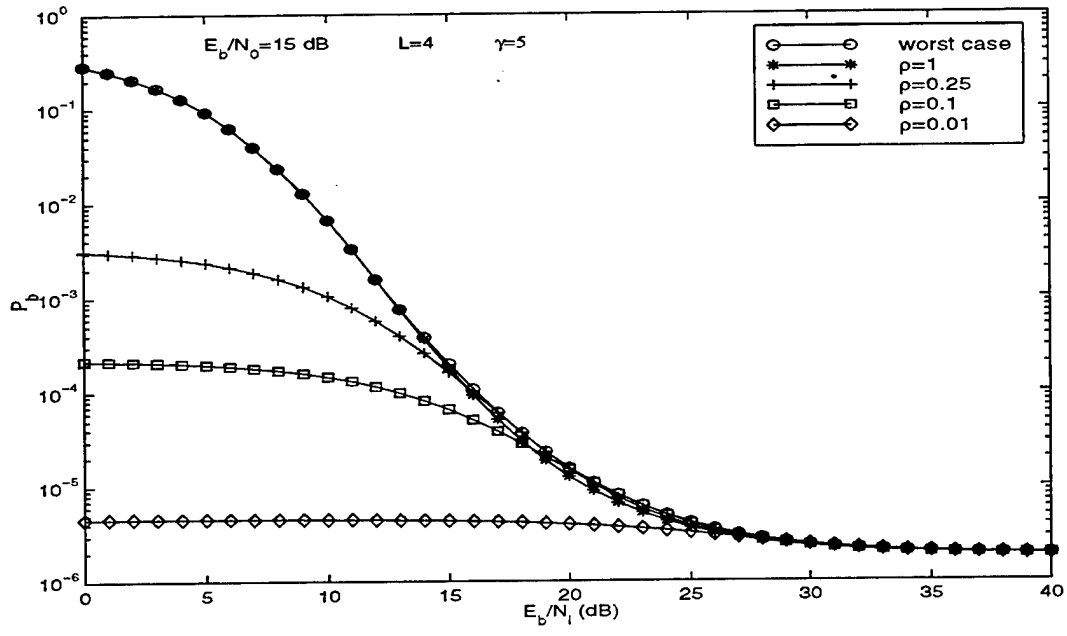

Figure 3.16: Performance of noise-normalized receiver for pulse jamming fractions $\rho = 1, 0.25, 0.1, 0.01$ and worst case for diversity order $L = 4$, $E_b/N_0 = 15$ dB and $\gamma = 5$.

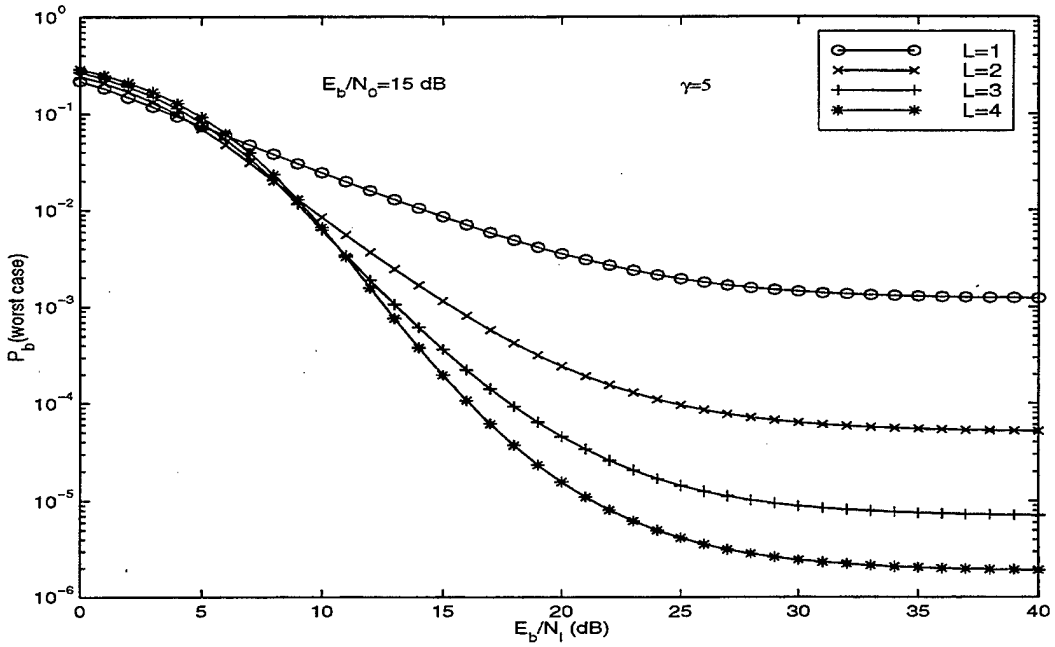

Figure 3.17: Worst case performance of noise-normalized receiver in presence of pulse noise interference for diversity orders L = 1,2,3,4, E_b/N_0 = 15 dB and γ = 5.

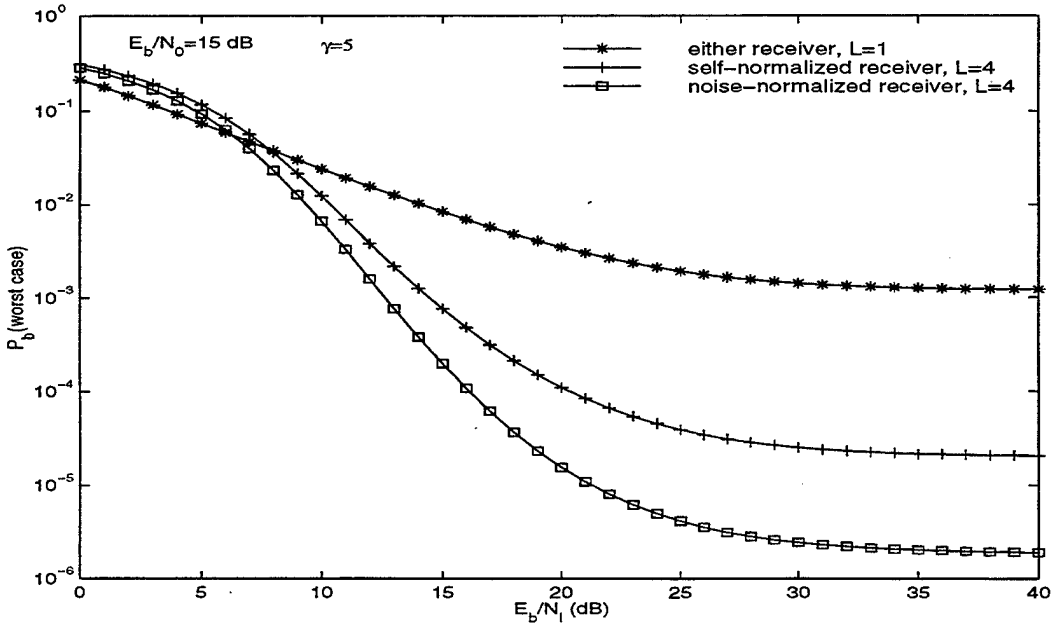

Figure 3.18: Worst case performance comparison between noise-normalized and self-normalized receivers in presence of pulse noise interference for diversity orders L = 1,4, E_b/N_0 = 15 dB and γ = 5.

Figure 3.19 shows the optimum value of ρ as a function of diversity order with a E_b/N_0 = 15 dB, $\gamma = 5$ and E_b/N_I as a parameter. As in the case for the self-normalized receiver, it is seen that the optimum value of ρ decreases as E_b/N_I increases and increases for increasing diversity order for a given E_b/N_I. Comparing to Figure 2.22, it is observed that for a given E_b/N_I and diversity order ($L \geq 2$), the value of ρ is higher for the noise-normalized receiver than the self-normalized receiver. This indicates that the noise-normalized receiver has forced the jammer to a more continuous jamming strategy compared to the self normalized receiver, making it a more effective countermeasure.

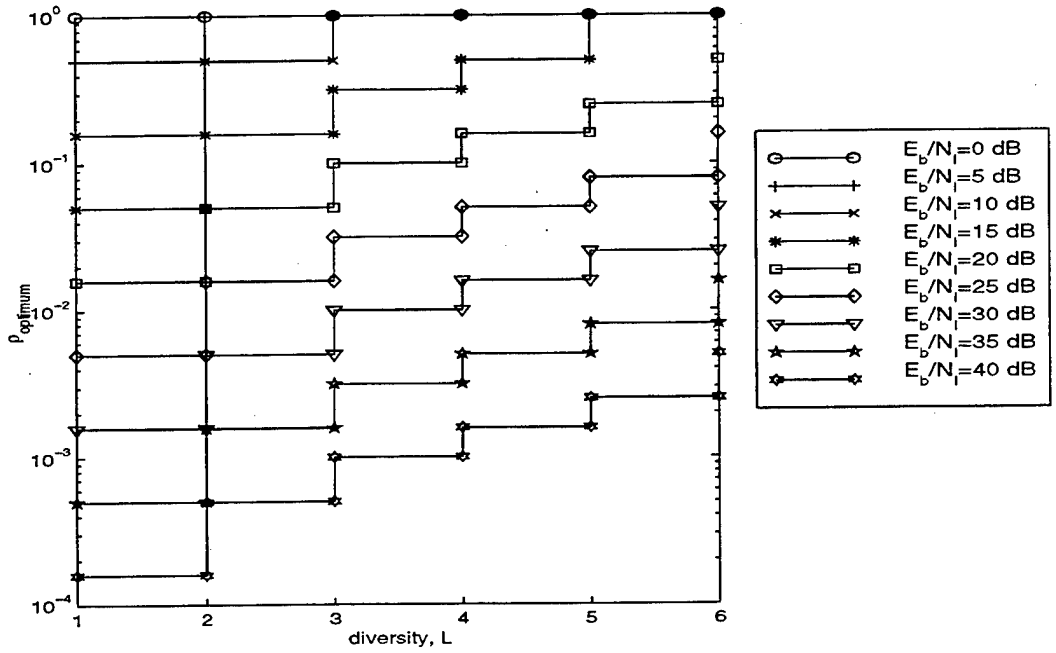

Figure 3.19: Optimum value of ρ as a function of diversity order with E_b/N_0 = 15 dB, $\gamma = 5$ and E_b/N_I as a parameter.

Figures 3.20 and 3.34 shows the optimum value of ρ as a function of γ with diversity order as a parameter and with E_b/N_0 = 15 dB for E_b/N_I equal to 20 and 30 dB respectively. As was the case for the self-normalized receiver, it is observed that the optimum value of ρ decreases for increasing γ. Comparing to the values of ρ in Figures 2.23 and 2.24, it is seen that over most of the range of γ, ρ is higher for the noise-normalized receiver than the self-normalized

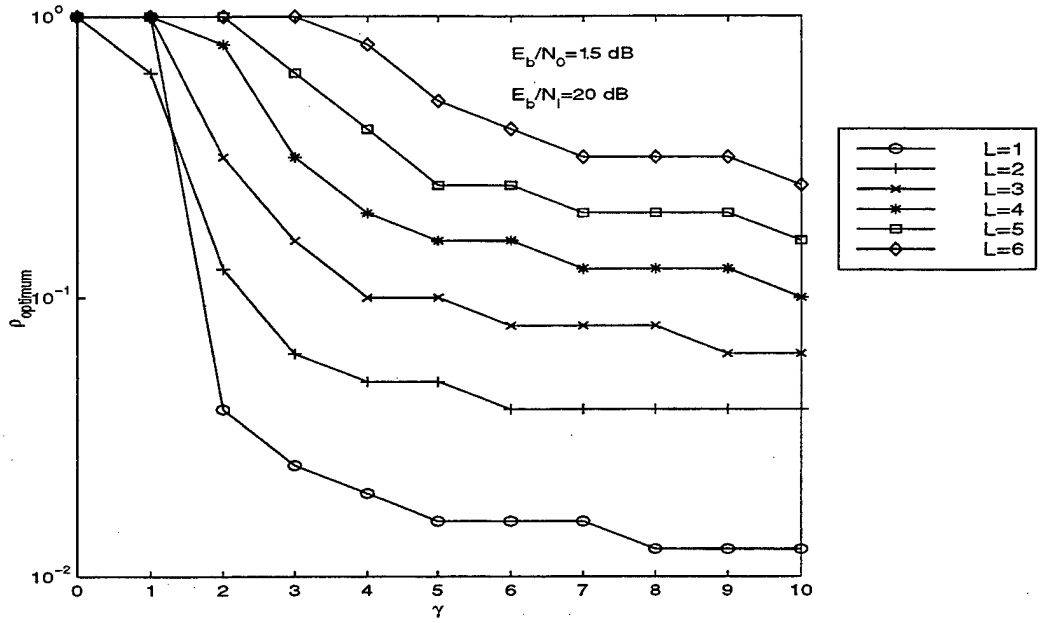

Figure 3.20: Optimum value of ρ as a function of γ with diversity order as a parameter for E_b/N_0 = 15 dB and E_b/N_I = 20 dB.

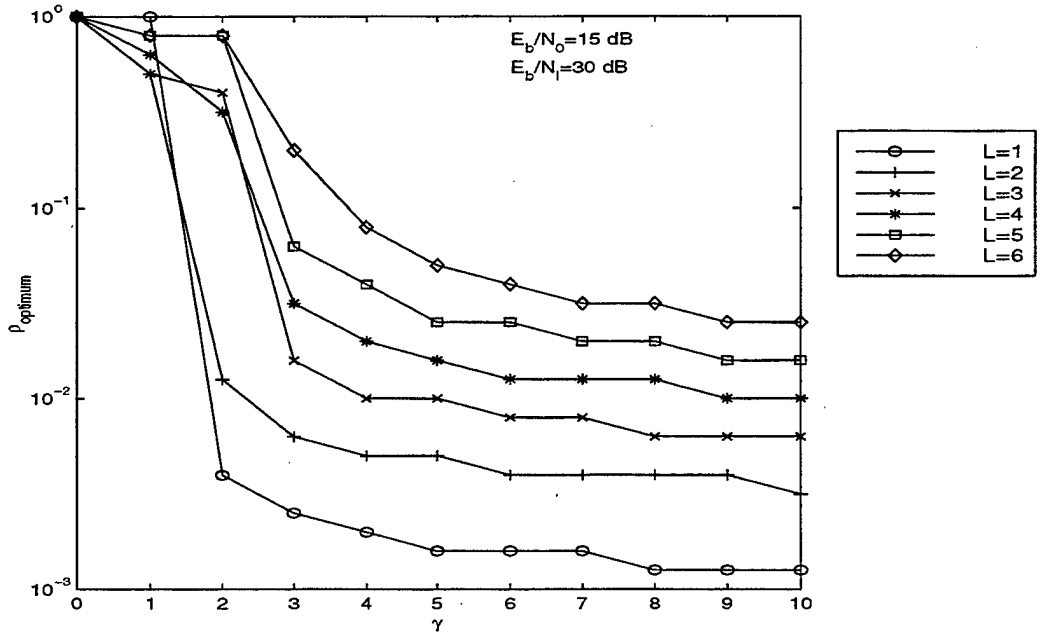

Figure 3.21: Optimum value of ρ as a function of γ with diversity order as a parameter for E_b/N_0 = 15 dB and E_b/N_I = 30 dB.

receiver. This is another indicator that the noise-normalized receiver is more effective against pulse noise jamming than the self-normalized receiver.

C. PERFORMANCE OF DS-DPSK WITH NON-IDEAL NOISE NORMALIZATION

While the system of Figure 3.1 is extremely effective in pulse noise mitigation as has been seen, it is as such not practically realizable. In this section, noise estimation errors are introduced and the performance of such a system is considered. A block diagram of the noise-normalized receiver with non-ideal noise normalization is depicted in Figure 3.22. The structure is seen to be the same as that of the noise-normalized receiver with ideal noise normalization with the exception that the symbol $\hat{\sigma}_j^2$ represents an estimate of σ_j^2, the true value of the measured noise. For the three interference cases I_1, I_2 and I_3, $\hat{\sigma}_j^2$ is given as

$$\hat{\sigma}_j^2 = \begin{cases} \sigma_n^2 + \hat{\sigma}_{I_1}^2, & \text{case } I_1 \\ \sigma_n^2 + \hat{\sigma}_{I_2}^2, & \text{case } I_2 \\ \sigma_n^2, & \text{case } I_3 \end{cases} \tag{3.16}$$

Here it is assumed that the thermal noise can be measured accurately and that measurement errors are caused by the interference components only. It is further assumed that on average the measurement errors for cases $I_1$and I_2 will be the same. For this analysis, $\hat{\sigma}_j^2$ is modeled as a random variable and also as a fixed parameter. In the former case, no knowledge of the estimation error is assumed *a priori* and as such $\hat{\sigma}_j^2$ is modeled as a uniform random variable. As a fixed parameter, $\hat{\sigma}_j^2$ represents some fixed bias introduced by the measurement circuitry. In the next section, the probability of bit error of this system will be derived. This will be followed by numerical results in the following subsection.

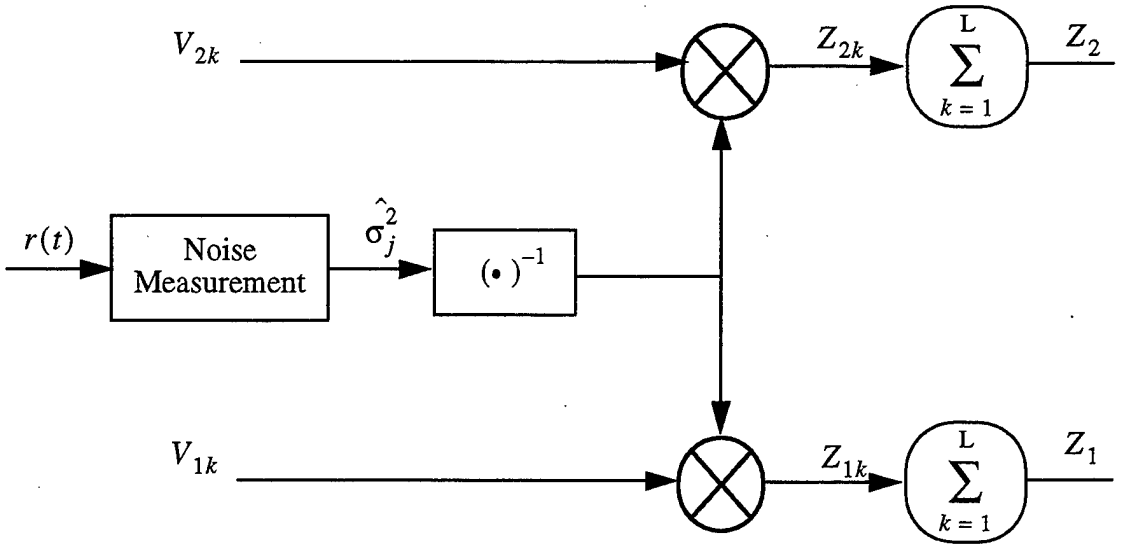

Figure 3.22: Noise-normalized receiver with non-ideal noise normalization.

1. Bit Error Probability

With $\hat{\sigma}_j^2$ modeled as a random variable, the conditional density for the random variable Z_1 can be expressed from equation 3.3 as

$$f_{Z_1}\left(z_1|0, I_j, \hat{\sigma}_j^2; L, i_1, i_2\right) = \mathcal{L}^{-1}\left(\left[\mathcal{L}\left(f_{Z_{1k}}\left(z_{1k}|0, I_1, \hat{\sigma}_1^2\right)^{\otimes i_1}\right)\right] \times \left[\mathcal{L}\left(f_{Z_{1k}}\left(z_{1k}|0, I_2, \hat{\sigma}_2^2\right)^{\otimes i_2}\right)\right] \times \left[\mathcal{L}\left(f_{Z_{1k}}\left(z_{1k}|0, I_3, \hat{\sigma}_3^2\right)^{\otimes (L-i_1-i_2)}\right)\right]\right) \quad (3.17)$$

The density function for the random variable $Z_{1k} = V_{1k}/\hat{\sigma}_j^2$ follows directly from equation 3.5

$$f_{Z_{1k}}\left(z_{1k}|0, I_j, \hat{\sigma}_j^2\right) = \frac{\hat{\sigma}_j^2}{2\sigma_{1_j}^2} \exp\left(-\frac{1}{2\sigma_{1_j}^2}\left(z_{1k}\hat{\sigma}_j^2 + 4\alpha^2\right)\right) I_0\left(\frac{2\alpha\sqrt{z_{1k}\hat{\sigma}_j^2}}{\sigma_{1_j}^2}\right) u(z_{1k}) \quad (3.18)$$

The Laplace transform of the density function for Z_{1k} is shown to be (Appendix B, section B.3)

$$F_{Z_{1k}}(s|0, I_j, \hat{\sigma_j^2}) = \frac{\hat{\sigma_j^2}}{2\sigma_{1_j}^2\left(s + \frac{\hat{\sigma_j^2}}{2\sigma_{1_j}^2}\right)} \exp\left(-\frac{2\alpha^2}{\sigma_{1_j}^2}\right) \exp\left(\frac{\alpha^2\hat{\sigma_j^2}}{\sigma_{1_j}^4\left(s + \frac{\hat{\sigma_j^2}}{2\sigma_{1_j}^2}\right)}\right) \tag{3.19}$$

The expression for $f_{Z_{1k}}\left(z_{1k}|0, I_j, \hat{\sigma_j^2}\right)^{\otimes i_j}$ is then given as

$$f_{Z_{1k}}\left(z_{1k}|0, I_j, \hat{\sigma_j^2}\right)^{\otimes i_j} = \mathcal{L}^{-1}\left(\left[F_{Z_{1k}}(s|0, I_j, \hat{\sigma_j^2})\right]^{i_j}\right) \tag{3.20}$$

which is shown to be (Appendix B, section B.4)

$$f_{Z_{1k}}\left(z_{1k}|0, I_j, \hat{\sigma_j^2}\right)^{\otimes i_j} = \left(\frac{(\hat{\sigma_j^2}/\sigma_j^2)(\gamma+1)\Gamma_L}{2(2+(\gamma+1)\Gamma_L)}\right) \exp\left(-\frac{4\gamma i_j + (\hat{\sigma_j^2}/\sigma_j^2)(\gamma+1)\Gamma_L z_{1k}}{2(2+(\gamma+1)\Gamma_L)}\right)$$

$$\left(\frac{(\hat{\sigma_j^2}/\sigma_j^2)z_{1k}(\gamma+1)\Gamma_L}{4\gamma i_j}\right)^{\left(\frac{i_j-1}{2}\right)} I_{i_j-1}\left(\sqrt{\frac{4(\hat{\sigma_j^2}/\sigma_j^2)\gamma(\gamma+1)\Gamma_L z_{1k} i_j}{(2+(\gamma+1)\Gamma_L)^2}}\right) u(z_{1k}) \tag{3.21}$$

From equation 3.10, the density function for the random variable Z_1 is

$$f_{Z_1}(z_1|0) = \sum_{i_2=0}^{L} \sum_{i_1=0}^{L-i_2} f_{Z_1}(z_1|0, I_j; L, i_1, i_2) \Pr(L, i_1, i_2) \tag{3.22}$$

where

$$f_{Z_1}(z_1|0, I_j; L, i_1, i_2) = \int_{\sigma_j^2-\delta}^{\sigma_j^2+\delta} f_{Z_1}\left(z_1|0, I_j, \hat{\sigma_j^2}; L, i_1, i_2\right) f_{\hat{\sigma_j^2}}(\hat{\sigma_j^2}) \tag{3.23}$$

$\Pr(L, i_1, i_2)$ is as defined in equation 3.11, $f_{\hat{\sigma_j^2}}(\hat{\sigma_j^2})$ is the probability density function for the random variable $\hat{\sigma_j^2}$ and δ is the maximum deviation of the estimated noise power from the actual noise power. Modeled as a uniform random variable, $\hat{\sigma_j^2}$ has mean σ_j^2 and variance $\delta^2/3$.

The conditional density for the random variable Z_2 can be expressed from equation 3.17 by letting $Z_1 \rightarrow Z_2$ and $Z_{1k} \rightarrow Z_{2k}$

$$f_{Z_2}\left(z_2|0, \mathrm{I}_j, \hat{\sigma}_j^2; \mathrm{L}, \mathrm{i}_1, \mathrm{i}_2\right) = \mathcal{L}^{-1}\left(\left[\mathcal{L}\left(f_{Z_{2k}}\left(z_{2k}|0, \mathrm{I}_1, \hat{\sigma}_1^2\right)^{\otimes \mathrm{i}_1}\right)\right] \times \left[\mathcal{L}\left(f_{Z_{2k}}\left(z_{2k}|0, \mathrm{I}_2, \hat{\sigma}_2^2\right)^{\otimes \mathrm{i}_2}\right)\right] \times \left[\mathcal{L}\left(f_{Z_{2k}}\left(z_{2k}|0, \mathrm{I}_3, \hat{\sigma}_3^2\right)^{\otimes (\mathrm{L}-\mathrm{i}_1-\mathrm{i}_2)}\right)\right]\right) \tag{3.24}$$

The density function for Z_{2k} is now given as

$$f_{Z_{2k}}\left(z_{2k}|0, \mathrm{I}_j, \hat{\sigma}_j^2\right) = \frac{\hat{\sigma}_j^2}{2\sigma_j^2}\exp\left(-\frac{\hat{\sigma}_j^2 z_{2k}}{2\sigma_j^2}\right)u(z_{2k}) \tag{3.25}$$

The expression for $f_{Z_{2k}}\left(z_{2k}|0, \mathrm{I}_j, \hat{\sigma}_j^2\right)^{\otimes \mathrm{i}_j}$ is derived from a *Chi-squared* probability density function with $2\mathrm{i}_j$ degrees of freedom [4, 5] and is given as

$$f_{Z_{2k}}\left(z_{2k}|0, \mathrm{I}_j, \hat{\sigma}_j^2\right)^{\otimes \mathrm{i}_j} = \frac{(\hat{\sigma}_j^2/\sigma_j^2)^{\mathrm{i}_j}\exp\left(-\frac{\hat{\sigma}_j^2 z_{2k}}{2\sigma_j^2}\right)z_{2k}^{(\mathrm{i}_j-1)}}{2^{\mathrm{i}_j}(\mathrm{i}_j-1)!}u(z_{2k}) \tag{3.26}$$

The density function for the random variable Z_2 is derived from equations 3.22 and 3.23 by letting $Z_1 \rightarrow Z_2$

$$f_{Z_2}(z_2|0) = \sum_{\mathrm{i}_2=0}^{\mathrm{L}} \sum_{\mathrm{i}_1=0}^{\mathrm{L}-\mathrm{i}_2} f_{Z_2}(z_2|0, \mathrm{I}_j; \mathrm{L}, \mathrm{i}_1, \mathrm{i}_2)\Pr(\mathrm{L}, \mathrm{i}_1, \mathrm{i}_2) \tag{3.27}$$

where

$$f_{Z_2}(z_2|0, \mathrm{I}_j; \mathrm{L}, \mathrm{i}_1, \mathrm{i}_2) = \int_{\sigma_j^2-\delta}^{\sigma_j^2+\delta} f_{Z_2}\left(z_2|0, \mathrm{I}_j, \hat{\sigma}_j^2; \mathrm{L}, \mathrm{i}_1, \mathrm{i}_2\right) f_{\hat{\sigma}_j^2}(\hat{\sigma}_j^2) \tag{3.28}$$

The probability of bit error may now be obtained directly through the numerical evaluation of equation 3.15. As a check for the analytical work here, substituting $\hat{\sigma}_j^2 = \sigma_j^2$ for the case of ideal noise-

normalization, equations 3.21 and 3.26 reduce to equations 3.9 and 3.13 which define the density functions for the random variables Z_1 and Z_2 under ideal noise-normalization.

2. Numerical Results

For the noise-normalized receiver with non-ideal noise-normalization, worst case performance was produced under the conditions outlined in equations 2.30 and 2.31. The values of ρ corresponding to equation 2.31 have been selected to be consistent with the values of ρ selected for the other receivers. Worst case performance curves for the noise-normalized receiver with non-ideal noise-normalization for a diversity order of L = 4, E_b/N_0 = 15 dB, $\gamma = 0$ and $\gamma = 5$ are shown in Figures 3.23 and 3.24 respectively. The uniform curve represents $\hat{\sigma}_j^2$ modeled as a uniform random variable with mean σ_j^2 and maximum error deviation $\delta = 0.5\sigma_j^2$. The (-50%) curve represents the case where the noise is underestimated by 50% and the (+50%) curve represents the case where the noise is overestimated by 50%. Also shown are the cases of ideal noise-normalization and the self-normalized receiver. It is seen that for either case of fading, performance degrades the most in comparison to the ideal case when the noise is underestimated. A less severe degradation occurs when the noise is overestimated. For either case however, the overall amount of degradation is not extremely significant and the overall performances are clearly superior to the performance of the self-normalized receiver. For the case of Rayleigh fading, having little knowledge of the estimation error (uniform curve) provides almost no change in performance compared to the ideal case over the entire range of signal-to-interference ratio. For moderate fading, the performance difference increases only slightly. It is therefore concluded that if one is willing to accept a slight degradation in performance, relatively crude measurement techniques may be utilized. This makes the noise-normalized receiver a practical and effective receiver in pulse-jammed environments. Throughout the rest of the dissertation, however, receiver comparisons will be based under the assumption of ideal noise-normalization.

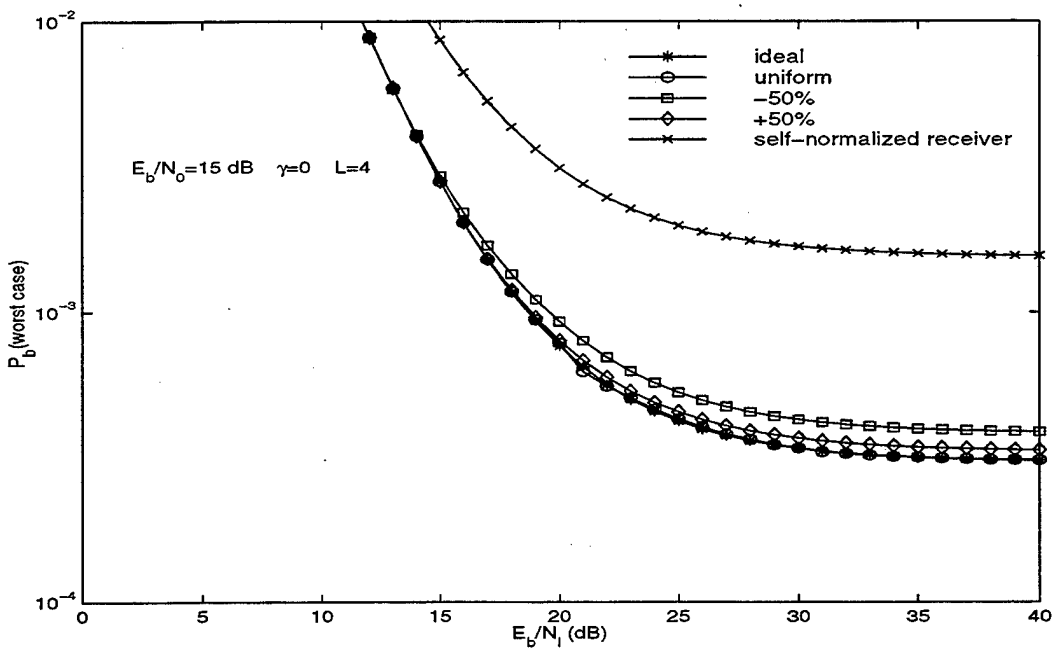

Figure 3.23: Worst case performance curves for the noise-normalized receiver with non-ideal noise-normalization for a diversity order L = 4, E_b/N_0 = 15 dB and $\gamma = 0$.

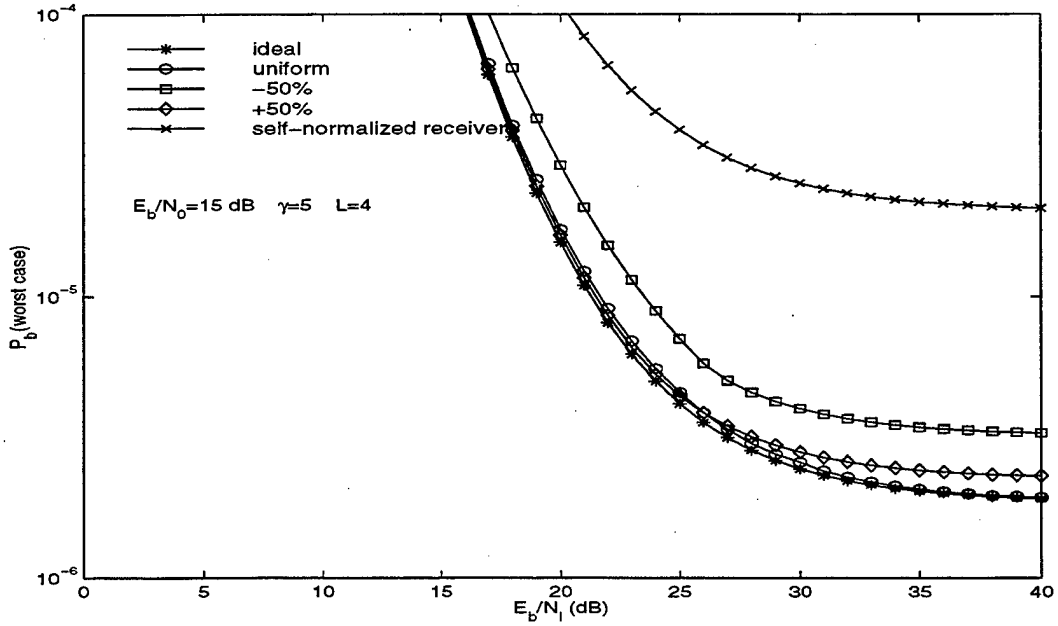

Figure 3.24: Worst case performance curves for the noise-normalized receiver with non-ideal noise-normalization for a diversity order L = 4, E_b/N_0 = 15 dB and $\gamma = 5$.

Before concluding this chapter, the performance of the linear receiver depicted in Figure 3.25 is investigated. With the linear receiver, it is seen that there is no attempt to mitigate the effects of the pulse noise jammer. The linear, self-normalized and noise-normalized receivers are called equal gain combining receivers since each diversity reception is given equal weight in the

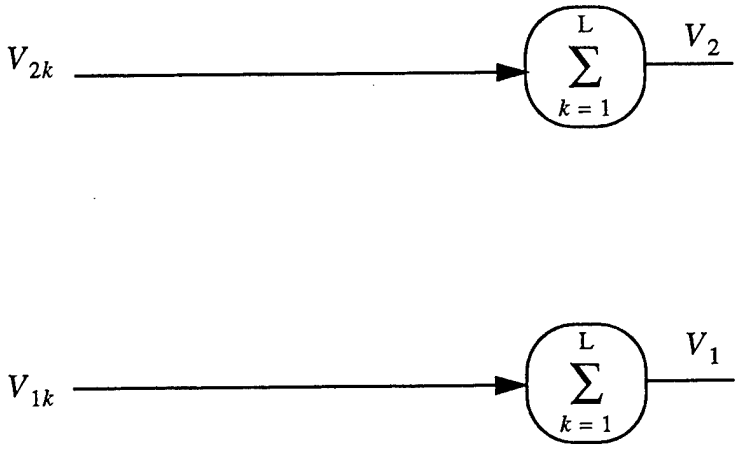

Figure 3.25: Linear receiver structure.

output decision statistic. The probability of bit error for the linear receiver is now derived and is followed by a performance comparison to the self-normalized and noise-normalized receivers.

D. PERFORMANCE COMPARISON OF SELF-NORMALIZED, NOISE NORMALIZED AND LINEAR RECEIVERS

1. Linear Receiver Bit Error Probability

Referring to Figure 3.25, the probability density functions for the random variables V_{1k} and V_{2k} given bit 0 is transmitted are given in equations 3.1 and 3.2 respectively. The conditional density for the random variable V_1 can be expressed as

$$f_{V_1}(v_1|0, I_j; L, i_1, i_2) = \mathcal{L}^{-1}([\mathcal{L}(f_{V_{1k}}(v_{1k}|0, I_1)^{\otimes i_1})] \times [\mathcal{L}(f_{V_{1k}}(v_{1k}|0, I_2)^{\otimes i_2})] \times [\mathcal{L}(f_{V_{1k}}(v_{1k}|0, I_3)^{\otimes (L-i_1-i_2)})]) \quad (3.29)$$

The Laplace transform of the density function for V_{1k} is shown to be (Appendix B, section B.5),

$$F_{V_{1k}}(s|0, \mathrm{I}_j) = \frac{1}{2\sigma_{1_j}^2\left(s + \frac{1}{2\sigma_{1_j}^2}\right)} \exp\left(-\frac{2\alpha^2}{\sigma_{1_j}^2}\right) \exp\left(\frac{\alpha^2}{\sigma_{1_j}^4\left(s + \frac{1}{2\sigma_{1_j}^2}\right)}\right) \tag{3.30}$$

The expression for $f_{V_{1k}}(v_{1k}|0, \mathrm{I}_j)^{\otimes \mathrm{i}_j}$ is given as

$$f_{V_{1k}}(v_{1k}|0, \mathrm{I}_j)^{\otimes \mathrm{i}_j} = \mathcal{L}^{-1}([F_{V_{1k}}(s|0, \mathrm{I}_j)]^{\mathrm{i}_j}) \tag{3.31}$$

which is shown to be (Appendix B, section B.6)

$$f_{V_{1k}}(v_{1k}|0, \mathrm{I}_j)^{\otimes \mathrm{i}_j} = \frac{1}{2\sigma_{1_j}^2} \exp\left(-\frac{v_{1k} + 4\alpha^2 \mathrm{i}_j}{2\sigma_{1_j}^2}\right)\left(\frac{v_{1k}}{4\alpha^2 \mathrm{i}_j}\right)^{\left(\frac{\mathrm{i}_j - 1}{2}\right)} \times$$

$$\mathrm{I}_{\mathrm{i}_j - 1}\left(\frac{2\alpha\sqrt{v_{1k}\mathrm{i}_j}}{\sigma_{1_j}^2}\right) u(v_{1k}) \tag{3.32}$$

The probability distribution of the random variable V_1 conditioned on a bit 0 transmission is given by

$$f_{V_1}(v_1|0) = \sum_{\mathrm{i}_2 = 0}^{\mathrm{L}} \sum_{\mathrm{i}_1 = 0}^{\mathrm{L} - \mathrm{i}_2} f_{V_1}(v_1|0, \mathrm{I}_j; \mathrm{L}, \mathrm{i}_1, \mathrm{i}_2) \Pr(\mathrm{L}, \mathrm{i}_1, \mathrm{i}_2) \tag{3.33}$$

where $\Pr(\mathrm{L}, \mathrm{i}_1, \mathrm{i}_2)$ is given in equation 3.11. Equation 3.33 must be evaluated numerically.

The conditional density function for the random variable V_2 is given as

$$f_{V_2}(v_2|0, \mathrm{I}_j; \mathrm{L}, \mathrm{i}_1, \mathrm{i}_2) = \mathcal{L}^{-1}([\mathcal{L}(f_{V_{2k}}(v_{2k}|0, \mathrm{I}_1)^{\otimes \mathrm{i}_1})] \times [\mathcal{L}(f_{V_{2k}}(v_{2k}|0, \mathrm{I}_2)^{\otimes \mathrm{i}_2})] \times$$

$$[\mathcal{L}(f_{V_{2k}}(v_{2k}|0, \mathrm{I}_3)^{\otimes (\mathrm{L} - \mathrm{i}_1 - \mathrm{i}_2)})]) \tag{3.34}$$

where expression for $f_{V_{2k}}(v_{2k}|0, \mathrm{I}_j)^{\otimes \mathrm{i}_j}$ is given as

$$f_{V_{2k}}(v_{2k}|0, \mathrm{I}_j)^{\otimes \mathrm{i}_j} = \frac{1}{(2\sigma_{2j}^2)^{\mathrm{i}_j}} \exp\left(-\frac{v_{2k}}{2\sigma_{2j}^2}\right) \frac{v_{2k}^{\mathrm{i}_j - 1}}{(\mathrm{i}_j - 1)!} u(v_{2k}) \tag{3.35}$$

which is recognizable as a *Chi-squared* probability density function with $2i_j$ degrees of freedom [4, 5]. The probability distribution of the random variable V_2 conditioned on a bit 0 transmission is given as

$$f_{V_2}(v_2|0) = \sum_{i_2=0}^{L} \sum_{i_1=0}^{L-i_2} f_{V_2}(v_2|0, I_j; L, i_1, i_2) \Pr(L, i_1, i_2) \tag{3.36}$$

where $\Pr(L, i_1, i_2)$ is given in equation 3.11. Equation 3.36 must also be evaluated numerically. The probability of bit error is given by

$$P_b = P_r(V_1 < V_2|0) \tag{3.37}$$

Expressing this in terms of the density functions for the random variables V_1 and V_2 yields

$$P_b = \int_0^{\infty} \int_0^{v_2} f_{V_1, V_2}(v_1, v_2|0) dv_1 dv_2 \tag{3.38}$$

The joint density function for the random variables Z_1 and Z_2 in equation 3.38 is the product of the two marginal density functions $f_{V_1}(v_1|0)$ and $f_{V_2}(v_2|0)$ since V_1 and V_2 are independent random variables. This last expression must also be evaluated numerically.

2. Performance Comparison between Self-Normalized, Noise-Normalized and Linear Receivers

The probability of bit error as a function of γ with no pulse noise jamming, a bit energy to thermal noise density ratio of $E_b/N_0 = 15$ dB and with diversity as a parameter is shown in Figure 3.2. It is seen that the linear receiver performance is identical to that of the noise-normalized receiver. It is noted that the best achievable performance for either receiver for a diversity of order $L = 4$ is $P_b \cong 3 \times 10^{-3}$ for $\gamma = 0$ and $P_b \cong 2 \times 10^{-6}$ for $\gamma = 5$. Worst case performance curves for the self-normalized, noise-normalized and linear receivers in the presence of pulse noise interference for diversity orders $L = 1,4$, $E_b/N_0 = 15$ dB and $\gamma = 0, 5$ are shown in Figures 3.26 and 3.27 respectively. For no diversity ($L = 1$), the performances are identical for all receivers. For $\gamma = 0$, it is seen that the linear receiver performance is inferior to the noise-normalized receiver. The performance difference is most significant in the region $10 \text{ dB} < E_b/N_I < 30 \text{ dB}$ where there is

as much as a 10 dB advantage for the noise-normalized receiver. The noise-normalized receiver has virtually rendered the pulse noise jammer ineffective at approximately $E_b/N_I = 25$ dB as it begins to approach its asymptotic limit of $P_b \cong 3 \times 10^{-3}$. The linear receiver does not begin to approach this limit until approximately $E_b/N_I = 40$ dB. The linear receiver is seen to be inferior to the self-normalized receiver over the range of approximately $8 \text{ dB} < E_b/N_I < 25$ dB. The maximum performance difference over this range however is on the order of 3 dB, much less than that observed for the noise-normalized receiver. For $E_b/N_I > 25$ dB, the linear receiver actually performs better than the self-normalized receiver. It is thus concluded that in this region the pulse noise jammer is less effective since the self-normalized receiver has lost any advantage it had over the linear receiver. The fact that the linear receiver performs better in this region is probably due to the fact that it does not limit the signal amplitude in any way as does the self-normalized receiver. This gives better overall combative qualities against signal fading.

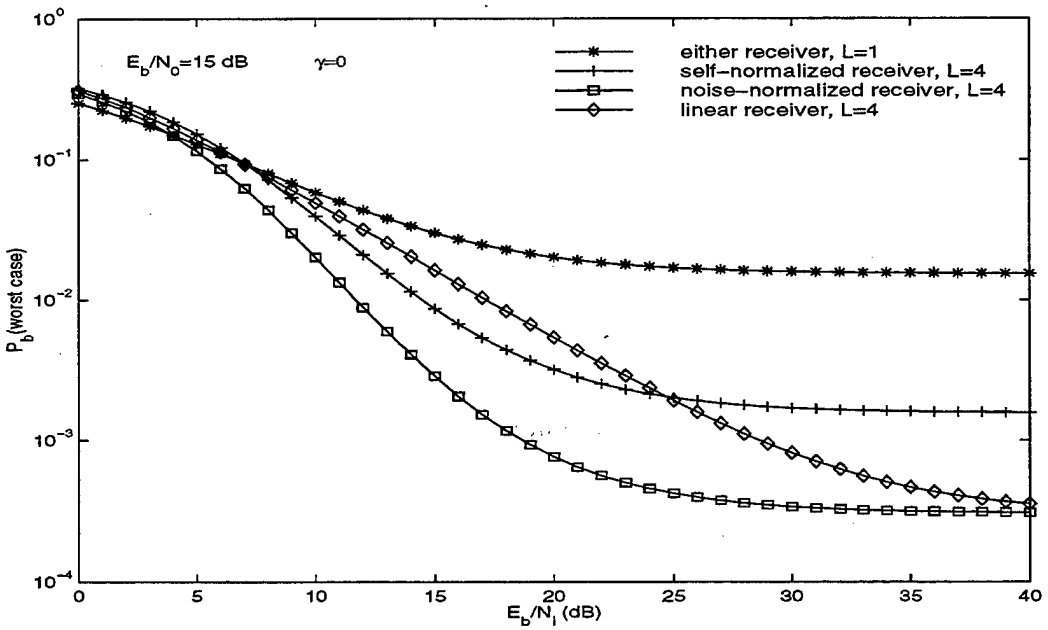

Figure 3.26: Worst case performance comparison between self-normalized, noise-normalized and linear receivers in the presence of pulse noise interference for diversity orders L = 1,4, $E_b/N_0 = 15$ dB and $\gamma = 0$.

For $\gamma = 5$, both noise-normalized and self-normalized receivers are superior to the linear receiver over the full range of signal-to-interference ratio. This difference is less notable for $E_b/N_I < 10$ dB but quite significant for larger values with the performance difference being as much as 20 dB for $P_b \cong 5 \times 10^{-5}$ for the self-normalized receiver and 25 dB for $P_b \cong 5 \times 10^{-5}$ for the noise-normalized receiver. The linear receiver is seen not to have even begun to approach its asymptotic performance limit of $P_b \cong 2 \times 10^{-6}$ at $E_b/N_I = 40$ dB. It is thus concluded that for moderate fading, the pulse noise jammer is extremely effective against the linear receiver at even very high signal-to-interference ratios.

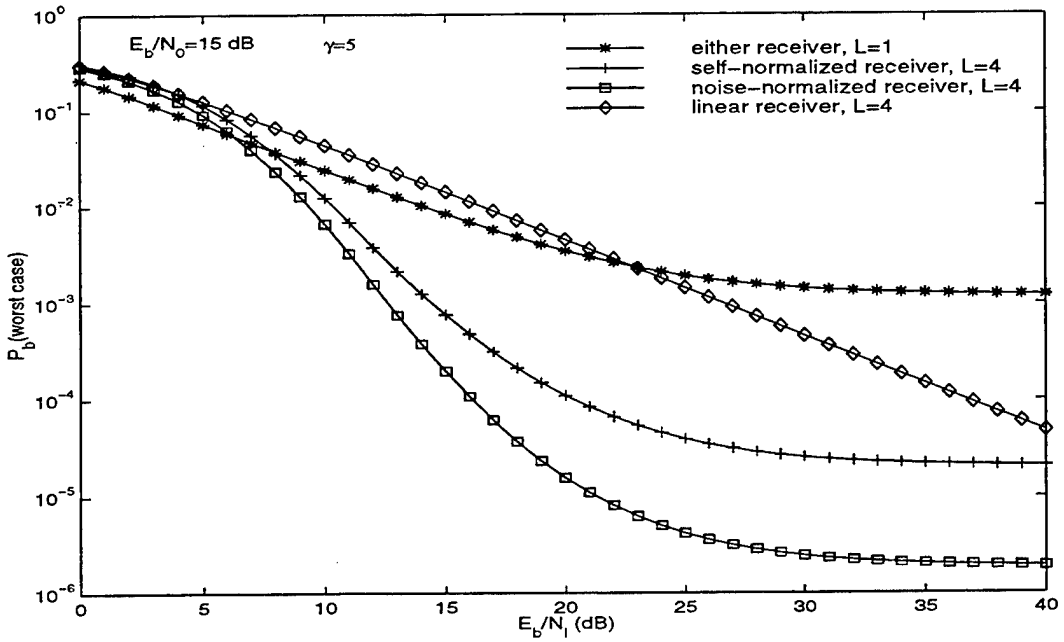

Figure 3.27: Worst case performance comparison between self-normalized, noise-normalized and linear receivers in the presence of pulse noise interference for diversity orders L = 1,4, E_b/N_0 = 15 dB and $\gamma = 5$.

E. CHAPTER CONCLUSIONS

The performance of a DS-DPSK spread spectrum system with noise-normalized receiver over a Rician frequency nonselective, slowly fading channel in the presence of pulsed noise interference and AWGN has been considered. The receiver employs L-fold time diversity and soft

decision equal gain combining. The same jammer model used for the self-normalized receiver analysis was employed here. As was concluded for the self-normalized receiver for severe and moderate fading, the best strategy for the jammer when ρ was fixed was to jam alternating bits rather than adjacent bits. The worst case performance of the noise-normalized receiver as a function of the parameter ρ under conditions of severe and moderate fading was analyzed. It was determined that the noise-normalized receiver was effective in mitigating the effects of pulse noise jamming for both fading conditions. For the moderate fading condition, the optimum value of ρ to produce worst case performance was observed as a function of diversity with E_b/N_I as a parameter. It was determined that pulse noise jamming is most effective at higher values of E_b/N_I and that increasing the diversity order forces the jammer to a more continuous form of jamming. It was noticed that higher diversity orders than those considered would be required to render the pulse noise jammer ineffective for less severe fading conditions. This was observed for values of γ between 0 and 10. The noise and self-normalized receivers were compared for their performance in conditions of severe and moderate fading. For severe fading, it was found that there was a marked difference in performance; the noise-normalized receiver is superior to the self-normalized over the full range of signal-to-interference ratio. For moderate fading, this difference grew for higher signal-to-interference ratios. Noncoherent combining losses were lesser in magnitude and occurred over a smaller range of signal-to-interference ratios for the noise-normalized receiver compared to the self-normalized receiver for both cases of severe and moderate fading.

The performance of the noise-normalized receiver with non-ideal noise-normalization was analyzed. It was seen that if one is willing to accept a slight degradation in performance, relatively crude measurement techniques may be utilized. This makes the noise-normalized receiver a practical as well as effective receiver in pulse-jammed environments. The worst case performance of the noise-normalized and self-normalized receivers were compared to the linear receiver. It was determined that the performance of the noise-normalized receiver was superior to that of the linear receiver for severe and moderate fading. The superiority was quite significant in the case of moderate fading with performance differences as much as 25 dB observed. The performance of the self-normalized receiver was seen to perform better than the linear receiver for severe fading for a limited range of signal-to-interference ratios. The performance difference was significantly less than that observed for the noise-normalized receiver. For moderate fading, the self-normalized

receiver demonstrated superior performance to that of the linear receiver over the full range of signal-to-interference ratios considered. The performance difference was less than that observed for the noise-normalized receiver.

IV. DS-DPSK WITH FIRST ORDER POST-DETECTION SELECTION COMBINING IN A FADING CHANNEL

In this chapter, the performance of DS-DPSK with first order post-detection selection combining (PDSC) in a Rician fading channel in the presence of pulsed noise interference and additive white Gaussian noise (AWGN) is considered. Consider the receiver structure of Figure 4.1 where M attenuated and delayed replicas of the DS-DPSK transmitted signal, denoted $r_k(t)$, k=1,2,....M, are received over M antennas. It is assumed that the antennas are spaced sufficiently far apart such that the resolvable multipath components in the signal have significantly different propagation delays at the antennas, providing M independently fading replicas of the DS-DPSK signal. Usually a separation of at least 10 signal wavelengths is required between two antennas in order to obtain signals that fade independently. This type of diversity is termed *spatial diversity.*

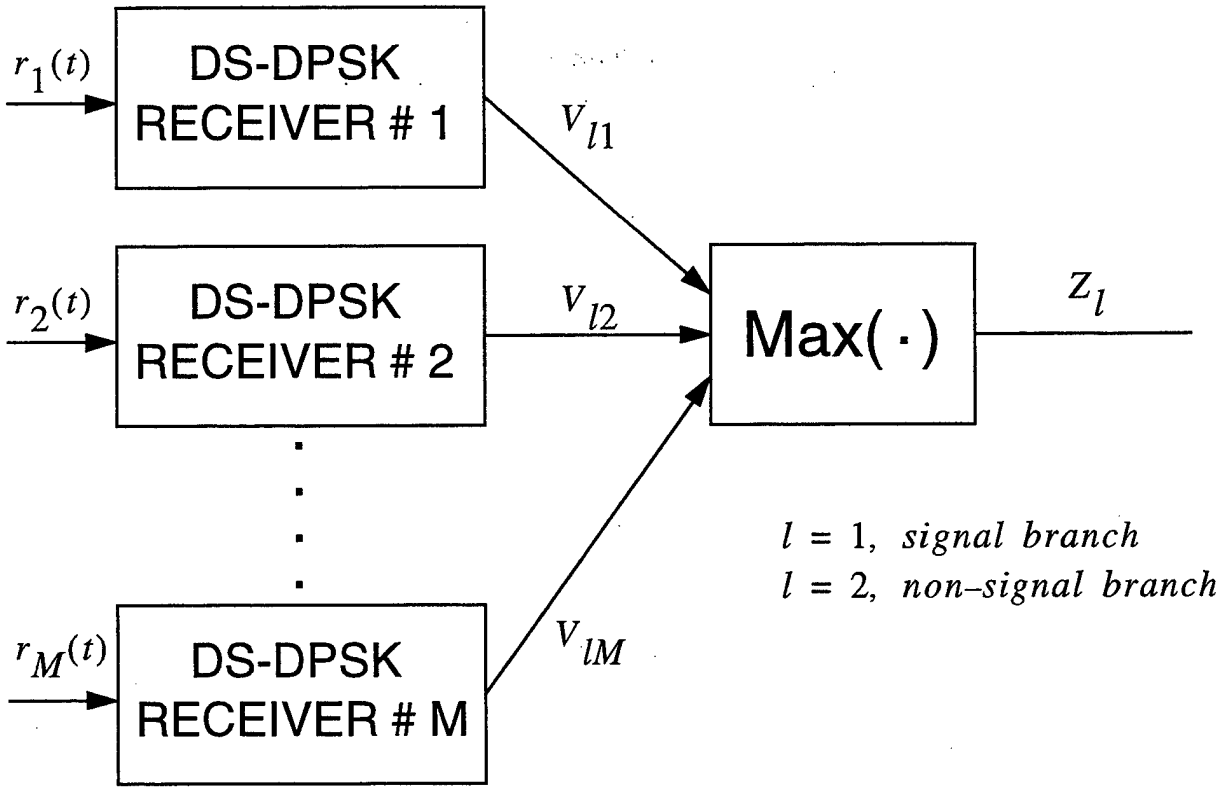

Figure 4.1: First order PDSC receiver.

With PDSC, the N largest outputs ($N < M$) are weighted equally and summed to produce the output decision variable Z_l. The receiver of Figure 4.1 is a first order combiner since it sets N = 1 (PDSC1). Equal gain combining (EGC) receivers, such as the self-normalized, noise-normalized and linear receivers, set N = M. It is assumed that the average received signal energy at the k^{th} antenna, denoted E_M, is identical at each of the M antennas. The output of a PDSC1 receiver then represents $(1/M)^{th}$ of the total recoverable signal energy ($E_M = E_b/M$) while the output of an EGC receiver represents the total recoverable signal energy.

Although PDSC receivers recover only a fraction of the total signal energy, they have several advantages over EGC receivers. First, PDSC receiver performance is *path independent.* To illustrate this, consider a scenario where one or more of the receive antennas are rendered inoperable. The corresponding receivers then contribute noise only to both the signal and non-signal branches. With EGC receivers, these noise branches contribute to the decision process where PDSC receivers would typically ignore these branches since they choose only the branches with the largest magnitudes. In such cases, the PDSC receiver would experience a more graceful performance degradation in comparison to the EGC receiver. Even with all antennas operable, the EGC receiver assumes that the spacing in between antennas is on the order of the delay between resolvable multipath components. Such may not be the case in reality since the terrain features of a particular geolocation dictate antenna spacing and the time delay between multipath arrivals may change over time. The result is that PDSC receivers suffer less deleterious effects due to noncoherent combining losses than do EGC receivers. In the case of N = 1, noncoherent combining losses do not exist at all. In addition to performance degradation due to noncoherent combining losses, EGC receiver complexity is *path dependent* since the number of receiver branches is assumed to be equal to the number of resolvable multipath components. The number of resolvable multipath components may vary with time and depends on geolocation. PDSC receiver complexity is the same regardless of time or location.

For the analysis undertaken here, the receiver performance of Figure 4.1 (PDSC1) over a Rician fading channel in the presence of pulse noise interference and AWGN is considered. The same jammer model is assumed as before except that since the diversity is now spatial instead of time. Assuming each of the M antennas experience the same level of jammer energy at any given

point in time, the probability density function for the pulse noise interference now has the following form:

$$\Pr(I_j) = \begin{cases} \rho_1, & case\ I_1 \\ \rho_2, & case\ I_2 \\ (1-\rho_1-\rho_2), & case\ I_3 \end{cases} \tag{4.1}$$

The rest of this chapter is structured as follows. The PDSC1 receiver performance over a Rayleigh fading channel is first considered since it provides an analytical solution for the conditional probability of bit error. The performance over a Rician fading channel is then considered in the sequel.

A. PERFORMANCE ANALYSIS OF DS-DPSK WITH FIRST ORDER POST-DETECTION SELECTION COMBINING OVER A RAYLEIGH FADING CHANNEL

1. Bit Error Probability for Rayleigh Fading Channel

The distribution for the random variable Z_l are now considered. The probability density function for the random variable Z_l can be determined from the following relation,

$$\Pr(z_l \le Z_l \le z_l + dz_l) = f_{Z_l}(z_l)dz_l \tag{4.2}$$

Expanding in terms of V_{lk}, $k = 1,2,....M$ gives

$$\Pr[z_l \le Z_l \le z_l + dz_l] = \Pr\left[(z_l \le V_{l1} \le z_l + dz_l) \bigcap_{i=2}^{M} V_{li} < z_l\right] \cup$$

$$\Pr\left[(z_l \le V_{l2} \le z_l + dz_l) \bigcap_{\substack{i=1 \\ i \ne 2}}^{M} V_{li} < z_l\right] \cup \ldots \cup \Pr\left[(z_l \le V_{lM} \le z_l + dz_l) \bigcap_{i=1}^{M-1} V_{li} < z_l\right] \tag{4.3}$$

Since the random variables V_{lk}, $k = 1,2,....M$, are assumed independent and identically distributed (iid), equation 4.3 becomes

$$\Pr(z_l \le Z_l \le z_l + dz_l) = \mathrm{M}\ \Pr\left[(z_l \le V_{lk} \le z_l + dz_l) \bigcap_{\substack{i=1 \\ i \ne k}}^{\mathrm{M}} V_{li} < z_l\right] \tag{4.4}$$

which can be expressed as

$$\Pr(z_l \le Z_l \le z_l + dz_l) = \mathrm{M} f_{V_{lk}}(z_l) dz_l \prod_{\substack{i=1 \\ i \ne k}}^{\mathrm{M}} F_{V_{li}}(z_l) \tag{4.5}$$

where $F_{V_{li}}(z_l)$ is the cumulative distribution function for the random variable V_{li}. The iid assumption further lets us simplify equation 4.5 to

$$\Pr(z_l \le Z_l \le z_l + dz_l) = \mathrm{M} f_{V_{lk}}(z_l) dz_l F_{V_{li}}^{(\mathrm{M}-1)}(z_l) \tag{4.6}$$

Comparing with equation 4.2, the probability density function for the random variable Z_l is

$$f_{Z_l}(z_l) = \mathrm{M} f_{V_{lk}}(z_l) F_{V_{li}}^{(\mathrm{M}-1)}(z_l) \tag{4.7}$$

The general form for the probability density function of Z_l for the N^{th} largest of M receiver outputs is

$$f_{Z_l}(z_l) = \frac{\mathrm{M}!}{(\mathrm{N}-1)!(\mathrm{M}-\mathrm{N})!} f_{V_{lk}}(z_l) F_{V_{li}}^{(\mathrm{N}-1)}(z_l)[1 - F_{V_{li}}(z_l)]^{(\mathrm{M}-\mathrm{N})} \tag{4.8}$$

Equations of this form provide the N^{th} order statistic for the random variable Z_l. A derivation of equation 4.8 may be found in [22].

The signal branch ($l = 1$) conditional probability density function may be obtained for the case of Rayleigh fading by setting $\alpha = 0$ and $v_{1k} = z_1$ in equation 3.1; the result is:

$$f_{V_{1k}}(z_1 | 0, \mathrm{I}_j) = \frac{1}{2\sigma_{1_j}^2} \exp\left(-\frac{z_1}{2\sigma_{1_j}^2}\right) u(z_1) \tag{4.9}$$

The conditional cumulative density function for the signal branch is given as

$$F_{V_{1k}}(z_1 | 0, \mathrm{I}_j) = \int_0^{z_1} f_{V_{1k}}(\lambda | 0, \mathrm{I}_j) d\lambda \tag{4.10}$$

Substituting equation 4.9 into 4.10 and carrying out the integration yields

$$F_{V_{1k}}(z_1|0, \mathrm{I}_j) = 1 - \exp\left(-\frac{z_1}{2\sigma_{1_j}^2}\right) \tag{4.11}$$

Substituting equations 4.9 and 4.11 into equation 4.7 produces the conditional probability density function for the random variable Z_1,

$$f_{Z_1}(z_1|0, \mathrm{I}_j) = \frac{\mathrm{M}}{2\sigma_{1_j}^2}\exp\left(-\frac{z_1}{2\sigma_{1_j}^2}\right)\left[1 - \exp\left(-\frac{z_1}{2\sigma_{1_j}^2}\right)\right]^{\mathrm{M}-1} u(z_1) \tag{4.12}$$

The conditional probability density function for the non-signal branch ($l = 2$) may be determined from equation 4.12 by setting $\sigma_{1_j}^2 = \sigma_{2_j}^2$ and $z_1 = z_2$; the result is:

$$f_{Z_2}(z_2|0, \mathrm{I}_j) = \frac{\mathrm{M}}{2\sigma_{2_j}^2}\exp\left(-\frac{z_2}{2\sigma_{2_j}^2}\right)\left[1 - \exp\left(-\frac{z_2}{2\sigma_{2_j}^2}\right)\right]^{\mathrm{M}-1} u(z_2) \tag{4.13}$$

The conditional probability of bit error equal to $\Pr(z_1 < z_2|0, \mathrm{I}_j)$ is derived in Appendix C, section C.1 and is given as

$$\mathrm{P_b}(\Gamma_{\mathrm{M}}|0, \mathrm{I}_j) = \sum_{p=0}^{\mathrm{M}-1}\sum_{r=0}^{\mathrm{M}-1}(-1)^{(p+r)}\binom{\mathrm{M}}{p+1}\binom{\mathrm{M}}{r+1}\times \left[\frac{1}{1 + \dfrac{(1+r)(2+\Gamma_{\mathrm{M}})}{(1+p)\Gamma_{\mathrm{M}}}}\right] \tag{4.14}$$

where $\Gamma_{\mathrm{M}} = \left(\dfrac{\mathrm{E_M}}{\mathrm{N_0}}\right)^{-1} + \left(\dfrac{\mathrm{E_M}}{\sigma_{\mathrm{I}_j}^2}\right)^{-1}$.

The probability of bit error is then given by

$$\mathrm{P_b} = \sum_{j=1}^{3}\mathrm{P_b}(\Gamma_{\mathrm{M}}|0, \mathrm{I}_j)\Pr(\mathrm{I}_j) \tag{4.15}$$

This last expression must be evaluated numerically.

2. Numerical Results for Rayleigh Fading Channel

In this section, the numerical results for the performance of the PDSC1 receiver over a Rayleigh fading channel when the jammer has a fixed peak power specification (fixed ρ) and for worst case jamming are presented. Figure 4.2 shows the performance curves of the PDSC1 receiver for $E_b/N_0 = 15$ dB, a diversity of $M = 4$ and $\rho = 0.05$ with β as a parameter. Note

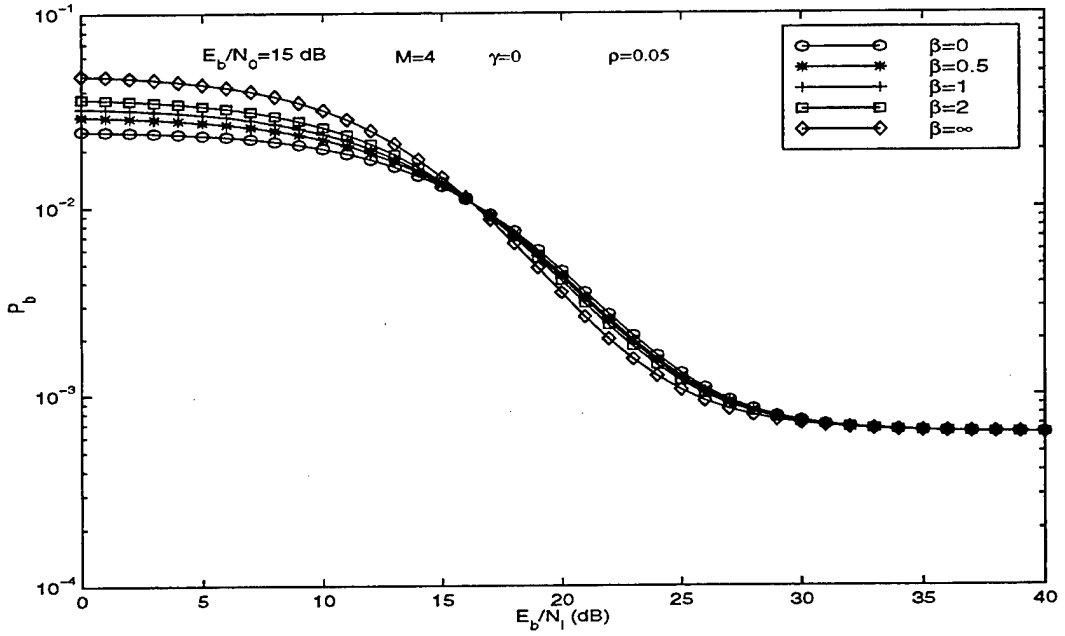

Figure 4.2: Performance of PDSC1 receiver for $E_b/N_0 = 15$ dB, a diversity of $M = 4$, $\gamma = 0$ and $\rho = 0.05$ with β as a parameter.

that for $E_b/N_I < 17$ dB, $\beta = \infty$ produces the worst performance. Above this value, $\beta = 0$ produces the worst performance. This is in contrast to the self-normalized and noise-normalized receivers where $\beta = \infty$ produces the worst performance for the full range of E_b/N_I. Figure 4.3 shows the performance curves of the PDSC1 receiver for $E_b/N_0 = 15$ dB, a diversity of $M = 4$ and $\rho = 0.5$ with β as a parameter. In this case $\beta = \infty$ produces the worst performance only for $E_b/N_I < 6$ dB with $\beta = 0$ producing the worst performance above this value. For low signal-to-interference ratios ($E_b/N_I < 10$ dB), the performance difference between the $\beta = 0$ and $\beta = \infty$ cases is at most 5 dB. This difference is substantially greater for the case of $\rho = 0.05$.

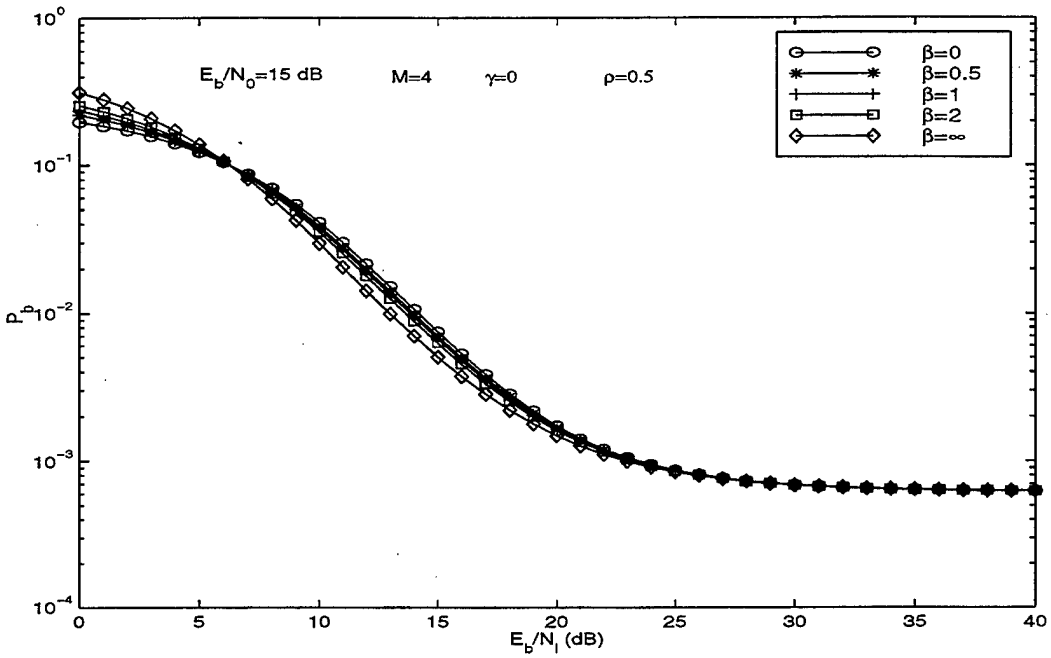

Figure 4.3: Performance of PDSC1 receiver for $E_b/N_0 = 15$ dB, a diversity of $M = 4$, $\gamma = 0$ and $\rho = 0.5$ with β as a parameter.

The worst case performance of the PDSC1 receiver over a Rayleigh channel is now considered. Worst case performance was determined through numerical search where it was determined that the worst case values of ρ for a particular value of E_b/N_I followed according to equations 2.30 and 2.31. The value of $\beta = 0$ has been selected for ease of comparison to the other receivers. Figures 4.4-4.6 show the performance curves of the PDSC1 receiver for diversity orders $M = 1,3,4$, $\rho = 0.01, 0.1, 0.25, 1$ and worst case performance and $E_b/N_0 = 15$ dB respectively. If Figure 4.4 ($M = 1$) is compared to Figures 2.14 and 3.9 ($L = 1$), it can be seen that the PDSC1 receiver produces identical performance to that of both the self-normalized and noise-normalized receivers. Again this is not surprising since the SNR at the outputs of all receivers is the same. It is also seen that for one antenna/no diversity ($M = 1$), pulse noise jamming is not effective since the worst case performance curve coincides with the continuous jamming curve. For $M = 3$ and $M = 4$, performance degradation due to pulse noise jamming is evident since the worst case performance curve is above the continuous jamming curve. The pulse noise jammer is seen to be

most effective in the range 10 dB < E_b/N_I < 30 dB. Figure 4.7 shows the worst case performance curves of the PDSC1 receiver in the presence of pulse noise interference for diversity orders M = 1 - 6, E_b/N_0 = 15 dB and $\gamma = 0$. It is seen that for relatively high signal-to-interference ratios (E_b/N_I > 25 dB), there is performance improvement for any increase in diversity order. For diversity orders higher than M = 3, the performance improvement is not as substantial and decreases for increasing diversity order. For E_b/N_I < 15 dB, increasing diversity order above M = 3 leads to a slight performance degradation. Below E_b/N_I = 5 dB, slight performance degradation occurs for any increase of diversity order. Figure 4.8 shows a worst case performance comparison between the self-normalized, noise-normalized, linear receivers (employing time diversity) and the PDSC1 receiver in the presence of pulse noise interference for diversity orders L = 1,4, M=1,4 (PDSC1), E_b/N_0 = 15 dB and $\gamma = 0$. It is seen that the PDSC1 receiver performance is comparable to (and slightly better than) the performance of the linear receiver for E_b/N_I < 25 dB. Above this value where the pulse noise jammer is less effective, the linear receiver outperforms the PDSC1 receiver. It is observed that the self-normalized receiver provides better performance against pulse noise jamming in the range 10 dB < E_b/N_I < 25 dB. It is seen that in the Rayleigh limit of high signal-to-interference ratio, the PDSC1 receiver performs better than the self-normalized receiver. The performance of all receivers at very low signal-to-interference ratios is very similar. For E_b/N_I > 5 dB, the noise-normalized receiver clearly is superior to all other receivers. Figure 4.9 plots the optimum value of ρ as a function of diversity order with E_b/N_0 = 15 dB, $\gamma = 0$ and E_b/N_I as a parameter. It is seen that increasing diversity order higher than M = 2 for a fixed value of E_b/N_I does not force the jammer to a more continuous strategy, since the optimum value of ρ remains constant.

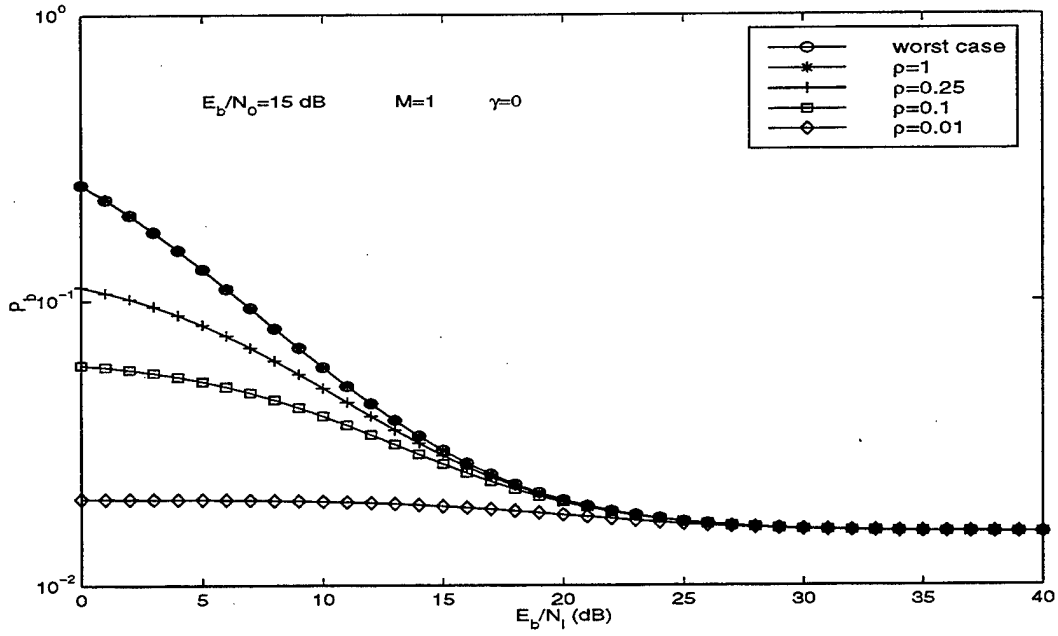

Figure 4.4: Performance of PDSC1 receiver for pulse jamming fractions $\rho = 1, 0.25, 0.1, 0.01$ and worst case for diversity order $M = 1$, $E_b/N_0 = 15$ dB and $\gamma = 0$.

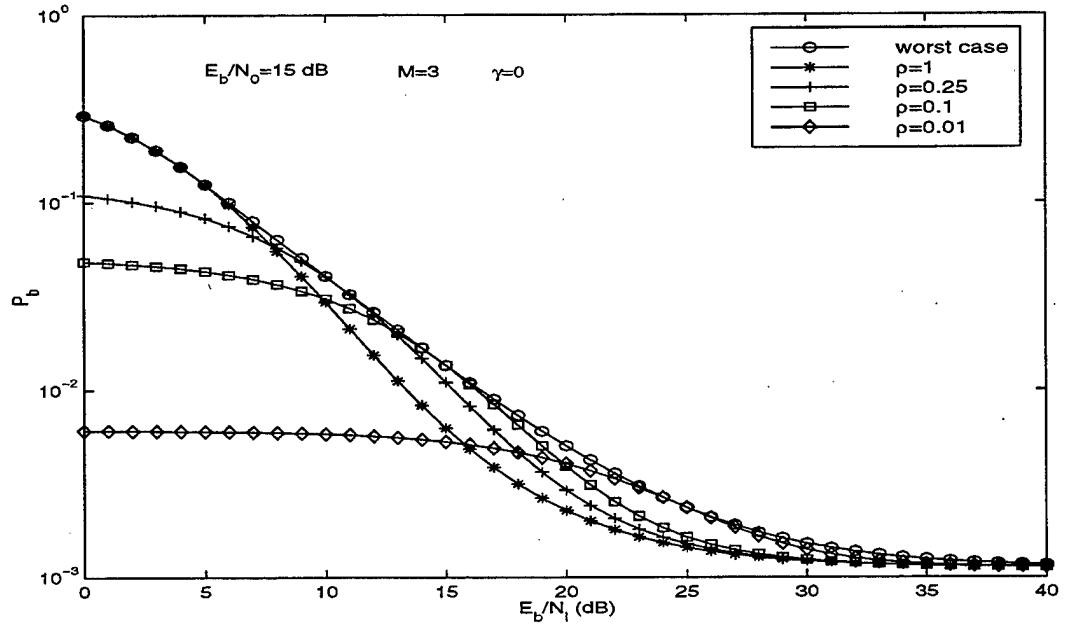

Figure 4.5: Performance of PDSC1 receiver for pulse jamming fractions $\rho = 1, 0.25, 0.1, 0.01$ and worst case for diversity order $M = 3$, $E_b/N_0 = 15$ dB and $\gamma = 0$.

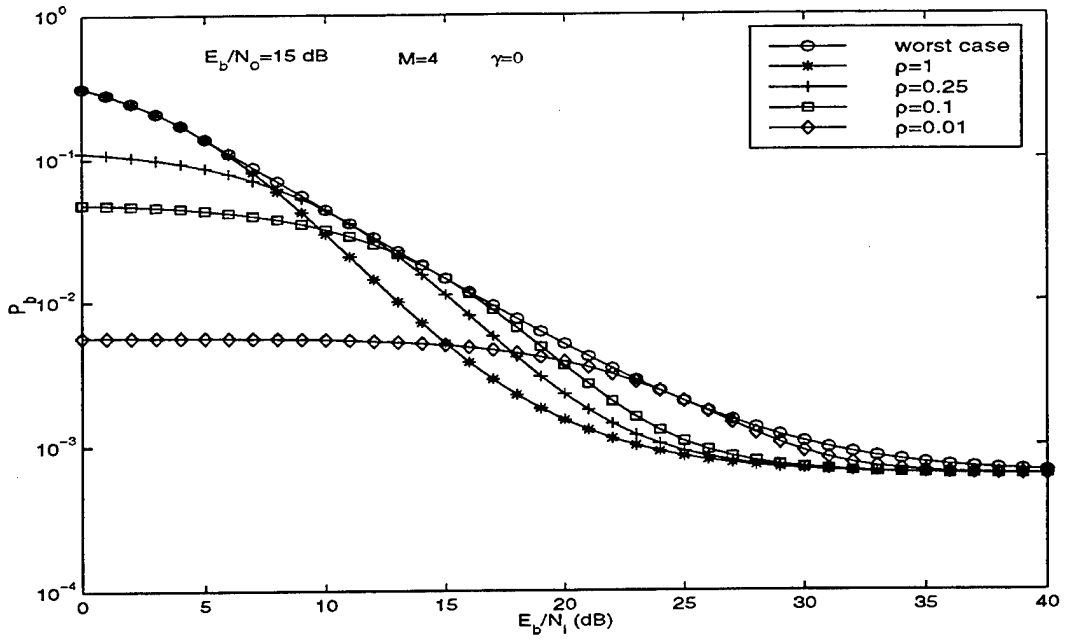

Figure 4.6: Performance of PDSC1 receiver for pulse jamming fractions $\rho = 1, 0.25, 0.1, 0.01$ and worst case for diversity order $M = 4$, $E_b/N_0 = 15$ dB and $\gamma = 0$.

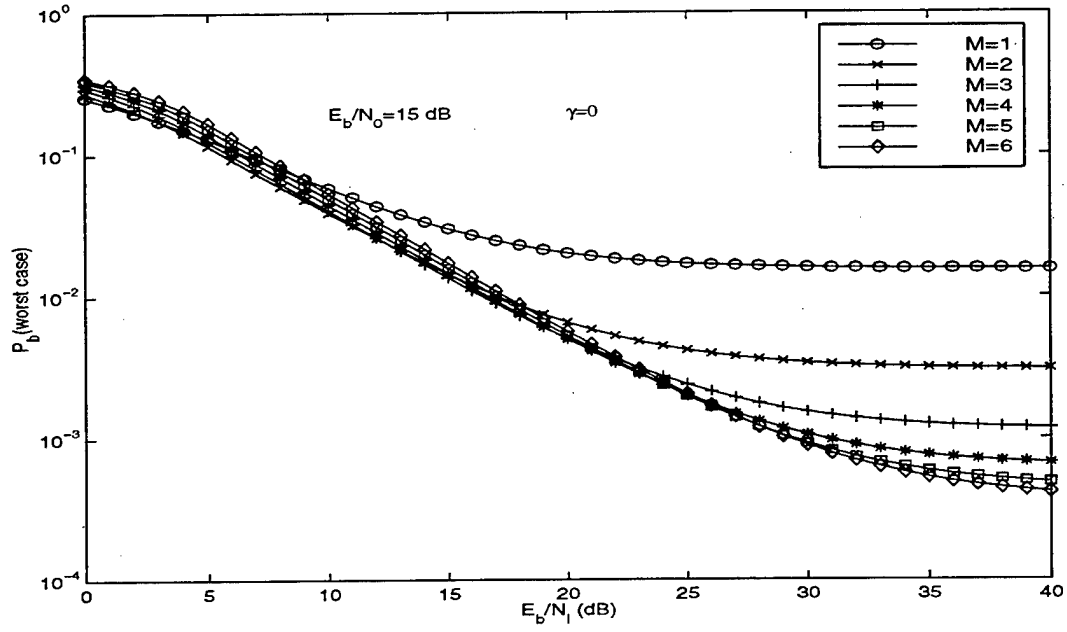

Figure 4.7: Worst case performance of PDSC1 receiver in presence of pulse noise interference for diversity orders M = 1-6, $E_b/N_0 = 15$ dB and $\gamma = 0$.

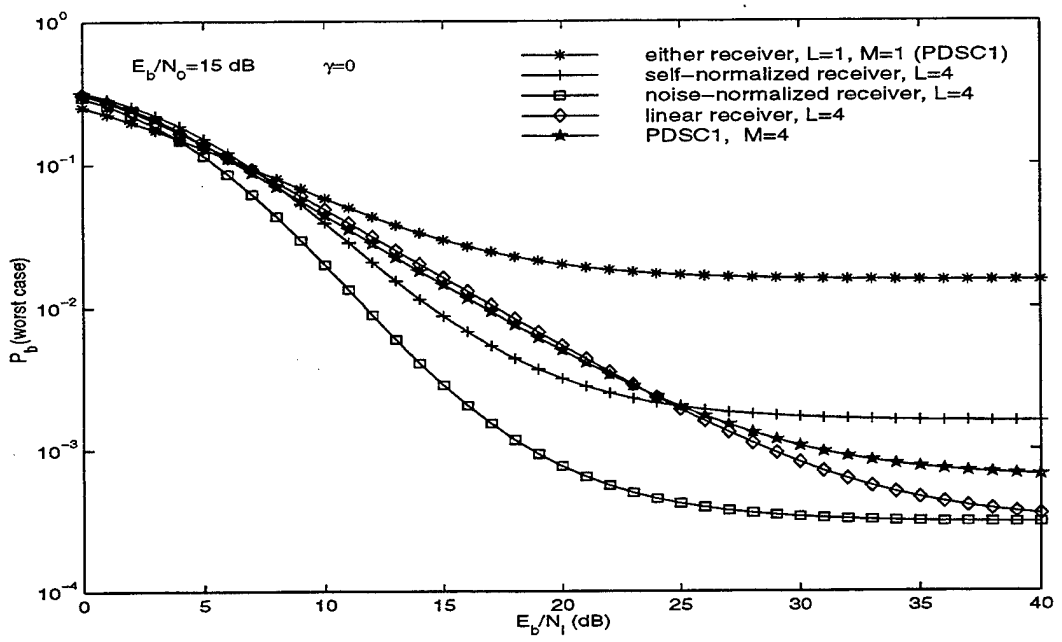

Figure 4.8: Worst case performance comparison between self-normalized, noise-normalized, linear and PDSC1 receivers in the presence of pulse noise interference for diversity orders L = 1,4, M=1,4 (PDSC1), E_b/N_0 = 15 dB and $\gamma = 0$.

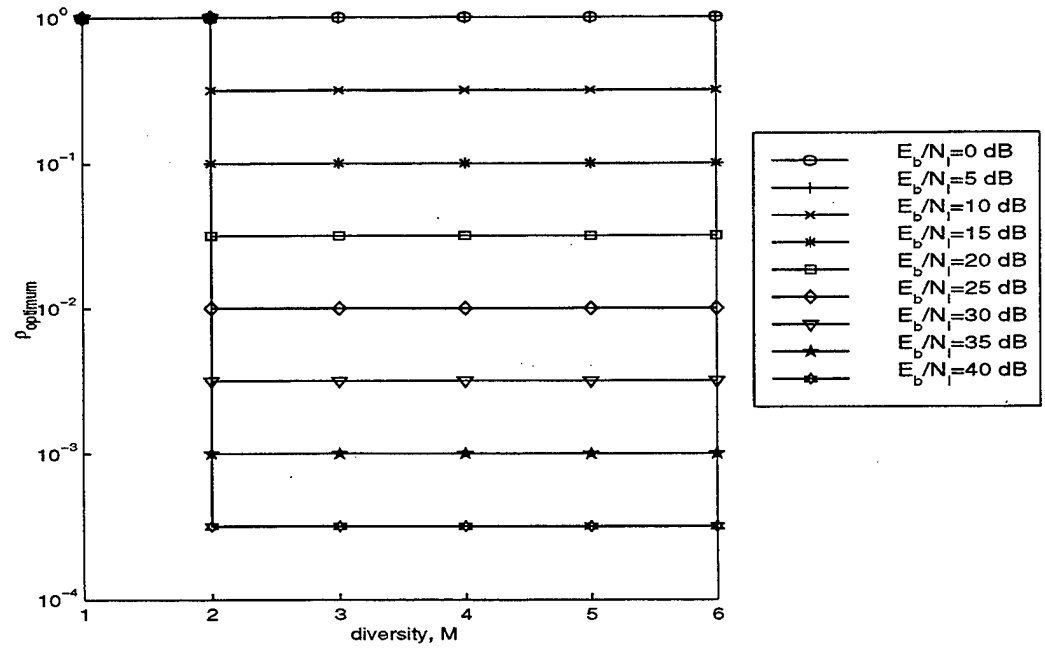

Figure 4.9: Optimum value of ρ as a function of diversity order with E_b/N_0 = 15 dB, $\gamma = 0$ and E_b/N_I as a parameter.

The performance of the PDSC1 receiver for the more general case of the Rician channel is now investigated. In the next section, the expression for the probability of bit error is derived followed by numerical results presented in the sequel.

B. PERFORMANCE ANALYSIS OF DS-DPSK WITH FIRST ORDER POST-DETECTION SELECTION COMBINING OVER A RICIAN FADING CHANNEL

1. Bit Error Probability for Rician Fading Channel

The form of the probability density function for random variable Z_1 is given is equation 4.8 with $l = 1$. The signal branch conditional probability density function for the Rician channel may be obtained by setting $v_{1k} = z_1$ in equation 3.1 and written as

$$f_{V_{1k}}(z_1|0, \mathrm{I}_j) = \frac{1}{2\sigma_{1_j}^2}\exp\left(-\frac{1}{2\sigma_{1_j}^2}(z_1 + 4\alpha^2)\right)\mathrm{I}_0\left(\frac{2\alpha\sqrt{z_1}}{\sigma_{1_j}^2}\right)u(z_1) \tag{4.16}$$

The conditional cumulative density function for the signal branch is given as

$$F_{V_{1k}}(z_1|0, \mathrm{I}_j) = \int_0^{z_1} f_{V_{1k}}(\lambda|0, \mathrm{I}_j)d\lambda \tag{4.17}$$

Substituting equation 4.16 into 4.17 and carrying out the integration yields

$$F_{V_{1k}}(z_1|0, \mathrm{I}_j) = 1 - Q\left(\frac{2\alpha}{\sigma_{1_j}}, \frac{\sqrt{z_1}}{\sigma_{1_j}}\right) \tag{4.18}$$

where $Q(a, b)$ is Marcum's Q-function. A derivation of equation 4.18 is given in Appendix C, section C.2. Substituting equations 4.16 and 4.18 into equation 4.8 for $l = 1$ gives the conditional probability density function for the random variable Z_1,

$$f_{Z_1}(z_1|0, \mathrm{I}_j) = \frac{\mathrm{M}}{2\sigma_{1_j}^2}\exp\left(-\frac{1}{2\sigma_{1_j}^2}(z_1 + 4\alpha^2)\right)\mathrm{I}_0\left(\frac{2\alpha\sqrt{z_1}}{\sigma_{1_j}^2}\right)\times$$

$$\left[1 - Q\left(\frac{2\alpha}{\sigma_{1_j}}, \frac{\sqrt{z_1}}{\sigma_{1_j}}\right)\right]^{\mathrm{M}-1} u(z_1) \tag{4.19}$$

From equation 4.13, the conditional probability density function for the random variable Z_2 is

$$f_{Z_2}(z_2|0, I_j) = \frac{M}{2\sigma_{2_j}^2}\exp\left(-\frac{z_2}{2\sigma_{2_j}^2}\right)\left[1-\exp\left(-\frac{z_2}{2\sigma_{2_j}^2}\right)\right]^{M-1} u(z_2) \qquad (4.20)$$

The conditional probability of bit error equal to $\Pr(z_1 < z_2|0, I_j)$ is derived in Appendix C, section C.3 and is given by

$$P_b(u|0, I_j) = \frac{M(\gamma+1)}{2(2+(\gamma+1)\Gamma_M)}\sum_{r=0}^{M-1}\binom{M}{r+1}(-1)^r\exp\left(-\frac{2\gamma}{2+(\gamma+1)\Gamma_M}\right) \times$$

$$\int_0^\infty \exp\left(-\frac{u}{2}\left[\frac{2(1+r)+(2+r)(\gamma+1)\Gamma_M}{(2+(\gamma+1)\Gamma_M)}\right]\right) I_0\left(\sqrt{\frac{4(\gamma+1)\gamma u}{(2+(\gamma+1)\Gamma_M)^2}}\right)\times$$

$$\left[1-Q\left(\sqrt{\frac{4\gamma}{2+(\gamma+1)\Gamma_M}}, \sqrt{\frac{u(\gamma+1)}{2+(\gamma+1)\Gamma_M}}\right)\right]^{M-1} du \qquad (4.21)$$

Equation 4.21 must be solved numerically. The recursive algorithm described in [23] can be used for the computation of Marcum's Q-function. The probability of bit error is then given by

$$P_b = \sum_{j=1}^{3} P_b(u|0, I_j)\Pr(I_j) \qquad (4.22)$$

This last expression must also be evaluated numerically.

2. Numerical Results for Rician Fading Channel

In this section, numerical results for the performance of the PDSC1 receiver over a Rician fading channel when the jammer has a fixed value of ρ and for worst case jamming are presented. Figure 4.10 shows the performance curves of the PDSC1 receiver for $E_b/N_0 = 15$ dB, $\gamma = 5$, a diversity of $M = 4$ and $\rho = 0.05$ with β as a parameter. Notice that for $E_b/N_I < 15$ dB, $\beta = \infty$ produces the worst performance. Above this value, $\beta = 0$ produces the worst performance. Figure 4.11 shows the performance curves of the PDSC1 receiver for $E_b/N_0 = 15$ dB,

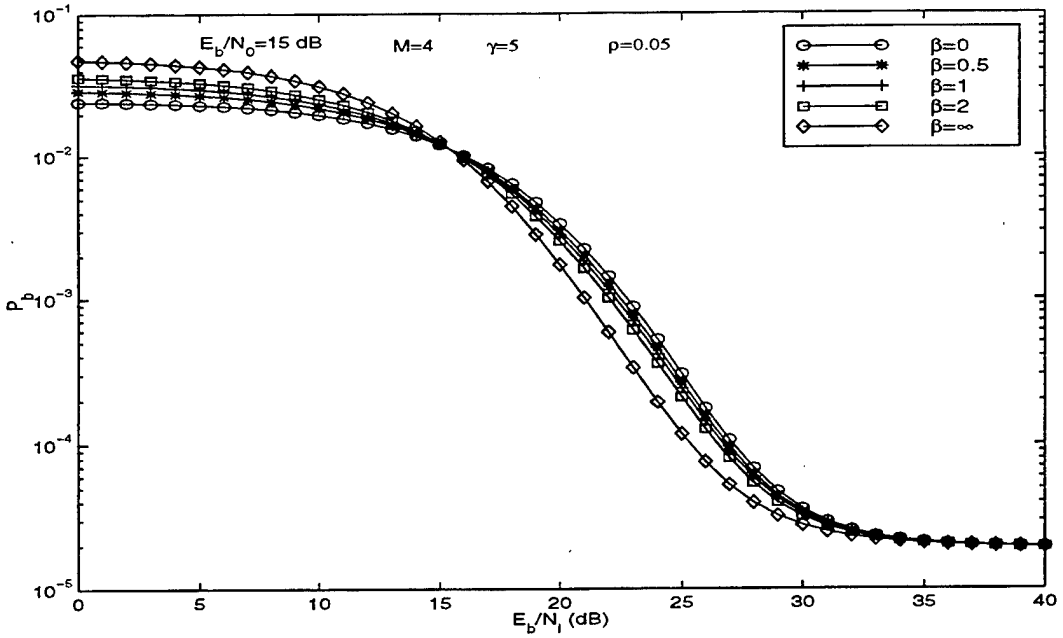

Figure 4.10: Performance of PDSC1 receiver for $E_b/N_0 = 15$ dB, a diversity of $M = 4$, $\gamma = 5$ and $\rho = 0.05$ with β as a parameter.

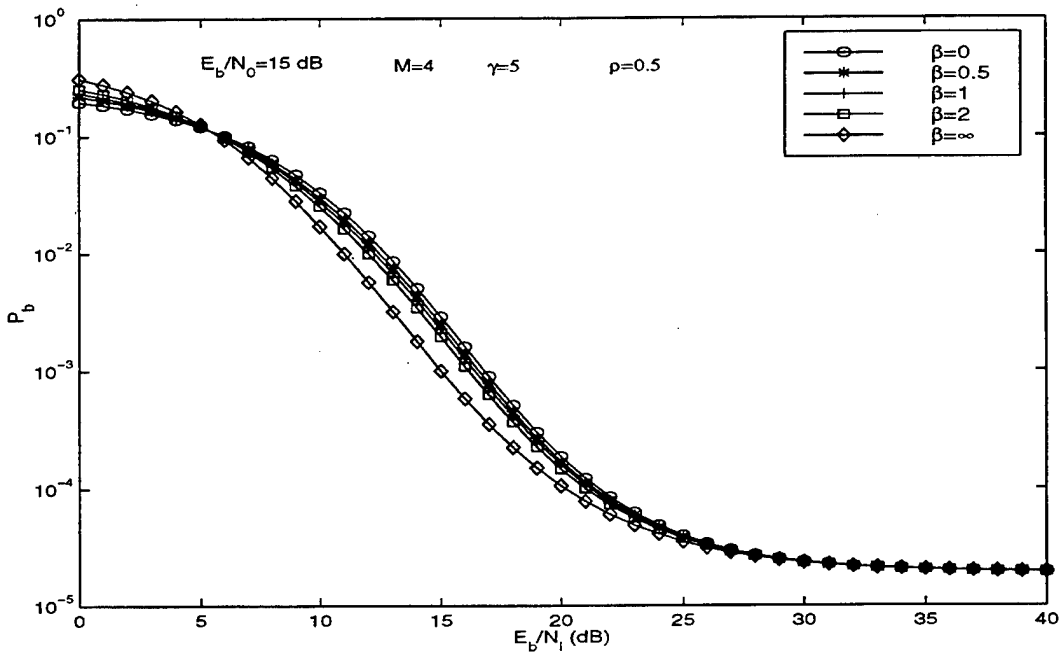

Figure 4.11: Performance of PDSC1 receiver for $E_b/N_0 = 15$ dB, a diversity of $M = 4$, $\gamma = 5$ and $\rho = 0.5$ with β as a parameter.

$\gamma = 5$, a diversity of M = 4 and $\rho = 0.5$ with β as a parameter. In this case $\beta = \infty$ produces the worst performance only for $E_b/N_I < 6$ dB with $\beta = 0$ producing the worst performance above this value. These results are similar to that observed for Rayleigh fading channel.

The worst case performance of the PDSC1 receiver is now considered. Worst case performance was determined through numerical search where it was determined that the worst case values of ρ for a particular value of E_b/N_I followed according to equations 2.30 and 2.31. The value of $\beta = 0$ has again been selected for ease of comparison to the other receivers. Figures 4.12-4.14 show the performance curves of the PDSC1 receiver for diversity orders M = 1,3,4, ρ = 0.01, 0.1, 0.25, 1 and worst case performance, $\gamma = 5$ and $E_b/N_0 = 15$ dB respectively. It is seen that there is significant performance degradation due to pulse noise jamming for all diversity cases considered. The degradation due to pulse jamming appears to increase for increasing diversity order since the separation between the worst case jamming curve and continuous jamming curve grows for higher diversity order. For example, the difference between the continuous and worst case performance curves in terms of BER for M = 1 and $E_b/N_I = 20$ dB is nearly half of an order of magnitude. For M = 4 and $E_b/N_I = 20$ dB, the difference is nearly 2 orders of magnitude, a 4 fold increase in performance degradation. In contrast, for the self-normalized and noise-normalized receivers, it was seen that performance degradation due to pulse noise jamming was diminished as diversity order was increased.

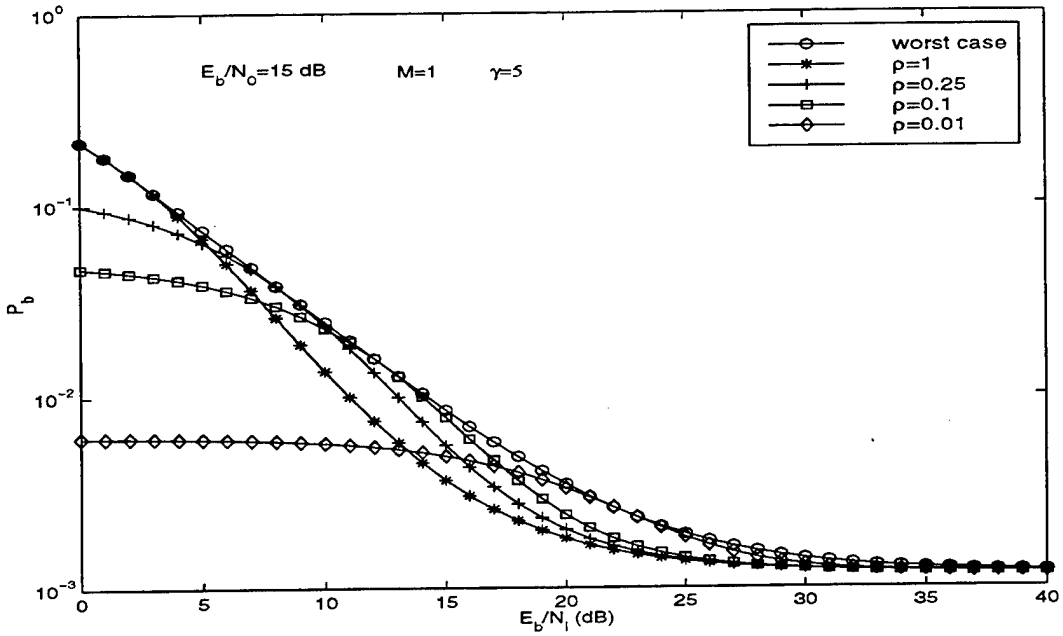

Figure 4.12: Performance of PDSC1 receiver for pulse jamming fractions $\rho = 1, 0.25, 0.1, 0.01$ and worst case for diversity order $M = 1$, $E_b/N_0 = 15$ dB and $\gamma = 5$.

Figure 4.15 shows the worst case performance curves of the PDSC1 receiver in the presence of pulse noise interference for diversity orders M = 1-6, $E_b/N_0 = 15$ dB and $\gamma = 5$. It is seen that for $E_b/N_I > 25$ dB, there is a significant performance improvement when moving from no diversity to a diversity of M = 2. Higher diversity order increases produce minimal change in performance. For $E_b/N_I < 20$ dB, increasing diversity order leads to a performance degradation. Figure 4.16 plots the worst case performance curves of the self-normalized, noise-normalized, linear receivers (employing time diversity) and the PDSC1 receiver in the presence of pulse noise interference for diversity orders L = 1,4, M=1,4 (PDSC1), $E_b/N_0 = 15$ dB and $\gamma = 5$. It is seen that the PDSC1 receiver has nearly identical performance to that of the linear receiver over the full range of signal-to-interference ratio. It is obvious that the PDSC1 receiver has some inherent advantages against degradation due to pulse noise jamming over the linear receiver since it produces the same performance utilizing one-fourth the signal energy available to the linear receiver. It is also seen that the self-normalized receiver performs better than the PDSC1 receiver over the full range of signal-to-interference ratios. This is in contrast to what was observed over the Rayleigh channel. The performance of the PDSC1 receiver for low signal-to-interference ratios is either the same or

slightly worse than that of the other receivers. Any improvements achieved against noncoherent combining losses in comparison to the other receivers at these low signal-to-interference ratios is not reflected in the performance curves.

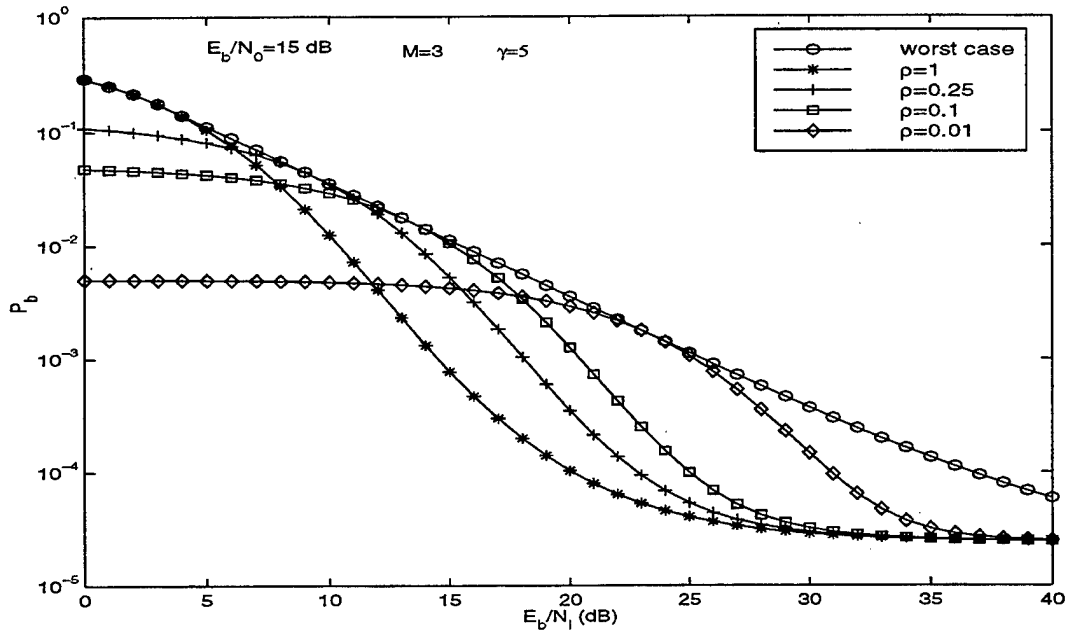

Figure 4.13: Performance of PDSC1 receiver for pulse jamming fractions $\rho = 1, 0.25, 0.1, 0.01$ and worst case for diversity order $M = 3$, $E_b/N_0 = 15$ dB and $\gamma = 5$.

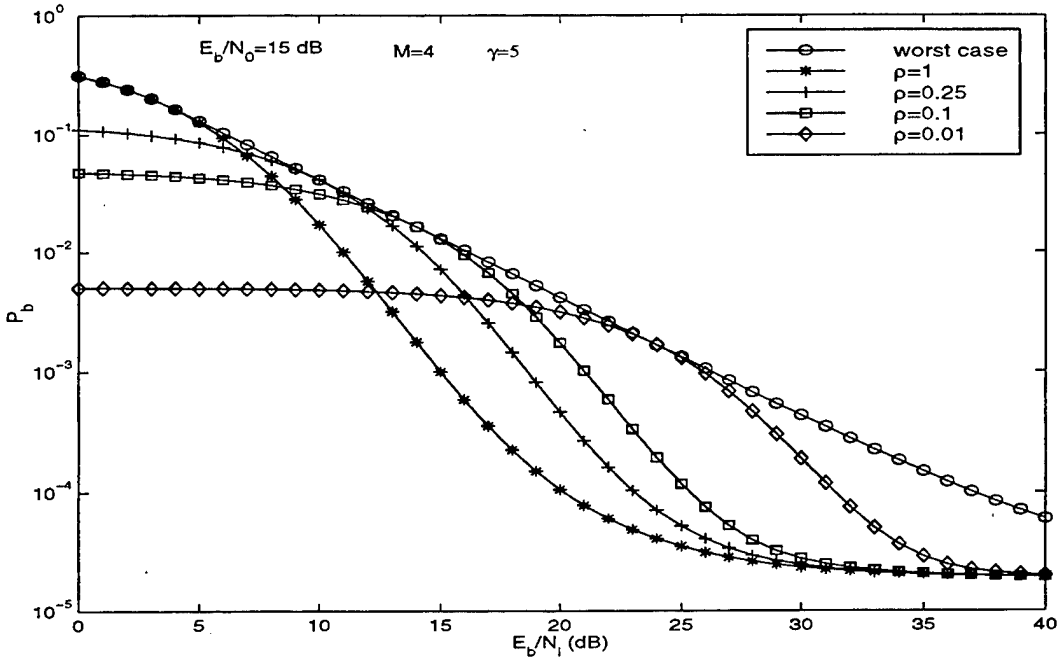

Figure 4.14: Performance of PDSC1 receiver for pulse jamming fractions $\rho = 1, 0.25, 0.1, 0.01$ and worst case for diversity order $M = 4$, $E_b/N_0 = 15$ dB and $\gamma = 5$.

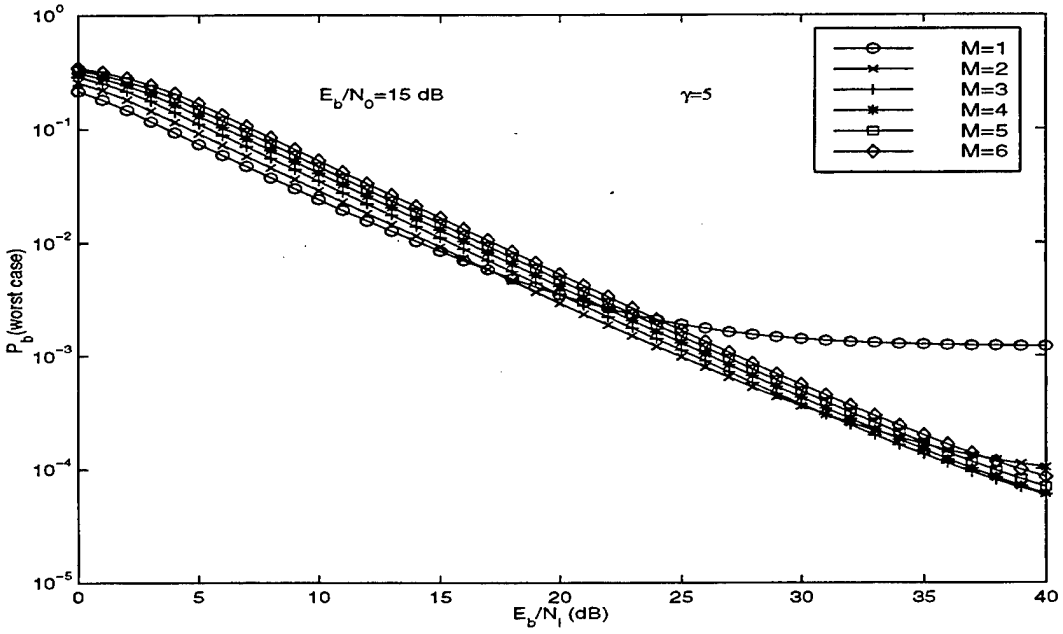

Figure 4.15: Worst case performance of PDSC1 receiver in presence of pulse noise interference for diversity orders $M = 1$-6, $E_b/N_0 = 15$ dB and $\gamma = 5$.

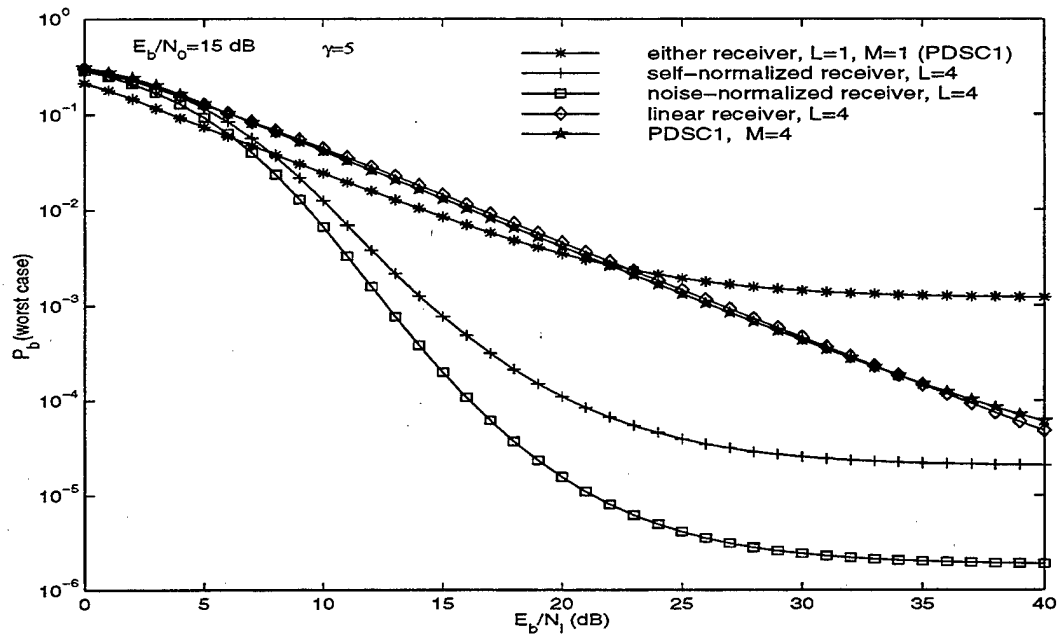

Figure 4.16: Worst case performance comparison between self-normalized, noise-normalized, linear and PDSC1 receivers in the presence of pulse noise interference for diversity orders L = 1,4, M=1,4 (PDSC1), E_b/N_0 = 15 dB and γ = 5.

Figure 4.17 plots the optimum value of ρ as a function of diversity order with E_b/N_0 = 15 dB, γ = 5 and E_b/N_I as a parameter. In contrast to the Rayleigh channel, the PDSC1 receiver does in this measure reduce the effectiveness of the pulse noise jammer since the jammer is moved towards a more continuous jamming strategy as diversity order is increased. The overall effect however is not as dramatic as that observed for the self-normalized and noise-normalized receivers where diversity order increases produced larger increases in ρ (compare to Figures 2.22 and 3.19).

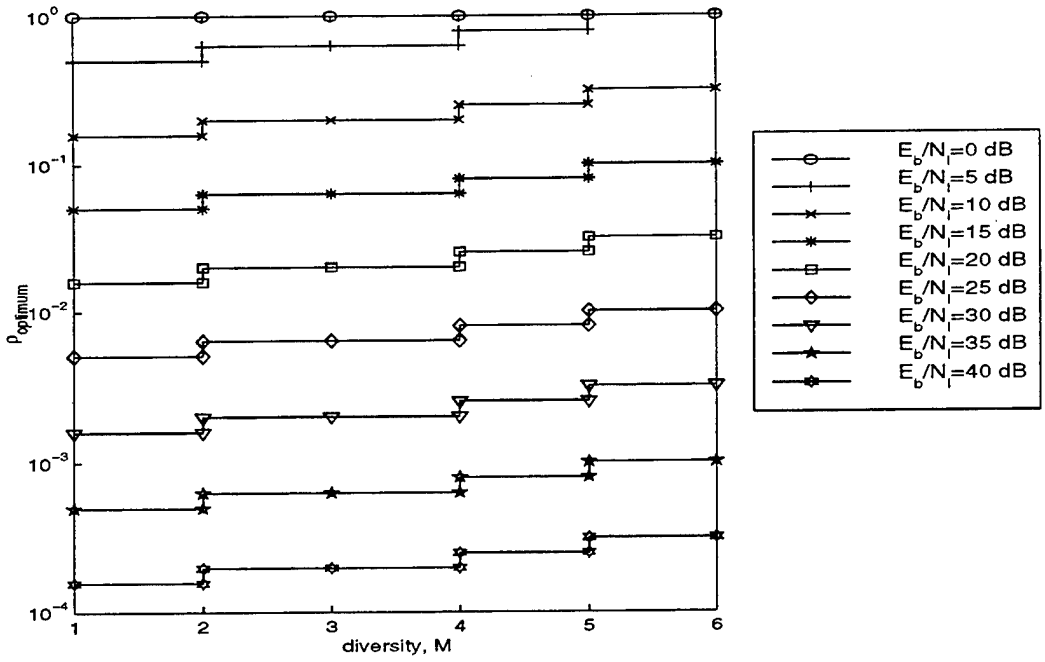

Figure 4.17: Optimum value of ρ as a function of diversity order with $E_b/N_0 = 15$ dB, $\gamma = 5$ and E_b/N_I as a parameter.

Figures 4.18 and 4.19 show the optimum value of ρ as a function of γ with diversity order as a parameter with $E_b/N_0 = 15$ dB for E_b/N_I equal to 20 dB and 30 dB respectively. It is seen in both cases that for a fixed γ ($\gamma > 3$), increasing diversity order through M = 5 moves the optimum value of ρ higher. Increasing diversity order from M = 5 to M = 6 has no further effect on the

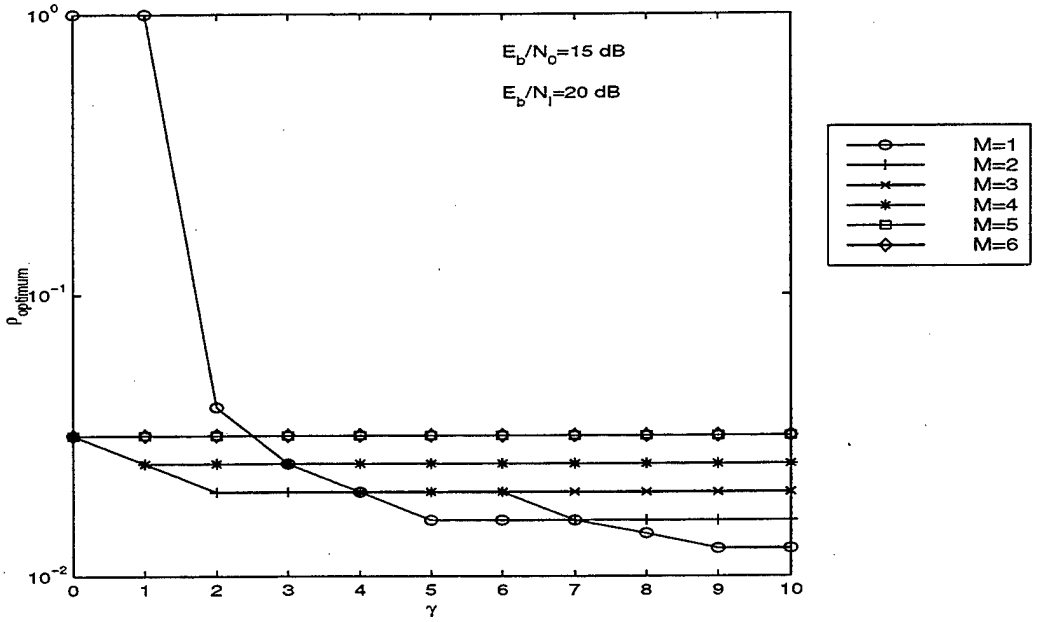

Figure 4.18: Optimum value of ρ as a function of γ with diversity order as a parameter for E_b/N_0 = 15 dB and E_b/N_I = 20 dB.

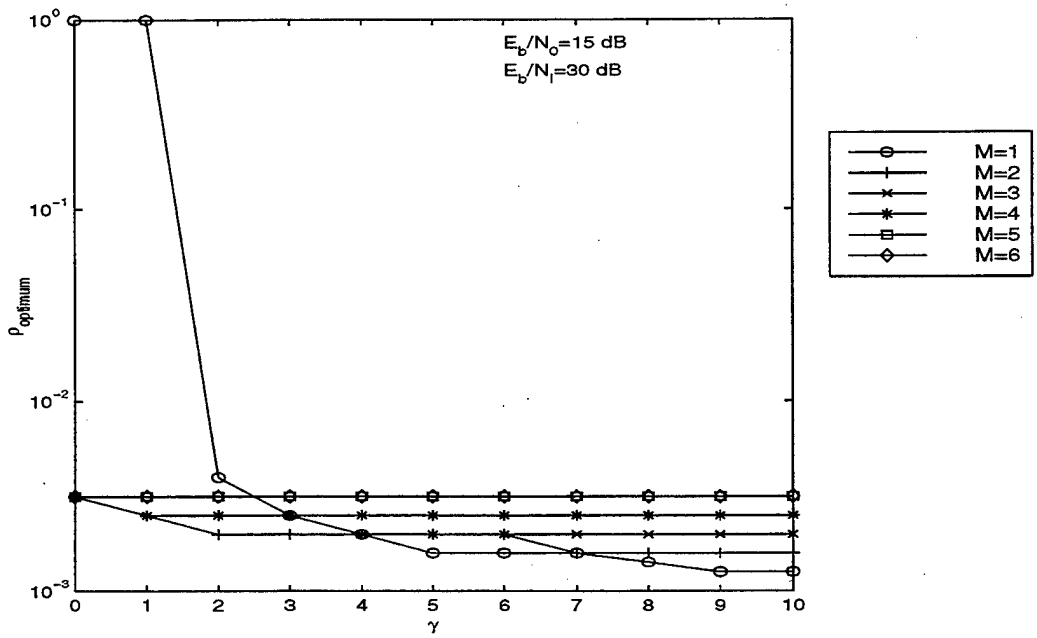

Figure 4.19: Optimum value of ρ as a function of γ with diversity order as a parameter for E_b/N_0 = 15 dB and E_b/N_I = 30 dB.

optimum value of ρ. This is in contrast to both the self-normalized and noise-normalized receivers where it was observed that the optimum value of ρ increased for all diversity order increases with $\gamma > 3$.

C. CHAPTER CONCLUSIONS

In this chapter, the performance of Direct Sequence Differential Phase Shift Keying (DS-DPSK) with first order post-detection selection combining (PDSC) in a Rician fading channel in the presence of pulsed noise interference and additive white Gaussian noise (AWGN) has been considered. The performance over a Rayleigh fading channel was considered separately since it provided an analytical solution for the conditional probability of bit error. In the case of the Rayleigh channel, for a very high peak power specification (ρ small), jamming alternating bits proved to be a more effective strategy than jamming adjacent bits for lower values of signal-to-interference ratios ($E_b/N_I < 17$ dB). For higher values of signal-to-interference ratio, jamming adjacent bits was shown to be most effective. For a lower peak power specification, jamming alternating bits proved to be the most effective jamming strategy but only over a smaller range of low signal-to-interference ratio. Similar results were observed for the case of moderate fading ($\gamma = 5$). For either the severe or moderate fading condition, it was observed that the PDSC1 receiver was not efficacious in mitigating pulse noise jamming. It was observed that the worst case performance curve did not move closer to the continuous jamming curve for increasing diversity order. In addition, the value of ρ remained constant for increasing diversity order over the Rayleigh channel and only increased slightly per increasing diversity order for the moderate fading condition. In general, the efficacy of the PDSC1 receiver against pulse noise jamming improved as the fading condition improved (higher γ).

For the Rayleigh channel it was observed that the worst case performance of the PDSC1 receiver was improved by increasing diversity order at higher values of signal-to-interference ratio. The amount of performance improvement between diversity orders was seen to decrease as diversity order was increased. The PDSC1 receiver demonstrated a slight performance degradation by increasing diversity order at lower values of signal-to-interference ratio. At the moderate fading level, performance improvement at high signal-to-interference ratio was significant between M = 1 and M = 2 with very little change for higher diversity orders. For the Rayleigh channel, it was

observed that where the pulse noise jammer was most effective, the performance of the PDSC1 receiver for M = 4 was comparable (and slightly better) to that of the linear receiver for L = 4. In the case of moderate fading, this result held true over the entire range of signal-to-interference ratios considered. It was also noticed that in the Rayleigh limit, the PDSC1 receiver outperformed the self-normalized receiver. In terms of noncoherent combining losses, any performance improvement in comparison to the other receivers was not apparent for both the severe and moderate fading cases.

V. DS-DPSK WITH FIRST ORDER POST-DETECTION SELECTION COMBINING AND L-FOLD TIME DIVERSITY IN A FADING CHANNEL

In this chapter, the performance of DS-DPSK with first order post-detection selection combining (PDSC1) and L-fold time diversity in a Rician fading channel in the presence of pulsed noise interference and additive white Gaussian noise (AWGN) is considered. Consider the receiver structure of Figure 5.1 where M attenuated and delayed replicas of the DS-DPSK transmitted signal, denoted $r_{kh}(t)$, k=1,2,....M, h= 1,2,....L are received over M antennas. The variables k and h represent the spatial and time indices respectively. The random variables V_{1h} and V_{2h} represent the PDSC1 receiver outputs for the signal and non-signal branch respectively. These random variables are then equally weighted and summed over the time index to produce the receiver outputs Z_1 and Z_2. It is noted that for a constant bit rate system, the received replicas $r_{kh}(t)$ represent $(1/ML)^{th}$ of the total recoverable signal energy ($E_{LM} = E_b/LM$) while the random variable Z_1 represents $(1/M)^{th}$ of the total recoverable signal energy. It is also noted that the special case of L = 1 produces the PDSC1 receiver while the case of M = 1 represents the linear receiver. It is also clear that this type of receiver has the same type of *path independence* as does the PDSC1 receiver since only 1 of M antennas are selected at any given point in time. In the next section, the expressions for the probability of bit error are derived.

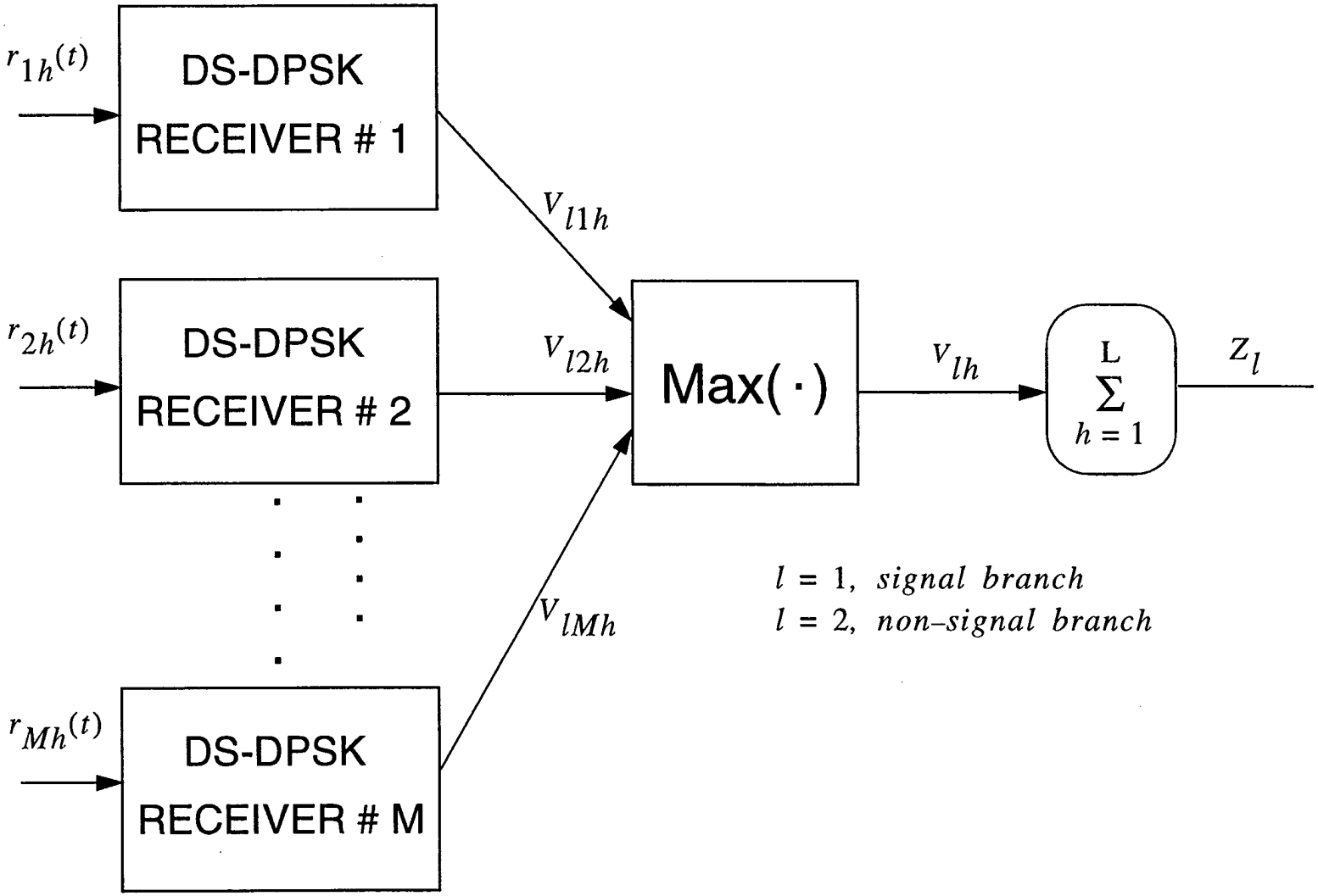

Figure 5.1: First Order PDSC receiver with L-fold time diversity.

A. BIT ERROR PROBABILITY

Considering the signal branch of Figure 5.1, the conditional probability density function for the random variable V_{1h} can be obtained from equation 4.19 by setting z_1 equal to v_{1h}

$$f_{V_{1h}}(v_{1h}|0, \mathrm{I}_j) = \frac{\mathrm{M}}{2\sigma_{1_j}^2}\exp\left(-\frac{1}{2\sigma_{1_j}^2}(v_{1h}+4\alpha^2)\right)\mathrm{I}_0\left(\frac{2\alpha\sqrt{v_{1h}}}{\sigma_{1_j}^2}\right)\times$$

$$\left[1-Q\left(\frac{2\alpha}{\sigma_{1_j}},\frac{\sqrt{v_{1h}}}{\sigma_{1_j}}\right)\right]^{\mathrm{M}-1} u(v_{1h}) \qquad (5.1)$$

The probability density function of the random variable V_{1h} conditioned on a bit 0 transmission is given as

$$f_{V_{1h}}(v_{1h}|0) = \sum_{j=1}^{3} f_{V_{1h}}(v_{1h}|0, \mathrm{I}_j)\Pr(\mathrm{I}_j) \qquad (5.2)$$

where

$$\Pr(\mathrm{I}_j) = \begin{cases} \rho_1, & case\ \mathrm{I}_1 \\ \rho_2, & case\ \mathrm{I}_2 \\ (1-\rho_1-\rho_2), & case\ \mathrm{I}_3 \end{cases} \qquad (5.3)$$

The conditional probability density function for the random variable Z_1 is given as

$$f_{Z_1}(z_1|0) = \mathcal{L}^{-1}([\mathcal{L}(f_{V_{1h}}(v_{1h}|0))]^{\mathrm{L}}) \qquad (5.4)$$

An analytical solution for Equation 5.4 does not exist and it must be evaluated numerically.

Considering the non-signal branch, the conditional probability density function for the random variable V_{2h} can be obtained from equation 4.20 by setting z_2 equal to v_{2h} and is given by

$$f_{V_{2h}}(v_{2h}|0, \mathrm{I}_j) = \frac{\mathrm{M}}{2\sigma_{2_j}^2}\exp\left(-\frac{v_{2h}}{2\sigma_{2_j}^2}\right)\left[1-\exp\left(-\frac{v_{2h}}{2\sigma_{2_j}^2}\right)\right]^{\mathrm{M}-1} u(v_{2h}) \qquad (5.5)$$

The probability density function of the random variable V_{2h} conditioned on a bit 0 transmission is given as

$$f_{V_{2h}}(v_{2h}|0) = \sum_{j=1}^{3} f_{V_{2h}}(v_{2h}|0, \mathrm{I}_j)\Pr(\mathrm{I}_j) \tag{5.6}$$

The conditional probability density function for Z_2 is given as

$$f_{Z_2}(z_2|0) = \mathcal{L}^{-1}([\mathcal{L}(f_{V_{2h}}(v_{2h}|0))]^{\mathrm{L}}) \tag{5.7}$$

which must also be evaluated numerically.The probability of bit error now becomes

$$\int_0^{\infty}\int_{z_1}^{\infty}[f_{Z_2}(z_2|0)dz_2]f_{Z_1}(z_1|0)dz_1 \tag{5.8}$$

and must also be evaluated numerically.

B. NUMERICAL RESULTS

In Figure 5.2, the probability of bit error curves of the PDSC1 receiver with L-fold time diversity (M = 4, L = 4), the noise-normalized and linear receivers (M = 1, L = 4) and the self-normalized receiver (M = 1, L = 4), are plotted as a function of γ with no pulse noise jamming and a bit energy to thermal noise density ratio of E_b/N_0 = 15 dB. It is first noted that the performance of the PDSC1 receiver with time diversity is relatively invariant to the fading condition being considered. The performance difference between the most severe and benign fading conditions in terms of the BER is approximately half an order of magnitude. This is in comparison to the other receivers where there is several orders of magnitude difference between the two extreme cases. In addition, it is noticed that the PDSC1 receiver approaches its Gaussian limit at approximately $\gamma = 10$ where the other receivers approach their Gaussian limit at approximately $\gamma = 1000$. It is seen that for cases of severe fading ($\gamma < 3$), the PDSC1 receiver with time diversity provides superior performance to the other receivers. In the Gaussian limit of all channels however where the signal amplitude is relatively unchanged, the performance of the PDSC1 receiver with time diversity is vastly inferior to the noise-normalized, linear and self-normalized receivers.

Figures 5.3 and 5.4 show the probability of bit error curves for the PDSC1 receiver with L-fold time diversity (M = 4, L = 4) and linear receiver (M = 1, L = 4) with no pulse noise jamming as a function of E_b/N_0 for $\gamma = 0$ and $\gamma = 5$ respectively. It is seen that for the severe fading case,

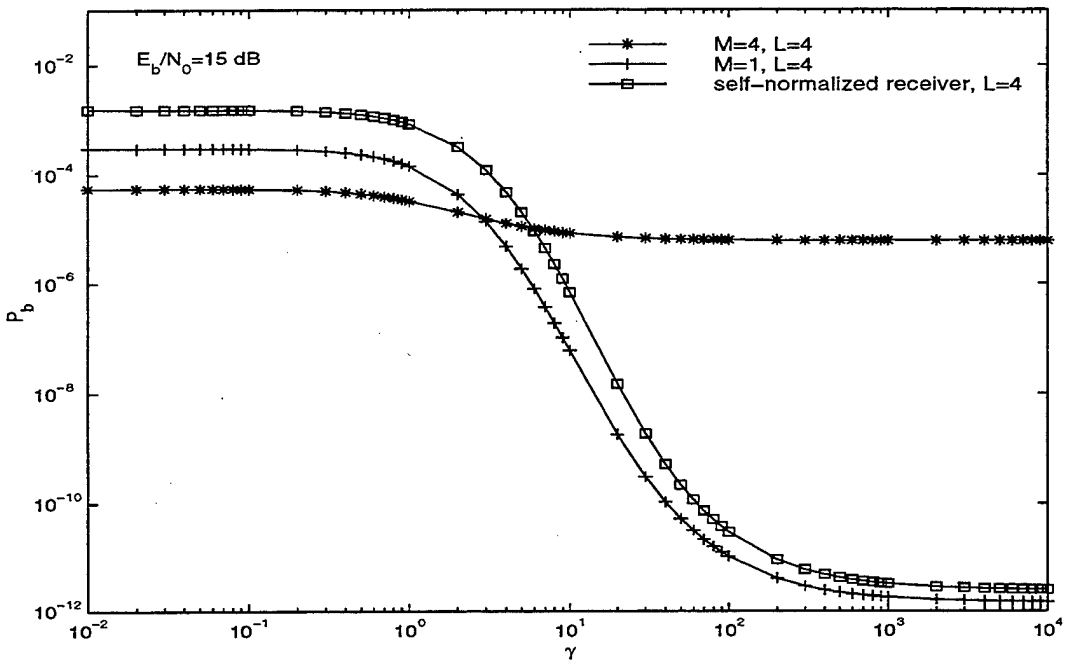

Figure 5.2: Probability of bit error for the PDSC1 receiver with L-fold time diversity (M = 4, L = 4), the noise-normalized and linear receivers (M = 1, L = 4) and the self-normalized receiver, (L = 4), as a function of γ with no pulse noise jamming and a bit energy to thermal noise density ratio of E_b/N_0 = 15 dB.

the PDSC1 receiver with time diversity provides performance superior to the linear receiver for bit error rates less than 10^{-3} ($E_b/N_0 > 13$ dB). Above this value of BER, the linear receiver provides a slightly better performance. It is seen that for the case of moderate fading, the range over which the PDSC1 receiver provides better performance in comparison to the linear receiver is reduced. In this case the enhanced performance region is valid for bit error rates on the order of 10^{-7} or lower and $E_b/N_0 > 16$ dB. It is thus seen that the PDSC1 receiver with time diversity requires a minimum signal energy to thermal noise density ratio to provide improved performance over the linear receiver.

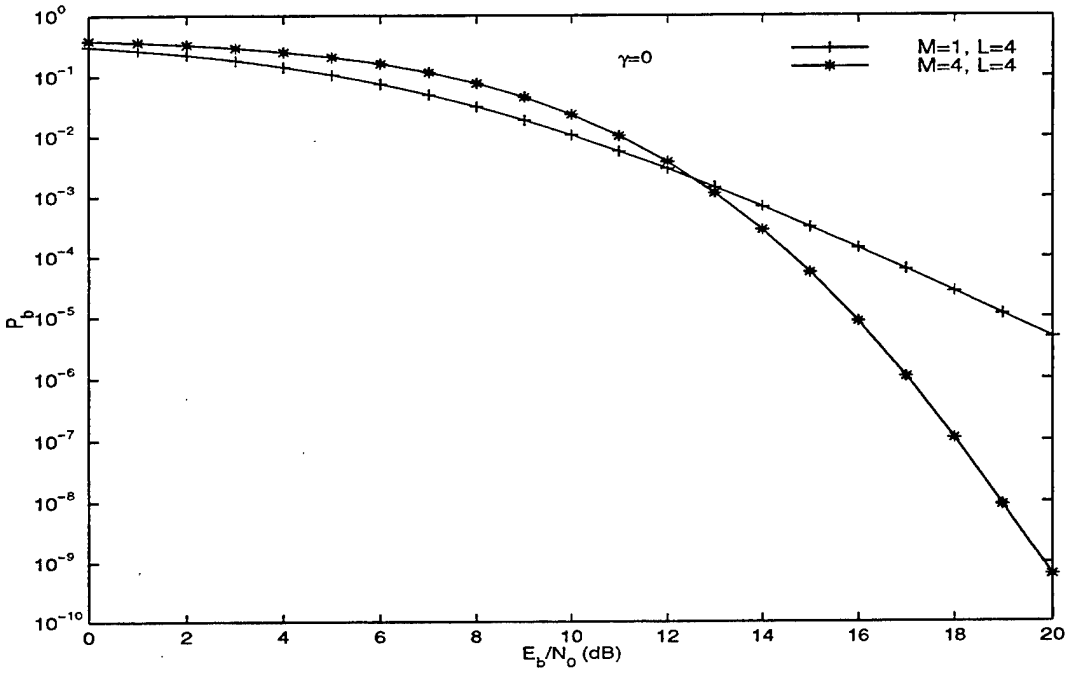

Figure 5.3: Probability of bit error for the PDSC1 receiver with L-fold time diversity (M = 4, L = 4) and linear receiver (M = 1, L = 4) as a function of E_b/N_0, $\gamma = 0$ with no pulse noise jamming.

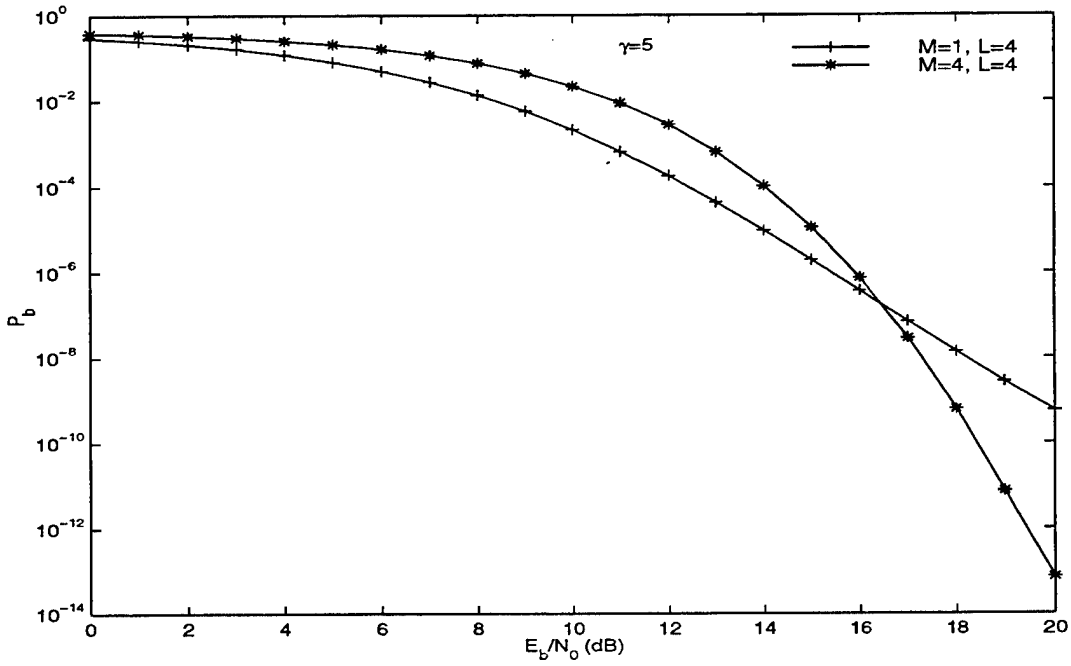

Figure 5.4: Probability of bit error for the PDSC1 receiver with L-fold time diversity (M = 4, L = 4) and linear receiver (M = 1, L = 4) as a function of E_b/N_0, $\gamma = 5$ with no pulse noise jamming.

Numerical results for the performance of the PDSC1 receiver with time diversity for a fixed jammer peak power specification (fixed ρ) and for worst case jamming are now presented. Figures 5.5 and 5.6 show the performance curves of the PDSC1 receiver for $E_b/N_0 = 15$ dB, a diversity of $L = 4$, $M = 4$ and $\rho = 0.05$ with β as a parameter for $\gamma = 0$ and $\gamma = 5$ respectively.

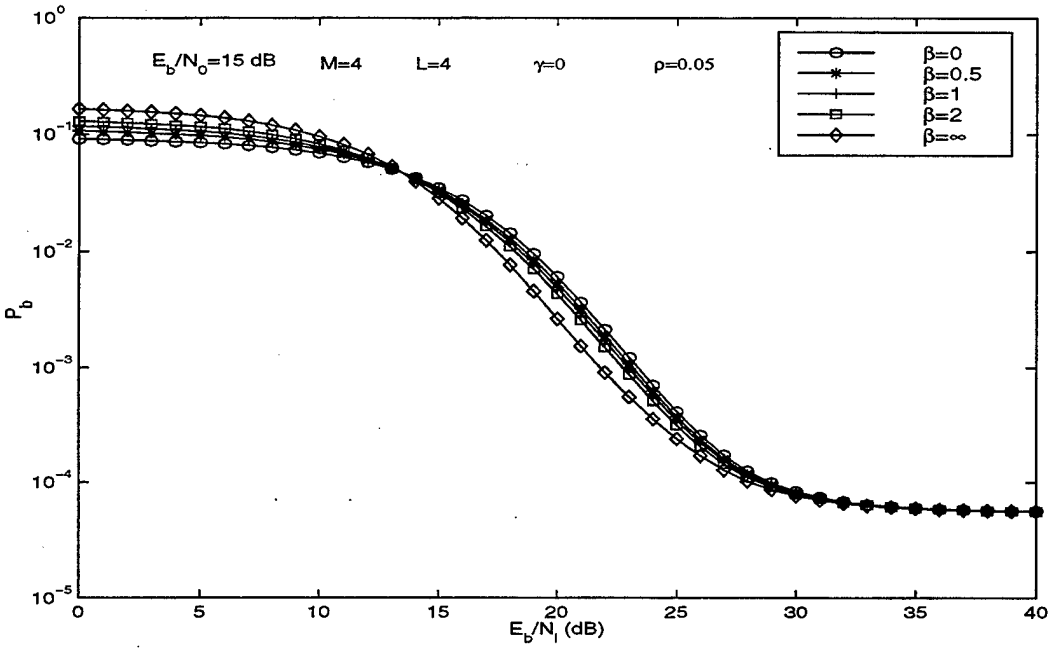

Figure 5.5: Performance of PDSC1 receiver with time diversity for $E_b/N_0 = 15$ dB, a diversity of $L = 4$, $M = 4$, $\gamma = 0$ and $\rho = 0.05$ with β as a parameter.

It is observed that for both fading conditions for fixed ρ, jamming alternating bits ($\beta = \infty$) produces the worst performance for the lower values of signal-to-interference ratios ($E_b/N_I < 13$ dB), while jamming consecutive bits ($\beta = 0$) produces the worst performance at the higher values. These results are similar to that observed for the PDSC1 receiver with no time diversity.

The worst case performance of the PDSC1 receiver with time diversity is now considered. Worst case performance was determined through numerical search where it was determined that the worst case values of ρ for a particular value of E_b/N_I followed according to equations 2.30 and 2.31. The value of $\beta = 0$ has been selected for ease of comparison to the other receivers. Figures 5.7-5.9 show the performance curves of the PDSC1 receiver with time diversity for $\rho = 0.01, 0.1,$

0.25, 1 and worst case performance, $\gamma = 0$ and $E_b/N_0 = 15$ dB for diversity orders M = 4, L = 1,3,4 respectively. It is seen that there is significant performance degradation due to pulse noise jamming for all cases considered. The degradation due to pulse jamming increases dramatically from L = 1 (no time diversity) to L = 3. It is seen that there is little performance difference between the L = 3 and L = 4 curves. Figure 5.10 shows the worst case performance curves of the PDSC1 receiver with time diversity in the presence of pulse noise interference for diversity orders L = 1-6, M = 4, $E_b/N_0 = 15$ dB and $\gamma = 0$. It is seen that at signal-to-interference ratios below 25 dB, increasing the time diversity order leads to a gradual performance decrease. At higher values of signal-to-interference ratio ($E_b/N_I > 33$ dB), any order of time diversity leads to a performance improvement compared to the case of no time diversity. It the range shown, a time diversity order of L = 2 or 3 provides the best performance improvement.

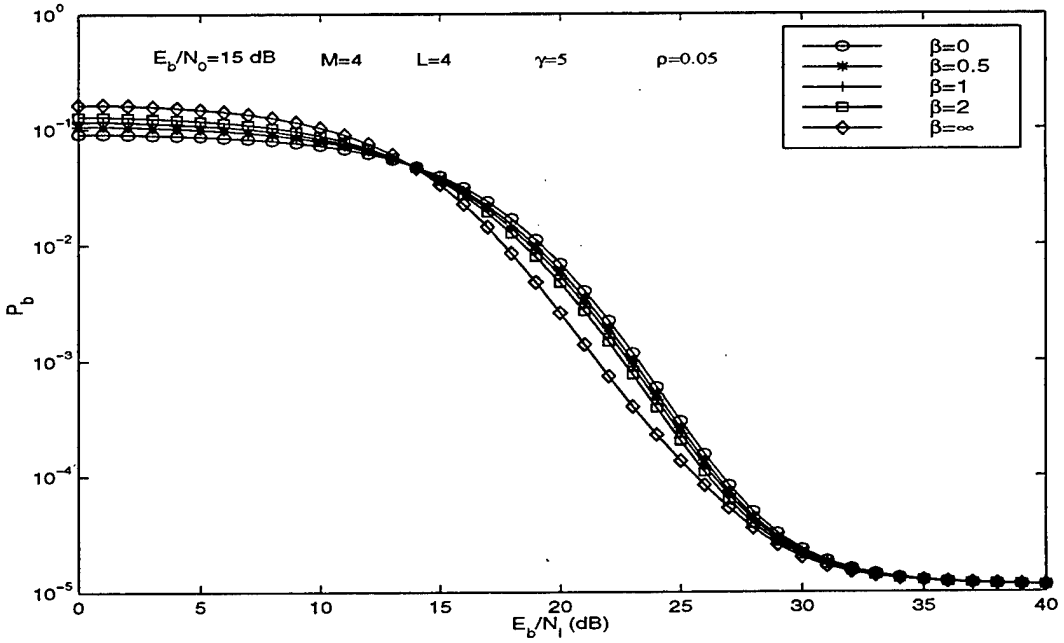

Figure 5.6: Performance of PDSC1 receiver with time diversity for $E_b/N_0 = 15$ dB, a diversity of L = 4, M = 4, $\gamma = 5$ and $\rho = 0.05$ with β as a parameter.

Figure 5.11 plots the optimum value of ρ as a function of time diversity order with M = 4, $E_b/N_0 = 15$ dB, $\gamma = 0$ and E_b/N_I as a parameter. As time diversity order is increased from L = 1-3, it is seen that the optimum value of ρ decreases. Above a time diversity order of L = 3, the optimum

ρ remains mostly constant over the range of E_b/N_I. Figures 5.12 and 5.13 show the performance curves of the PDSC1 receiver with time diversity for ρ = 0.01, 0.1, 0.25, 1 and worst case performance, γ = 0 and E_b/N_0 = 15 dB for diversity orders L = 4, M = 1,3 respectively. It is again seen that there is significant performance degradation due to pulse noise jamming for all cases considered. The degradation due to pulse jamming increases dramatically from M = 1 (no spatial diversity) to M = 3. It is seen that there is little performance difference between the M = 3 curve and M = 4 curve (Figure 5.9). Figure 5.14 shows the worst case performance curves of the PDSC1 receiver with time diversity in the presence of pulse noise interference for diversity orders M = 1-6, L = 4, E_b/N_0 = 15 dB and γ = 0. It is seen that at signal

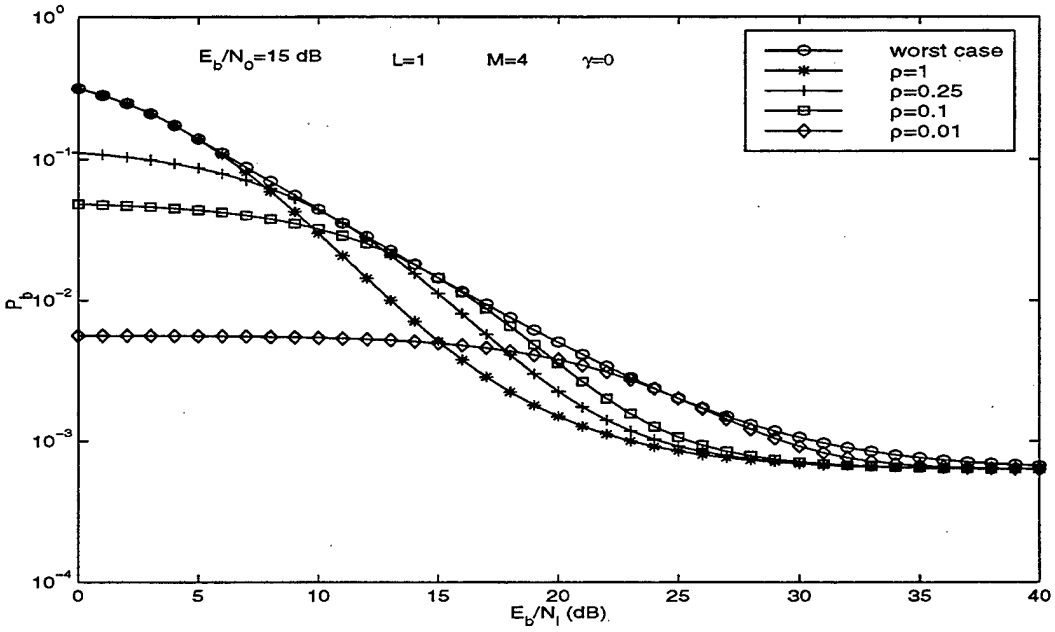

Figure 5.7: Performance of PDSC1 receiver with time diversity for pulse jamming fractions ρ = 1, 0.25, 0.1, 0.01 and worst case for diversity order L = 1, M = 4, E_b/N_0 = 15 dB and γ = 0.

to interference ratios below 30 dB, increasing the spatial diversity order leads to a gradual performance decrease. For E_b/N_I higher than this, a spatial diversity order of M = 2 provides the best performance improvement. Figure 5.15 plots the optimum value of ρ as a function of spatial diversity order with L = 4, E_b/N_0 = 15 dB, γ = 0 and E_b/N_I as a parameter. As spatial diversity order is increased, it is seen that the optimum value of ρ increases over the full range of signal-to-

interference ratio, effectively forcing the jammer to a more continuous jamming strategy. Figure 5.16 plots the worst case performance curves of the self-normalized, noise-normalized, linear receivers (L = 4) and PDSC1 receiver without time diversity (L = 1, M = 4) and with time diversity (L = 4, M = 4) in the presence of pulse noise interference with E_b/N_0 = 15 dB and $\gamma = 0$. It is seen that the PDSC1 receiver with time diversity is inferior to the other diversity receivers for $E_b/N_I <$ 28 dB. As signal-to-interference ratio is increased higher and the Rayleigh limit of the channel is approached, the PDSC1 receiver with time diversity provides superior performance compared to any of the other receivers. It is also noted that the PDSC1 receiver with time diversity of L = 4 only begins to approach its Rayleigh limit of $P_b = 5.5 \times 10^{-5}$ where the others have nearly converged to their Rayleigh limits. For low values of signal-to-interference ratio (E_b/N_I < 10 dB), losses in comparison to the PDSC1 receiver without time diversity are likely attributable to noncoherent combining losses.

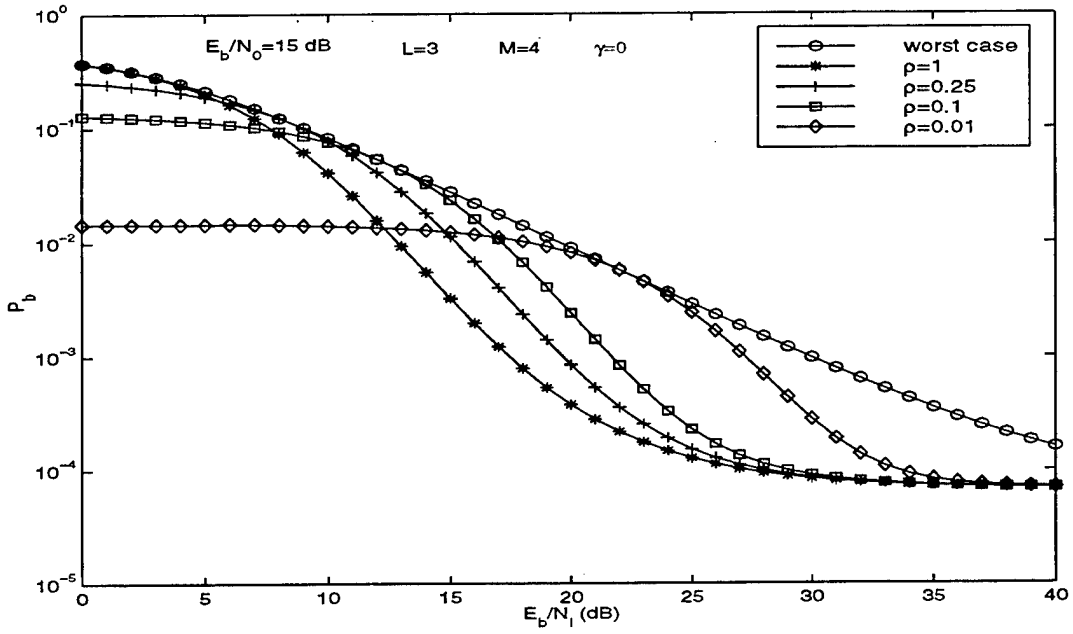

Figure 5.8: Performance of PDSC1 receiver with time diversity for pulse jamming fractions ρ = 1, 0.25, 0.1, 0.01 and worst case for diversity order L = 3, M = 4, E_b/N_0 = 15 dB and $\gamma = 0$.

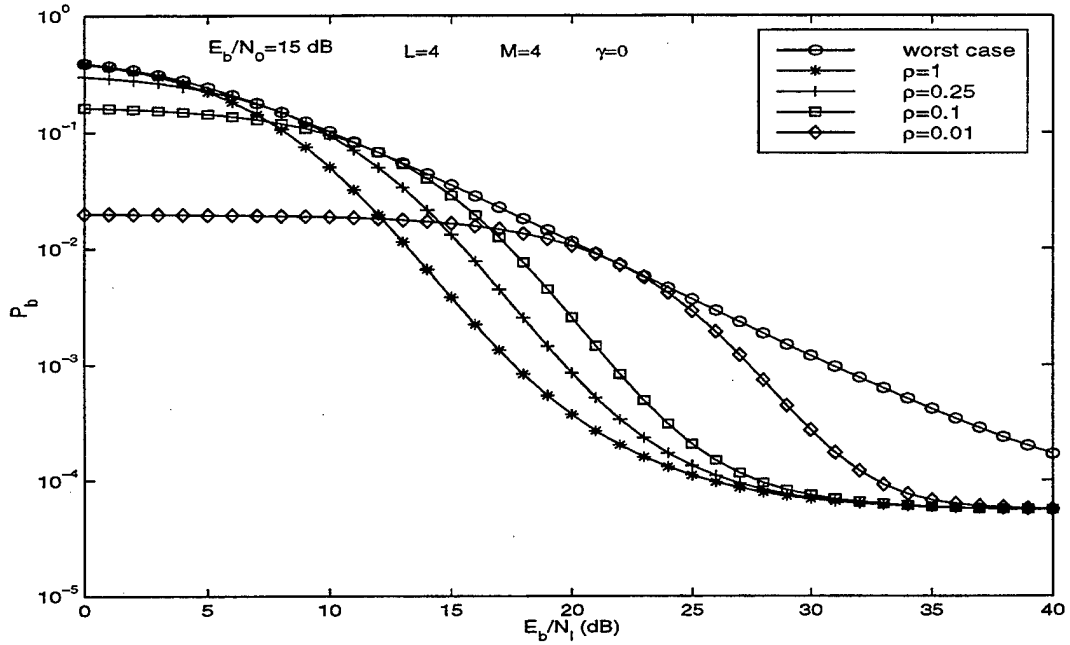

Figure 5.9: Performance of PDSC1 receiver with time diversity for pulse jamming fractions ρ = 1, 0.25, 0.1, 0.01 and worst case for diversity order L = 4, M = 4, E_b/N_0 = 15 dB and γ = 0.

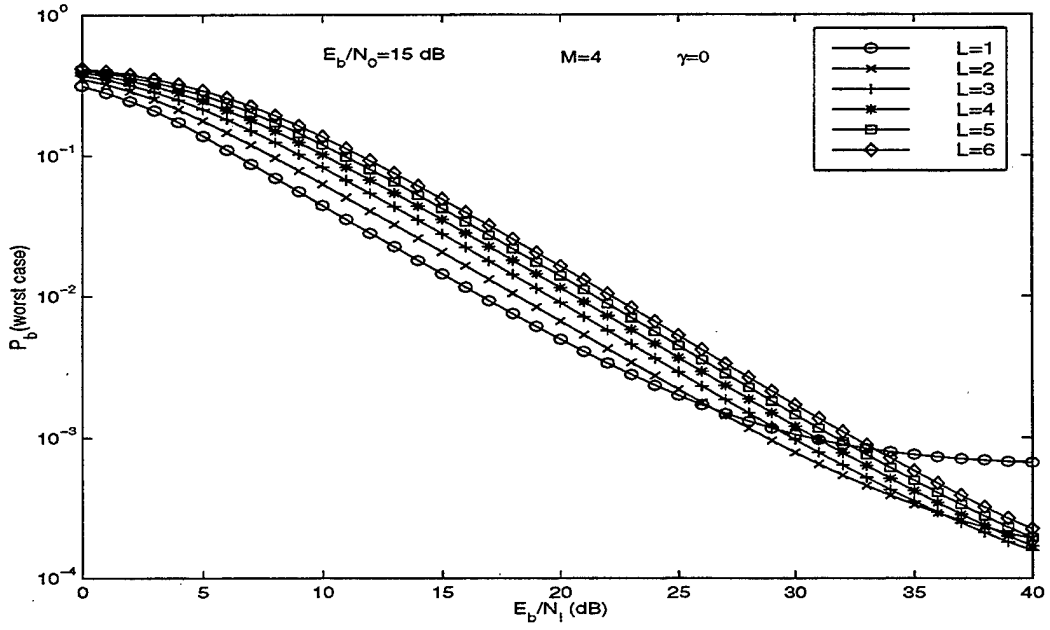

Figure 5.10: Worst case performance of PDSC1 receiver with time diversity in the presence of pulse noise interference for diversity orders L = 1-6, M = 4, E_b/N_0 = 15 dB and γ = 0.

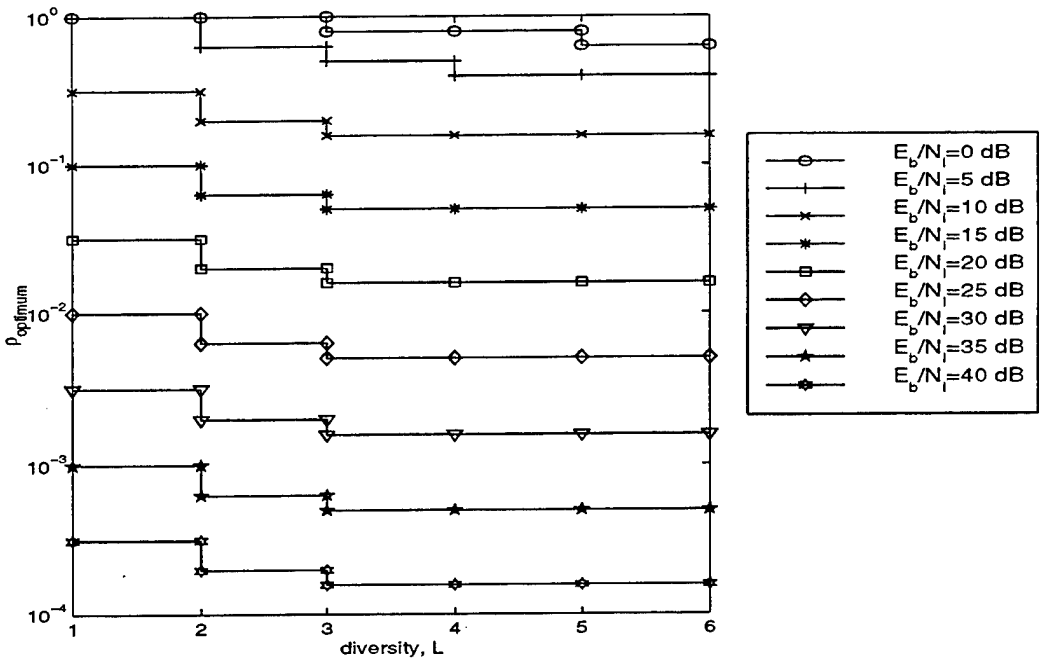

Figure 5.11: Optimum value of ρ as a function of time diversity order with $M = 4$, $E_b/N_0 = 15$ dB, $\gamma = 0$ and E_b/N_I as a parameter.

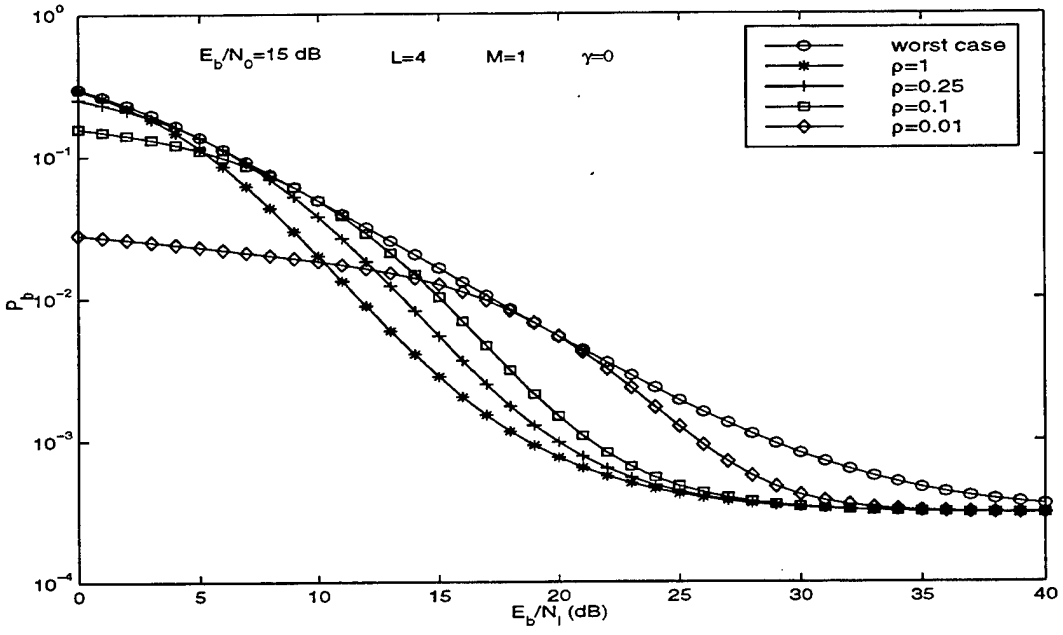

Figure 5.12: Performance of PDSC1 receiver with time diversity for pulse jamming fractions ρ = 1, 0.25, 0.1, 0.01 and worst case for diversity order $L = 4$, $M = 1$, $E_b/N_0 = 15$ dB and $\gamma = 0$.

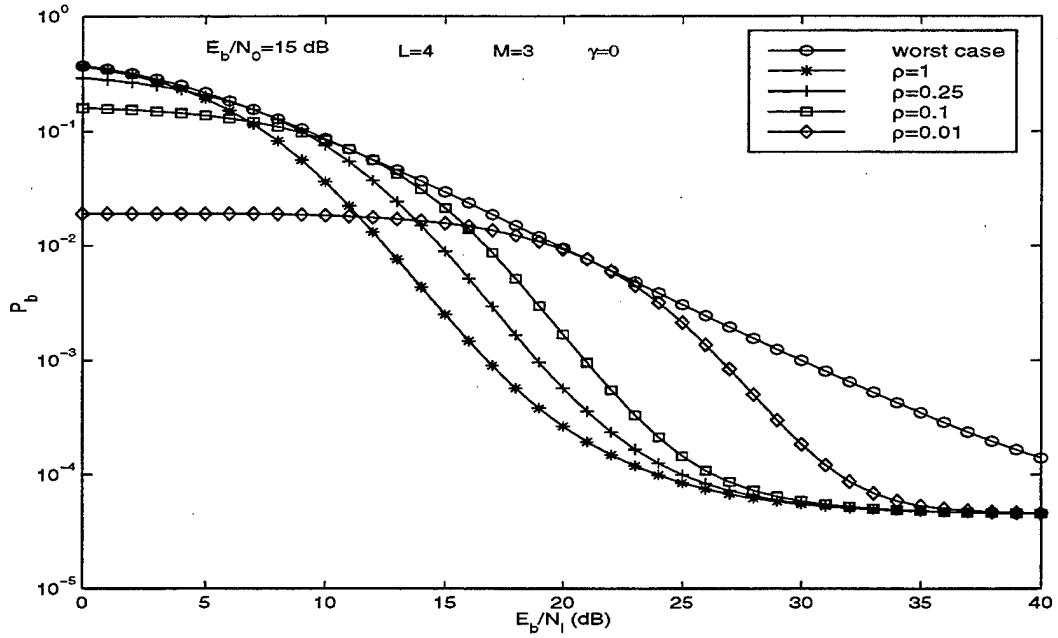

Figure 5.13: Performance of PDSC1 receiver with time diversity for pulse jamming fractions ρ = 1, 0.25, 0.1, 0.01 and worst case for diversity order L = 4, M = 3, E_b/N_0 = 15 dB and γ = 0.

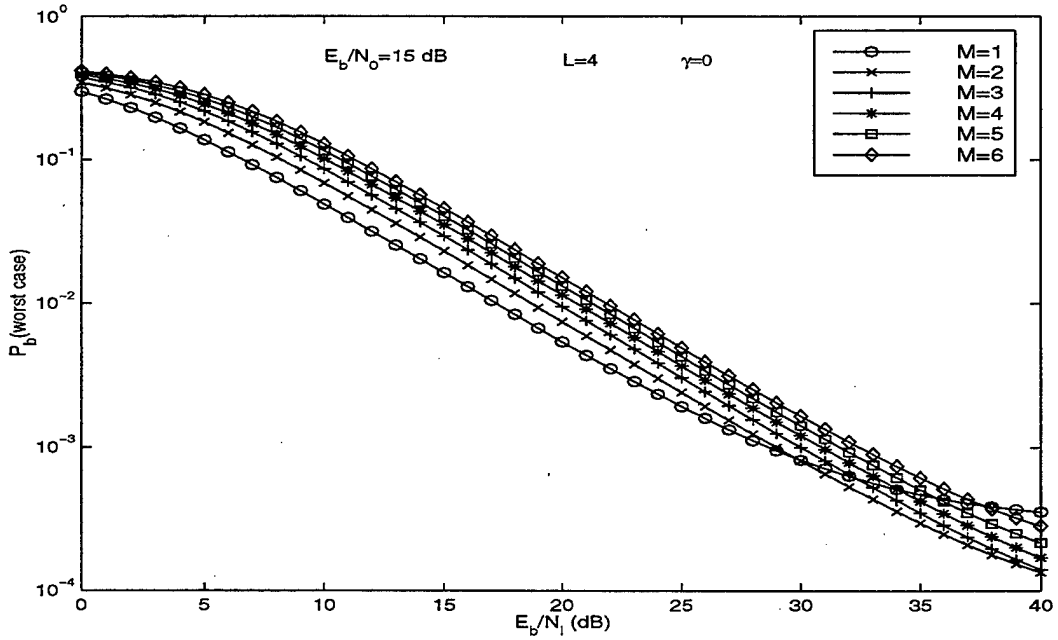

Figure 5.14: Worst case performance of PDSC1 receiver with time diversity in the presence of pulse noise interference for diversity orders L = 4, M = 1-6, E_b/N_0 = 15 dB and γ = 0.

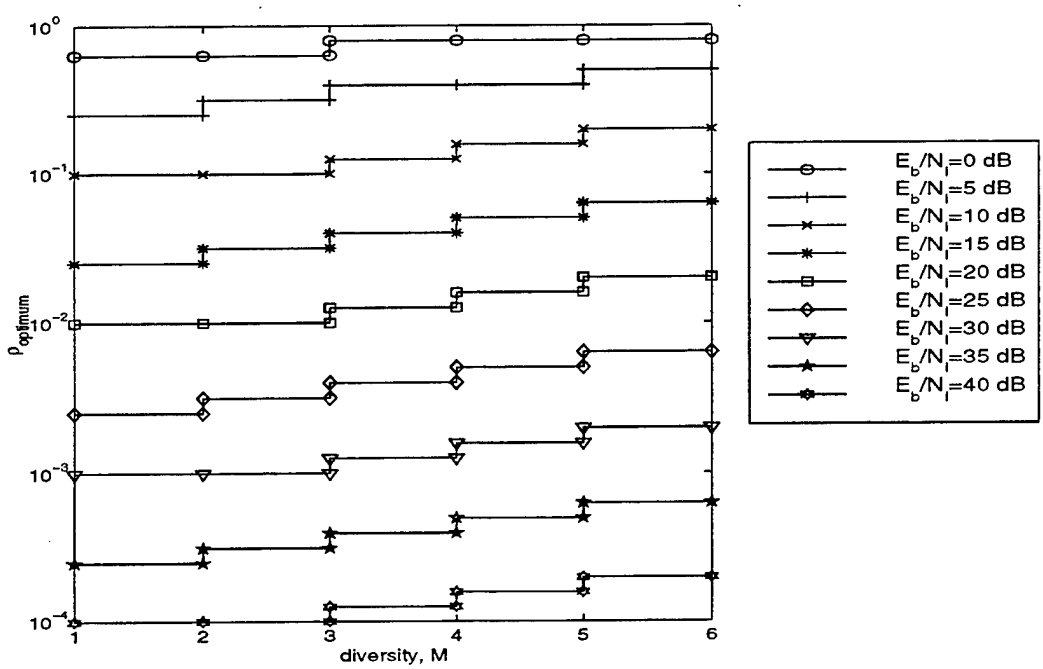

Figure 5.15: Optimum value of ρ as a function of spatial diversity order with L = 4, E_b/N_0 = 15 dB, γ = 0 and E_b/N_I as a parameter.

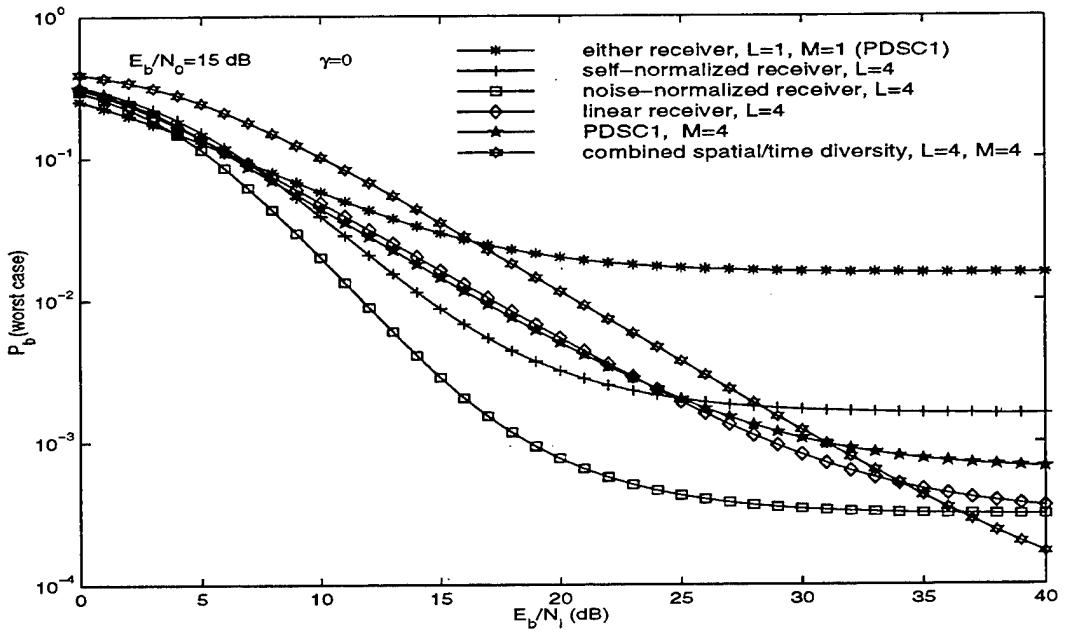

Figure 5.16: Worst case performance comparison between self-normalized, noise-normalized, linear receivers (L = 4) and PDSC1 receiver without time diversity (L = 1, M = 4) and with time diversity (L = 4, M = 4) in the presence of pulse noise interference with E_b/N_0 = 15 dB and γ = 0.

Figures 5.17 - 5.19 show the performance curves of the PDSC1 receiver with time diversity for ρ = 0.01, 0.1, 0.25, 1 and worst case performance, γ = 5 and E_b/N_0 = 15 dB for diversity orders M = 4, L = 1,3,4 respectively. It is seen that there is significant performance degradation due to pulse noise jamming for all cases considered. It is also noted that the worst case performance degrades for increasing time diversity order. This is also seen in Figure 5.20 where the worst case performance curves of the PDSC1 receiver with time diversity in the presence of pulse noise interference for diversity orders L = 1-6, M = 4, E_b/N_0 = 15 dB and γ = 5 are shown. Here any increase in time diversity order leads to a performance degradation over the full range of signal-to-interference ratio.

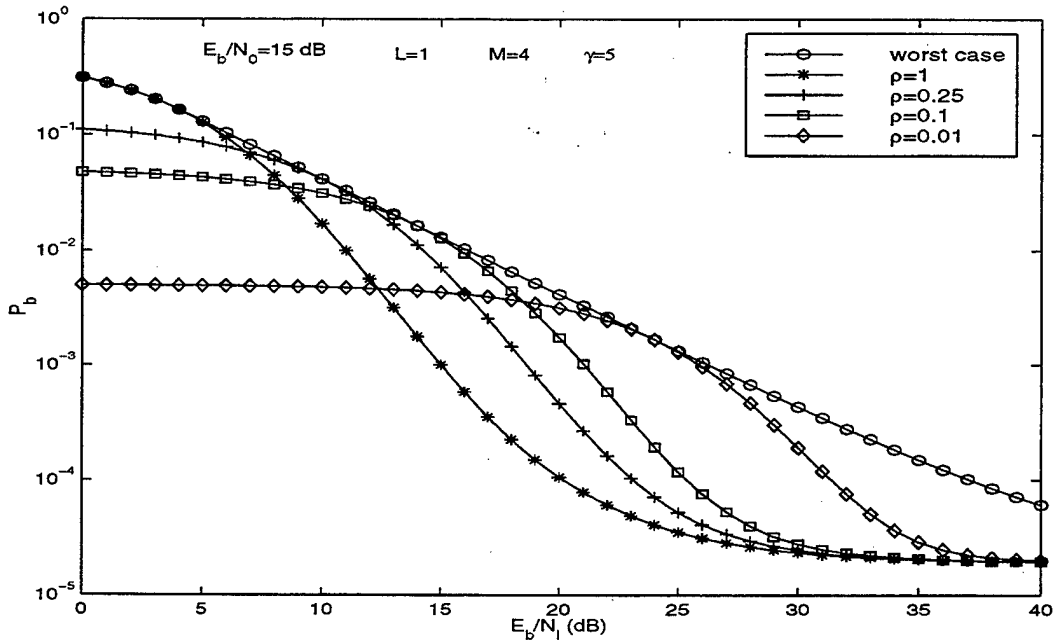

Figure 5.17: Performance of PDSC1 receiver with time diversity for pulse jamming fractions ρ = 1, 0.25, 0.1, 0.01 and worst case for diversity order L = 1, M = 4, E_b/N_0 = 15 dB and γ = 5.

Figure 5.21 plots the optimum value of ρ as a function of time diversity order with M = 4, E_b/N_0 = 15 dB, γ = 5 and E_b/N_I as a parameter. It is seen that seen that the optimum value of ρ decreases for increasing time diversity order. Figures 5.22 and 5.23 show the performance curves of the PDSC1 receiver with time diversity for ρ = 0.01, 0.1, 0.25, 1 and worst case performance, γ = 5 and E_b/N_0 = 15 dB for diversity orders L = 4, M = 1,3 respectively. It is again seen that

there is severe performance degradation due to pulse noise jamming. When comparing to the case of diversity order L = 4, M = 4 (Figure (5.9), it is noticed that performance worsens as the spatial order is increased. This is also depicted in Figure 5.24 which shows the worst case performance curves of the PDSC1 receiver with time diversity in the presence of pulse noise interference for diversity orders L = 4, M = 1-6, E_b/N_0 = 15 dB and γ = 5. It is seen that any increase in spatial diversity order leads to performance degradation over the full range of signal-to-interference ratio. Figure 5.25 plots the optimum value of ρ as a function of spatial diversity order with L = 4, E_b/N_0 = 15 dB, γ = 5 and E_b/N_I as a parameter. As spatial diversity order is increased, it is seen that the optimum value of ρ increases over the full range of signal-to-interference ratio. This result is similar to that which was observed for the Rayleigh fading channel. Again it is seen that although performance worsens as the spatial order is increased, the jammer has been forced to a more continuous jamming strategy. Figure 5.26 plots the worst case performance curves of the self-normalized, noise-normalized, linear receivers (L = 4) and PDSC1 receiver without time diversity (L = 1, M = 4) and with time diversity (L = 4, M = 4) in the presence of pulse noise interference with E_b/N_0 = 15 dB and γ = 5. It is seen that the PDSC1 receiver with time diversity is inferior to all other diversity receivers over the full range of signal-to-interference ratio.

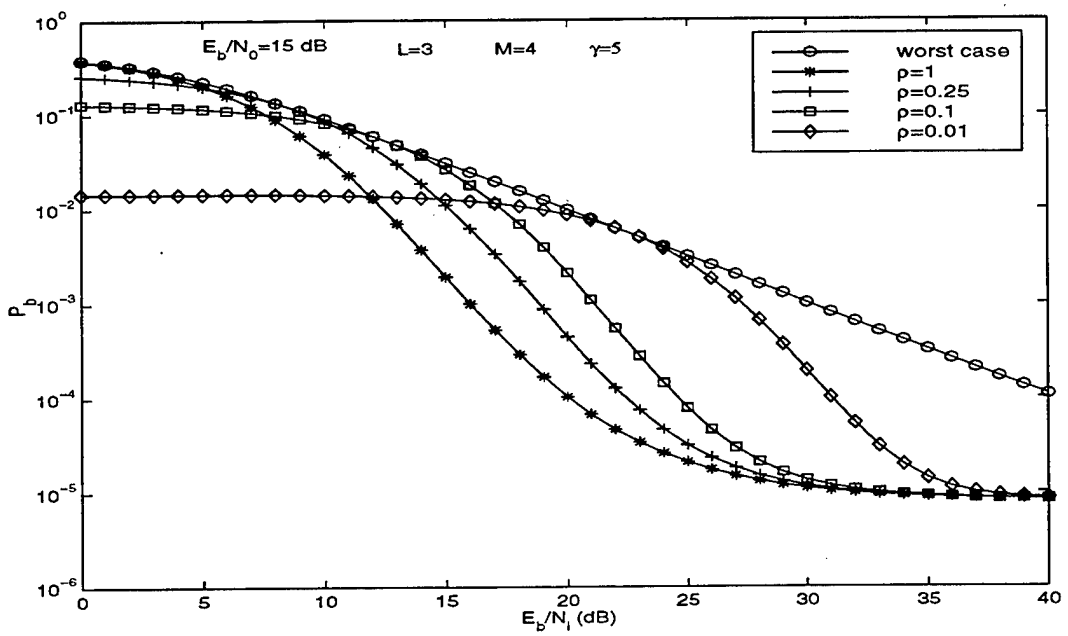

Figure 5.18: Performance of PDSC1 receiver with time diversity for pulse jamming fractions ρ = 1, 0.25, 0.1, 0.01 and worst case for diversity order L = 3, M = 4, E_b/N_0 = 15 dB and γ = 5.

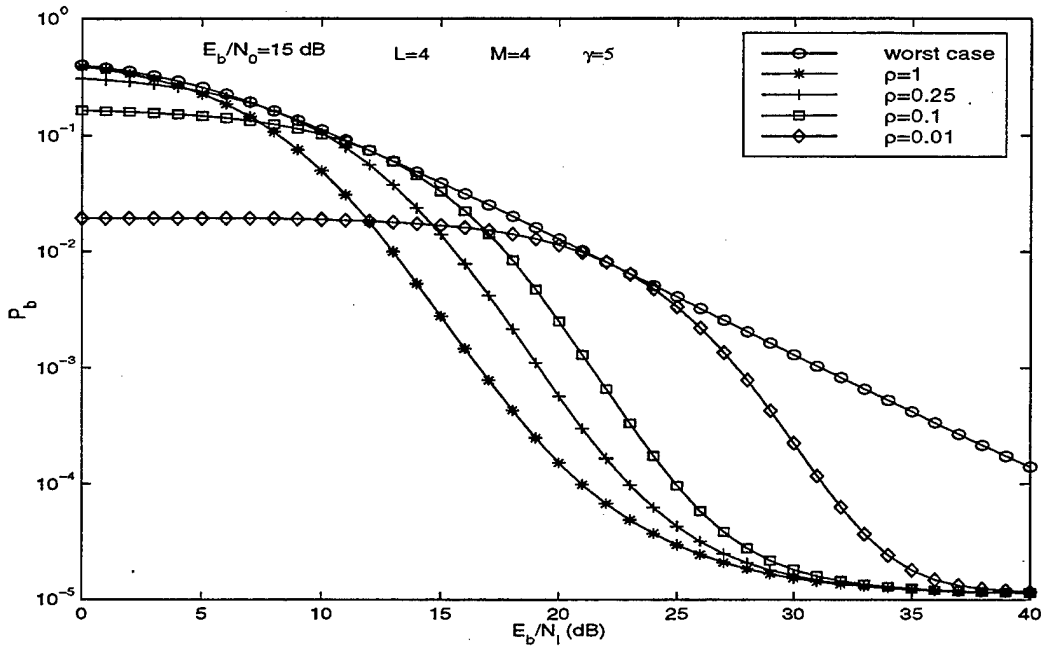

Figure 5.19: Performance of PDSC1 receiver with time diversity for pulse jamming fractions ρ = 1, 0.25, 0.1, 0.01 and worst case for diversity order L = 4, M = 4, E_b/N_0 = 15 dB and γ = 5.

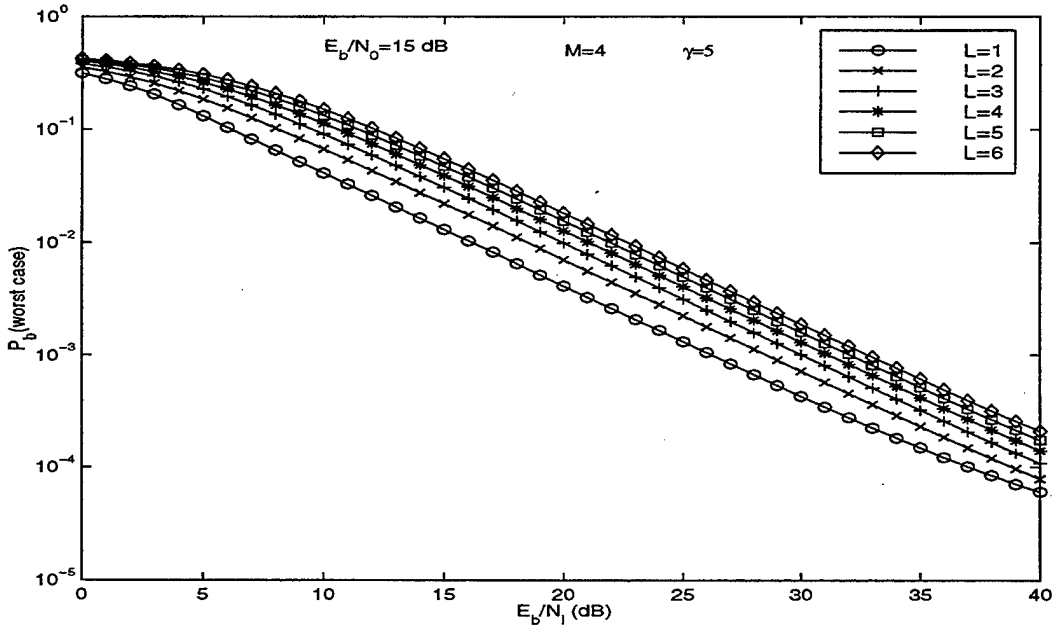

Figure 5.20: Worst case performance of PDSC1 receiver with time diversity in the presence of pulse noise interference for diversity orders L = 1-6, M = 4, E_b/N_0 = 15 dB and γ = 5.

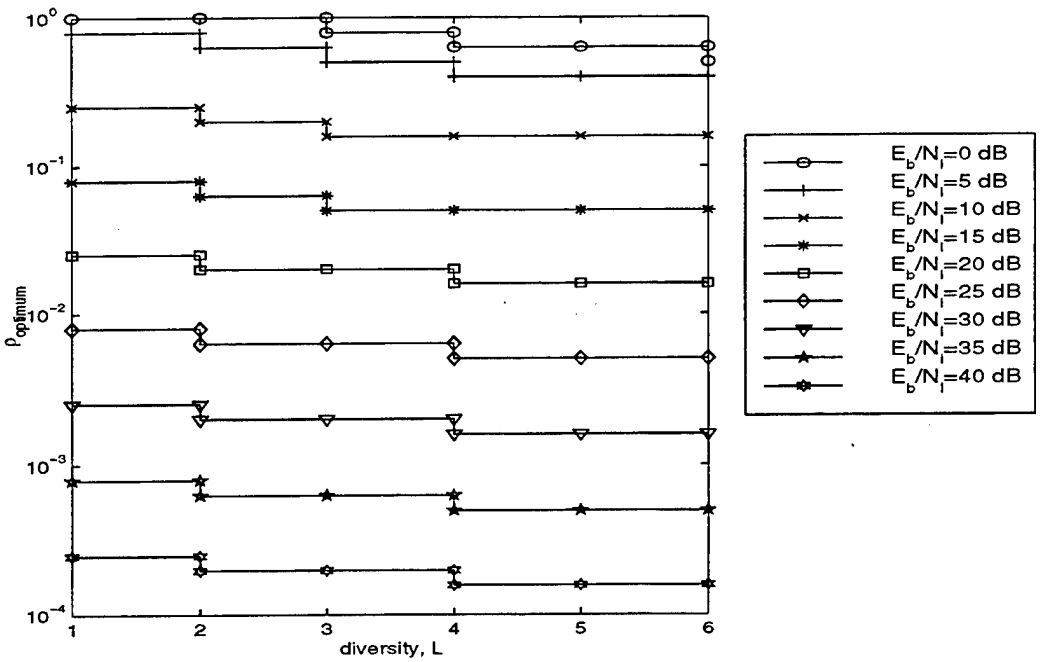

Figure 5.21: Optimum value of ρ as a function of time diversity order with $M = 4$, $E_b/N_0 = 15$ dB, $\gamma = 5$ and E_b/N_I as a parameter.

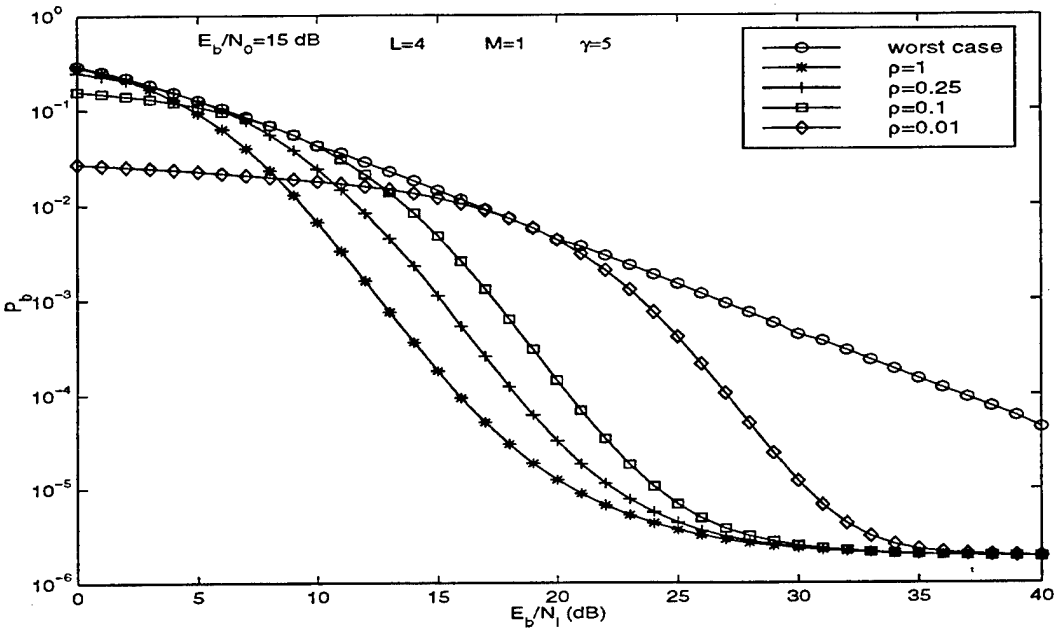

Figure 5.22: Performance of PDSC1 receiver with time diversity for pulse jamming fractions ρ = 1, 0.25, 0.1, 0.01 and worst case for diversity order $L = 4$, $M = 1$, $E_b/N_0 = 15$ dB and $\gamma = 5$.

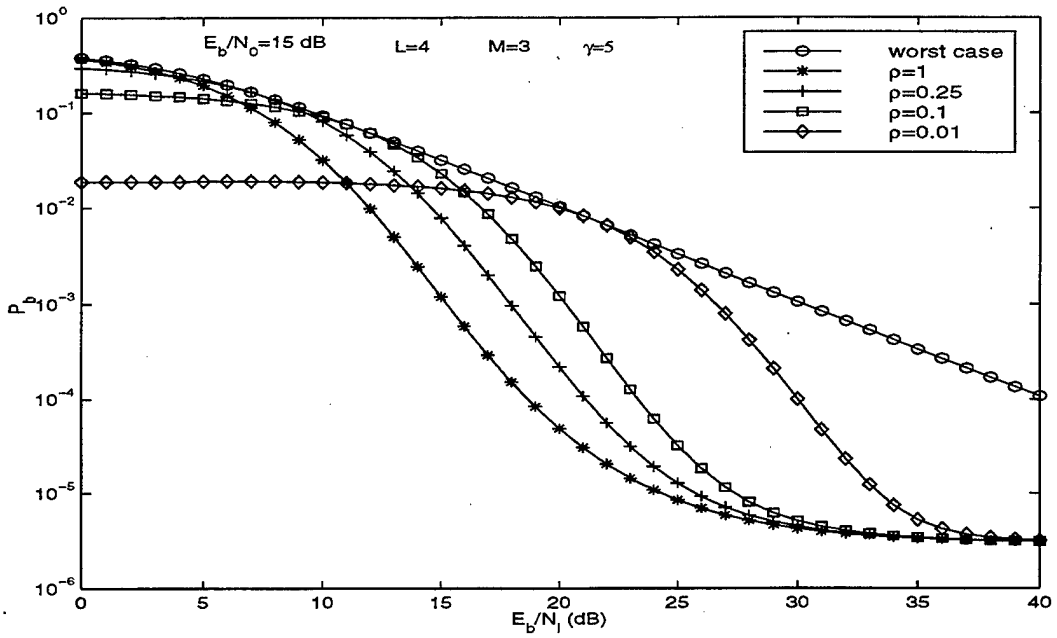

Figure 5.23: Performance of PDSC1 receiver with time diversity for pulse jamming fractions ρ = 1, 0.25, 0.1, 0.01 and worst case for diversity order L = 4, M = 3, E_b/N_0 = 15 dB and γ = 5.

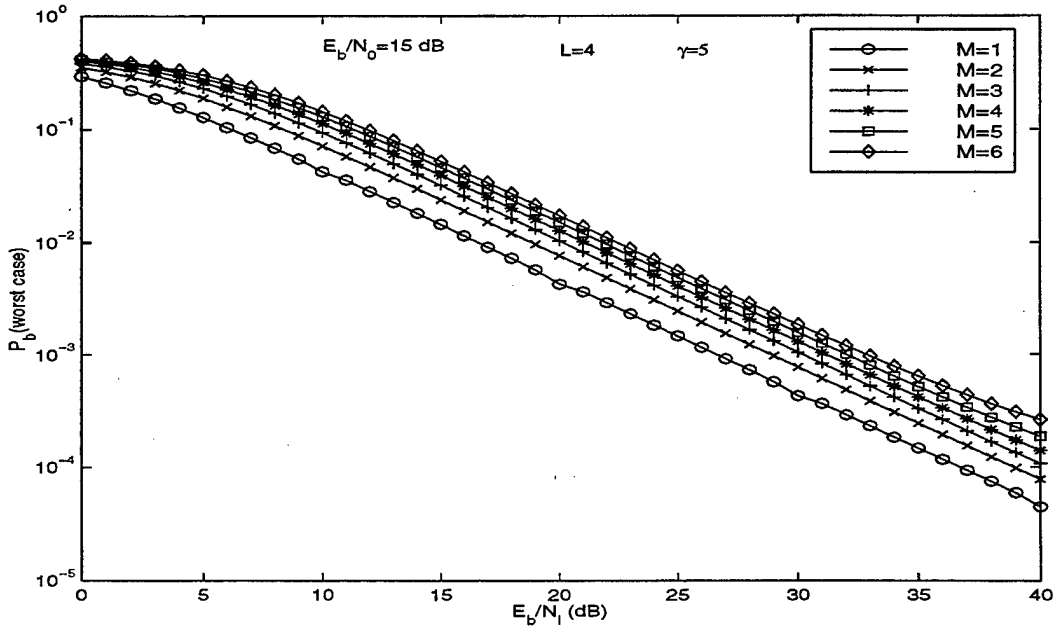

Figure 5.24: Worst case performance of PDSC1 receiver with time diversity in the presence of pulse noise interference for diversity orders L = 4, M = 1-6, E_b/N_0 = 15 dB and γ = 5.

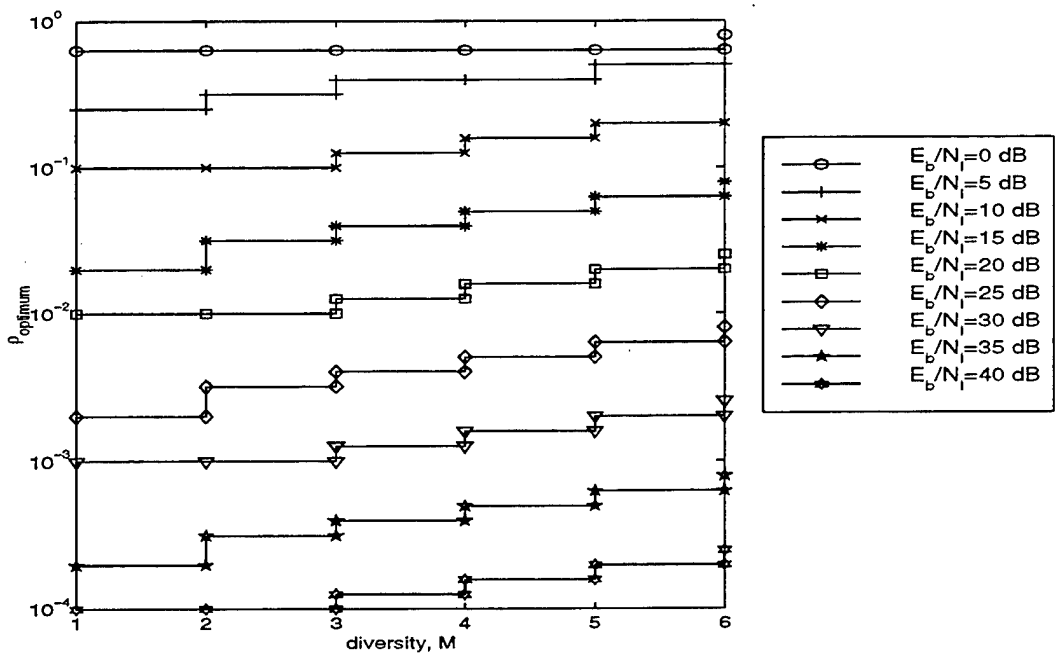

Figure 5.25: Optimum value of ρ as a function of spatial diversity order with L = 4, E_b/N_0 = 15 dB, γ = 5 and E_b/N_I as a parameter.

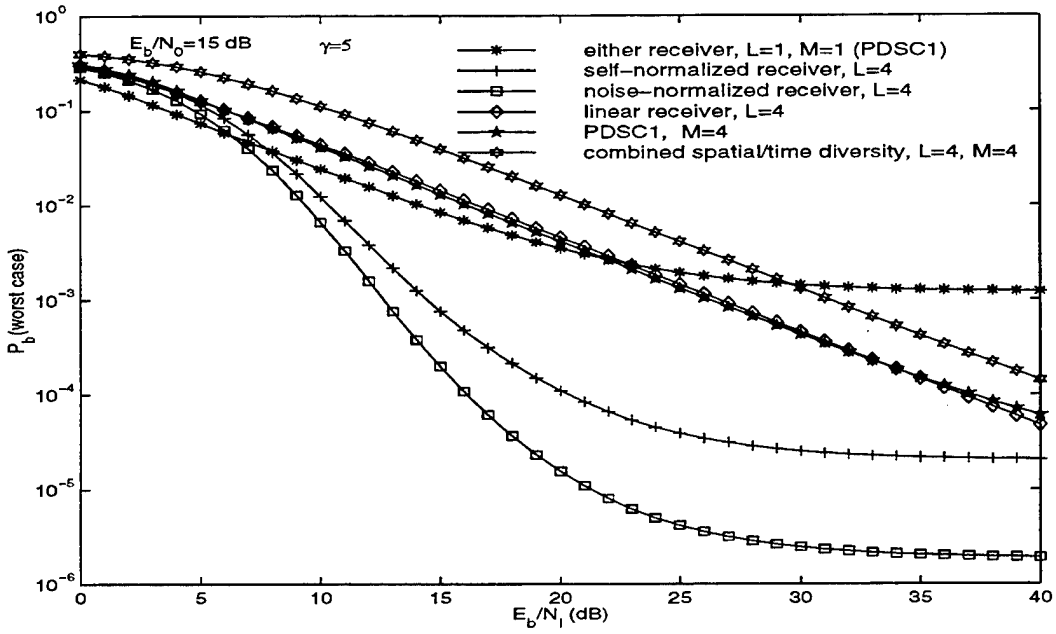

Figure 5.26: Worst case performance comparison between self-normalized, noise-normalized, linear receivers (L = 4) and PDSC1 receiver without time diversity (L =1, M =4) and with time diversity (L = 4, M= 4) in the presence of pulse noise interference with E_b/N_0 = 15 dB and γ = 5.

Figure 5.27 is a plot of the optimum value of ρ as a function of γ with time diversity order as a parameter for M = 4, E_b/N_0 = 15 dB and E_b/N_I = 10 dB. It is observed that the optimum value of ρ decreases for increasing time diversity order over the full range of γ. Figure 5.28 shows the optimum value of ρ as a function of γ with spatial diversity order as a parameter for L = 4, E_b/N_0 = 15 dB and E_b/N_I = 10 dB. Here it is observed that the optimum value of ρ increases for increasing spatial diversity order over the full range of γ. Similar results are observed at a higher value of signal-to-interference ratio (E_b/N_I = 30 dB) in Figure 5.29 in the case of increasing time diversity order with M = 4 and Figure 5.30 in the case of increasing spatial diversity order with L = 4. These results are consistent with what was observed for the Rayleigh channel and moderate fading channel (γ = 5).

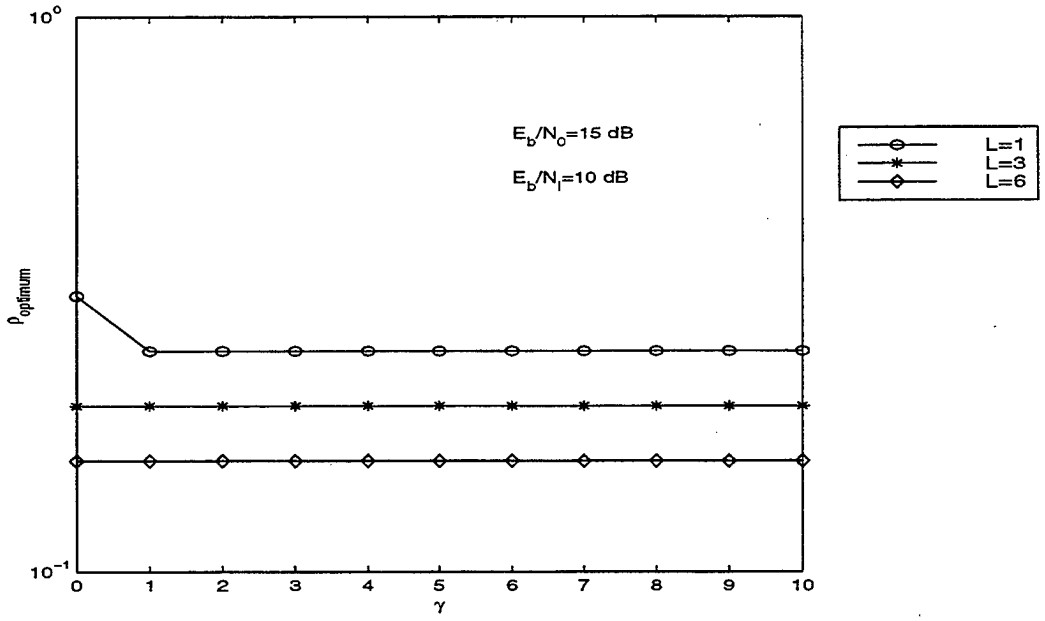

Figure 5.27: Optimum value of ρ as a function of γ with time diversity order as a parameter for M = 4, E_b/N_0 = 15 dB and E_b/N_I = 10 dB.

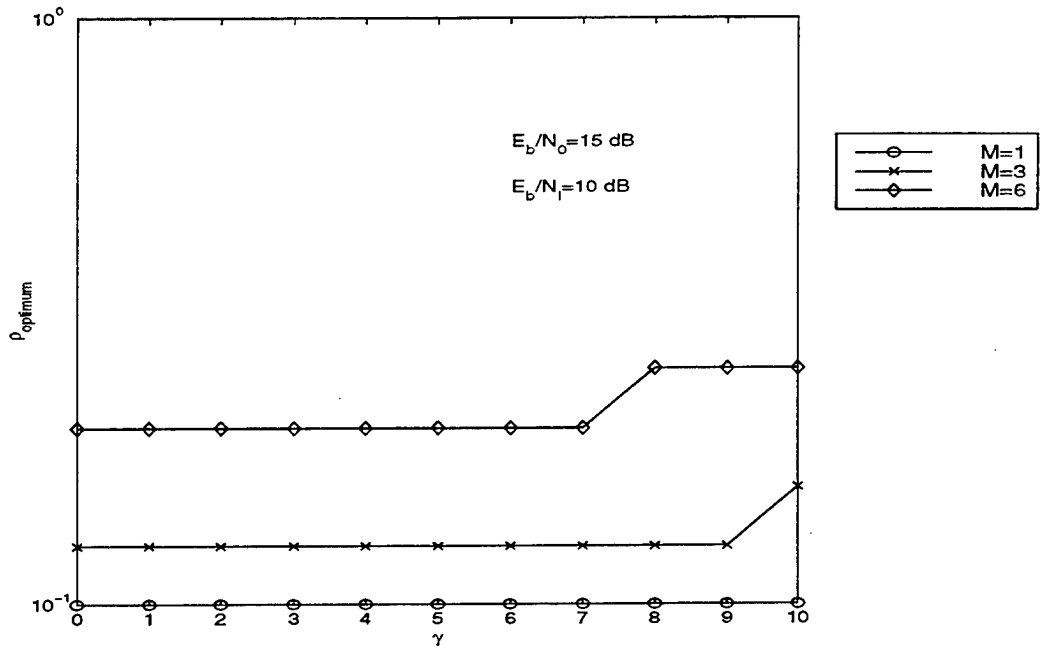

Figure 5.28: Optimum value of ρ as a function of γ with spatial diversity order as a parameter for L = 4, E_b/N_0 = 15 dB and E_b/N_I = 10 dB.

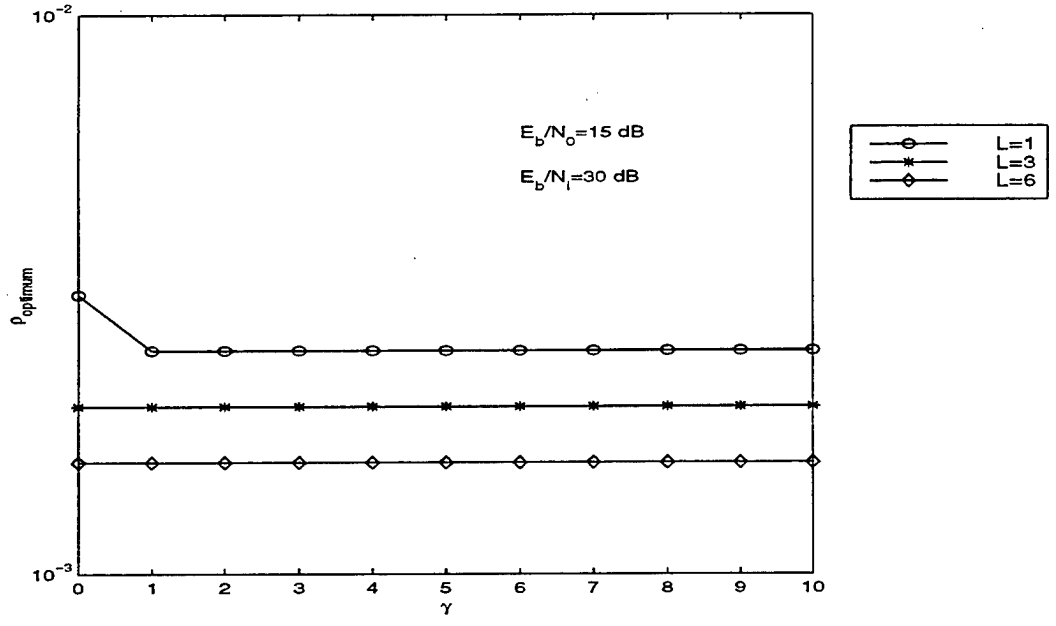

Figure 5.29: Optimum value of ρ as a function of γ with time diversity order as a parameter for M = 4, E_b/N_0 = 15 dB and E_b/N_I = 30 dB.

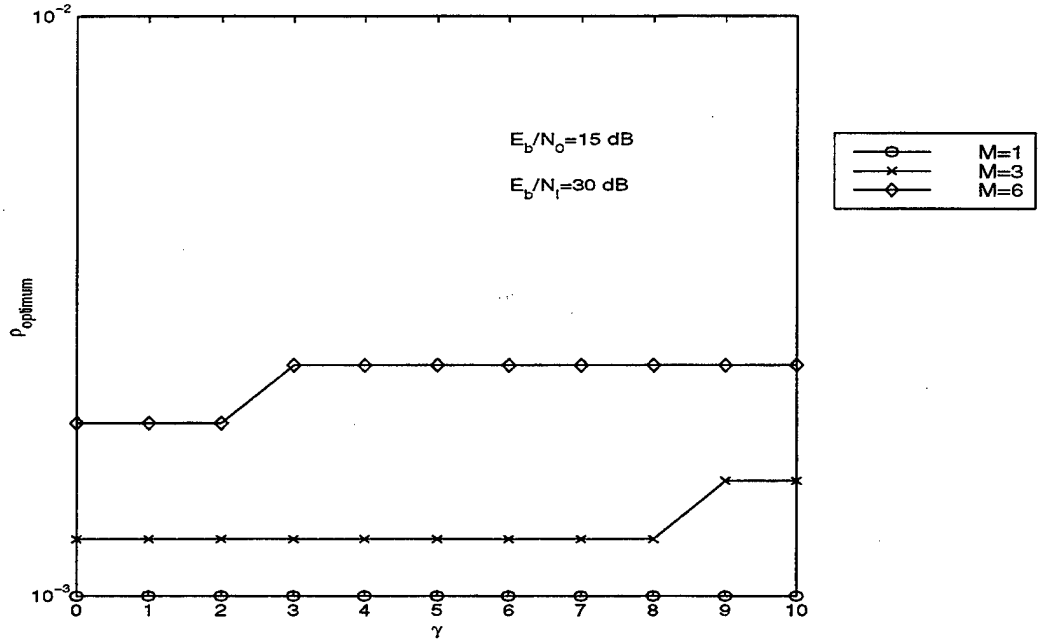

Figure 5.30: Optimum value of ρ as a function of γ with spatial diversity order as a parameter for L = 4, E_b/N_0 = 15 dB and E_b/N_I = 30 dB.

C. CHAPTER CONCLUSIONS

In this chapter, the performance of Direct Sequence Differential Phase Shift Keying (DS-DPSK) with first order post-detection selection combining (PDSC1) and L-fold time diversity in a Rician fading channel in the presence of pulsed noise interference and additive white Gaussian noise (AWGN) has been considered. Closed form solutions for the probability of bit error were not available for either the Rayleigh or Rician channels so numerical solution was required. The performance of the PDSC1 receiver with time diversity in a fading environment with no pulse noise jamming was investigated. It was determined that the performance of the PDSC1 receiver with time diversity was relatively insensitive to the fading condition in comparison to the self-normalized, noise-normalized and linear receivers. Given a sufficient signal energy to thermal noise density ratio, the PDSC1 receiver was shown to perform better than the other receivers under severe and moderate fading conditions. The performance of the PDSC1 receiver with time diversity for a fixed jammer peak power specification under severe and moderate fading conditions was analyzed. It was determined that for both fading conditions, jamming alternating bits produced the worst performance for the lower values of signal-to-interference ratios, while jamming

consecutive bits produces the worst performance at the higher values. These results are similar to those observed for the PDSC1 receiver with no time diversity.

The worst case performance of the PDSC1 receiver with time diversity was also investigated. For either the severe or moderate fading condition, it was observed that the PDSC1 receiver with time diversity was not effective in mitigating pulse noise jamming. It was observed that the worst case performance curve did not move closer to the continuous jamming curve for increasing spatial diversity order with fixed time diversity order (L = 4) or for increasing time diversity order with fixed spatial diversity order (M = 4). For either the Rayleigh channel or the moderate fading condition, the optimum value of ρ was seen to decrease slightly for increasing time diversity order with M = 4. A slight increase in ρ was observed per increasing spatial diversity order with L = 4. This observation also held for other values of γ between 0 and 10. For the Rayleigh channel, it was seen that for signal-to-interference ratios below 25 dB, increasing the time diversity order for a fixed spatial diversity order of M = 4 led to a gradual performance decrease. Above this value of signal-to-interference ratio, a time diversity order of L = 2 or 3 produced a modest performance improvement. Similar results were observed when the spatial order was varied as the time diversity order remain fixed. For moderate fading, any increase in time or spatial diversity order led to a performance degradation. For severe and moderate fading, it was observed that the optimum value of ρ decreased as time diversity order was increased for a fixed spatial diversity order and increased as spatial diversity order was increased for a fixed time diversity order. In the latter case, it is seen that the jammer is forced to a more continuous form of jamming strategy. These results also hold true for $0 \leq \gamma \leq 10$. The worst case performance of the PDSC1 receiver with time diversity was compared with the worst case performance of the self-normalized, noise-normalized, linear and PDSC1 receivers under severe and moderate fading conditions. For the Rayleigh fading channel, it was seen that the PDSC1 receiver with time diversity is inferior to the other receivers for $E_b/N_I < 28$ dB. As signal-to-interference ratio is increased above this in the Rayleigh limit of the channel, the PDSC1 receiver with time diversity provides superior performance in comparison to that of any of the other receivers. For the moderate fading channel, it was seen that the PDSC1 receiver with time diversity was inferior to the other receivers over the full range of signal-to-interference ratio.

VI. DS-DPSK WITH CONVOLUTIONAL CODING AND SOFT DECISION VITERBI DECODING

In this chapter, the performance of Direct Sequence Differential Phase Shift Keying (DS-DPSK) with convolutional coding and soft decision Viterbi decoding in a Rician fading channel in the presence of pulsed noise interference and additive white Gaussian noise (AWGN) is considered. The transmitter of the coded DS-DPSK system is shown in Figure 6.1.

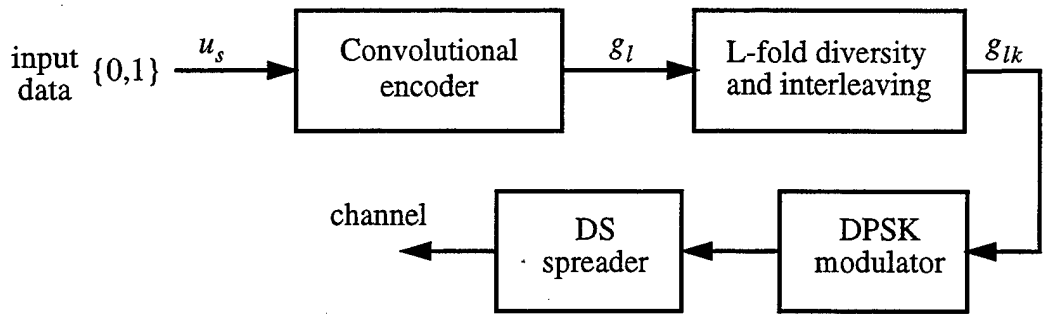

Figure 6.1: Transmitter model of DS-DPSK with convolutional coding and L-fold time diversity.

Here a sequence of binary information bits $\{u_s, s = 1, 2...kB\}$ of length kB is input to the convolutional encoder producing a coded binary data sequence $\{g_l, l = 1, 2...nB\}$ of length nB. For every k information bits taken at the information bit rate, R_b, n output coded bits are produced at the coded bit rate, R_c. The time required to transmit n coded bits must be equal to the time required to transmit k uncoded information bits. The resultant is that the coded bit rate $R_c = R_b/r_c$ and the energy per each coded bit, denoted $E_c = r_c E_b$, where $r_c = k/n$ $(r_c < 1)$ is the code rate. The parameter B is an integer that is determined by the length of a particular code word.

A general convolutional encoder may be implemented with k shift registers and n modulo-2 adders. At each clock interval, k information bits are multiplexed into the first stages of the k shift registers, and the previous information bits are shifted one shift register stage to the right. In a convolutional encoder, each set of n coded bits is determined by the k data bits and between $\nu - 1$ and $k(\nu - 1)$ of the preceding data bits. The parameter ν is termed the *constraint length* of the convolutional code and is defined as the maximum number of shifts over which a single information bit can effect the encoder output.

Although convolutional codes are not necessarily finite in length, the performance analysis initially assumes a fixed length code and is then generalized to an infinite length code. In general coding theory, the Hamming distance represents the number of bits for which 2 code words are different. The Hamming weight is the number of nonzero components in a code word. The Hamming distance between 2 code words may be determined as the Hamming weight of the modulo-2 addition of the 2 code words. In notational form, the distance between the p^{th} code word sequence $\{g_l^{(p)}, l = 1, 2...nB\}$ and the q^{th} code word sequence $\{g_l^{(q)}, l = 1, 2...nB\}$ is expressed as $d(g_l^{(p)}, g_l^{(q)}, l = 1, 2...n) = w(g_l^{(p)} + g_l^{(q)}, l = 1, 2...n)$. Convolutional codes are linear. A linear code is one where the modulo-2 addition of any 2 code words results in another code word. It is therefore seen that the set of Hamming distances between any one code word and the rest of the code words is the same for all code words. Any one code word may then be selected in considering the performance of the convolutional code then without loss of generality. The ability of a convolutional code to perform error correction is strongly related to its minimum free distance, d_{free} defined to be the minimum Hamming distance between any 2 possible code words. Convolutional codes can be characterized by a transfer function relating the input to the output from which the minimum free distance may be ascertained. A more detailed treatment of convolutional codes and their properties may be found in [25]. Referring again to Figure 6.1, each bit at the output of the convolutional encoder is repeated L times producing the new binary sequence for the p^{th} code word $\{g_{lk}^{(p)}, l = 1, 2...nB; k = 1, 2...L\}$. This sequence is interleaved and fed to the DPSK modulator for carrier modulation. The modulator output is then fed to the Direct Sequence Spread Spectrum module for "spreading" before transmission over the channel.

A block diagram of the linear receiver for the DS-DPSK coded system is shown in Figure 6.2. The sequence of events prior to decoding are seen to be exactly the same as that for the

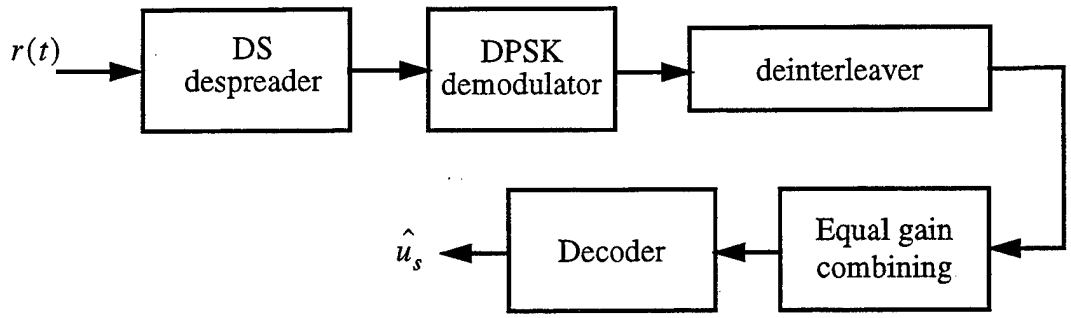

Figure 6.2: Block diagram of the linear receiver for the coded DS-DPSK system.

uncoded system. The only fundamental difference is that the system now operates at the coded bit rate rather than the information bit rate.

In this analysis, a maximum likelihood estimate is sought. The Viterbi decoder is a maximum likelihood decoder which utilizes a decoding trellis to maximize a set of path metrics. The trellis is an efficient representation of all possible code words generated by the encoder where each code word is represented as a path through the trellis. Path metrics are formed as a sum of branch metrics, which are produced as the sum of bit metrics. In this analysis, it is assumed the code word path is of length nB bits, where B is the number of branches along any one path and n is the number of bits per branch. At the B^{th} branch node, path metrics are compared and the path with the highest metric is selected as the correct path through the trellis. The equal gain combining structure between the demodulator output and the input to the decoder in Figure 6.2 is shown in Figure 6.3. The random variables forming the sequence

$\{V_{1lmk}, l = 1, 2...n; m = 1, 2...B; k = 1, 2...\mathrm{L}\}$ represent the deinterleaved, demodulator outputs representing bit 0. The random variables forming the sequence

$\{V_{2lmk}, l = 1, 2...n; m = 1, 2...B; k = 1, 2...\mathrm{L}\}$ represent the deinterleaved, demodulator outputs representing bit 1. The random variables forming the sequences

$\{V_{1lm}, l = 1, 2...n; m = 1, 2...B\}$ and $\{V_{2lm}, l = 1, 2...n; m = 1, 2...B\}$ serve as inputs to the decoder.

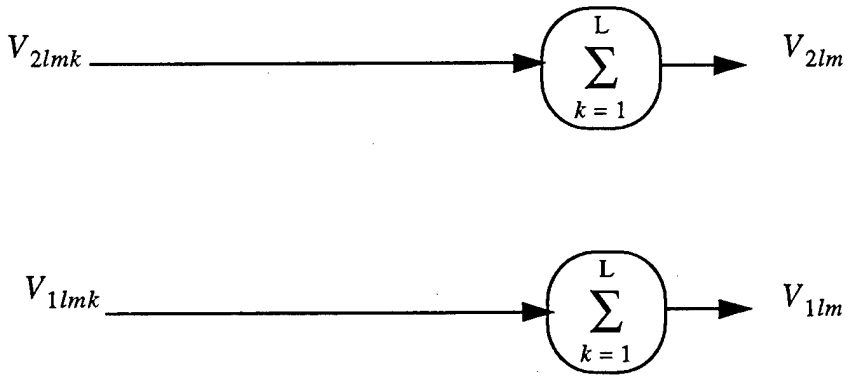

Figure 6.3: Equal gain combining structure for the linear receiver.

A maximum likelihood estimate of the path metric for the p^{th} path may be produced by considering the *log-likelihood* function

$$PM^{(p)} = \sum_{m=1}^{B} \sum_{l=1}^{n} \log(f_{V_{1lm}, V_{2lm}}(V_{1lm}, V_{2lm} | g_{lm}^{(p)})) \qquad (6.1)$$

In [5], it was shown that maximizing $\log(f_{V_{1lm}, V_{2lm}}(V_{1lm}, V_{2lm} | g_{lm}^{(p)}))$ is equivalent to maximizing a pair of correlation metrics obtained through cross-correlation of the received signal with the transmitted signals representing bit 0 and bit 1. Since the coupled operation of the receiver of Figure 2.3 and combiner of Figure 6.3 producing the random variables V_{1lm} and V_{2lm} may be represented as a cross-correlation between the received signal and the transmitted signals representing bit 0 and bit 1, a suitable correlation metric for the l^{th} bit of the m^{th} branch of the p^{th} path is

$$CM_{lm}^{(p)} = ([1 - g_{lm}^{(p)}]V_{1lm} + g_{lm}^{(p)} V_{2lm}) \qquad (6.2)$$

This metric aligns the signal representing bit 0 with detector branch 1 and the signal branch representing bit 1 with detector branch 2. Maximizing this metric at each bit interval over the entire coded word sequence is performed by receivers employing hard decision decoding. In soft decision receivers, individual bit metrics are summed over the entire the code word path before a decision

is made. Using the correlation metric of equation 6.2 in place of $\log(f_{V_{1lm},\,V_{2lm}}(V_{1lm},\,V_{2lm}|g_{lm}^{(p)}))$ in equation 6.1, the path metric for the p^{th} path may now be reexpressed as

$$PM^{(p)} = \sum_{m=1}^{B}\sum_{l=1}^{n} CM_{lm}^{(p)} \tag{6.3}$$

Defining the branch metric for the m^{th} branch of the p^{th} path to be

$$BM_{m}^{(p)} = \sum_{l=1}^{n} CM_{lm}^{(p)} \tag{6.4}$$

the path metric for the p^{th} path may be expressed as

$$PM^{(p)} = \sum_{m=1}^{B} BM_{m}^{(p)} \tag{6.5}$$

In the error analysis, the performance of a convolutional code will be derived from the probability of first error event. A first error event is defined as the probability that another path that merges with the all-zero path for the first time at branch node B has a larger path metric than that of the all-zero code word. From equations 6.2 and 6.3, the path metric for the all-zero code word is

$$PM^{(1)} = \sum_{m=1}^{B}\sum_{l=1}^{n} V_{1lm} \tag{6.6}$$

since for the all-zero code word $g_{lm}^{(p)} = 0, \forall(l,m)$. By substituting the known relation $V_{1lm} = \sum_{k=1}^{L} V_{1lmk}$, equation 6.6 can be written as

$$PM^{(1)} = \sum_{m=1}^{B}\sum_{l=1}^{n}\sum_{k=1}^{L} V_{1lmk} \tag{6.7}$$

Denoting the code word path length $N = nB$ bits, equation 6.7 may now be expressed as

$$PM^{(1)} = \sum_{i=1}^{N}\sum_{k=1}^{L} V_{1ki} \tag{6.8}$$

where i is an index that runs over all bits along the path. A decoder error occurs when the path metric for the p^{th} path at branch node B is greater than the path metric for the all-zero path

$$PM^{(p)} > PM^{(1)} \tag{6.9}$$

Assuming the code word for the p^{th} path has weight d, its path metric is

$$PM^{(p)} = \sum_{i=1}^{d} \sum_{k=1}^{L} V_{2ki} + \sum_{i=d+1}^{N} \sum_{k=1}^{L} V_{1ki} \tag{6.10}$$

Rewriting equation 6.8 as

$$PM^{(1)} = \sum_{i=1}^{d} \sum_{k=1}^{L} V_{1ki} + \sum_{i=d+1}^{N} \sum_{k=1}^{L} V_{1ki} \tag{6.11}$$

and substituting equations 6.10 and 6.11 into equation 6.9, it is seen that a decoding error occurs when

$$\sum_{i=1}^{d} \sum_{k=1}^{L} V_{2ki} > \sum_{i=1}^{d} \sum_{k=1}^{L} V_{1ki} \tag{6.12}$$

More generally, since the code is linear, the probability of decoder error between any 2 code words with Hamming distance d is

$$P_2(d) = \Pr\left(\sum_{i=1}^{d} \sum_{k=1}^{L} V_{2ki} > \sum_{i=1}^{d} \sum_{k=1}^{L} V_{1ki} \right) \tag{6.13}$$

It is seen through this relation that the coded system with L^{th} order time diversity is equivalent to the uncoded system with dL^{th} order time diversity. This statement is general and therefore applies to any condition of fading or pulse noise jamming. In addition, since the use of the correlation metric of equation 6.2 is applicable to the other receivers analyzed in this work, the result of equation 6.13 extends to these other receivers. The coded noise-normalized and self-normalized systems with L^{th} order time diversity are equivalent to the respective uncoded systems with dL^{th} order time diversity. The coded PDSC1 system with M^{th} order spatial diversity is equivalent to the uncoded system with M^{th} order spatial diversity and d^{th} order time diversity. The coded

PDSC1 system with M^{th} order spatial diversity and L^{th} order time diversity is equivalent to the uncoded system with M^{th} order spatial diversity with dL^{th} order time diversity.

Since there may be many possible pairs of code words with distance d, it is more general to consider the probability of an error event over all pairs of code words with distance d, $P_e(d)$. $P_e(d)$ is then a union of all error events over all possible pairs of code words with distance d. When considering the all-zero code word, this is equivalent to stating that $P_e(d)$ is a union over all possible error events between the all-zero code word and code words of weight d. If there are a total of A_d possible code words with weight d, the probability of an error event is upper-bounded in the following way

$$P_e(d) \leq A_d P_2(d) \tag{6.14}$$

Since individual paths may overlap over certain portions of the code, the events forming the union are not in general disjoint. The result is that the bound of equation 6.14 may not be very tight. This is especially true at low values of signal-to-noise ratio.

If the total information weight of all code words of weight d is B_d, the probability of bit error for all code words of weight d is upper-bounded by

$$P_b(d) < \frac{1}{k} B_d P_2(d) \tag{6.15}$$

Here $B_d P_2(d)$ represents the average number of bits in error and k is used as a normalization for the total number of information bits along the path. Extending to the case of an infinite length code, the upper bound on the unconditional probability of bit error is obtained by summing over all possible Hamming distances, the expression for which is

$$P_b < \frac{1}{k} \sum_{d = d_{free}}^{\infty} B_d P_2(d) \tag{6.16}$$

The values of A_d and B_d are parameters of the transfer function of a particular code and are available by table look-up. The best convolutional codes in terms of their distance properties have been determined through numerical search. In the next sections, the performance of the noise-normalized, self-normalized, PDSC1 and linear receivers is considered. Due to the numerical complexity, the numerical analysis is not extended to the PDSC1 receiver with time diversity.

A. PERFORMANCE ANALYSIS FOR NOISE-NORMALIZED RECEIVER AND SOFT DECISION VITERBI DECODING

A block diagram of the DS-DPSK coded receiver system with noise-normalization is shown in Figure 6.4. The sequence of events prior to decoding are seen to be exactly the same as that for the uncoded system.

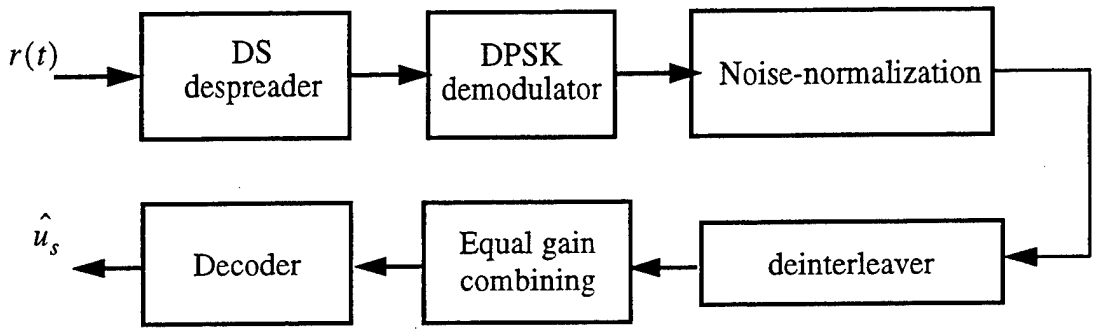

Figure 6.4: Block diagram of the DS-DPSK coded receiver system with noise-normalization.

1. Numerical Results

In this section, the performance of the coded noise-normalized receiver system in a pulse noise jamming environment is analyzed. In the numerical analysis, the worst case performance was produced by those conditions outlined in equations 2.30 and 2.31 as was previously the case for the uncoded system. To keep this analysis consistent with the analysis done for the uncoded system, equation 2.31 ($\rho_1 = 0$, $\rho = \rho_2$) is selected to represent worst case performance. Performance curves for the noise-normalized receiver for diversity orders L = 1 and 4 and jammer fractions $\rho = 0.01, 0.1, 0.25, 1$ and worst case, $E_b/N_0 = 15$ dB, $\gamma = 0$, $\nu = 3$ and $r_c = 0.5$ are shown in Figures 6.5 and 6.6 respectively. It is seen that pulse noise jamming is not effective for either diversity case since the continuous jamming curves correspond to the worst case performance curves. It is seen for very high signal-to-interference ratio ($E_b/N_I > 30$ dB), that there is significant performance improvement when moving from no diversity to a diversity order of L = 4. This is clearly seen in Figure 6.7 where the worst case performance curves for the coded and

uncoded systems are shown for L = 1 and 4, E_b/N_0 = 15 dB, $\gamma = 0$, $\nu = 3$ and $r_c = 0.5$. It is also seen that the net performance improvement between uncoded and coded systems is significantly greater for a diversity order of L = 4 compared to the case of no diversity for $E_b/N_I >$ 20 dB. Figure 6.8 compares the worst case performance curves for the coded and uncoded systems for L = 1 and 4, E_b/N_0 = 15 dB, $\gamma = 0$, $\nu = 5$ and $r_c = 0.75$. By comparing these to Figure 6.7, it is seen that the performance improvement afforded by the code rate of $r_c = 0.75$ with constraint length of $\nu = 5$ is not as great as the improvement given by the code rate $r_c = 0.5$, constraint length $\nu = 3$ system for any diversity case considered.

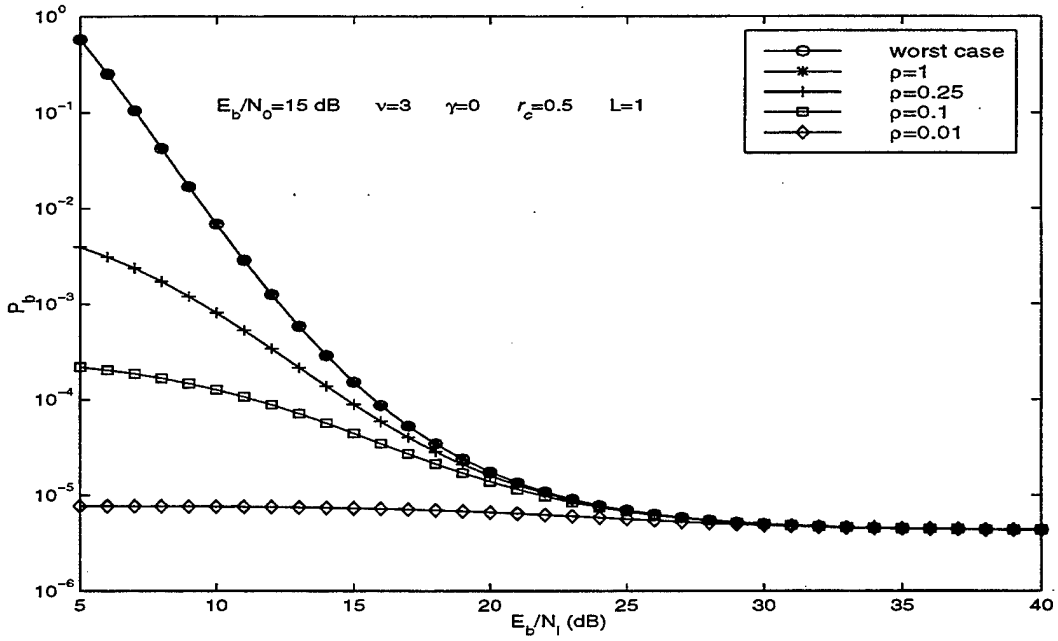

Figure 6.5: Performance of noise-normalized receiver for pulse jamming fractions $\rho = 1, 0.25, 0.1,$ 0.01 and worst case for diversity order L = 1, E_b/N_0 = 15 dB, $\gamma = 0$, $\nu = 3$ and $r_c = 0.5$.

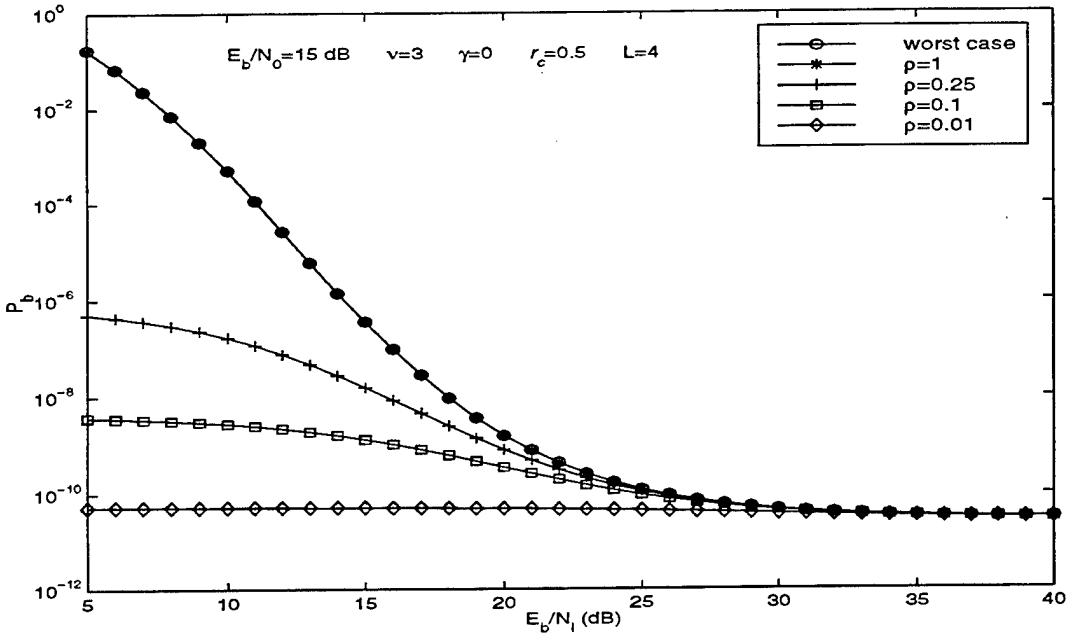

Figure 6.6: Performance of noise-normalized receiver for pulse jamming fractions $\rho = 1, 0.25, 0.1, 0.01$ and worst case for diversity order $L = 4$, $E_b/N_0 = 15$ dB, $\gamma = 0$, $\nu = 3$ and $r_c = 0.5$.

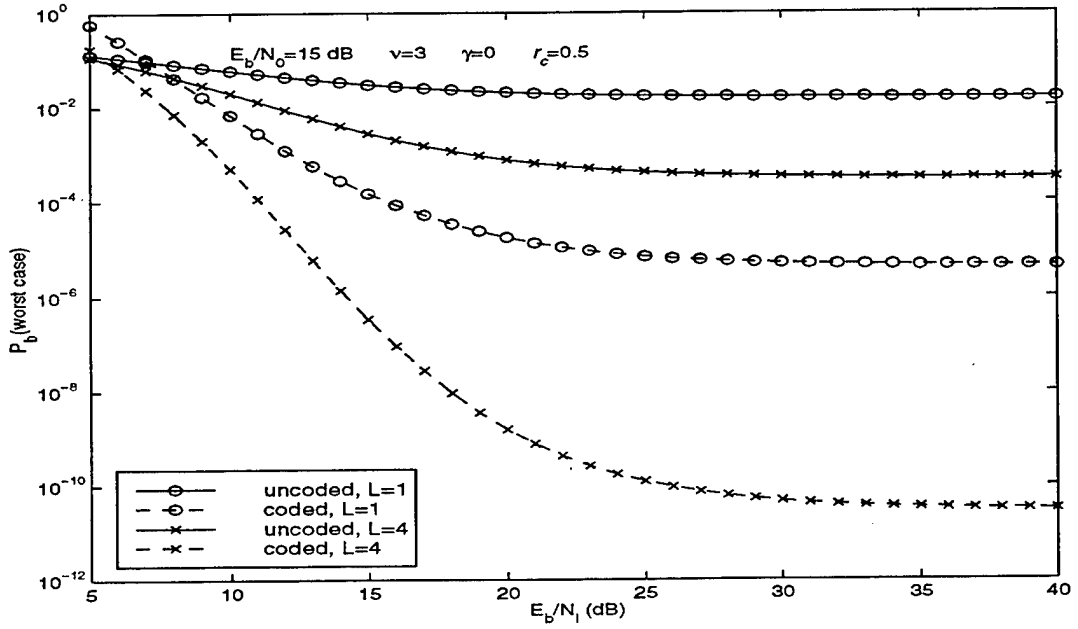

Figure 6.7: Worst case performance comparison of coded and uncoded system for noise-normalized receiver for diversity orders $L = 1$ and 4, $E_b/N_0 = 15$ dB, $\gamma = 0$, $\nu = 3$ and $r_c = 0.5$.

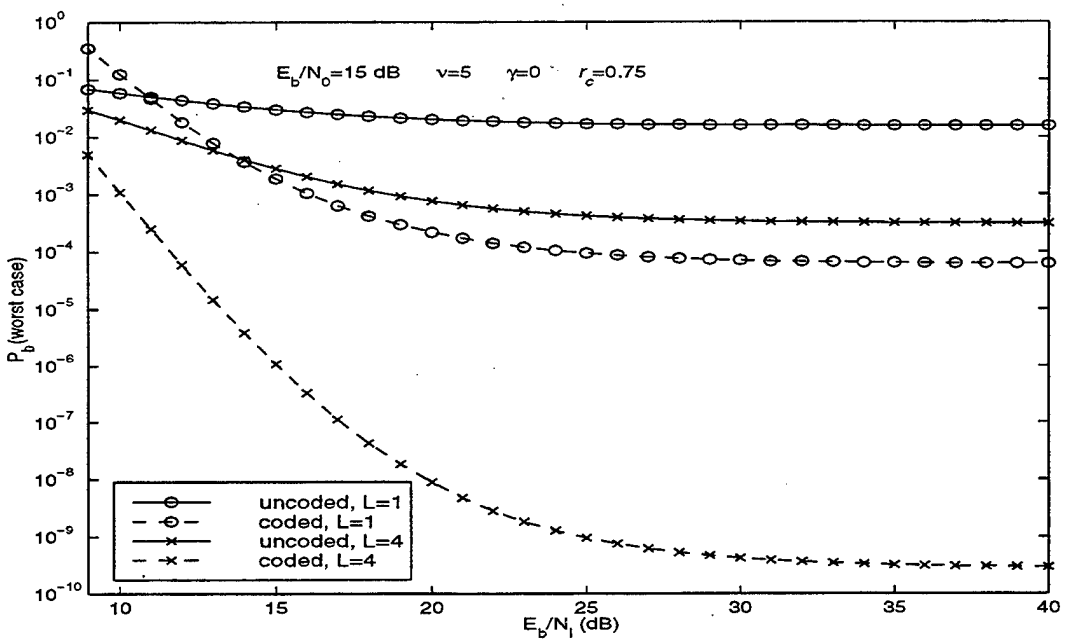

Figure 6.8: Worst case performance comparison of coded and uncoded system for noise-normalized receiver for diversity orders L = 1 and 4, $E_b/N_0 = 15$ dB, $\gamma = 0$, $\nu = 5$ and $r_c = 0.75$.

Performance curves for the noise-normalized receiver for diversity orders L = 1 and 4 and jammer fractions $\rho = 0.01, 0.1, 0.25, 1$ and worst case, $E_b/N_0 = 10$ dB, $\gamma = 0$, $\nu = 5$ and $r_c = 0.5$ are shown in Figures 6.9 and 6.10 respectively. Again it is seen that pulse noise jamming is not effective for either diversity case. Figure 6.11 shows the worst case performance curves for the coded and uncoded systems for L = 1 and 4, $E_b/N_0 = 10$ dB, $\gamma = 0$, $\nu = 5$ and $r_c = 0.5$. For very high signal-to-interference ratio, it is again seen that the performance improvement between uncoded and coded systems is significant with the diversity order L = 4 demonstrating the larger net performance improvement. The amount of improvement however is not as great as was demonstrated at $E_b/N_0 = 15$ dB and $r_c = 0.5$. Figure 6.12 shows the worst case performance curves for the coded and uncoded systems for L = 1 and 4, $E_b/N_0 = 10$ dB, $\gamma = 0$, $\nu = 7$ and $r_c = 0.75$. It is seen that there is very little performance difference between the coded and uncoded systems when no diversity is employed. When diversity is utilized however, the difference between the coded and uncoded systems is substantial. This result differs from the case

of higher signal to thermal noise ratio and code rate (E_b/N_0 = 15 dB and $r_c = 0.75$) and lower constraint length ($\nu = 5$) illustrated in Figure 6.8 where the difference between coded and uncoded systems was significant for both cases of diversity (L = 4) and no diversity (L = 1).

Performance curves for the noise-normalized receiver for diversity orders L = 1 and 4 and jammer fractions $\rho = 0.01, 0.1, 0.25, 1$ and worst case, E_b/N_0 = 15 dB, $\gamma = 5$, $\nu = 3$ and $r_c = 0.5$ are shown in Figures 6.13 and 6.14 respectively. For the case of no diversity, it is seen that pulse noise jamming is effective in the range 10 dB < E_b/N_I < 30 dB. At E_b/N_I = 20 dB; it is seen that the difference between the continuous jamming curve and the worst case performance curve is approximately 3 dB. For the case of diversity L = 4, jammer effectiveness has been negated. The worst case performance curves for the coded and uncoded systems are shown for L = 1 and 4, E_b/N_0 = 15 dB, $\gamma = 5$, $\nu = 3$ and $r_c = 0.5$ in Figure 6.15. The performance improvement between the uncoded and coded systems for both diversity cases is significant with the L = 4 diversity case again showing the larger net improvement. These observations also apply to the higher code rate system worst case performance curves shown in Figure 6.16 for L = 1 and 4, E_b/N_0 = 15 dB, $\gamma = 5$, $\nu = 5$ and $r_c = 0.75$. These observations are similar to those made under the Rayleigh fading analysis. Performance curves for the noise-normalized receiver for diversity orders L = 1 and 4 and jammer fractions $\rho = 0.01, 0.1, 0.25, 1$ and worst case, E_b/N_0 = 10 dB, $\gamma = 5$, $\nu = 5$ and $r_c = 0.5$ are shown in Figures 6.17 and 6.18 respectively. It is seen that pulse noise jamming is not effective at either diversity order. It is recalled that the pulse noise jammer was effective at E_b/N_0 = 15 dB and L = 1 for $\gamma = 5$, $r_c = 0.5$ and $\nu = 5$. The lack of jammer effectiveness at E_b/N_0 = 10 dB is most likely attributable to the fact that the overall signal-to-noise (thermal noise plus interference noise) ratio is lower. Continuous jamming is generally more effective for this condition. Figure 6.19 shows the worst case performance curves for the coded and uncoded systems for diversity orders L = 1 and 4, E_b/N_0 = 10 dB, $\gamma = 5$, $\nu = 5$ and $r_c = 0.5$. The performance improvement between the uncoded and coded systems for each diversity order is significant with again the case of L = 4 having the larger net improvement. These observations also apply to the higher code rate system where in Figure 6.20 the worst case

performance curves for the coded and uncoded systems are shown for L = 1 and 4, E_b/N_0 = 10 dB, $\gamma = 5$, $\nu = 7$ and $r_c = 0.75$. In the case of no diversity, this differs from that observed for the Rayleigh channel in Figure 6.12 where the difference between the uncoded and coded systems for E_b/N_0 = 10 dB, $\nu = 7$ and $r_c = 0.75$ was rather small.

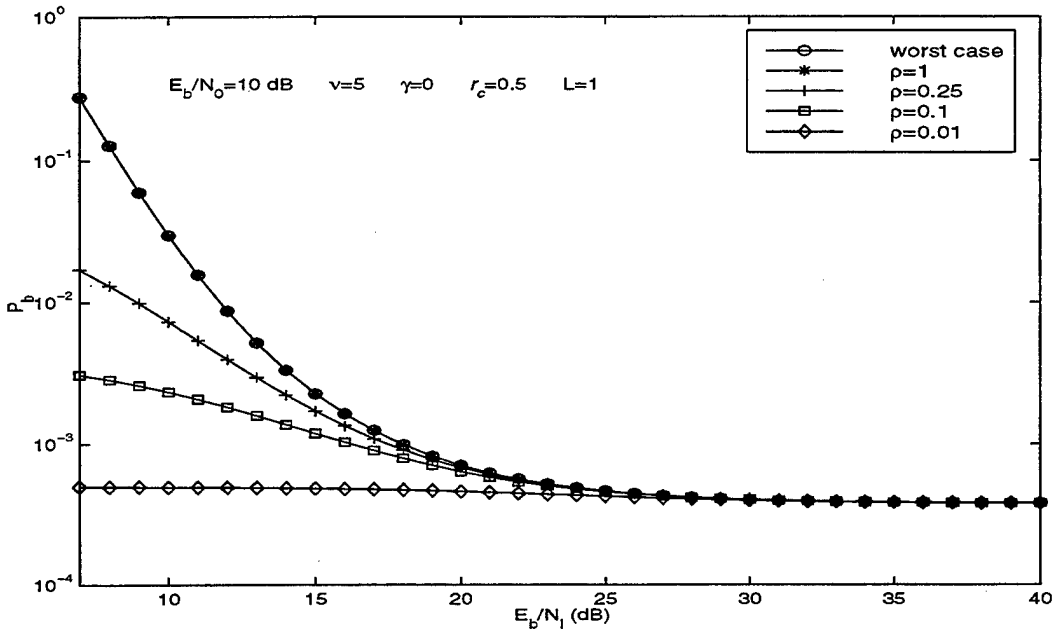

Figure 6.9: Performance of noise-normalized receiver for pulse jamming fractions ρ = 1, 0.25, 0.1, 0.01 and worst case for diversity order L = 1, E_b/N_0 = 10 dB, $\gamma = 0$, $\nu = 5$ and $r_c = 0.5$.

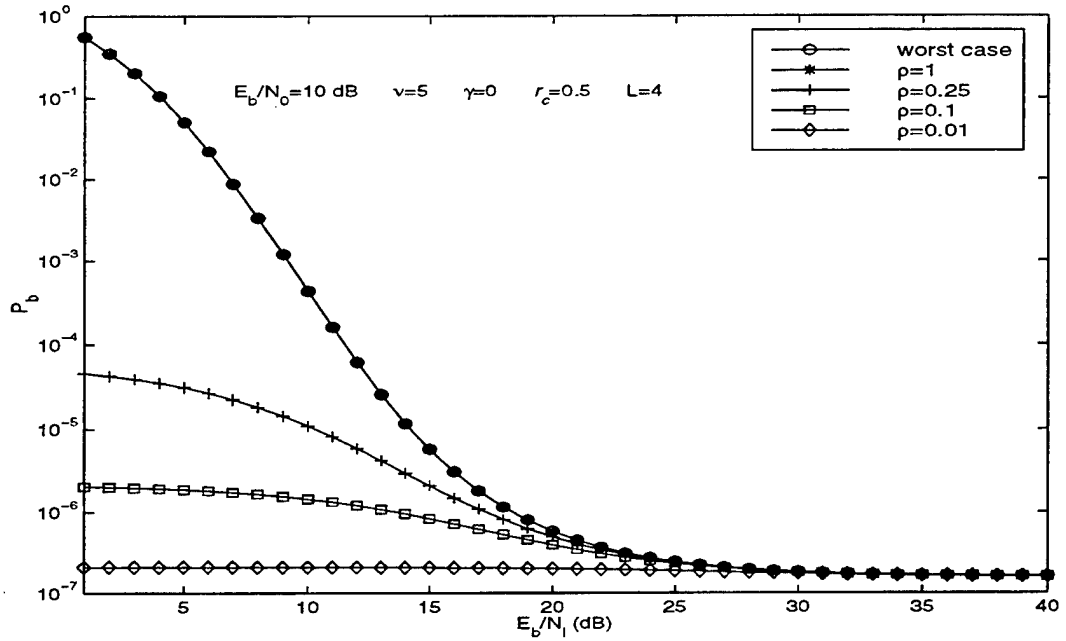

Figure 6.10: Performance of noise-normalized receiver for pulse jamming fractions $\rho = 1, 0.25, 0.1, 0.01$ and worst case for diversity order $L = 4$, $E_b/N_0 = 10$ dB, $\gamma = 0$, $\nu = 5$ and $r_c = 0.5$.

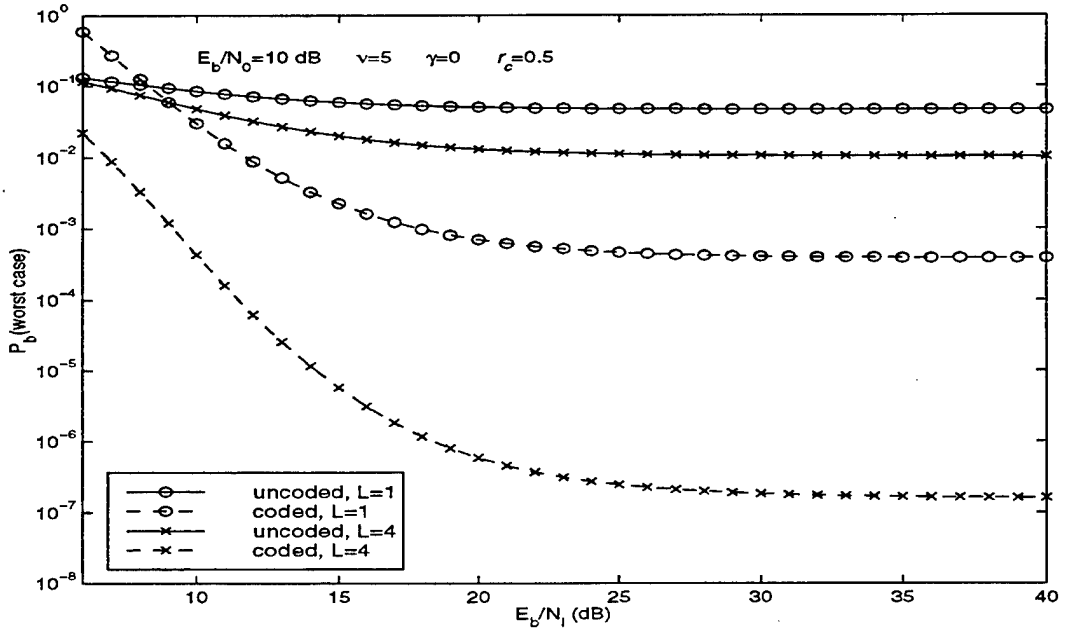

Figure 6.11: Worst case performance comparison of coded and uncoded system for noise-normalized receiver for diversity orders $L = 1$ and 4, $E_b/N_0 = 10$ dB, $\gamma = 0$, $\nu = 5$ and $r_c = 0.5$.

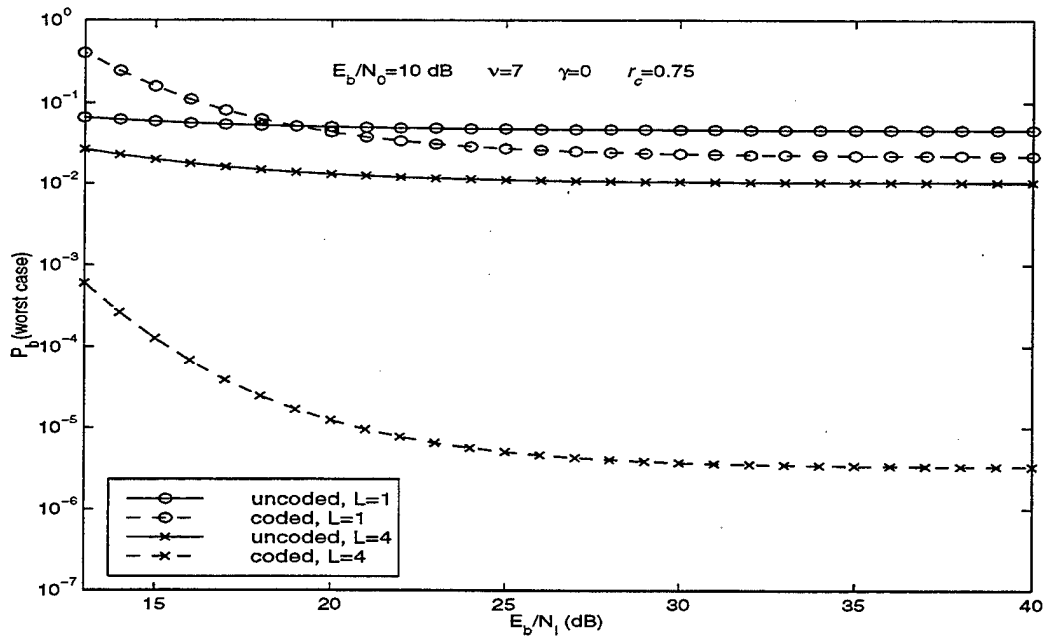

Figure 6.12: Worst case performance comparison of coded and uncoded system for noise-normalized receiver for diversity orders L = 1 and 4, $E_b/N_0 = 10$ dB, $\gamma = 0$, $\nu = 7$ and $r_c = 0.75$.

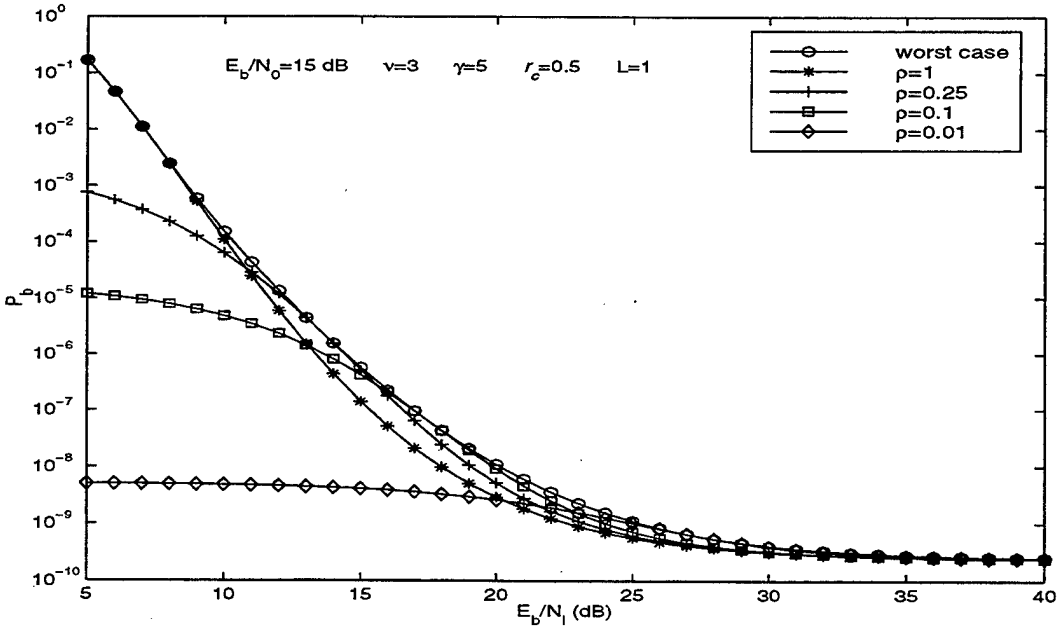

Figure 6.13: Performance of noise-normalized receiver for pulse jamming fractions $\rho = 1$, 0.25, 0.1, 0.01 and worst case for diversity order L = 1, $E_b/N_0 = 15$ dB, $\gamma = 5$, $\nu = 3$ and $r_c = 0.5$.

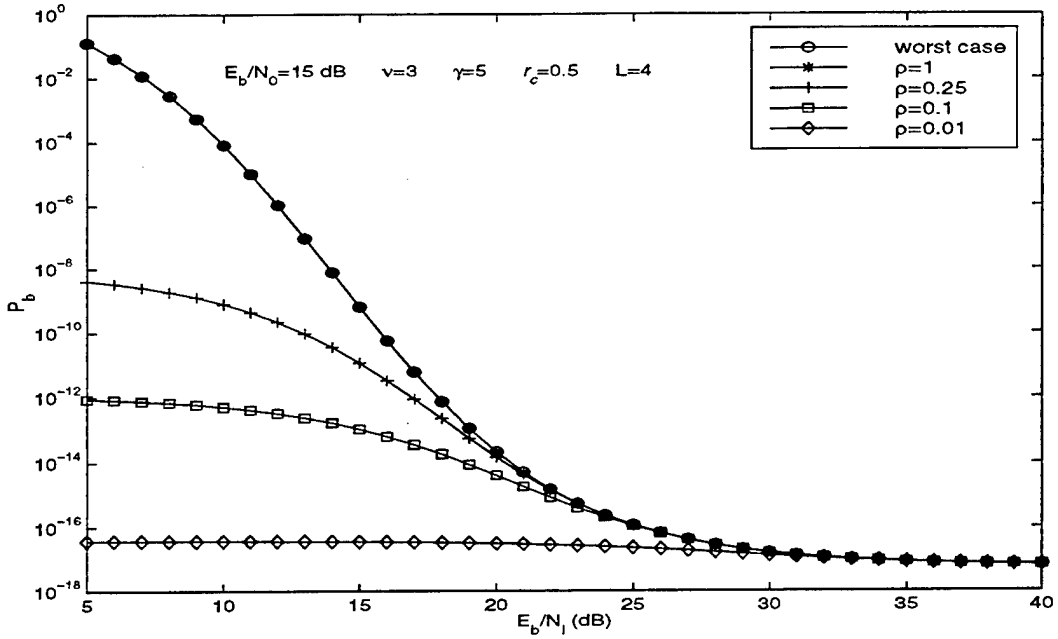

Figure 6.14: Performance of noise-normalized receiver for pulse jamming fractions $\rho = 1, 0.25, 0.1, 0.01$ and worst case for diversity order $L = 4$, $E_b/N_0 = 15$ dB, $\gamma = 5$, $\nu = 3$ and $r_c = 0.5$.

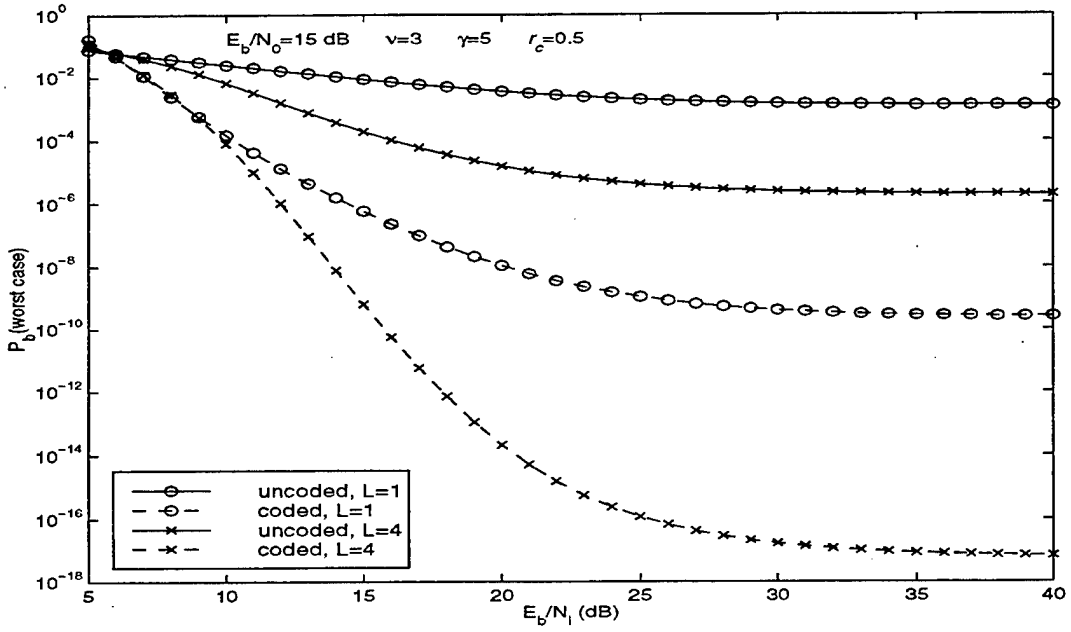

Figure 6.15: Worst case performance comparison of coded and uncoded system for noise-normalized receiver for diversity orders $L = 1$ and 4, $E_b/N_0 = 15$ dB, $\gamma = 5$, $\nu = 3$ and $r_c = 0.5$.

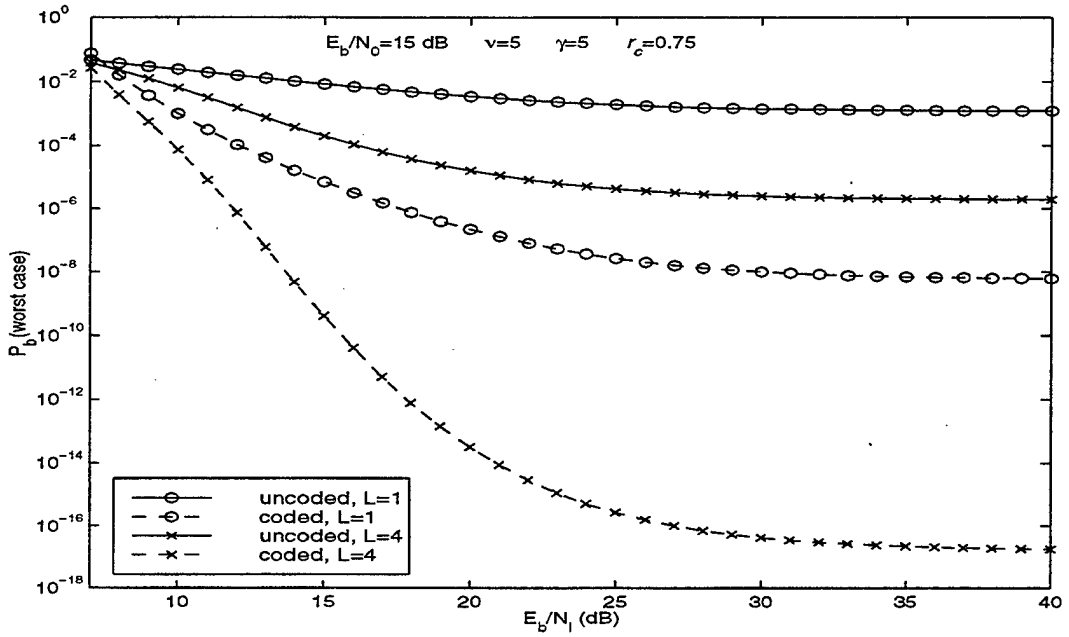

Figure 6.16: Worst case performance comparison of coded and uncoded system for noise-normalized receiver for diversity orders L = 1 and 4, $E_b/N_0 = 15$ dB, $\gamma = 5$, $\nu = 5$ and $r_c = 0.75$.

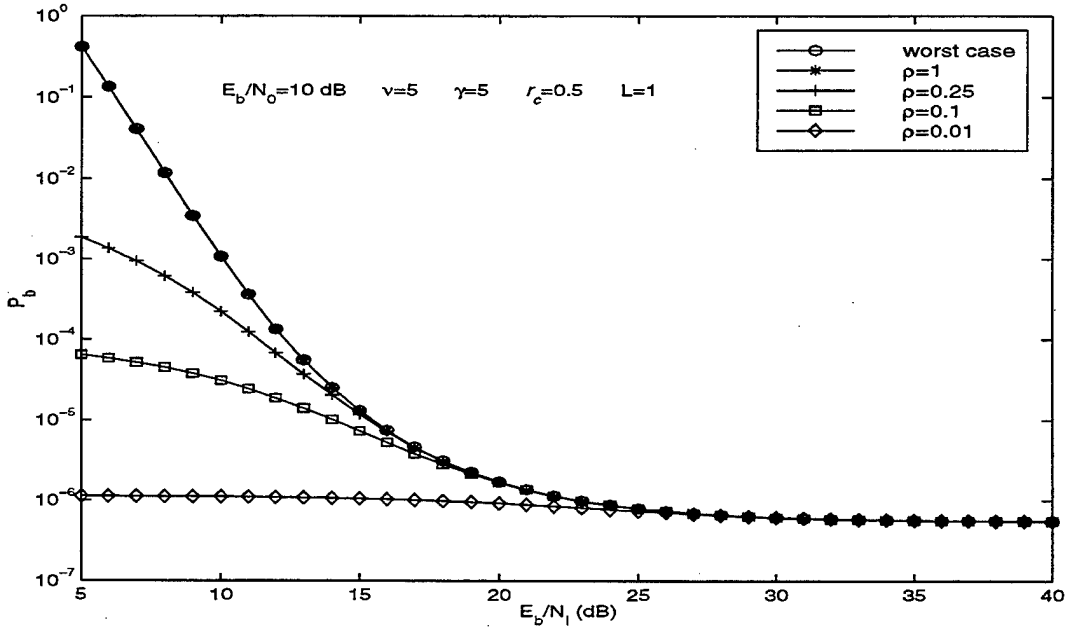

Figure 6.17: Performance of noise-normalized receiver for pulse jamming fractions $\rho = 1$, 0.25, 0.1, 0.01 and worst case for diversity order L = 1, $E_b/N_0 = 10$ dB, $\gamma = 5$, $\nu = 5$ and $r_c = 0.5$.

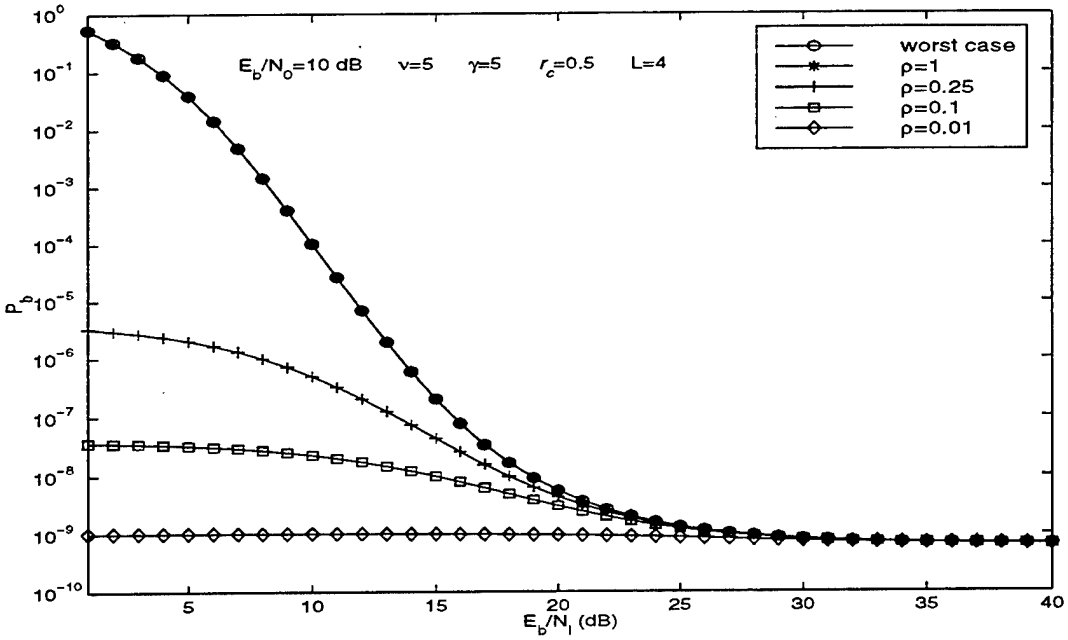

Figure 6.18: Performance of noise-normalized receiver for pulse jamming fractions $\rho = 1, 0.25, 0.1, 0.01$ and worst case for diversity order $L = 4$, $E_b/N_0 = 10$ dB, $\gamma = 5$, $\nu = 5$ and $r_c = 0.5$.

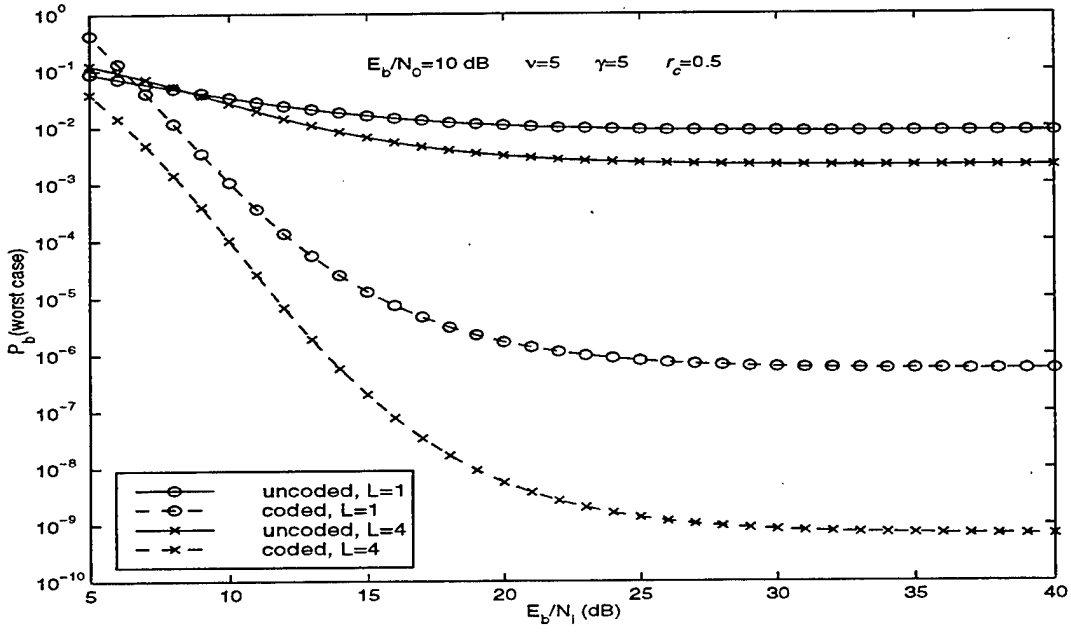

Figure 6.19: Worst case performance comparison of coded and uncoded system for noise-normalized receiver for diversity orders $L = 1$ and 4, $E_b/N_0 = 10$ dB, $\gamma = 5$, $\nu = 5$ and $r_c = 0.5$.

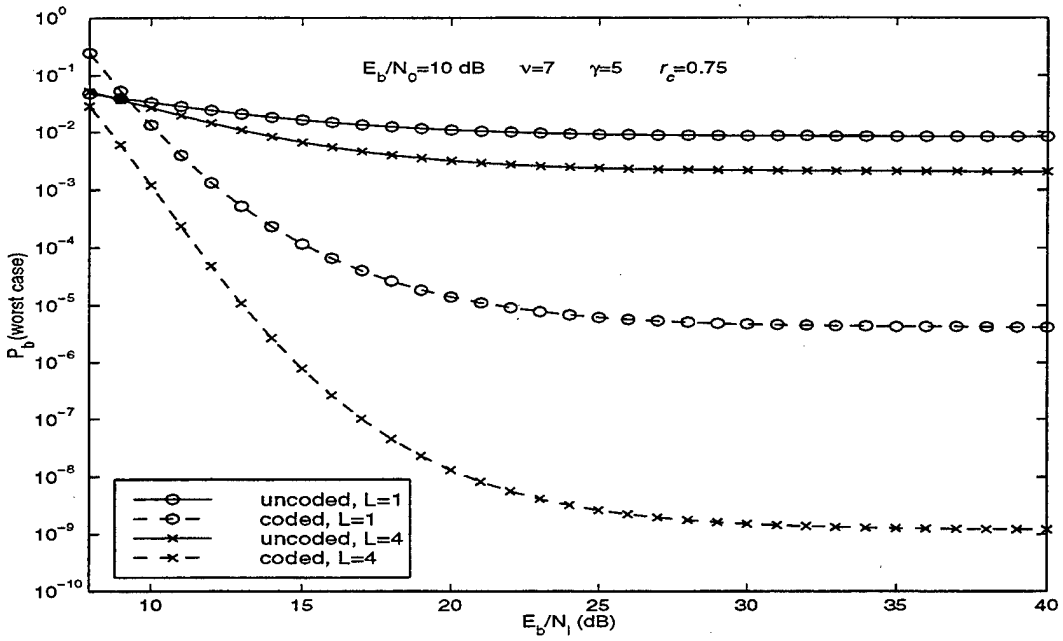

Figure 6.20: Worst case performance comparison of coded and uncoded system for noise-normalized receiver for diversity orders L = 1 and 4, $E_b/N_0 = 10$ dB, $\gamma = 5$, $\nu = 7$ and $r_c = 0.75$.

B. PERFORMANCE ANALYSIS FOR THE PDSC1 RECEIVER AND SOFT DECISION VITERBI DECODING FOR A RAYLEIGH FADING CHANNEL

A block diagram of the DS-DPSK/PDSC1 receiver coded system is shown in Figure 6.21. Prior to deinterleaving, it is seen that the overall receiver structure is exactly the same as the uncoded PDSC1 receiver system. Due to the computational complexity involved in the numerical analysis of the performance of the coded PDSC1 system, only a few cases were able to be analyzed. The performance of the coded PDSC1 system will be compared to the coded noise-normalized, self-normalized and linear receiver systems towards the end of the chapter.

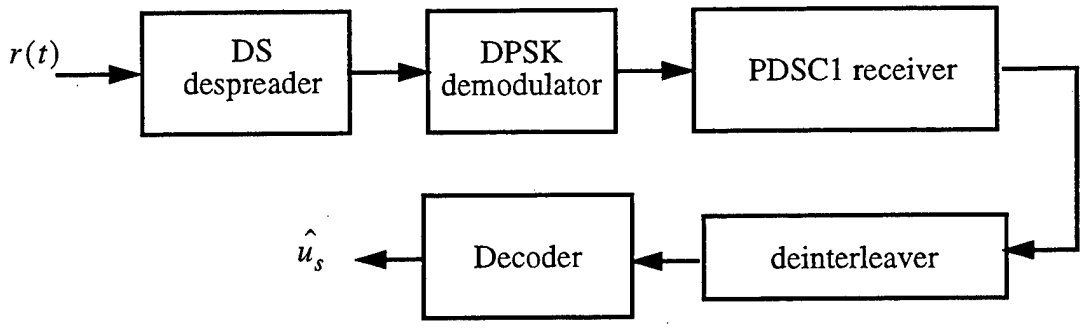

Figure 6.21: Block diagram of the DS-DPSK/PDSC1 receiver coded system.

C. PERFORMANCE ANALYSIS FOR THE SELF-NORMALIZED RECEIVER AND SOFT DECISION VITERBI DECODING

A block diagram of the DS-DPSK/self-normalized receiver coded system is shown in Figure 6.22. It is seen that the receiver structure is exactly the same as the coded noise-normalized receiver system with the noted exception of the type of normalization.

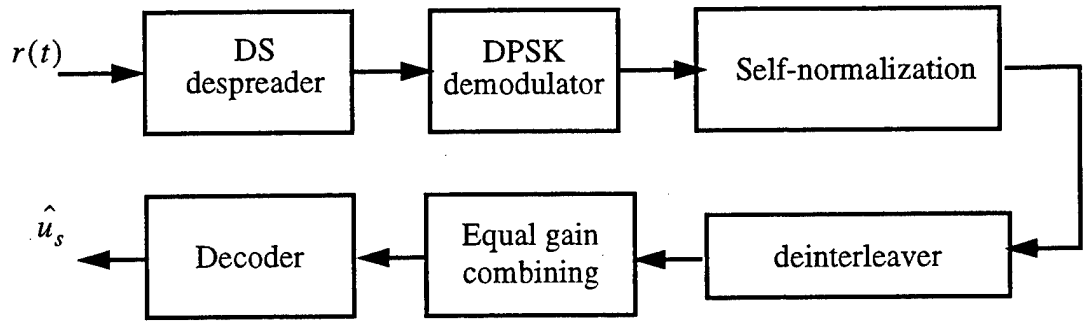

Figure 6.22: Block diagram of the DS-DPSK receiver coded system with self-normalization.

1. Numerical Results

In this section, the performance of the coded self-normalized receiver system in a pulse noise jamming environment is analyzed. As in the case of the coded noise-normalized system, the worst case performance for the coded self-normalized receiver system was produced by those conditions outlined in equations 2.30 and 2.31. To keep this analysis consistent with the analysis of the uncoded self-normalized receiver system, equation 2.31 ($\rho_1 = 0$, $\rho = \rho_2$) is selected to represent worst case performance. Performance curves for the self-normalized receiver for diversity orders L = 1 and 4 and jammer fractions $\rho = 0.01, 0.1, 0.25, 1$ and worst case, $E_b/N_0 =$ 15 dB, $\gamma = 0$, $\nu = 3$ and $r_c = 0.5$ are shown in Figures 6.23 and 6.24 respectively. It is seen that pulse noise jamming is not effective for either diversity case since the continuous jamming curves correspond to the worst case performance curves. It is seen for most of the range of E_b/N_I there is significant performance improvement when moving from no diversity to a diversity order of L = 4. This is clearly seen in Figure 6.25 where the worst case performance curves for the coded and uncoded systems are shown for L = 1 and 4, $E_b/N_0 = 15$ dB, $\gamma = 0$, $\nu = 3$ and $r_c = 0.5$. In addition, the performance improvement between the uncoded and coded systems is significant with the case of L = 4 demonstrating the larger net performance increase. This is similar to what was observed for the noise-normalized receiver. Figure 6.26 compares the worst case performance curves for the coded and uncoded systems for L = 1 and 4, $E_b/N_0 = 15$ dB, $\gamma = 0$, $\nu = 5$ and $r_c = 0.75$. It is seen that there is little difference between the uncoded and coded performance curves for no diversity. In contrast, there is a significant performance improvement in favor of the coded system over the uncoded system for L = 4. Comparing to Figure 6.25, it is seen that the performance improvement afforded by the code rate of $r_c = 0.75$ with constraint length of $\nu = 5$ is not as great as that for the code rate $r_c = 0.5$, constraint length $\nu = 3$ system for any diversity case considered. This is similar to what was observed for the noise-normalized receiver.

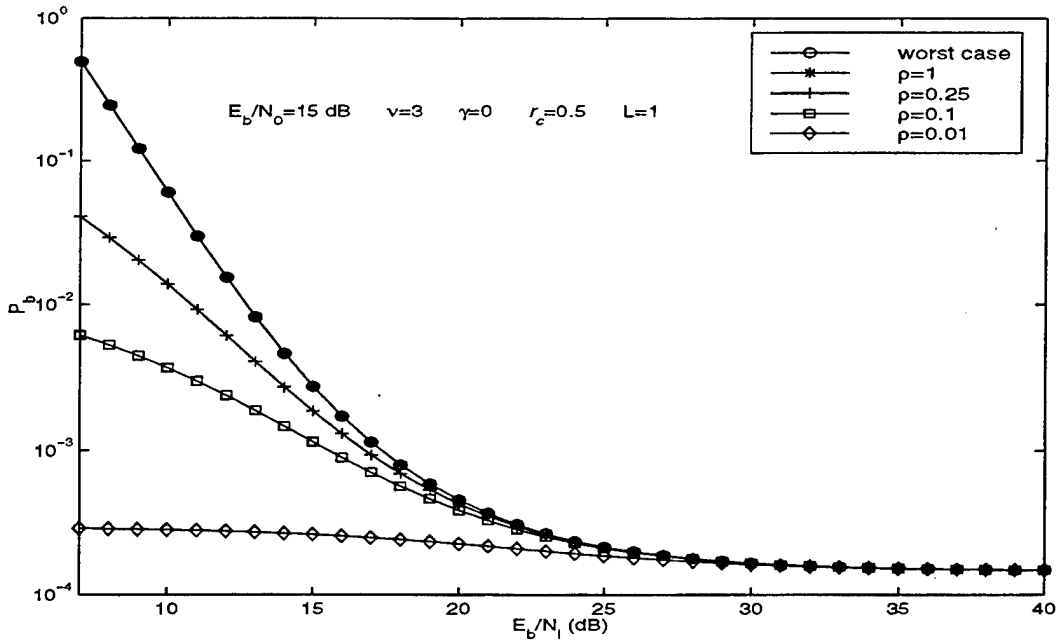

Figure 6.23: Performance of self-normalized receiver for pulse jamming fractions $\rho = 1, 0.25, 0.1, 0.01$ and worst case for diversity order $L = 1$, $E_b/N_0 = 15$ dB, $\gamma = 0$, $\nu = 3$ and $r_c = 0.5$.

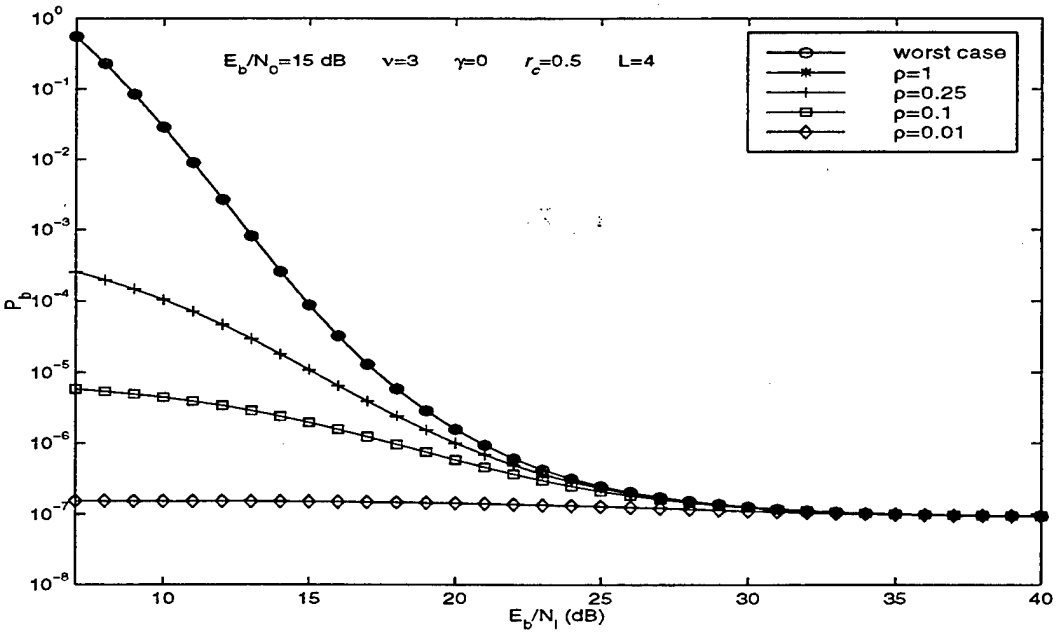

Figure 6.24: Performance of self-normalized receiver for pulse jamming fractions $\rho = 1, 0.25, 0.1, 0.01$ and worst case for diversity order $L = 4$, $E_b/N_0 = 15$ dB, $\gamma = 0$, $\nu = 3$ and $r_c = 0.5$.

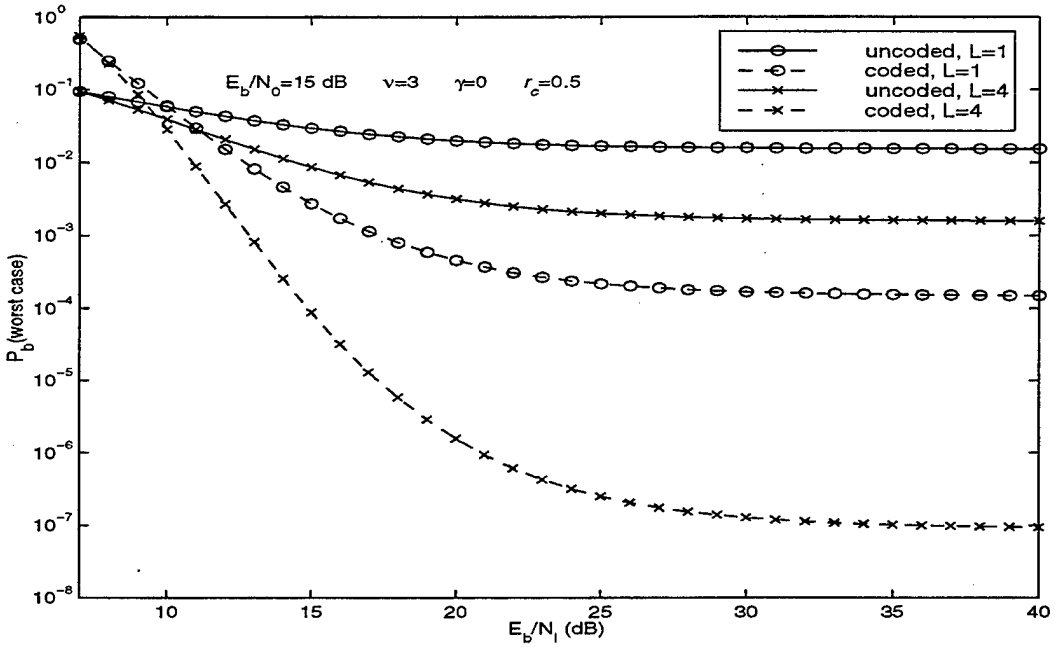

Figure 6.25: Worst case performance comparison of coded and uncoded system for self-normalized receiver for diversity orders L = 1 and 4, $E_b/N_0 = 15$ dB, $\gamma = 0$, $\nu = 3$ and $r_c = 0.5$.

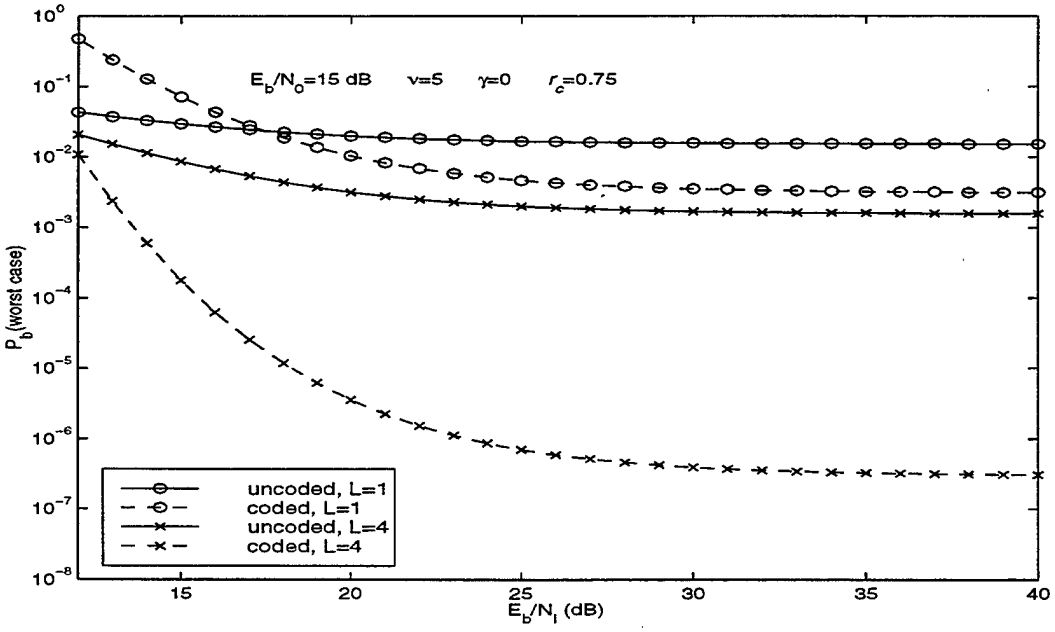

Figure 6.26: Worst case performance comparison of coded and uncoded system for self-normalized receiver for diversity orders L = 1 and 4, $E_b/N_0 = 15$ dB, $\gamma = 0$, $\nu = 5$ and $r_c = 0.75$.

Performance curves for the self-normalized receiver for diversity orders L = 1 and 4 and jammer fractions ρ = 0.01, 0.1, 0.25, 1 and worst case, E_b/N_0 = 10 dB, γ = 0, ν = 5 and r_c = 0.5 are shown in Figures 6.27 and 6.28 respectively. It is seen that pulse noise jamming is ineffective for both diversity cases. Figure 6.29 shows the worst case performance curves for the coded and uncoded systems for L = 1 and 4, E_b/N_0 = 10 dB, γ = 0, ν = 5 and r_c = 0.5. It is seen that for E_b/N_I > 15 dB, the coded system performs better than the uncoded system for both diversity orders with the L = 4 diversity case showing a slightly larger net performance improvement. In comparison to the case of same code rate and higher signal-to-thermal noise ratio (Figure 6.25), the performance improvement between uncoded and coded systems is substantially less.

Performance curves for the self-normalized receiver for diversity orders L = 1 and 4 and jammer fractions ρ = 0.01, 0.1, 0.25, 1 and worst case, E_b/N_0 = 15 dB, γ = 5, ν = 3 and r_c = 0.5 are shown in Figures 6.30 and 6.31 respectively. For the case of no diversity, it is seen that pulse noise jamming is effective in the range 10 dB < E_b/N_I < 30 dB. At E_b/N_I = 20 dB; it is also seen that the difference between the continuous jamming curve and the worst case performance curve is approximately 3 dB. This is the same observation that was made for the noise-normalized receiver. For the case of diversity L = 4, it is seen that jammer effectiveness has been negated. The worst case performance curves for the coded and uncoded systems are shown for L = 1 and 4, E_b/N_0 = 15 dB, γ = 5, ν = 3 and r_c = 0.5 in Figure 6.32. The performance improvement between the uncoded and coded systems for both diversity cases is significant with the diversity order L = 4 showing a slightly larger net improvement. Figure 6.33 shows the worst case performance curves for the coded and uncoded systems for L = 1 and 4, E_b/N_0 = 15 dB, γ = 5, ν = 5 and r_c = 0.75. It is observed that there is significant performance improvement between the uncoded and coded systems for both diversity cases. For the case of L = 1, this differs from what was observed for the Rayleigh channel (Figure 6.26) where relatively little performance improvement was obtained when comparing uncoded and coded systems.

Performance curves for the self-normalized receiver for diversity orders L = 1 and 4 and jammer fractions ρ = 0.01, 0.1, 0.25, 1 and worst case, E_b/N_0 = 10 dB, γ = 5, ν = 5 and

$r_c = 0.5$ are shown in Figures 6.34 and 6.35 respectively. It is seen that pulse noise jamming is not effective at either diversity order. This is similar to what was observed for the noise-normalized receiver. Figure 6.36 shows the worst case performance curves for the coded and uncoded systems for diversity orders L = 1 and 4, $E_b/N_0 = 10$ dB, $\gamma = 5$, $\nu = 5$ and $r_c = 0.5$. The performance improvement between the uncoded and coded systems for each diversity order is significant. Note however, that the coded system with no diversity actually outperforms the coded system with diversity. For the same code rate, this is opposite to what was observed at the higher signal to thermal noise ratio ($E_b/N_0 = 15$ dB) and lower constraint length ($\nu = 3$, Figure 6.32), where the coded system with diversity outperformed the coded system with no diversity. These results may be explained by the additional noncoherent combining losses incurred at the lower signal-to-noise ratio. In addition, the higher constraint length code has larger values of d, contributing more to noncoherent combining loss. Figure 6.37 shows the worst case performance curves for the coded and uncoded systems for L = 1 and 4, $E_b/N_0 = 10$ dB, $\gamma = 5$, $\nu = 7$ and $r_c = 0.75$. In contrast to the previous case, it is seen that coded system with diversity now outperforms the coded system without diversity. This can be explained by the fact that the higher code rate system suffers less from noncoherent combining losses.

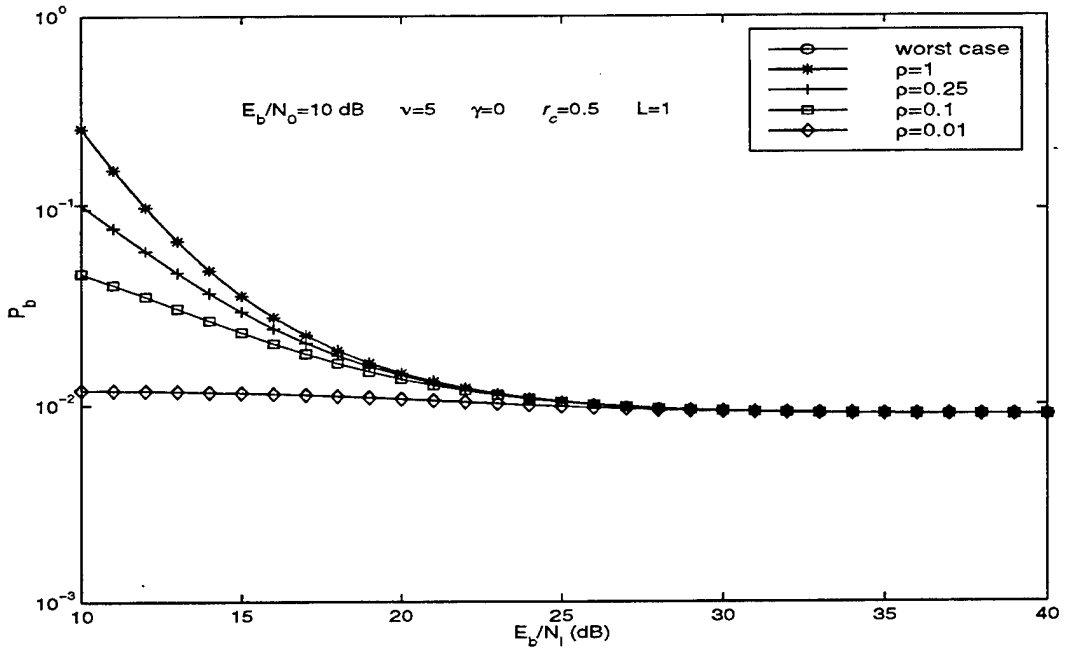

Figure 6.27: Performance of self-normalized receiver for pulse jamming fractions $\rho = 1, 0.25, 0.1, 0.01$ and worst case for diversity order $L = 1$, $E_b/N_0 = 10$ dB, $\gamma = 0$, $\nu = 5$ and $r_c = 0.5$.

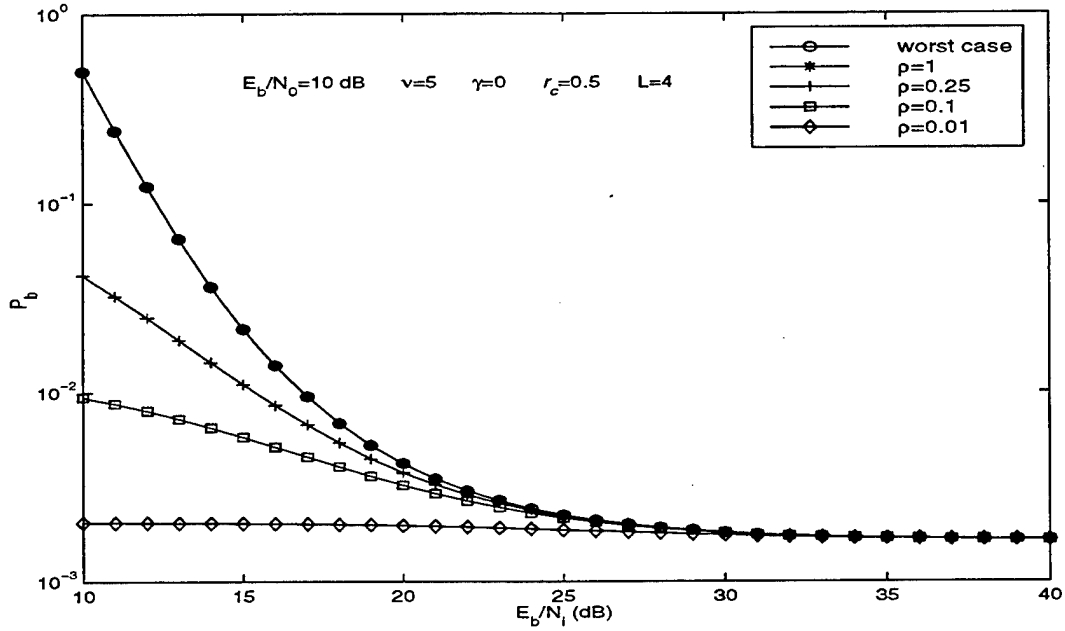

Figure 6.28: Performance of self-normalized receiver for pulse jamming fractions $\rho = 1, 0.25, 0.1, 0.01$ and worst case for diversity order $L = 4$, $E_b/N_0 = 10$ dB, $\gamma = 0$, $\nu = 5$ and $r_c = 0.5$.

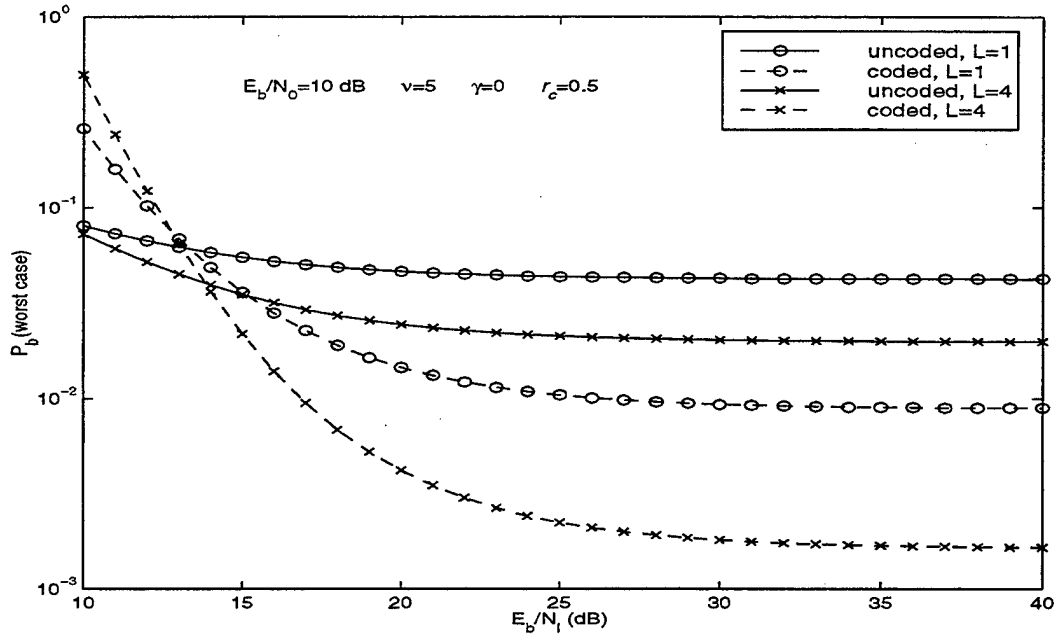

Figure 6.29: Worst case performance comparison of coded and uncoded system for self-normalized receiver for diversity orders L = 1 and 4, $E_b/N_0 = 10$ dB, $\gamma = 0$, $\nu = 5$ and $r_c = 0.5$.

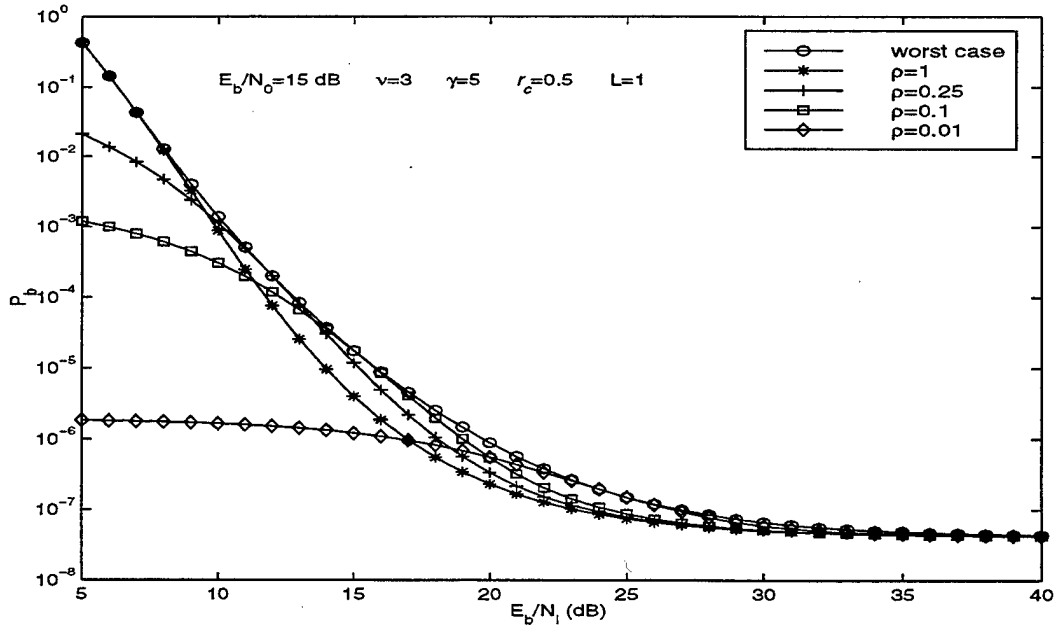

Figure 6.30: Performance of self-normalized receiver for pulse jamming fractions $\rho = 1, 0.25, 0.1,$ 0.01 and worst case for diversity order L = 1, $E_b/N_0 = 15$ dB, $\gamma = 5$, $\nu = 3$ and $r_c = 0.5$.

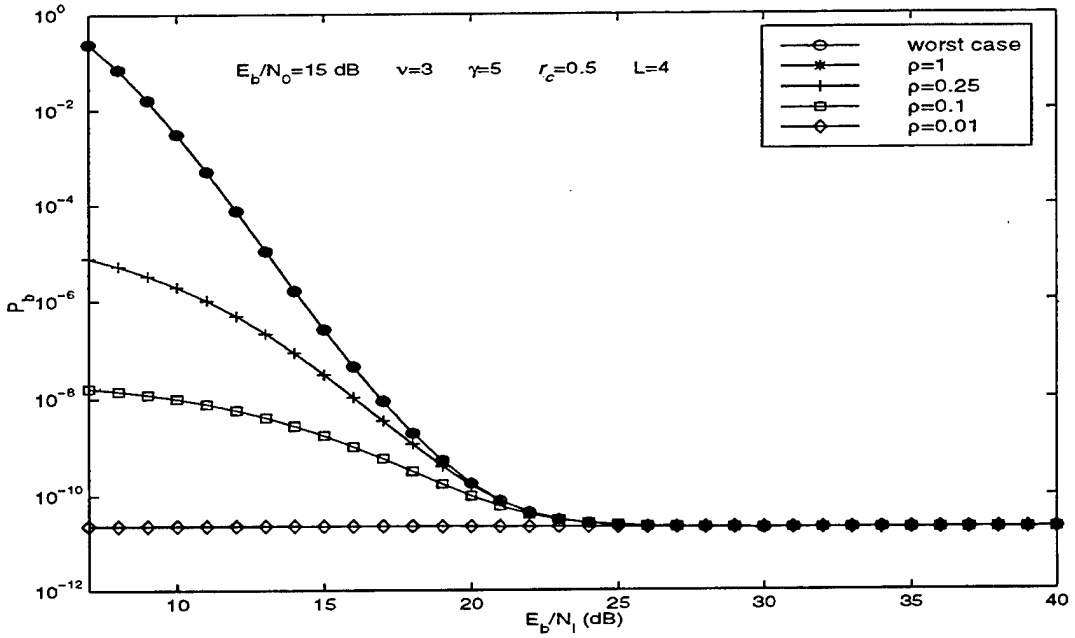

Figure 6.31: Performance of self-normalized receiver for pulse jamming fractions $\rho = 1, 0.25, 0.1,$ 0.01 and worst case for diversity order $L = 4$, $E_b/N_0 = 15$ dB, $\gamma = 5$, $\nu = 3$ and $r_c = 0.5$.

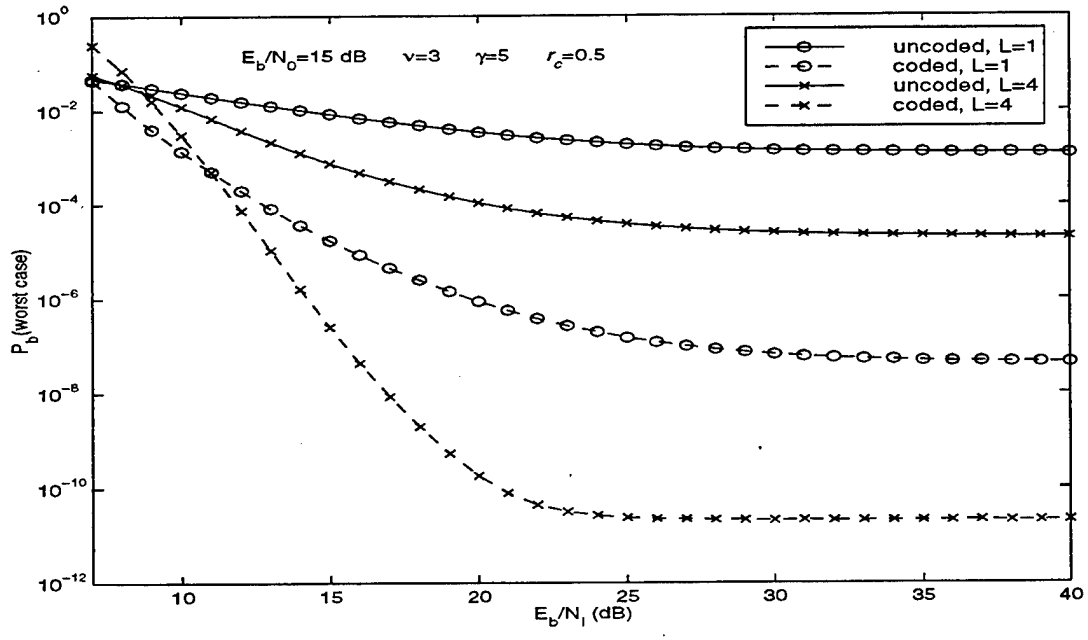

Figure 6.32: Worst case performance comparison of coded and uncoded system for self-normalized receiver for diversity orders $L = 1$ and 4, $E_b/N_0 = 15$ dB, $\gamma = 5$, $\nu = 3$ and $r_c = 0.5$.

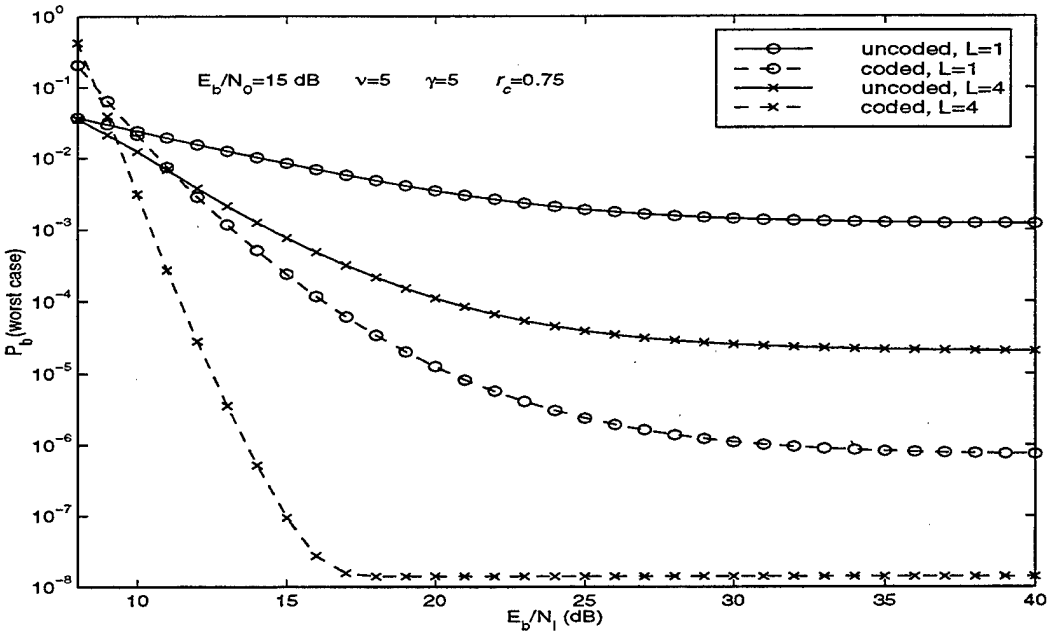

Figure 6.33: Worst case performance comparison of coded and uncoded system for self-normalized receiver for diversity orders L = 1 and 4, $E_b/N_0 = 15$ dB, $\gamma = 5$, $\nu = 5$ and $r_c = 0.75$.

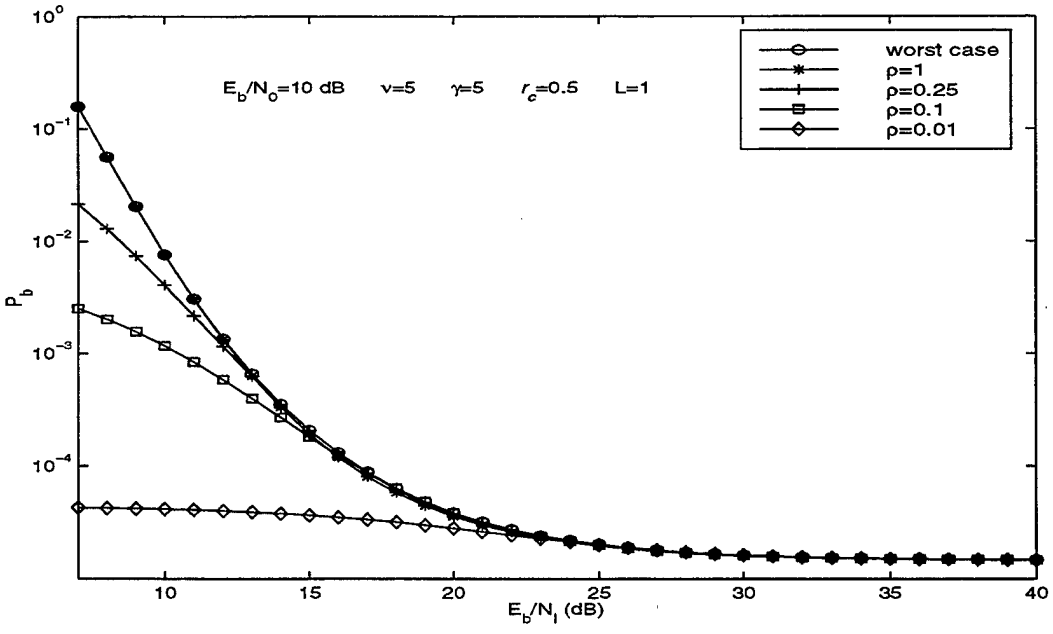

Figure 6.34: Performance of self-normalized receiver for pulse jamming fractions $\rho = 1, 0.25, 0.1, 0.01$ and worst case for diversity order L = 1, $E_b/N_0 = 10$ dB, $\gamma = 5$, $\nu = 5$ and $r_c = 0.5$.

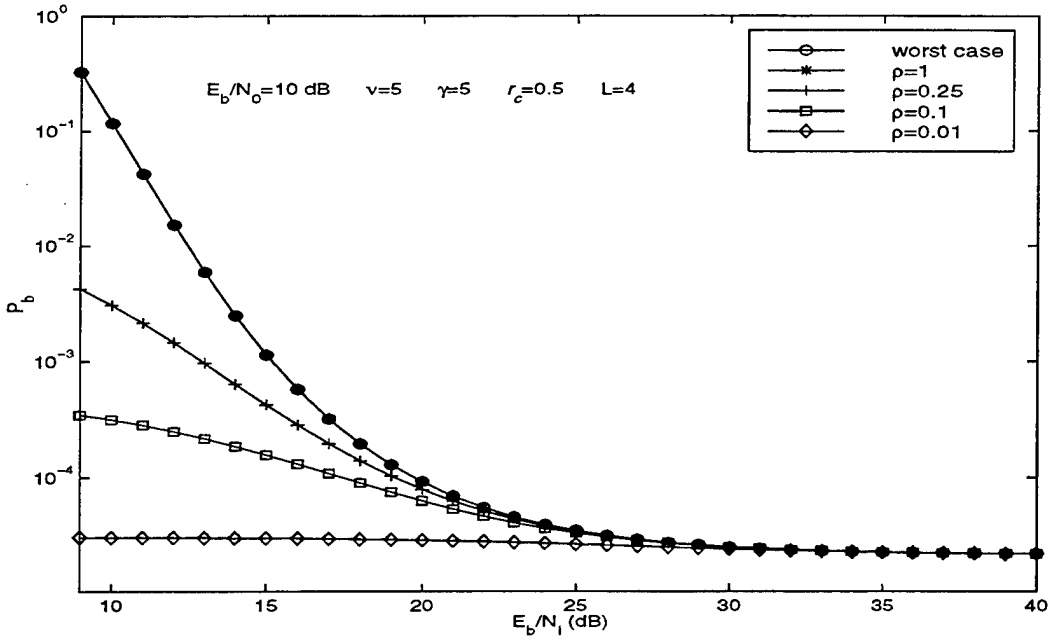

Figure 6.35: Performance of self-normalized receiver for pulse jamming fractions $\rho = 1, 0.25, 0.1,$ 0.01 and worst case for diversity order $L = 4$, $E_b/N_0 = 10$ dB, $\gamma = 5$, $\nu = 5$ and $r_c = 0.5$.

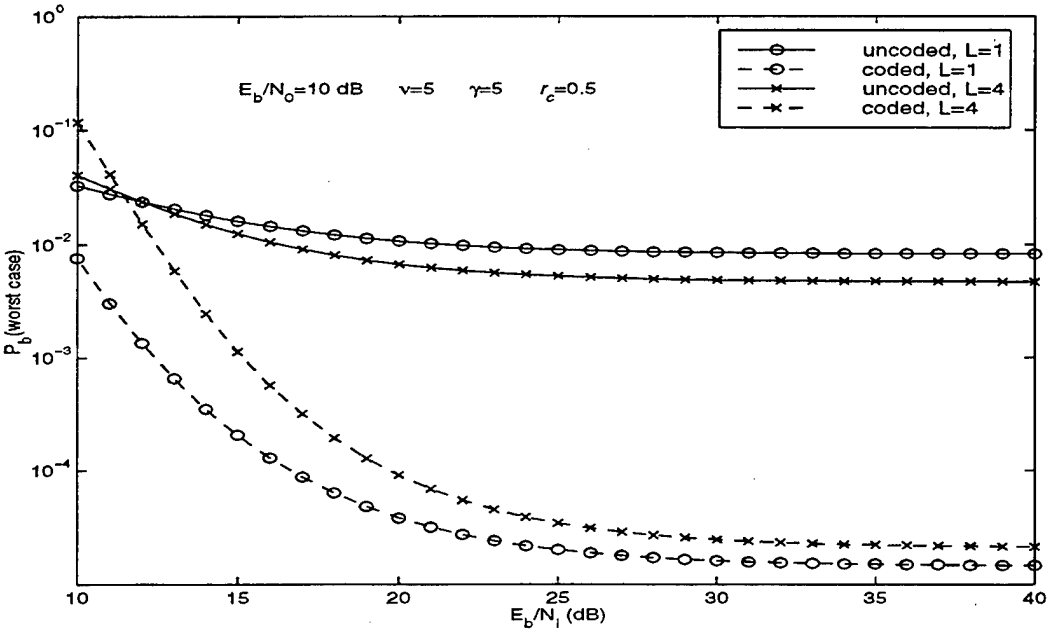

Figure 6.36: Worst case performance comparison of coded and uncoded system for self-normalized receiver for diversity orders $L = 1$ and 4, $E_b/N_0 = 10$ dB, $\gamma = 5$, $\nu = 5$ and $r_c = 0.5$.

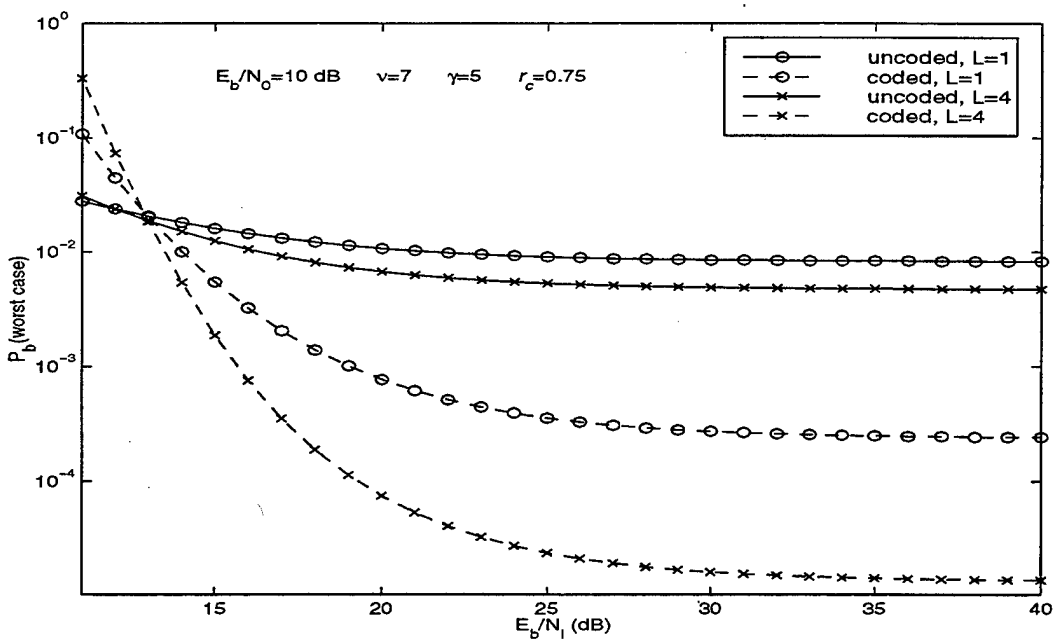

Figure 6.37: Worst case performance comparison of coded and uncoded system for self-normalized receiver for diversity orders L = 1 and 4, $E_b/N_0 = 10$ dB, $\gamma = 5$, $\nu = 7$ and $r_c = 0.75$.

D. PERFORMANCE COMPARISON BETWEEN NOISE-NORMALIZED, SELF-NORMALIZED, LINEAR AND PDSC1 RECEIVERS FOR A RAYLEIGH FADING CHANNEL

In this section, a worst case performance comparison of the coded systems between the noise-normalized, self-normalized, linear and PDSC1 receivers over a Rayleigh fading channel in the presence of pulse noise jamming and AWGN is presented. Figure 6.38 shows the comparison for the parameters $E_b/N_0 = 15$ dB, $\nu = 3$, $r_c = 0.5$ with a time diversity of L = 4 for the noise-normalized, self-normalized and linear receivers and a spatial diversity of M = 4 for the PDSC1 receiver. It is seen that the performance of the linear and PDSC1 receivers is inferior to that of either the self-normalized or noise-normalized receivers with the noise-normalized receiver demonstrating the better performance. It is seen that pulse noise jamming is extremely effective against the linear receiver over the full range of E_b/N_I since the performance curve for the linear receiver has not yet converged to the performance for the Rayleigh limit of the channel. In the limit of very high signal-to-interference ratio where the pulse noise jammer is no longer effective, it is known from previous results that the performance of the linear receiver should equal that of the

noise-normalized receiver. At E_b/N_I = 40 dB, it is seen that performance curve for the linear receiver in terms of its probability of bit error is still several orders of magnitude higher than that of the noise-normalized receiver.

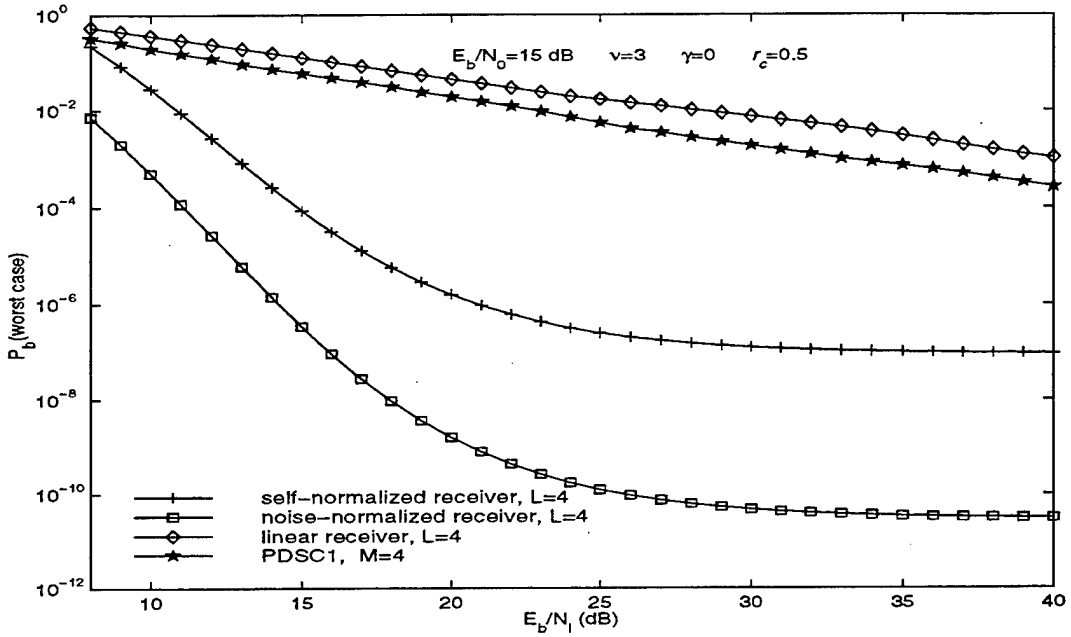

Figure 6.38: Worst case performance comparison between the noise-normalized, self-normalized, linear and PDSC1 receivers for E_b/N_0 = 15 dB, $\gamma = 0$, $\nu = 3$ and $r_c = 0.5$.

Figure 6.39 shows the comparison for the parameters E_b/N_0 = 10 dB, $\nu = 5$, $r_c = 0.5$ with a time diversity of L = 4 for the noise-normalized, self-normalized and linear receivers and a spatial diversity of M = 4 for the PDSC1 receiver. It is seen that the performance of the noise-normalized receiver is clearly superior to all other receivers. It is also seen that for $E_b/N_I > 38$ dB, the linear and PDSC1 receivers outperform the self-normalized receiver. At a relatively strong signal-to-interference ratio of E_b/N_I = 20 dB however the self-normalized receiver clearly performs better than the linear or PDSC1 receivers.

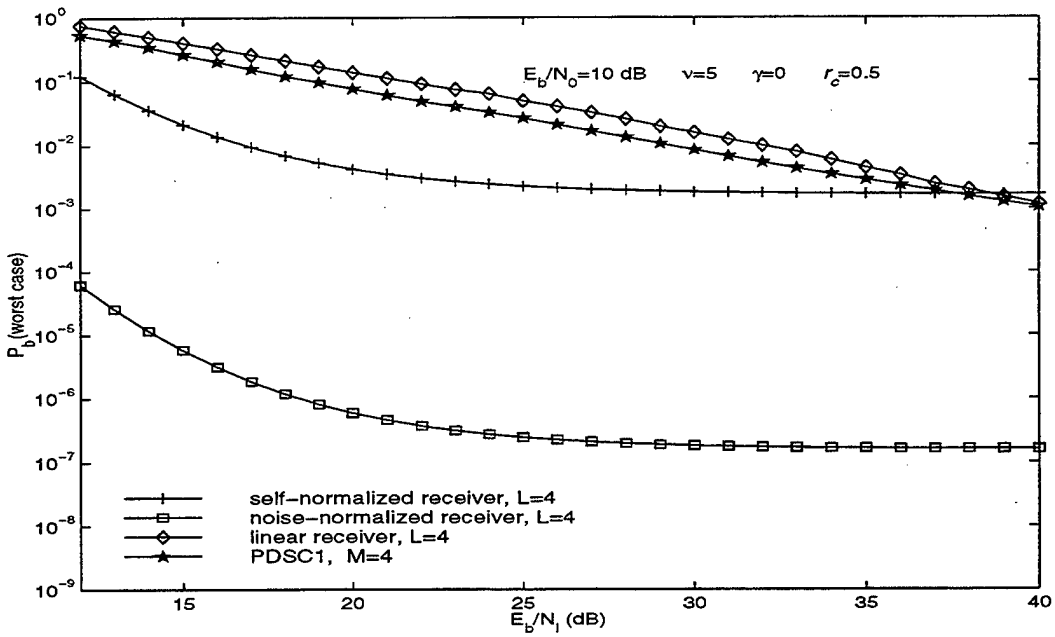

Figure 6.39: Worst case performance comparison between the noise-normalized, self-normalized, linear and PDSC1 receivers for $E_b/N_0 = 10$ dB, $\gamma = 0$, $\nu = 5$ and $r_c = 0.5$.

E. CHAPTER CONCLUSIONS

In this chapter, the performance of Direct Sequence Differential Phase Shift Keying (DS-DPSK) with convolutional coding and soft decision Viterbi decoding in a Rician fading channel in the presence of pulsed noise interference and additive white Gaussian noise (AWGN) has been considered. Upper bounds on the probability of decoder error and bit error were derived. It was shown that the operation of the coded noise-normalized, self-normalized and linear DS-DPSK systems with L^{th} order time diversity was equivalent to the respective uncoded DS-DPSK systems with dL^{th} order time diversity. The coded PDSC1 system with M^{th} order spatial diversity was shown to be equivalent to the uncoded system with M^{th} order spatial diversity and d^{th} order time diversity. The coded PDSC1 system with M^{th} order spatial diversity and L^{th} order time diversity was shown to be equivalent to the uncoded system with M^{th} order spatial diversity and dL^{th} order time diversity. These results were shown to be independent of the condition of fading or pulse noise jamming.

In the numerical analysis of the noise-normalized receiver for the Rayleigh channel, for E_b/N_0 = 10 dB or 15 dB with or without diversity, it was seen that the effects of pulse noise jamming had been completely negated. For moderate fading ($\gamma = 5$), for E_b/N_0 = 15 dB and no diversity, pulse noise jamming was effective. The effects of pulse noise jamming had been negated with a diversity order of L = 4. Pulse noise jamming was seen not to be effective at the lower signal to thermal noise ratio considered (E_b/N_0 = 10 dB) for either case of diversity. The lack of jammer effectiveness was attributed to the fact that the overall signal-to-noise ratio (thermal noise plus interference ratio) was smaller, generally a better condition for continuous jamming. For both fading conditions considered, it was seen that the net performance improvement between uncoded and coded systems was significantly greater when diversity was employed. In addition, the net performance improvement was greater at higher signal to thermal noise ratio. For the Rayleigh channel at the higher code rate, E_b/N_0 = 10 dB and no diversity, it was seen that there was little difference in performance between the uncoded and coded system. At the moderate fading condition, this difference grew substantially.

In the numerical analysis of the self-normalized receiver for the Rayleigh channel, for E_b/N_0 = 10 dB or 15 dB with or without diversity, it was seen that the effects of pulse noise jamming had been completely negated. For moderate fading, E_b/N_0 = 15 dB and no diversity, pulse noise jamming was seen to be effective. These effects were negated when diversity was employed. Pulse noise jamming was not effective at the lower signal to thermal noise ratio considered for either diversity case considered. In contrast to what was observed for the noise-normalized receiver, the coded self-normalized system did not always benefit from the combined use of diversity and coding. For the Rayleigh channel, the coded system with diversity always outperformed the coded system without diversity. For the moderate fading condition considered, it was seen that with E_b/N_0 = 10 dB, $\nu = 5$, and $r_c = 0.5$, the coded system without diversity outperformed the coded system with diversity. This was best explained by the additional noncoherent combining losses that could occur at the moderate fading condition with the proper combination of signal-to-noise ratio, code rate, constraint length and diversity.

The worst case performance of the coded noise-normalized, self-normalized, linear and PDSC1 systems over a Rayleigh fading channel in the presence of pulse noise jamming and AWGN were compared for a diversity of L = 4 and M = 4 (PDSC1). At E_b/N_0 = 15 dB, it was seen

that the performance of the linear and PDSC1 receivers was inferior to that of either the self-normalized or noise-normalized receivers with the noise-normalized receiver demonstrating the better performance. At $E_b/N_0 = 10$ dB, the noise-normalized receiver remained superior to all other receivers. At very high signal-to-interference ratio, the PDSC1 and linear receivers performed slightly better than the self-normalized receiver. At lower signal-to-interference ratios, the self-normalized receiver performed better than either the PDSC1 or the linear receiver.

VII. CONCLUSIONS

A. SUMMARY OF WORK

The performance of a Direct Sequence Differential Phase Shift-Keying (DS-DPSK) spread spectrum system over a Rician frequency-nonselective, slowly fading channel in the presence of pulsed noise interference and AWGN has been considered. The performance of several receiver configurations, that of the self-normalized, noise-normalized, linear, PDSC1 and PDSC1 with time diversity receivers has been analyzed. In addition, the performance of the coded self-normalized, noise-normalized, linear and PDSC1 receiver systems utilizing soft decision Viterbi decoding has been analyzed. A wideband pulse noise interference model was employed which allowed the possibility that either 1, 2 consecutive or no bits were jammed over the 2-bit signaling interval. For all receiver configurations, the worst case performance as a function of the parameter ρ, the fraction of time or bits the pulse noise jammer is in the "on" state was analyzed. For all receivers, the value of ρ was determined through numerical search for each value of signal-to-interference ratio. It was determined that two values of ρ produced identical worst case performance, but that the variances over any 2-bit signaling interval were the same for both cases. For the uncoded systems, the worst case performance for a fixed value of ρ as a function of signal-to-interference ratio and of the parameter β, the ratio of fraction of 1-bit jammed events to 2-bit jammed events, was also analyzed. Several measures of efficacy with respect to mitigating the effects of pulse noise jamming for each receiver configuration were considered. The probability of bit error as a function of signal-to-interference ratio with diversity level as a parameter was first analyzed. A particular receiver configuration was considered effective in pulse noise mitigation if the worst case performance curve moved closer to the continuous jamming curve as diversity level was increased. For the uncoded systems, another measure of efficacy was determined by observing the optimum value of ρ as a function of diversity and γ, the direct-to-diffuse signal energy ratio. Here, a particular receiver configuration was considered efficient in pulse noise jamming mitigation if the value of ρ increased for increasing diversity level. For all receiver configurations, it was determined that pulse noise jamming became more effective as the signal-to-interference ratio and/

or the value of γ increased. The worst case performance of the receivers was compared for both the uncoded and coded systems.

For the uncoded self-normalized receiver system, a closed form expression for the conditional probability density function of the random variable at the output of the normalizer prior to combining was available. A closed form solution for the probability of bit error however was not available and the probability of bit error had to be determined through numerical analysis. In the numerical analysis, for fixed values of the jamming fraction ρ, worst case performance as a function of the signal-to-interference ratio and β demonstrated that for severe and moderate fading, the best strategy for the jammer was to jam alternating bits rather than adjacent bits. In the worst case performance analysis of the self-normalized receiver as a function of the parameter ρ, it was determined that the self-normalized receiver was effective in mitigating the effects of pulse noise jamming for both severe and moderate fading conditions. For moderate fading conditions, the optimum value of ρ to produce worst case performance was observed as a function of diversity. It was seen that increasing the diversity order forced the jammer to a more continuous form of jamming. The optimum value of ρ to produce worst case performance was observed as a function of γ with diversity as a parameter. It was concluded that pulse noise jamming effectiveness increased with increasing γ and decreased with increasing diversity order. This was observed for values of γ between 0 and 10.

The noise-normalized receiver was described to be an idealization of the self-normalized receiver since the normalization variable contained noise only components. For the uncoded noise-normalized receiver system, a closed form expression for the joint probability density function for the random variables at the output of the normalizer was available. For the signal branch, the marginal conditional probability density function for the random variable at the output of the combiner was not available. A closed form solution to the probability of bit error was also not available and the probability of bit error had to be determined through numerical analysis. The numerical burden was alleviated to some degree through determination of the signal branch marginal probability density function at the output of the combiner conditioned on homogeneous jamming events. As was the case for the self-normalized receiver with fixed ρ, the best strategy for the jammer was to jam alternating bits rather than adjacent bits for severe and moderate fading.

In the worst case performance analysis as a function of ρ, the noise-normalized receiver was also seen to be effective in mitigating pulse noise jamming. For the moderate fading condition as diversity order was increased, the worst case performance curve moved closer to the continuous jamming curve. The value of ρ also increased for increasing diversity order. Pulse noise jamming was also seen to be more effective at higher values of γ. The performance of the noise-normalized receiver with non-ideal noise-normalization was analyzed. It was seen that if one is willing to accept a slight degradation in performance, relatively crude measurement techniques may be utilized. This makes the noise-normalized receiver a practical as well as effective receiver in pulse-jammed environments.

Where the self-normalized and noise-normalized receivers utilized time diversity, the set of PDSC1 receivers utilized spatial diversity. PDSC receivers are premised on the fact that not all multipath components of the received signal may arrive at the same antenna. Their performance is said to be path independent since only the antenna with the largest output is selected. PDSC1 receivers have the advantage that they do not suffer noncoherent combining losses as do EGC receivers. For the PDSC1 receiver, a closed form solution for the conditional probability of bit error over a Rayleigh fading channel was available. A closed form solution for the conditional probability of bit error over a Rician fading channel was not available and required numerical solution. In the case of the Rayleigh channel, for a very high peak power specification (ρ small), jamming alternating bits proved to be a more effective jamming strategy than jamming adjacent bits for lower values of signal-to-interference ratios ($E_b/N_I < 17$ dB). For higher values of signal-to-interference ratio, jamming adjacent bits was shown to be most effective. For a lower peak power specification, jamming alternating bits proved to be the most effective jamming strategy but only over a smaller range of low signal-to-interference ratio. Similar results were observed for the case of moderate fading ($\gamma = 5$).

For either the severe or moderate fading condition, it was observed that the PDSC1 receiver was not effective in mitigating pulse noise jamming. It was observed that the worst case performance curve did not move closer to the continuous jamming curve for increasing diversity order. For the Rayleigh channel, the optimum value of ρ remained constant as diversity order was increased. For the moderate fading condition, it was observed that ρ increased slightly as diversity order was increased. The amount of increase was not as great as that observed for either the self-

normalized or noise-normalized receivers however. In general, the efficacy of the PDSC1 receiver against pulse noise jamming improved as the fading condition improved (higher γ). For the Rayleigh channel, it was observed that the worst case performance of the PDSC1 receiver was improved by increasing diversity order at higher values of signal-to-interference ratio. The amount of performance improvement between diversity orders was seen to decrease as diversity order was increased. Also for the Rayleigh channel, the PDSC1 receiver demonstrated a slight performance degradation by increasing diversity order at lower values of signal-to-interference ratio. At the moderate fading level, the performance improvement at high signal-to-interference ratio was significant between M = 1 and M = 2 with very little change for higher diversity orders.

For the PDSC1 receiver with time diversity, closed form solutions for the probability of bit error were not available for either the Rayleigh or Rician channels and required numerical solution. The performance of the PDSC1 receiver with time diversity for a fixed jammer peak power specification under severe and moderate fading conditions was analyzed. It was determined that for both fading conditions, jamming alternating bits produced the worst performance for the lower values of signal-to-interference ratios, while jamming consecutive bits produces the worst performance at the higher values. These results are similar to that observed for the PDSC1 receiver with no time diversity. For either the severe or moderate fading condition, it was observed that the PDSC1 receiver with time diversity was not effective in mitigating pulse noise jamming. It was observed that the worst case performance curve did not move closer to the continuous jamming curve for increasing spatial diversity order with fixed time diversity order (L = 4) or for increasing time diversity order with fixed spatial diversity order (M = 4). For either the Rayleigh channel or the moderate fading condition, the optimum value of ρ was seen to decrease slightly for increasing time diversity order with M = 4. A slight increase in ρ was observed per increasing spatial diversity order with L = 4. This observation also held for other values of γ between 0 and 10. For the Rayleigh channel, it was seen that for signal-to-interference ratios below 25 dB, increasing the time diversity order for a fixed spatial diversity order of M = 4 led to a gradual performance decrease. Above this value of signal-to-interference ratio, a time diversity order of L = 2 or 3 produced a modest performance improvement. Similar results were observed when the spatial order was varied as the time diversity order remain fixed. For moderate fading, any increase in time

or spatial diversity order led to a performance degradation over the full range of signal-to-interference ratio.

The worst case performance of the uncoded self-normalized, noise-normalized, linear, PDSC1 and PDSC1 with time diversity receiver systems under severe and moderate fading conditions were compared. For the Rayleigh fading channel, it was seen that the PDSC1 receiver with time diversity was inferior to the other receivers for $E_b/N_I < 28$ dB. As the signal-to-interference ratio was increased above $E_b/N_I = 35$ dB in the Rayleigh limit of the channel, the PDSC1 receiver with time diversity was seen to provide the best performance of all receivers. Over most of the range of signal-to-interference ratio considered however, the noise-normalized receiver provided superior performance to all other receivers. The self-normalized receiver provided the next best performance below $E_b/N_I = 25$ dB and was inferior to all other receivers above $E_b/N_I = 30$ dB in the Rayleigh limit of the channel. The performances of the PDSC1 and linear receivers were similar over the full range of signal-to-interference ratios considered. For the moderate fading channel, it was seen that the PDSC1 receiver with time diversity was inferior to the other receivers over the full range of signal-to-interference ratio. In this case, the noise-normalized receiver provided superior performance to all other receivers with the self-normalized receiver attaining the next best performance. The linear and PDSC1 receivers exhibited similar performances again.

In the last chapter, the performance of DS-DPSK with convolutional coding and soft decision Viterbi decoding in a fading channel in the presence of pulsed noise interference and additive white Gaussian noise (AWGN) was considered. Upper bounds on the probability of decoder error and bit error were derived. It was shown that the operation of the coded noise-normalized, self-normalized and linear DS-DPSK systems with L^{th} order time diversity was equivalent to the respective uncoded DS-DPSK systems with dL^{th} order time diversity. The coded PDSC1 system with M^{th} order spatial diversity was shown to be equivalent to the uncoded system with M^{th} order spatial diversity and d^{th} order time diversity. The coded PDSC1 system with M^{th} order spatial diversity and L^{th} order time diversity was shown to be equivalent to the uncoded system with M^{th} order spatial diversity with dL^{th} order time diversity. These results were shown to be independent of the condition of fading or pulse noise jamming.

In the numerical analysis of the coded noise-normalized receiver, it was seen that pulse noise jamming was effective for the moderate fading condition at E_b/N_0 = 15 dB and without diversity. It was seen that the effects of pulse noise jamming had been negated with a diversity order of L = 4. For both severe and moderate fading, it was seen that the net performance improvement between the uncoded and coded systems was significantly greater when diversity was employed. In addition, the net performance improvement was greater at higher signal-to-thermal noise ratio.

In the numerical analysis of the coded self-normalized receiver, it was seen that pulse noise jamming was effective for the moderate fading condition at E_b/N_0 = 15 dB and without diversity. It was seen that the effects of pulse noise jamming had been negated with a diversity order of L = 4. In contrast to what was observed for the noise-normalized receiver, the coded self-normalized system did not always benefit from the combined use of diversity and coding. For the Rayleigh channel, the coded system with diversity always outperformed the coded system without diversity. For the moderate fading condition considered, it was seen that with E_b/N_0 = 10 dB, $\nu = 5$, and $r_c = 0.5$, the coded system without diversity outperformed the coded system with diversity. This was best explained by the additional noncoherent combining losses that could occur at the moderate fading condition with the proper combination of lower signal-to-noise ratio, code rate, constraint length and diversity.

The worst case performance of the coded noise-normalized, self-normalized, linear and PDSC1 systems over a Rayleigh fading channel in the presence of pulse noise jamming and AWGN were compared for a diversity of L = 4 and M = 4 (PDSC1). At E_b/N_0 = 15 dB, it was seen that the performance of the linear and PDSC1 receivers was inferior to that of either the self-normalized or noise-normalized receivers with the noise-normalized receiver demonstrating the better performance. At the lower signal-to-thermal noise ratio, the noise-normalized receiver remained superior to all other receivers. At very high signal-to-interference ratio, the PDSC1 and linear receivers performed slightly better than the self-normalized receiver. At lower signal-to-interference ratios, the self-normalized receiver performed better than either the PDSC1 or linear receiver.

This main contributions of this work are now summarized. First a novel implementation of a DPSK detector was successfully employed in several receiver configurations to mitigate the

combined effects of pulse noise interference and signal fading. A full analytical development and numerical analyses was provided for all receiver types. As part of the modeling effort, a pulse noise interference model was adopted which allowed for the possibility that one, two or none of the modulated bits experienced interference. The coded operation of the nonlinear systems were derived in terms of an equivalent uncoded operation. This led to a straightforward approach for which to evaluate coded system performances.

B. SUGGESTIONS FOR FUTURE WORK

In the analysis of DS-DPSK over a Rician fading channel in the presence of pulse noise interference and AWGN, the performance of several receiver types has been considered. It has been seen that the noise-normalized and self-normalized receivers were very efficient in mitigating the effects of pulse noise jamming. The performance of the set of PDSC1 receivers suffered where pulse noise jamming was most effective. The most probable cause of this outcome is the fact that the set of M antenna outputs which form the decision statistic, experience the same level of interference at any point in time. Therefore some output decisions will be heavily biased from the effects of pulse noise jamming, while others will experience little or no effect. One way to make the decision process fairer would be to distribute the effects of pulse jamming out more equitably amongst the bits in time. One might accomplish this by utilizing L-fold time diversity with interleaving coupled with M-fold spatial diversity and picking the largest output over a (L x M) sample grid. Such a configuration would also preserve the desirable quality of path independence inherit in the PDSC1 receiver. One also might consider the use of the PDSC1 receiver in tandem with either the self-normalized receiver or noise-normalized receiver.

It has been seen that closed form expressions for the probability of bit error were not always available throughout this work. A simpler distribution for the effects of fading in terms of its mathematical description such as the Nakagami-m distribution [30] might lead to closed form solutions. This would also relieve some of the numerical burden encountered with the relatively complex mathematical description of the Rician distribution. In addition, the Nakagami-m distribution is considered a more general description of the fading phenomenon than the Rician distribution. One of the reasons the Rician distribution is commonly used in the literature is its intuitive appeal where the direct path signal energy and the diffuse signal energy are identified as separate parameters of the distribution.

APPENDIX A

The conditional density function for the random variable Z_{1k} is derived here. From Chapter II, recall the following relations:

$$f_{Z_{1k},W}(z_{1k}, w|0, \mathrm{I}_j) = \frac{w}{4\sigma_{1_j}^2\sigma_{2_j}^2}\exp\left(-\frac{w(1-z_{1k})}{2\sigma_{2_j}^2}\right)\exp\left(-\frac{wz_{1k}+4\alpha^2}{2\sigma_{1_j}^2}\right)\mathrm{I}_0\left(\frac{2\alpha\sqrt{wz_{1k}}}{\sigma_{1_j}^2}\right)\times$$

$$u(w)u(z_{1k}) \tag{A.1}$$

$$f_{Z_{1k}}(z_{1k}|0, \mathrm{I}_j) = \int_0^\infty f_{Z_{1k},W}(z_{1k}, w|0, \mathrm{I}_j)dw \tag{A.2}$$

If a substitution $x = \frac{w}{\sigma_{1_j}^2}$ is made in equation A.1, equation A.2 may be reexpressed as

$$f_{Z_{1k}}(z_{1k}|0, \mathrm{I}_j) = \frac{\exp(-2\alpha^2/\sigma_{1_j}^2)\sigma_{1_j}^2}{4\sigma_{2_j}^2}\int_0^\infty x\exp\left(-\frac{x(\sigma_{1_j}^2(1-z_{1k})+\sigma_{2_j}^2z_{1k})}{2\sigma_{2_j}^2}\right)\times$$

$$\mathrm{I}_0\left(\frac{2\alpha\sqrt{xz_{1k}}}{\sigma_{1_j}}\right)u(z_{1k})dx \tag{A.3}$$

With the application of the following relation

$$\mathrm{I}_n(z) = \mathrm{i}^{-n}\mathrm{J}_n(\mathrm{i}z) \tag{A.4}$$

(see equation 8.406.3, page 961 of [19]), equation A.3 can be rewritten as

$$f_{Z_{1k}}(z_{1k}|0, \mathrm{I}_j) = \frac{\exp(-2\alpha^2/\sigma_{1_j}^2)\sigma_{1_j}^2}{4\sigma_{2_j}^2}\int_0^\infty x\exp\left(-\frac{x(\sigma_{1_j}^2(1-z_{1k})+\sigma_{2_j}^2z_{1k})}{2\sigma_{2_j}^2}\right)\times$$

$$\mathrm{J}_0\left(\frac{\mathrm{i}2\alpha\sqrt{xz_{1k}}}{\sigma_{1_j}}\right)u(z_{1k})dx \tag{A.5}$$

where $\mathrm{i} = \sqrt{-1}$ .With the application of the following relation

$$\int_0^\infty x^{n+\frac{1}{2}\nu} \exp(-\Omega x) J_\nu(2\lambda\sqrt{x})dx = n!\lambda^\nu \exp\left(-\frac{\lambda^2}{\Omega}\right)\Omega^{-n-\nu-1} L_n^\nu(\lambda^2/\Omega) \qquad (A.6)$$

(see equation 6.643.4, page 741 of [19]), A.5 can be expressed as

$$f_{Z_{1k}}(z_{1k}|0, I_j) = \frac{\exp(-2\alpha^2/\sigma_{1_j}^2)\sigma_{1_j}^2}{4\sigma_{2_j}^2} \times \frac{\exp(-\lambda^2/\Omega)L_1^0(\lambda^2/\Omega)}{\Omega^2} u(z_{1k}) \qquad (A.7)$$

where $L_n^\nu(m)$ is the Laguerre polynomial of order n, $\lambda = \frac{i\alpha\sqrt{z_{1k}}}{\sigma_{1_j}}$, and

$$\Omega = \frac{(\sigma_{1_j}^2(1-z_{1k}) + \sigma_{2_j}^2 z_{1k})}{2\sigma_{2_j}^2}.$$

With the application of the following relation

$$L_n^\Omega(x) = \sum_{m=0}^{n} (-1)^m \binom{n+\Omega}{n-m} \frac{x^m}{m!} \qquad (A.8)$$

(see equation 8.970.1, page 1061 of [19]), equation A.7 may be reexpressed as

$$f_{Z_{1k}}(z_{1k}|0, I_j) = \frac{\exp(-2\alpha^2/\sigma_{1_j}^2)\sigma_{1_j}^2}{4\sigma_{2_j}^2} \times \frac{\exp(-\lambda^2/\Omega)\left(1-\frac{\lambda^2}{\Omega}\right)}{\Omega^2} u(z_{1k}) \qquad (A.9)$$

Now recall from Chapter II that the average signal energy per bit, E_b equals $\alpha^2 + 2\sigma_a^2$. Letting γ equal $\frac{\alpha^2}{2\sigma_a^2}$, the ratio of direct to diffuse signal power, then the diffuse signal power, $2\sigma_a^2$, may be equivalently expressed as $\frac{E_b}{(\gamma+1)}$. Recall also that $\sigma_{1_j}^2 = (4\sigma_a^2 + \sigma_j^2)$ and $\sigma_{2_j}^2 = \sigma_j^2$ where $\sigma_j^2 = \sigma_n^2 + \sigma_{I_j}^2$ for $j = 1,2,3$ is the total conditional noise variance, represent the total conditional variances for branches 1 and 2 respectively. With the use of these relations and some algebraic simplifications, equation A.9 can be reexpressed as

$$f_{Z_{1k}}(z_{1k}|0, I_j) = \left(\frac{[((\gamma+1)\Gamma_L)^3 + 2((\gamma+1)\Gamma_L)^2(1+(1-z_{1k})) + 4(\gamma+1)\Gamma_L(1-z_{1k})]}{[(\gamma+1)\Gamma_L + 2(1-z_{1k})]^3} + \right.$$

$$\frac{[2\gamma z_{1k}((\gamma+1)\Gamma_L)^2]}{[(\gamma+1)\Gamma_L+2(1-z_{1k})]^3}\Bigg)\times\exp\Bigg(-\frac{2\gamma(1-z_{1k})}{(\gamma+1)\Gamma_L+2(1-z_{1k})}\Bigg)u(z_{1k}) \qquad \text{(A.10)}$$

where $\Gamma_L = \left(\frac{E_L}{N_0}\right)^{-1} + \left(\frac{E_L}{\sigma_{I_j}^2}\right)^{-1} \cdot \left(\frac{E_L}{N_0}\right)$ is the average bit energy to thermal noise density ratio and

$\left(\frac{E_L}{\sigma_{I_j}^2}\right)$ is the average bit energy to jammer noise power ratio for case I_j, $j = 1,2,3$.

APPENDIX B

B.1 DERIVATION OF LAPLACE TRANSFORM OF $f_{Z_{1k}}(z_{1k}|0, \mathrm{I}_j)$

The Laplace transform of $f_{Z_{1k}}(z_{1k}|0, \mathrm{I}_j)$ is given by

$$F_{Z_{1k}}(s|0, \mathrm{I}_j) = \int_0^\infty f_{Z_{1k}}(z_{1k}|0, \mathrm{I}_j)\exp(-sz_{1k})dz_{1k} \tag{B.11}$$

Substituting in the expression for $f_{Z_{1k}}(z_{1k}|0, \mathrm{I}_j)$ (equation 3.5) into equation B.11 yields

$$F_{Z_{1k}}(s|0, \mathrm{I}_j) = \frac{\sigma_j^2}{2\sigma_{1_j}^2}\exp\left(-\frac{2\alpha^2}{\sigma_{1_j}^2}\right)\int_0^\infty \exp\left(-z_{1k}\left(s + \frac{\sigma_j^2}{2\sigma_{1_j}^2}\right)\right)\mathrm{I}_0\left(\frac{2\alpha\sqrt{z_{1k}\sigma_j^2}}{\sigma_{1_j}^2}\right)dz_{1k} \tag{B.12}$$

By defining a new variable $x = \sqrt{z_{1k}}$, equation B.12 can be rewritten as

$$F_{Z_{1k}}(s|0, \mathrm{I}_j) = \frac{\sigma_j^2}{\sigma_{1_j}^2}\exp\left(-\frac{2\alpha^2}{\sigma_{1_j}^2}\right)\int_0^\infty x\exp\left(-x^2\left(s + \frac{\sigma_j^2}{2\sigma_{1_j}^2}\right)\right)\mathrm{I}_0\left(\frac{2\alpha\sigma_j x}{\sigma_{1_j}^2}\right)dx \tag{B.13}$$

With the application of the following relation

$$\mathrm{I}_n(z) = \mathrm{i}^{-n}\mathrm{J}_n(\mathrm{i}z) \tag{B.14}$$

(see equation 8.406.3, page 961 of [19]), equation B.13 may be rewritten as

$$F_{Z_{1k}}(s|0, \mathrm{I}_j) = \frac{\sigma_j^2}{\sigma_{1_j}^2}\exp\left(-\frac{2\alpha^2}{\sigma_{1_j}^2}\right)\int_0^\infty x\exp\left(-x^2\left(s + \frac{\sigma_j^2}{2\sigma_{1_j}^2}\right)\right)\mathrm{J}_0\left(\frac{\mathrm{i}2\alpha\sigma_j x}{\sigma_{1_j}^2}\right)dx \tag{B.15}$$

where $\mathrm{i} = \sqrt{-1}$. With the application of the following relation

$$\int_0^\infty x^{\nu+1}\exp(-\Omega x^2)\mathrm{J}_\nu(\beta x)dx = \frac{\beta^\nu}{(2\Omega)^{\nu+1}}\exp\left(-\frac{\beta^2}{4\Omega}\right) \tag{B.16}$$

(see equation 6.6314 on page 738 of [19]), equation B.15 may be expressed as

$$F_{Z_{1k}}(s|0,\mathrm{I}_j) = \frac{\sigma_j^2}{2\sigma_{1_j}^2\left(s+\frac{\sigma_j^2}{2\sigma_{1_j}^2}\right)}\exp\left(-\frac{2\alpha^2}{\sigma_{1_j}^2}\right)\exp\left(\frac{\alpha^2\sigma_j^2}{\sigma_{1_j}^4\left(s+\frac{\sigma_j^2}{2\sigma_{1_j}^2}\right)}\right) \qquad \text{(B.17)}$$

B.2 DERIVATION OF $f_{Z_{1k}}(z_{1k}|0,\mathrm{I}_1)^{\otimes \mathrm{i}_j}$

The function $f_{Z_{1k}}(z_{1k}|0,\mathrm{I}_1)^{\otimes \mathrm{i}_j}$ may be derived as the inverse Laplace transform of $[F_{Z_{1k}}(s|0,\mathrm{I}_j)]^{\mathrm{i}_j}$, defined to be

$$f_{Z_{1k}}(z_{1k}|0,\mathrm{I}_j)^{\otimes \mathrm{i}_j} = \int_0^\infty [F_{Z_{1k}}(s|0,\mathrm{I}_j)]^{\mathrm{i}_j}\exp(sz_{1k})ds \qquad \text{(B.21)}$$

Substituting equation B.17 into B.21,

$$f_{Z_{1k}}(z_{1k}|0,\mathrm{I}_j)^{\otimes \mathrm{i}_j} = \left(\frac{\sigma_j^2}{2\sigma_{1_j}^2}\right)^{\mathrm{i}_j}\exp\left(-\frac{2\alpha^2\mathrm{i}_j}{\sigma_{1_j}^2}\right)\int_0^\infty\left(s+\frac{\sigma_j^2}{2\sigma_{1_j}^2}\right)^{-\mathrm{i}_j}\times$$

$$\exp\left(\frac{\alpha^2\sigma_j^2\mathrm{i}_j}{\sigma_{1_j}^4\left(s+\frac{\sigma_j^2}{2\sigma_{1_j}^2}\right)}\right)\exp(sz_{1k})ds \qquad \text{(B.22)}$$

Applying the known relation $\mathcal{L}\{\exp(-bz)f(z)\} = F_z(s+b)$, where $\mathcal{L}$ denotes the forward Laplace transform, equation B.14 and the following relation

$$\mathcal{L}\{a^{-\nu/2}z^{\nu/2}\mathrm{J}_\nu(2\sqrt{az})\} = \frac{1}{s^{\nu+1}}\exp\left(-\frac{a}{s}\right), \quad \nu > -1 \qquad \text{(B.23)}$$

(see equation 30 on page 185 of [20]), equation B.22 can be expressed as

$$f_{Z_{1k}}(z_{1k}|0,\mathrm{I}_j)^{\otimes \mathrm{i}_j} = \left(\frac{\sigma_j^2}{2\sigma_{1_j}^2}\right)^{\mathrm{i}_j}\left(\frac{\alpha^2\sigma_j^2\mathrm{i}_j}{\sigma_{1_j}^4}\right)^{-\left(\frac{\mathrm{i}_j-1}{2}\right)}\exp\left(-\frac{\sigma_j^2 z_{1k}}{2\sigma_{1_j}^2}\right)\exp\left(-\frac{2\alpha^2\mathrm{i}_j}{\sigma_{1_j}^2}\right)\times$$

$$I_{i_j-1}\left(\frac{2\alpha\sigma_j\sqrt{z_{1k}i_j}}{\sigma_{1_j}^2}\right)z_{1k}^{\left(\frac{i_j-1}{2}\right)}u(z_{1k}) \tag{B.24}$$

$$f_{Z_{1k}}(z_{1k}|0,I_j)^{\otimes i_j} = \frac{\sigma_j^2}{2\sigma_{1_j}^2}\exp\left(-\frac{\sigma_j^2 z_{1k}+4\alpha^2 i_j}{2\sigma_{1_j}^2}\right)\left(\frac{\sigma_j^2 z_{1k}}{4\alpha^2 i_j}\right)^{\left(\frac{i_j-1}{2}\right)}\times$$

$$I_{i_j-1}\left(\frac{2\alpha\sigma_j\sqrt{z_{1k}i_j}}{\sigma_{1_j}^2}\right)u(z_{1k}) \tag{B.25}$$

It is now desired to express this equation in terms of the signal to thermal noise density ratio (E_b/N_0) and the signal to noise interference ratio ($E_b/\sigma_{I_j}^2$), where $\sigma_{I_j}^2$ is the conditional noise variance for the jammer as before. Recalling that $\sigma_j^2 = \sigma_n^2 + \sigma_{I_j}^2$ is the total conditional noise variance and $\sigma_{1_j}^2 = (4\sigma_a^2 + \sigma_j^2)$ is the total conditional variance for branch 1 of our receiver, the following relations hold,

$$\frac{\sigma_j^2}{\sigma_{1_j}^2} = \frac{(\gamma+1)\Gamma_L}{2+(\gamma+1)\Gamma_L} \tag{B.26a}$$

$$\frac{\alpha^2}{\sigma_{1_j}^2} = \frac{\gamma}{2+(\gamma+1)\Gamma_L} \tag{B.26b}$$

$$\frac{\sigma_j^2}{\alpha^2} = \frac{(\gamma+1)\Gamma_L}{\gamma} \tag{B.26c}$$

where $\gamma = \frac{\alpha^2}{2\sigma_a^2}$ is the ratio of direct signal power to diffuse signal power and $\Gamma_L = \left(\frac{E_L}{N_0}\right)^{-1} + \left(\frac{E_L}{\sigma_{I_j}^2}\right)^{-1}$. Substituting equation B.26a and B.26b into equation B.25 gives

$$f_{Z_{1k}}(z_{1k}|0, \mathrm{I}_1)^{\otimes \mathrm{i}_j} = \left(\frac{(\gamma+1)\Gamma_{\mathrm{L}}}{2(2+(\gamma+1)\Gamma_{\mathrm{L}})}\right)\exp\left(-\frac{4\gamma \mathrm{i}_j + (\gamma+1)\Gamma_{\mathrm{L}} z_{1k}}{2(2+(\gamma+1)\Gamma_{\mathrm{L}})}\right)\times$$

$$\left(\frac{z_{1k}(\gamma+1)\Gamma_{\mathrm{L}}}{4\gamma \mathrm{i}_j}\right)^{\left(\frac{\mathrm{i}_j-1}{2}\right)} \mathrm{I}_{\mathrm{i}_j-1}\left(\sqrt{\frac{4\gamma(\gamma+1)\Gamma_{\mathrm{L}} z_{1k} \mathrm{i}_j}{(2+(\gamma+1)\Gamma_{\mathrm{L}})^2}}\right) u(z_{1k}) \qquad \text{(B.27)}$$

B.3 DERIVATION OF LAPLACE TRANSFORM OF $f_{Z_{1k}}\left(z_{1k}|0, \mathrm{I}_j, \hat{\sigma_j^2}\right)$

The Laplace transform of $f_{Z_{1k}}\left(z_{1k}|0, \mathrm{I}_j, \hat{\sigma_j^2}\right)$ is given by

$$F_{Z_{1k}}(s|0, \mathrm{I}_j, \hat{\sigma_j^2}) = \int_0^\infty f_{Z_{1k}}\left(z_{1k}|0, \mathrm{I}_j, \hat{\sigma_j^2}\right)\exp(-sz_{1k})dz_{1k} \qquad \text{(B.31)}$$

Substituting in the expression for $f_{Z_{1k}}\left(z_{1k}|0, \mathrm{I}_j, \hat{\sigma_j^2}\right)$ (equation 3.18) into equation B.31,

$$F_{Z_{1k}}(s|0, \mathrm{I}_j, \hat{\sigma_j^2}) = \frac{\hat{\sigma_j^2}}{2\sigma_{1_j}^2}\exp\left(-\frac{2\alpha^2}{\sigma_{1_j}^2}\right)\int_0^\infty \exp\left(-z_{1k}\left(s+\frac{\hat{\sigma_j^2}}{2\sigma_{1_j}^2}\right)\right)\mathrm{I}_0\left(\frac{2\alpha\sqrt{z_{1k}\hat{\sigma_j^2}}}{\sigma_{1_j}^2}\right)dz_{1k} \qquad \text{(B.32)}$$

By defining a new variable $x = \sqrt{z_{1k}}$, equation B.32 can be rewritten as

$$F_{Z_{1k}}(s|0, \mathrm{I}_j, \hat{\sigma_j^2}) = \frac{\hat{\sigma_j^2}}{\sigma_{1_j}^2}\exp\left(-\frac{2\alpha^2}{\sigma_{1_j}^2}\right)\int_0^\infty x\exp\left(-x^2\left(s+\frac{\hat{\sigma_j^2}}{2\sigma_{1_j}^2}\right)\right)\mathrm{I}_0\left(\frac{2\alpha\hat{\sigma_j}x}{\sigma_{1_j}^2}\right)dx \qquad \text{(B.33)}$$

Upon applying equation B.14, equation B.33 may be rewritten as

$$F_{Z_{1k}}(s|0, \mathrm{I}_j, \hat{\sigma_j^2}) = \frac{\hat{\sigma_j^2}}{\sigma_{1_j}^2}\exp\left(-\frac{2\alpha^2}{\sigma_{1_j}^2}\right)\int_0^\infty x\exp\left(-x^2\left(s+\frac{\hat{\sigma_j^2}}{2\sigma_{1_j}^2}\right)\right)\mathrm{J}_0\left(\frac{\mathrm{i}2\alpha\hat{\sigma_j}x}{\sigma_{1_j}^2}\right)dx \qquad \text{(B.34)}$$

With the application of equation B.16, equation B.34 may be expressed as

$$F_{Z_{1k}}(s|0, \mathrm{I}_j, \hat{\sigma}_j^2) = \frac{\hat{\sigma}_j^2}{2\sigma_{1_j}^2\left(s + \frac{\hat{\sigma}_j^2}{2\sigma_{1_j}^2}\right)} \exp\left(-\frac{2\alpha^2}{\sigma_{1_j}^2}\right) \exp\left(\frac{\alpha^2\hat{\sigma}_j^2}{\sigma_{1_j}^4\left(s + \frac{\hat{\sigma}_j^2}{2\sigma_{1_j}^2}\right)}\right) \qquad \text{(B.35)}$$

B.4 DERIVATION OF $f_{Z_{1k}}\left(z_{1k}|0, \mathrm{I}_j, \hat{\sigma}_j^2\right)^{\otimes \mathrm{i}_j}$

The function $f_{Z_{1k}}\left(z_{1k}|0, \mathrm{I}_j, \hat{\sigma}_j^2\right)^{\otimes \mathrm{i}_j}$ may be derived as the inverse Laplace transform of $\left[F_{Z_{1k}}(s|0, \mathrm{I}_j, \hat{\sigma}_j^2)\right]^{\mathrm{i}_j}$, defined to be

$$f_{Z_{1k}}\left(z_{1k}|0, \mathrm{I}_j, \hat{\sigma}_j^2\right)^{\otimes \mathrm{i}_j} = \int_0^\infty \left[F_{Z_{1k}}(s|0, \mathrm{I}_j, \hat{\sigma}_j^2)\right]^{\mathrm{i}_j} \exp(sz_{1k})ds \qquad \text{(B.41)}$$

Substituting equation B.35 into B.41 yields

$$f_{Z_{1k}}\left(z_{1k}|0, \mathrm{I}_j, \hat{\sigma}_j^2\right)^{\otimes \mathrm{i}_j} = \left(\frac{\hat{\sigma}_j^2}{2\sigma_{1_j}^2}\right)^{\mathrm{i}_j} \exp\left(-\frac{2\alpha^2 \mathrm{i}_j}{\sigma_{1_j}^2}\right) \int_0^\infty \left(s + \frac{\hat{\sigma}_j^2}{2\sigma_{1_j}^2}\right)^{-\mathrm{i}_j} \times$$

$$\exp\left(\frac{\alpha^2\hat{\sigma}_j^2 \mathrm{i}_j}{\sigma_{1_j}^4\left(s + \frac{\hat{\sigma}_j^2}{2\sigma_{1_j}^2}\right)}\right) \exp(sz_{1k})ds \qquad \text{(B.42)}$$

Applying the relation $\mathcal{L}\{\exp(-bz)f(z)\} = F_z(s+b)$, equations B.14 and B.23, equation B.42 can be expressed as

$$f_{Z_{1k}}\left(z_{1k}|0, I_j, \hat{\sigma_j^2}\right)^{\otimes i_j} = \left(\frac{\hat{\sigma_j^2}}{2\sigma_{1_j}^2}\right)^{i_j}\left(\frac{\alpha^2\hat{\sigma_j^2}i_j}{\sigma_{1_j}^4}\right)^{-\left(\frac{i_j-1}{2}\right)}\exp\left(-\frac{\hat{\sigma_j^2}z_{1k}}{2\sigma_{1_j}^2}\right)\exp\left(-\frac{2\alpha^2 i_j}{\sigma_{1_j}^2}\right)\times$$

$$I_{i_j-1}\left(\frac{2\alpha\hat{\sigma}_j\sqrt{z_{1k}i_j}}{\sigma_{1_j}^2}\right)z_{1k}^{\left(\frac{i_j-1}{2}\right)}u(z_{1k}) \qquad \text{(B.43)}$$

$$f_{Z_{1k}}\left(z_{1k}|0, I_j, \hat{\sigma_j^2}\right)^{\otimes i_j} = \frac{\hat{\sigma_j^2}}{2\sigma_{1_j}^2}\exp\left(-\frac{\hat{\sigma_j^2}z_{1k}+4\alpha^2 i_j}{2\sigma_{1_j}^2}\right)\left(\frac{\hat{\sigma_j^2}z_{1k}}{4\alpha^2 i_j}\right)^{\left(\frac{i_j-1}{2}\right)}\times$$

$$I_{i_j-1}\left(\frac{2\alpha\hat{\sigma}_j\sqrt{z_{1k}i_j}}{\sigma_{1_j}^2}\right)u(z_{1k}) \qquad \text{(B.44)}$$

It is again desired to express these equations in terms of the signal to thermal noise density ratio (E_b/N_0) and the signal to noise interference ratio ($E_b/\sigma_{I_j}^2$). Applying the following relationships:

$$\frac{\hat{\sigma_j^2}}{\sigma_{1_j}^2} = \frac{(\hat{\sigma_j^2}/\sigma_j^2)(\gamma+1)\Gamma_L}{2+(\gamma+1)\Gamma_L} \qquad \text{(B.45a)}$$

$$\frac{\alpha^2}{\sigma_{1_j}^2} = \frac{\gamma}{2+(\gamma+1)\Gamma_L} \qquad \text{(B.45b)}$$

$$\frac{\hat{\sigma_j^2}}{\alpha^2} = \frac{(\hat{\sigma_j^2}/\sigma_j^2)(\gamma+1)\Gamma_L}{\gamma} \qquad \text{(B.45c)}$$

equation B.44 may be rewritten as

$$f_{Z_{1k}}\left(z_{1k}|0, I_j, \hat{\sigma_j^2}\right)^{\otimes i_j} = \left(\frac{(\hat{\sigma_j^2}/\sigma_j^2)(\gamma+1)\Gamma_L}{2(2+(\gamma+1)\Gamma_L)}\right)\exp\left(-\frac{4\gamma i_j+(\hat{\sigma_j^2}/\sigma_j^2)(\gamma+1)\Gamma_L z_{1k}}{2(2+(\gamma+1)\Gamma_L)}\right)\times$$

$$\left(\frac{(\hat{\sigma_j^2}/\sigma_j^2)z_{1k}(\gamma+1)\Gamma_L}{4\gamma i_j}\right)^{\left(\frac{i_j-1}{2}\right)}I_{i_j-1}\left(\sqrt{\frac{4(\hat{\sigma_j^2}/\sigma_j^2)\gamma(\gamma+1)\Gamma_L z_{1k}i_j}{(2+(\gamma+1)\Gamma_L)^2}}\right)u(z_{1k}) \qquad \text{(B.46)}$$

B.5 DERIVATION OF LAPLACE TRANSFORM OF $f_{V_{1k}}(v_{1k}|0, \mathrm{I}_j)$

The Laplace transform of $f_{V_{1k}}(v_{1k}|0, \mathrm{I}_j)$ is given by

$$F_{V_{1k}}(s|0, \mathrm{I}_j) = \int_0^\infty f_{V_{1k}}(v_{1k}|0, \mathrm{I}_j)\exp(-sv_{1k})dv_{1k} \tag{B.51}$$

Substituting in the expression for $f_{V_{1k}}(v_{1k}|0, \mathrm{I}_j)$ (equation 3.1) into equation B.51 yields

$$F_{V_{1k}}(s|0, \mathrm{I}_j) = \frac{1}{2\sigma_{1_j}^2}\exp\left(-\frac{2\alpha^2}{\sigma_{1_j}^2}\right)\int_0^\infty \exp\left(-v_{1k}\left(s+\frac{1}{2\sigma_{1_j}^2}\right)\right)\mathrm{I}_0\left(\frac{2\alpha\sqrt{v_{1k}}}{\sigma_{1_j}^2}\right)dv_{1k} \tag{B.52}$$

By defining a new variable $x = \sqrt{v_{1k}}$, equation B.52 can be rewritten as

$$F_{V_{1k}}(s|0, \mathrm{I}_j) = \frac{1}{\sigma_{1_j}^2}\exp\left(-\frac{2\alpha^2}{\sigma_{1_j}^2}\right)\int_0^\infty x\exp\left(-x^2\left(s+\frac{1}{2\sigma_{1_j}^2}\right)\right)\mathrm{I}_0\left(\frac{2\alpha x}{\sigma_{1_j}^2}\right)dx \tag{B.53}$$

With the application of equation B.14, equation B.53 may be rewritten as

$$F_{V_{1k}}(s|0, \mathrm{I}_j) = \frac{1}{\sigma_{1_j}^2}\exp\left(-\frac{2\alpha^2}{\sigma_{1_j}^2}\right)\int_0^\infty x\exp\left(-x^2\left(s+\frac{1}{2\sigma_{1_j}^2}\right)\right)\mathrm{J}_0\left(\frac{\mathrm{i}2\alpha x}{\sigma_{1_j}^2}\right)dx \tag{B.54}$$

Now by applying equation B.16, equation B.54 may be expressed as

$$F_{V_{1k}}(s|0, \mathrm{I}_j) = \frac{1}{2\sigma_{1_j}^2\left(s+\frac{1}{2\sigma_{1_j}^2}\right)}\exp\left(-\frac{2\alpha^2}{\sigma_{1_j}^2}\right)\exp\left(\frac{\alpha^2}{\sigma_{1_j}^4\left(s+\frac{1}{2\sigma_{1_j}^2}\right)}\right) \tag{B.55}$$

B.6 DERIVATION OF $f_{V_{1k}}(v_{1k}|0, \mathrm{I}_1)^{\otimes \mathrm{i}_j}$

The function $f_{V_{1k}}(v_{1k}|0, \mathrm{I}_1)^{\otimes \mathrm{i}_j}$ may be derived as the inverse Laplace transform of $[F_{V_{1k}}(s|0, \mathrm{I}_j)]^{\mathrm{i}_j}$, defined to be

$$f_{V_{1k}}(v_{1k}|0, \mathrm{I}_j)^{\otimes \mathrm{i}_j} = \int_0^\infty [F_{V_{1k}}(s|0, \mathrm{I}_j)]^{\mathrm{i}_j}\exp(sv_{1k})ds \tag{B.61}$$

Substituting equation B.55 into B.61 yields

$$f_{V_{1k}}(v_{1k}|0,\mathrm{I}_j)^{\otimes \mathrm{i}_j} = \left(\frac{1}{2\sigma_{1_j}^2}\right)^{\mathrm{i}_j}\exp\left(-\frac{2\alpha^2\mathrm{i}_j}{\sigma_{1_j}^2}\right)\int_0^\infty\left(s+\frac{1}{2\sigma_{1_j}^2}\right)^{-\mathrm{i}_j}\times$$

$$\exp\left(\frac{\alpha^2\mathrm{i}_j}{\sigma_{1_j}^4\left(s+\frac{1}{2\sigma_{1_j}^2}\right)}\right)\exp(sv_{1k})ds \qquad \text{(B.62)}$$

By applying the relation $\mathcal{L}\{\exp(-bz)f(z)\} = F_z(s+b)$ and equations B.14 and B.23, equation B.62 can be expressed as

$$f_{V_{1k}}(v_{1k}|0,\mathrm{I}_j)^{\otimes \mathrm{i}_j} = \left(\frac{1}{2\sigma_{1_j}^2}\right)^{\mathrm{i}_j}\left(\frac{\alpha^2\mathrm{i}_j}{\sigma_{1_j}^4}\right)^{-\left(\frac{\mathrm{i}_j-1}{2}\right)}\exp\left(-\frac{v_{1k}}{2\sigma_{1_j}^2}\right)\exp\left(-\frac{2\alpha^2\mathrm{i}_j}{\sigma_{1_j}^2}\right)\times$$

$$\mathrm{I}_{\mathrm{i}_j-1}\left(\frac{2\alpha\sqrt{v_{1k}\mathrm{i}_j}}{\sigma_{1_j}^2}\right)v_{1k}^{\left(\frac{\mathrm{i}_j-1}{2}\right)}u(v_{1k}) \qquad \text{(B.63)}$$

$$f_{V_{1k}}(v_{1k}|0,\mathrm{I}_j)^{\otimes \mathrm{i}_j} = \frac{1}{2\sigma_{1_j}^2}\exp\left(-\frac{v_{1k}+4\alpha^2\mathrm{i}_j}{2\sigma_{1_j}^2}\right)\left(\frac{v_{1k}}{4\alpha^2\mathrm{i}_j}\right)^{\left(\frac{\mathrm{i}_j-1}{2}\right)}\times$$

$$\mathrm{I}_{\mathrm{i}_j-1}\left(\frac{2\alpha\sqrt{v_{1k}\mathrm{i}_j}}{\sigma_{1_j}^2}\right)u(v_{1k}) \qquad \text{(B.64)}$$

APPENDIX C

C.1 DERIVATION OF THE CONDITIONAL PROBABILITY OF BIT ERROR FOR PDSC1 RECEIVER OVER RAYLEIGH FADING CHANNEL

The conditional probability of bit error $\Pr(z_1 < z_2 | 0, \mathrm{I}_j)$ may be expressed as

$$\mathrm{P_b}(z_1, z_2 | 0, \mathrm{I}_j) = \int_0^{\infty} \int_0^{z_2} f_{Z_1, Z_2}(z_1, z_2 | 0, \mathrm{I}_j) dz_1 dz_2 \tag{C.15}$$

Since Z_1 and Z_2 are independent random variables, equation C.15 can be written as

$$\mathrm{P_b}(z_1, z_2 | 0, \mathrm{I}_j) = \int_0^{\infty} \left[\int_0^{z_2} f_{Z_1}(z_1 | 0, \mathrm{I}_j) dz_1 \right] f_{Z_2}(z_2 | 0, \mathrm{I}_j) dz_2 \tag{C.16}$$

With the use of equation 4.12, the inner integral of equation C.16 becomes

$$\int_0^{z_2} f_{Z_1}(z_1 | 0, \mathrm{I}_j) dz_1 = \int_0^{z_2} \frac{\mathrm{M}}{2\sigma_{1_j}^2} \exp\left(- \frac{z_1}{2\sigma_{1_j}^2} \right) \left[1 - \exp\left(- \frac{z_1}{2\sigma_{1_j}^2} \right) \right]^{\mathrm{M}-1} dz_1 \tag{C.17}$$

Then by applying the binomial theorem

$$(a+b)^n = \sum_{p=0}^{n} \binom{n}{p} a^{n-p} b^p \tag{C.18}$$

equation C.17 can be expressed as

$$\int_0^{z_2} f_{Z_1}(z_1 | 0, \mathrm{I}_j) dz_1 = \int_0^{z_2} \frac{\mathrm{M}}{2\sigma_{1_j}^2} \exp\left(- \frac{z_1}{2\sigma_{1_j}^2} \right) \sum_{p=0}^{\mathrm{M}-1} \binom{\mathrm{M}-1}{p} (-1)^p \exp\left(- \frac{p z_1}{2\sigma_{1_j}^2} \right) dz_1 \tag{C.19}$$

Rearranging terms then gives

$$\int_0^{z_2} f_{Z_1}(z_1 | 0, \mathrm{I}_j) dz_1 = \frac{\mathrm{M}}{2\sigma_{1_j}^2} \sum_{p=0}^{\mathrm{M}-1} \binom{\mathrm{M}-1}{p} (-1)^p \int_0^{z_2} \exp\left(- \frac{z_1 (1+p)}{2\sigma_{1_j}^2} \right) dz_1 \tag{C.110}$$

Carrying out the integration yields

$$\int_0^{z_2} f_{Z_1}(z_1|0, I_j)dz_1 = M\sum_{p=0}^{M-1}\binom{M-1}{p}\frac{(-1)^p}{(1+p)}\left[1-\exp\left(-\frac{z_2(1+p)}{2\sigma_{1_j}^2}\right)\right] \qquad \text{(C.111)}$$

Substituting equation C.111 into equation C.16 yields

$$P_b(z_2, \sigma_{1_j}^2|0, I_j) = \int_0^{\infty} M\sum_{p=0}^{M-1}\binom{M-1}{p}\frac{(-1)^p}{(1+p)}\left[1-\exp\left(-\frac{z_2(1+p)}{2\sigma_{1_j}^2}\right)\right] f_{Z_2}(z_2|0, I_j)dz_2 \qquad \text{(C.112)}$$

Substituting equation 4.13 into equation C.112 gives

$$P_b(z_2, \sigma_{1_j}^2, \sigma_{2_j}^2|0, I_j) = \int_0^{\infty} M\sum_{p=0}^{M-1}\binom{M-1}{p}\frac{(-1)^p}{(1+p)}\left[1-\exp\left(-\frac{z_2(1+p)}{2\sigma_{1_j}^2}\right)\right]\times$$

$$\frac{M}{2\sigma_{2_j}^2}\exp\left(-\frac{z_2}{2\sigma_{2_j}^2}\right)\left[1-\exp\left(-\frac{z_2}{2\sigma_{2_j}^2}\right)\right]^{M-1} dz_2 \qquad \text{(C.113)}$$

Again applying the binomial theorem (C.18) and rearranging terms yields

$$P_b(z_2, \sigma_{1_j}^2, \sigma_{2_j}^2|0, I_j) = \sum_{p=0}^{M-1}\sum_{r=0}^{M-1}\frac{M^2(-1)^{(p+r)}}{2\sigma_{2_j}^2(1+p)}\binom{M-1}{p}\binom{M-1}{r}\times$$

$$\int_0^{\infty}\left[1-\exp\left(-\frac{z_2(1+p)}{2\sigma_{1_j}^2}\right)\right]\exp\left(-\frac{z_2(1+r)}{2\sigma_2^2}\right)dz_2 \qquad \text{(C.110)}$$

After evaluating the integral, equation C.110 may be expressed as

$$P_b(\sigma_{1_j}^2, \sigma_2^2|0, I_j) = \sum_{p=0}^{M-1}\sum_{r=0}^{M-1}\frac{M^2(-1)^{(p+r)}}{(1+p)(1+r)}\binom{M-1}{p}\binom{M-1}{r}\times$$

$$\left[1-\frac{1}{1+\dfrac{(1+p)\sigma_2^2}{(1+r)\sigma_{1_j}^2}}\right] \qquad \text{(C.111)}$$

Further simplifying the leading terms yields

$$P_b(\sigma_{1_j}^2, \sigma_2^2 | 0, I_j) = \sum_{p=0}^{M-1} \sum_{r=0}^{M-1} (-1)^{(p+r)} \binom{M}{p+1} \binom{M}{r+1} \times \left[1 - \frac{1}{1 + \frac{(1+p)\sigma_2^2}{(1+r)\sigma_{1_j}^2}} \right] \quad \text{(C.112)}$$

Expressing equation C.112 in terms of the signal to thermal noise and signal to interference ratio yields

$$P_b(\Gamma_M | 0, I_j) = \sum_{p=0}^{M-1} \sum_{r=0}^{M-1} (-1)^{(p+r)} \binom{M}{p+1} \binom{M}{r+1} \times \left[1 - \frac{1}{1 + \frac{(1+p)\Gamma_M}{(1+r)(2+\Gamma_M)}} \right] \quad \text{(C.113)}$$

or

$$P_b(\Gamma_M | 0, I_j) = \sum_{p=0}^{M-1} \sum_{r=0}^{M-1} (-1)^{(p+r)} \binom{M}{p+1} \binom{M}{r+1} \times \left[\frac{1}{1 + \frac{(1+r)(2+\Gamma_M)}{(1+p)\Gamma_M}} \right] \quad \text{(C.114)}$$

where $\Gamma_M = \left(\frac{E_M}{N_0}\right)^{-1} + \left(\frac{E_M}{\sigma_{I_j}^2}\right)^{-1}$.

C.2 DERIVATION OF EQUATION 4.18

Substituting equation 4.16 into 4.17 yields

$$F_{V_{1k}}(z_1 | 0, I_j) = \int_0^{z_1} \frac{1}{2\sigma_{1_j}^2} \exp\left(- \frac{1}{2\sigma_{1_j}^2} (\lambda + 4\alpha^2) \right) I_0\left(\frac{2\alpha\sqrt{\lambda}}{\sigma_{1_j}^2} \right) d\lambda \quad \text{(C.21)}$$

With the application of the known relation

$$F_Y(y) = \int_0^y \frac{1}{2\sigma^2}\left(\frac{u}{s^2}\right)^{(n-2)/4} \exp\left(-\frac{s^2+u}{2\sigma^2}\right) I_{n/2-1}\left(\sqrt{u}\frac{s}{\sigma^2}\right) du \qquad \text{(C.22)}$$

(see equation (2-1-121) of [5]) and equation (2-1-124) of [5]

$$F_Y(y) = 1 - Q\left(\frac{s}{\sigma}, \frac{\sqrt{y}}{\sigma}\right) \qquad \text{(C.23)}$$

equation C.21 can be expressed as

$$F_{V_{1k}}(z_1|0, \mathrm{I}_j) = 1 - Q\left(\frac{2\alpha}{\sigma_{1_j}}, \frac{\sqrt{z_1}}{\sigma_{1_j}}\right) \qquad \text{(C.24)}$$

C.3 DERIVATION OF THE CONDITIONAL PROBABILITY OF BIT ERROR FOR PDSC1 RECEIVER OVER RICIAN FADING CHANNEL

The conditional probability of bit error equal to $\Pr(z_1 < z_2|0, \mathrm{I}_j)$ may be expressed as

$$\mathrm{P_b}(z_1, z_2|0, \mathrm{I}_j) = \int_0^\infty \left[\int_{z_1}^\infty f_{Z_2}(z_2|0, \mathrm{I}_j) dz_2\right] f_{Z_1}(z_1|0, \mathrm{I}_j) dz_1 \qquad \text{(C.31)}$$

Applying equation C.18 to equation 4.20, the inner integral of equation C.31 may be evaluated to be

$$\int_{z_1}^\infty f_{Z_2}(z_2|0, \mathrm{I}_j) dz_2 = \mathrm{M} \sum_{r=0}^{\mathrm{M}-1} \binom{\mathrm{M}-1}{r} \frac{(-1)^r}{(1+r)} \exp\left(-\frac{z_1(1+r)}{2\sigma_{2_j}^2}\right) \qquad \text{(C.32)}$$

Substituting equations 4.19 and C.32 into C.31 and simplifying the factorial terms gives

$$\mathrm{P_b}(z_1|0, \mathrm{I}_j) = \frac{\mathrm{M}}{2\sigma_{1_j}^2} \sum_{r=0}^{\mathrm{M}-1} \binom{\mathrm{M}}{r+1} (-1)^r \int_0^\infty \exp\left(-\frac{z_1(1+r)}{2\sigma_{2_j}^2}\right) \times$$

$$\exp\left(-\frac{1}{2\sigma_{1_j}^2}(z_1 + 4\alpha^2)\right) \mathrm{I}_0\left(\frac{2\alpha\sqrt{z_1}}{\sigma_{1_j}^2}\right) \left[1 - Q\left(\frac{2\alpha}{\sigma_{1_j}}, \frac{\sqrt{z_1}}{\sigma_{1_j}}\right)\right]^{\mathrm{M}-1} dz_1 \qquad \text{(C.33)}$$

Combining the exponential terms yields

$$P_b(z_1|0,I_j) = \frac{M}{2\sigma_{1_j}^2}\sum_{r=0}^{M-1}\binom{M}{r+1}(-1)^r \exp\left(-\frac{2\alpha^2}{\sigma_{1_j}^2}\right)\int_0^\infty \exp\left(-\frac{z_1(1+r)\sigma_{1_j}^2+\sigma_{2_j}^2}{2\sigma_{1_j}^2\sigma_{2_j}^2}\right)\times$$

$$I_0\left(\frac{2\alpha\sqrt{z_1}}{\sigma_{1_j}^2}\right)\left[1-Q\left(\frac{2\alpha}{\sigma_{1_j}},\frac{\sqrt{z_1}}{\sigma_{1_j}}\right)\right]^{M-1} dz_1 \qquad \text{(C.34)}$$

It is desired to put equation C.34 in terms of $\gamma = \frac{\alpha^2}{2\sigma_a^2}$ and $\Gamma_M = \left(\frac{E_M}{N_0}\right)^{-1} + \left(\frac{E_M}{\sigma_{I_j}^2}\right)^{-1}$. This can be done in several steps. Recalling that $\sigma_{1_j}^2 = (4\sigma_a^2 + N_0 + \sigma_{I_j}^2)$ and $\sigma_{2_j}^2 = (N_0 + \sigma_{I_j}^2)$, the following relations hold:

$$\sigma_{1_j}^2 = \frac{E_M}{(\gamma+1)}(2+(\gamma+1)\Gamma_M) \qquad \text{(C.35a)}$$

$$\frac{\alpha^2}{\sigma_{1_j}^2} = \frac{\gamma}{2+(\gamma+1)\Gamma_M} \qquad \text{(C.35b)}$$

$$\frac{\sigma_{1_j}^2}{\sigma_{2_j}^2} = \frac{2+(\gamma+1)\Gamma_M}{(\gamma+1)\Gamma} \qquad \text{(C.35c)}$$

With these relations, equation C.34 may be reexpressed as

$$P_b(z_1|0,I_j) = \frac{M(\gamma+1)}{2E_M(2+(\gamma+1)\Gamma_M)}\sum_{r=0}^{M-1}\binom{M}{r+1}(-1)^r \exp\left(-\frac{2\gamma}{2+(\gamma+1)\Gamma_M}\right)\times$$

$$\int_0^\infty \exp\left(-\frac{z_1}{2E_M}\left[\frac{2(1+r)+(2+r)(\gamma+1)\Gamma_M}{2+(\gamma+1)\Gamma_M}\right]\right) I_0\left(\sqrt{\frac{4(\gamma+1)\gamma z_1}{E_M(2+(\gamma+1)\Gamma_M)^2}}\right)\times$$

$$\left[1-Q\left(\sqrt{\frac{4\gamma}{2+(\gamma+1)\Gamma_M}},\sqrt{\frac{z_1(\gamma+1)}{E_M(2+(\gamma+1)\Gamma_M)}}\right)\right]^{M-1} dz_1 \qquad \text{(C.36)}$$

Letting $u = \frac{z_1}{E_M}$, equation C.36 may be expressed as

$$P_b(u|0,I_j) = \frac{M(\gamma+1)}{2(2+(\gamma+1)\Gamma_M)} \sum_{r=0}^{M-1} \binom{M}{r+1} (-1)^r \exp\left(-\frac{2\gamma}{2+(\gamma+1)\Gamma_M}\right) \times$$

$$\int_0^\infty \exp\left(-\frac{u}{2}\left[\frac{2(1+r)+(2+r)(\gamma+1)\Gamma_M}{(2+(\gamma+1)\Gamma_M)}\right]\right) I_0\left(\sqrt{\frac{4(\gamma+1)\gamma u}{(2+(\gamma+1)\Gamma_M)^2}}\right) \times$$

$$\left[1 - Q\left(\sqrt{\frac{4\gamma}{2+(\gamma+1)\Gamma_M}}, \sqrt{\frac{u(\gamma+1)}{2+(\gamma+1)\Gamma_M}}\right)\right]^{M-1} du \qquad \text{(C.37)}$$

LIST OF REFERENCES

1. Rappaport, Theodore S., *Wireless Communications, Principles and Practice,* Prentice-Hall Inc., Upper Saddle River, New Jersey, 1996.

2. Sklar, B., "Rayleigh fading channels in mobile digital communication systems, Part I: characterization," *IEEE Communications Magazine*, pp. 136-155, September, 1997.

3. Pahlavan, Kaveh and Levesque, Allen H., *Wireless Information Networks,* John Wiley & Sons, Inc., New York, New York, 1995.

4. Van Trees, Harry L., *Detection, Estimation, and Modulation Theory, Part I,* John Wiley & Sons, Inc., New York, New York, 1971.

5. Proakis, John G., *Digital Communications*, 3rd ed., McGraw-Hill, Inc., New York, NY, 1995.

6. Haykin, Simon, *Communication Systems,* 3rd ed., John Wiley and Sons, New York, NY, 1994.

7. Sklar, B., *Digital Communications: Fundamentals and Applications,* Prentice-Hall Inc., Englewood Cliffs, New Jersey, 1988.

8. Whalen, Anthony D., *Detection of Signals in Noise*, Academic Press Inc., San Diego, CA., 1971.

9. Leon-Garcia, Alberto, *Probability and Random Processes for Electrical Engineering,* 2nd ed., Addison-Wesley Publishing Company, Inc., Reading, Massachusetts, 1994.

10. Peterson, Roger L., Ziemer, Rodger E. and Borth, David E., *Introduction to Spread Spectrum Communications,* John Wiley and Sons, New York, NY, 1995.

11. Simon, M. K., Omura, J. K., Scholtz, R.A., and Levitt B. K., *Spread Spectrum Communications, Vol I, II.* Computer Science Press, Rockville, MD, 1985.

12. Simon M. K., *et al., Spread Spectrum Communications Handbook,* McGraw-Hill, Inc., New York, NY, 1994.

13. Turin, G.L., "The effects of multipath and fading on the performance of direct-sequence CDMA systems," *IEEE Journal on Selected Areas in Communications,* vol. SAC-2, pp. 59-63, July 1984.

14. Robertson, R. Clark and Ha, Tri T., "Error probabilities of fast frequency-hopped FSK with self-normalization combining in a fading channel with partial-band interference," *IEEE Journal on Selected Areas in Communications,* vol. 10, no. 4, pp. 714-722, May 1992.

15. Robertson, R. Clark and Ha, Tri T., "Error probabilities of fast frequency-hopped MFSK with noise-normalization combining in a fading channel with partial-band interference," *IEEE Transactions on Communications,* vol. 40, no. 2, pp. 404-412, February 1992.

16. Robertson, R. Clark and Iwasaki, H., "Performance of a Fast Frequency-Hopped Noncoherent MFSK Receiver with Nonideal Adaptive Gain Control," *IEEE Transactions on Communications,* vol. 46, no. 1, pp. 104-114, January 1998.

17. Lee, J. S., Miller, L. E., and French, R. H., "Probability of Error Analysis of a BFSK frequency-hopping system with diversity under partial-band jamming interference-Part II: Performance of square-law nonlinear combining soft decision receivers," *IEEE Transactions on Communications,* vol. COM-32, no. 2, pp. 1243-1250, December 1984.

18. Miller, L. E., Lee, J. S., and Kadrichu, A. P., "Probability of Error Analysis of a BFSK frequency-hopping system with diversity under partial-band jamming interference-Part III: Performance of a square-law self-normalizing soft decision receiver," *IEEE Transactions on Communications,* vol. COM-34, no. 7, pp. 669-675, July 1986.

19. Gradshteyn, I. S. and Ryzhik, I. M., *Table of Integrals, Series, and Products,* 5th ed., Academic Press, Inc., New York, NY, 1994.

20. Erdelyi, A., *Tables of Integral Transforms,* vol. 1, McGraw-Hill Inc., New York, 1954.

21. Eng, T., Kong, N. and Milstein, L. B., "Comparison of diversity combining techniques for Rayleigh-fading channels," *IEEE Transactions on Communications,* vol. 44, no. 9, September 1996.

22. Papoulis, A., *Probability, Random Variables, and Stochastic Processes,* 3rd ed., McGraw-Hill, Inc., New York, NY, 1991.

23. McGee, W. F., "Another recursive method for computing the Q-function," *IEEE Transactions on Information Theory,* July 1970.

24. Abramowitz, M. and Stegun, I., *Handbook of Mathematical Functions,* Dover Publications, Inc., 1972.

25. Clark, G. C. and Cain, J. B., *Error Correction Coding for Digital Communications,* Plenum, New York, NY, 1981.

26. Lin, Shu and Costello, Daniel J., *Error Control Coding: Fundamentals and Applications,* Prentice-Hall Inc., Englewood Cliffs, New Jersey, 1983.

27. Forney, G. D., "The Viterbi Algorithm," *Proceedings IEEE,* vol. 61, no. 3, pp. 268-278, 1978.

28. Chang, I. K., Stuber, G. L., and Bush, A. M., Performance of diversity combining techniques for DS/DPSK signaling over a pulse jammed multipath-fading channel," *IEEE Transactions on Communications,* vol. 38, no. 10, pp. 1823-1834, October 1990.

29. Chang, I. K., Stuber, G. L., "Soft-limiter RAKE receivers for coded DS/ DPSK systems over pulse jammed multipath-fading channels," *IEEE Transactions on Communications,* vol. 44, no. 9, pp. 1163-1171, September 1996.

30. Nakagami, M., "The *m*-Distribution--A General Formula of Intensity Distribution of Rapid Fading," in *Statistical Methods of Radio Wave Propagation,* W.C. Hoffman (ed.), pp. 3-36, Pergamon Press, New York, 1960.

INITIAL DISTRIBUTION LIST

1.	Defense Technical Information Center 8725 John Kingman Rd., STE 0944 Fort Belvoir, VA 22060-6218	2
2.	Dudley Knox Library Naval Postgraduate School 411 Dyer Road Monterey, CA 93943-5101	2
3.	Chairman, Code EC Department of Electrical and Computer Engineering Naval Postgraduate School Monterey, CA 93943-5121	1
4.	Prof. Charles W. Therrien, Code EC/Ti Department of Electrical and Computer Engineering Naval Postgraduate School Monterey, CA 93943-5121	1
5.	Prof. Tri T. Ha, Code EC/Ha Department of Electrical and Computer Engineering Naval Postgraduate School Monterey, CA 93943-5121	2
6.	Prof. Murali Tummala, Code EC/Tu Department of Electrical and Computer Engineering Naval Postgraduate School Monterey, CA 93943-5121	1
7.	Prof. Roberto Cristi, Code EC/Cx Department of Electrical and Computer Engineering Naval Postgraduate School Monterey, CA 93943-5121	1
8.	Prof. Andres Larraza, Code PH/La Department of Physics Naval Postgraduate School Monterey, CA 93943-5121	1

9. RADM John A. Gauss
Commander
Space and Naval Warfare Systems Command
4301 Pacific Highway
San Diego, CA 92110-3127 — 1

10. Mr. Kin Searcy
Space and Naval Warfare Systems Command
Code PMW-133
Bldg. C60, Electron Drive
San Diego, CA 92152 — 1

11. Ms. Michelle McGuire
Space and Naval Warfare Systems Command
Code PMW-133
Bldg. C60, Electron Drive
San Diego, CA 92152 — 1

12. LCDR Charles W. Victory
19393 Via Cuesta Road
Ramona, CA 92065 — 7

13. Mr. James Victory
Chemin Du Sautoir/DOR 7
1294 Genthod, Switzerland — 1

14. Ashraf M. Aziz
15 Hussien Ahmed St.
ELSHARABIA
Cairo, Egypt — 1